UNIVERSITY OF CALIFORNIA SAN DIEGO

Physiology of bacteria in anaerobic environments

A Dissertation submitted in partial satisfaction of the requirements
for the degree Doctor of Philosophy

in

Physics with a Specialization in Quantitative Biology

by

Brian Robert Taylor

Committee in charge:

Professor Terence Hwa, Chair
Professor Lin Chao
Professor Alexander Groisman
Professor Suckjoon Jun
Professor Amir Zarrinpar

2022

The Dissertation of Brian Robert Taylor is approved, and it is acceptable in quality and form for publication on microfilm and electronically.

University of California San Diego

2022

DEDICATION

To my family.

EPIGRAPH

The most beautiful stories always start with wreckage

-Jack London

TABLE OF CONTENTS

LIST OF FIGURES

LIST OF TABLES

LIST OF SUPPLEMENTAL FILES

tableS2a.xlsx

tableS2b.xlsx

tableS3a.xlsx

tableS3b.xlsx

tableS3c.xlsx

LIST OF ABBREVIATIONS

Ac	Acetate
ATP	Adenosine triphosphate
ADP	Adenosine diphosphate
AMP	Adenosine monophosphate
cTc	Chlortetracycline
HAc	Acetic acid
PP_i	Pyrophosphate

ACKNOWLEDGMENTS

I would like to thank my advisor, Terry Hwa, for supporting me all these years no matter how far down I fell into the rabbit hole. His unique knowledge and critical eye have provided a valuable perspective that has allowed me to grow as a scientist. I would also like to thank my other committee members, past and present, Suckjoon Jun, Amir Zarrinpar, Karsten Zengler, Alex Groisman, and Lin Chao for their helpful and insightful comments.

I would also like to thank the many friends and colleagues I've met over the years, especially in the Hwa lab both past and present: Jonas Cremer and Markus Arnoldini for the challenging work of showing this greenhorn how to do experiments, Vadim Patsalo, for his deep cynicism that thoroughly challenged my own, Kapil Amarnath for his realistic optimism, Hiro Okano and Zhongge Zhang for sharing their deep knowledge of experimental technique, Ghita Guessous for grading those homeworks, and many others including Tomo, Rohan, Chenhao, Matteo, Jacob, Gabe, Avaneesh, Nate, Leo, Lance, and Jack. Special thanks to Nate and Jack for the super useful edits to this dissertation.

I'd also like to thank my collaborators from over the years, including Yihui Shen, Joshua Rabinowitz, and James Williamson. Special thanks as well to Brian Tenner and Linda Joosen for teaching me everything there is to know about Gibson cloning.

Chapter 2, in full, has been submitted for publication as Tradeoff between cytoplasmic accumulation and acidification governs bacterial response to short-chain fatty acid stress. Brian R. Taylor, Vadim Patsalo, Hiroyuki Okano, Yihui Shen, Zhongge Zhang, James R. Williamson, Joshua D. Rabinowitz, Terence Hwa, 2022. The dissertation author was the primary author of this paper.

Chapter 3, in part, is currently being prepared for submission for publication of the material. Brian R. Taylor, Vadim Patsalo, James R. Williamson, Terence Hwa, 2022. The dissertation author was the primary author of this paper.

Chapter 4, in part, is currently being prepared for submission for publication of the material. Brian R. Taylor, Vadim Patsalo, Zhongge Zhang, James R. Williamson, Terence Hwa, 2022. The dissertation author was the primary author of this paper.

VITA

2014 Bachelor of Science in Physics, University of Illinois at Urbana Champaign

2016 Master of Science in Physics, University of California San Diego

2019 Candidate of Philosophy in Physics, University of California San Diego

2022 Doctor of Philosophy in Physics with a Specialization in Quantitative Biology, University of California San Diego

PUBLICATIONS

Taylor, B. R., Patsalo, V., Okano, H., Shen, Y., Zhang, Z., Williamson, J. R., Rabinowitz, J. D., Hwa, T. Tradeoff between cytoplasmic accumulation and acidification governs bacterial response to short-chain fatty acid stress, Under review (2022).

Wu, S.-Y., Wen, Y., Serre, N. B. C., Laursen, C. C. H., Dietz, A. G., **Taylor, B. R.**, Aggarwal, A., Rancic, V., Becker, M., Ballanyi, K., Podgorski, K., Hirase, H., Nedergaard, M., Fendrych, M., Lemieux, M. J., Eberl, D. F., Kay, A. R., Campbell, R. E., & Shen, Y. (2021). A sensitive and specific genetically encodable biosensor for potassium ions. bioRxiv.

Amarnath, K., Narla, A. V., Pontrelli, S., Dong, J., Caglar, T., **Taylor, B. R.**, Schwartzman, J., Sauer, U., Cordero, O. X., & Hwa, T. (2021). Stress-induced cross-feeding of internal metabolites provides a dynamic mechanism of microbial cooperation. bioRxiv.

Basan, M., Honda, T., Christodoulou, D., Hörl, M., Chang, Y.-F., Leoncini, E., Mukherjee, A., Okano, H., **Taylor, B. R.**, Silverman, J. M., Sanchez, C., Williamson, J. R., Paulsson, J., Hwa, T., & Sauer, U. (2020). A universal trade-off between growth and lag in fluctuating environments. Nature, 584(7821), 470–474.

ABSTRACT OF THE DISSERTATION

Physiology of bacteria in anaerobic environments

by

Brian Robert Taylor

Doctor of Philosophy in Physics with a Specialization in Quantitative Biology

University of California San Diego, 2022

Professor Terence Hwa, Chair

Heterotrophic bacteria growing in anaerobic environments face two related problems. First, metabolism of carbon is less efficient without oxygen because cells must get energy through fermentation rather than aerobic respiration. As a result, cells have to either find ways to uptake more carbon or reduce the inefficiency caused by fermentation. Second, these fermentation waste products inhibit the growth of these bacteria. The human gut is an environment that is low in oxygen, yet bacteria thrive and grow to high densities. In this dissertation, I study the adaptations

that gut resident bacteria *Bacteroides thetaiotaomicron*, and *Escherichia coli* have developed in order to overcome these problems caused by low oxygen.

In chapter 2, we study the tolerance of *E. coli* to acetate stress. Short-chain fatty acids (SCFAs) accumulate in the mammalian gut and other fermentative environments, inhibiting the growth of many bacteria. The cause of growth inhibition and bacterial strategy resisting SCFA stress are however unclear. Through quantitative physiological study of *E. coli* under acetate stress complemented by proteomic and metabolomic analysis, we establish that acetate accumulation reduces growth by acting as a "useless metabolite" that excludes other metabolites. This accumulation can be blocked by cytosolic acidification, which however has its own deleterious effect. Strikingly, *E. coli* acidifies its cytosol to an extent that minimizes the combined effect of acidification and acetate accumulation on cell growth. Tolerance to both stress factors would require numerous cytosolic proteins to improve their activities at acidic pH, resulting in an obligatory tradeoff between SCFA tolerance and fast growth in neutral pH as has been reported for various gut bacterial species.

In chapter 3, we study the physiology of gut symbiote, *Bacteroides thetaiotaomicron*. *Bacteroides thetaiotaomicron* is a dominant member of the intestinal microbiota of humans and other mammals. One reason for *B. theta*'s dominance is its abundant machinery for utilizing a large variety of complex polysaccharides as a source of carbon and energy. This machinery is organized into localized clusters of genes that coordinate to breakdown polysaccharides of great complexity. While much knowledge has been developed about the individual genes involved in polysaccharide utilization, a quantitative picture is still incomplete. Here, we present a quantitative model describing the growth of *B. theta* on single and multiple carbon substrates. We find that a dominant obstacle for *B. theta*'s growth arises from a constant demand for carbon that is

independent of growth. This obstacle is partially overcome by *B. theta*'s ability to utilize multiple carbon sources with existing polysaccharide utilization machinery can provide this flux without a significant proteome cost.

In chapter 4, we study the role of pyrophosphate (PP_i) in mediating the energy efficiency of bacteria. PP_i is a universally abundant molecule found in all domains of life. Despite its ubiquity, many organisms treat it as a waste product, simply degrading the molecule into phosphate. However, some organisms use PP_i as a substitute for the energy-carrying ATP. *B. theta* has multiple enzymes that fulfill this role. Here, we find that depriving *B. theta* of PP_i significantly decreases its yield, which is consistent with PP_i's role as an energy substitute. However, this benefit of PP_i also comes at a cost as we also find increasing PP_i concentration, a necessity for using it as an energy currency, reduces the rate of protein synthesis and growth. Such a growth-yield tradeoff provides a reason why many organisms don't take advantage of the free energy benefit provided by substitution of ATP with PP_i, often restricted to organisms that would otherwise have a low yield, such as anaerobic bacteria.

Chapter 1

Introduction and Background

1.1 Introduction

For many living beings, possibly including yourself, a consistent supply of oxygen is necessary to continue living. Additionally, all known living things need water to live. However, for living beings that require oxygen, the need for water presents a problem, because oxygen dissolves poorly in water. Large organisms like mammals, can get around this problem by pumping oxygen around with cardiovascular systems, which in mammals include features such as the protein hemoglobin to help dissolve oxygen and carry it through veins and arteries. But, for microbes, a cardiovascular system is not an available option. They are large, complicated to build, and it's hard to keep competing microbes from taking advantage of it. As a result, environments where bacteria grow to high density are often oxygen deprived because any available oxygen is often quickly depleted (*1*).

How do these microbes living in low oxygen environments adapt to these conditions? Some organisms have alternative metabolisms where they create their own oxygen, such as the light-harvesting cyanobacteria (*2*). Other organisms can use so-called alternative electron acceptors which, similar to oxygen, can be used for respiration (*3*). Alternatively, organisms can metabolize via fermentation, converting carbohydrates into energy and fermentation waste products, such as acetic acid, lactic acid, and ethanol, which are found in everyday products such as vinegar, yogurt, and beer, respectively (*4*, *5*).

The microbes studied in this dissertation, *Escherichia coli* (*E. coli*) and *Bacteroides thetaiotaomicron* (*B. theta*) are both capable of fermentation, which is useful for growth in the environment they both live in: the human colon, which is anoxic (*6*, *7*). However, they still have many other differences in their metabolism. While *E. coli* can grow with oxygen, converting carbohydrates to CO_2 and biomass, *B. theta* will stop growing if exposed to more than nanomolar concentrations of oxygen (*8*). *B. theta* has unique fermentation pathways compared to *E. coli*, which contributes to its oxygen sensitivity as enzymes involved in those fermentation pathways are sensitive to oxygen (*9*). Because of their similarities and differences, *E. coli* and *B. theta* are useful organisms to compare, and our understanding of one complements our understanding of the other.

1.2 Growth of bacteria

E. coli cells can be cultured in defined media which contain a carbon source, nitrogen source, trace nutrients, and salts. When cells are placed into a well-defined media, they gradually adapt to grow in that media. As cells adapt, their constituent parts, RNA, DNA, and protein grow exponentially in proportion (*10*). This growth can continue over many generations until some limiting nutrient, such as oxygen, carbon, nitrogen, or other trace nutrient is depleted (*11*). When cells are grown in different environments, for example by changing the carbon source, nitrogen source, temperature, osmolarity, or antibiotic stress, their biomass composition changes in response to this environment (*12*). These changes have been described at different levels of abstraction, ranging from molecular mechanisms to physical and physiological constraints (*13*–*16*).

1.3 Background on acetate stress in bacteria

1.3.1 Short chain fatty acids

Bacteria that live in the mammalian intestinal system have to face two types of stress related to acids. The first is the very low pH of the stomach where pH can reach as low as 2. The second is the relatively more neutral colon where pH can range from 5-7 (*17*). The relative abundance of bacteria in these two environments differs greatly with the colon containing much higher densities of bacteria compared to the stomach. The difference in abundances between these two environments reflects the relative harshness of these two environments. When environmental pHs are below 4, *E. coli* is unable to grow and is instead more focused on survival (*18–21*). Our focus is on growth in the colon.

Contrary to the case of the stomach, bacteria aren't inhibited by the low pH itself. *E. coli* is able to maintain growth even when external pH reaches values as low as 4.5 (*20*). Instead, the environment of the gut is inhibitory to bacteria because of high concentrations of short chain fatty acids (SCFAs). Concentrations of these SCFAs can reach values as high as 100 mM (*22*, *23*). Approximately half of these SCFAs are acetate, with the rest being made up of propionate and butyrate along with lesser concentrations of other organic acids such as branched SCFAs. These SCFAs are known to inhibit or prevent the growth of many different kinds of bacteria (*24*). In addition to the human gut, SCFAs play an important role in the rumen (*25*).

SCFAs also are found in high concentrations in many other environments. Concentrations of SCFAs are relevant to bioproduction. Acetate excretion is a common byproduct of bacterial metabolism. Acetate is excreted in both aerobic (*26*, *27*) and anaerobic conditions (*6*). Acetate, as a metabolite, is found in conditions varying from sludge fermenters (*28*, *29*), marine environments, soil environments, and the mammalian gut (*23*). In high density environments, metabolism of acetate is associated with gene expression changes (*30*).

There has also been an increased interest in short chain fatty acids due to their effect on the gut microbiome. SCFAs play a role in the health of both the microbiome and the human host (*31–33*). Of particular interest are butyrate and propionate (*34*). Butyrate is consumed by the human host's gut epithelial tissue where it helps with tissue healing by down-regulating bacterial virulence (*35*). Furthermore, mammalian guts have free fatty acid (FFA) sensors such as GPR-41 and GPR-43 that monitor concentrations of SCFAs and provide information to the host about nutrient availability (*36*, *37*).

SCFAs play an important role in modulating the microbial ecosystem of the microbiome. Surprisingly, this modulation seems to be separated at the phylum level. *Bacteroidetes* appear to be significantly more sensitive to SCFAs at low pH than their *Firmicutes* competitors (*38*). The differential sensitivity to pH is important as an intermediatory in models considering nutrient flow and water uptake in the gut (*39*), which explains phyla level differences in bacterial abundance based on stool consistency (*40*). Furthermore, pH serves a role in the chemical output of the microbiome in addition to its composition (*41*). At a species level, butyrate appears to affect different *Bacteroides* species based on their Acyl-CoA transferase expression (*42*). SCFA accumulation also affects pathogenicity. For example, *Salmonella* is particularly sensitive to propionate, which is secreted by certain *Bacteroidetes* species (*43*). SCFAs also serve as important intermediates of cross feeding. Lactate also appears to regulate species interactions as an intermediate metabolite (*44*, *45*). The resident gut archaeon, *Methanobrevibactor smithii*, uses SCFAs such as acetate for its growth (*46*, *47*). Elucidating the bacterial response to SCFA is a critical element in managing and manipulating gut microbes (*32*, *48–51*).

There have been several proposed mechanisms for why bacterial cells are inhibited by SCFAs. While many studies have suggested that SCFAs have an uncoupling effect, it has been

shown that there are multiple physiological differences between acetate stress and stress imposed by the uncoupler carbonylcyanide-m-chlorophenylhydrazone (CCCP) (*52*). Additionally, work has also shown that acetate perturbs many ions in the cells, especially by partially replacing glutamate (*53*). Recovery after acetate removal appears to be dependent on glutamate synthesis. In some strains of *E. coli*, acetate sensitivity appears to be related to a defect in methionine metabolism (*54*). Acetate tolerance can be improved by the addition of certain amino acids and nucleotides (*55*). Expression of genes involved in the tricarboxylic acid (TCA) cycle and the glyoxylate shunt is reduced in acidic media with acetate (*56*). However, latter studies found that mutations disrupting acetate uptake did not change the cell's tolerance to acetate stress (*57*).

In chapter 2, we extend previous knowledge of acetic acid stress by connecting the accumulation of acetate and resulting loss of metabolites as a source of the growth defect by showing that these effects can be replicated with other useless metabolites.

1.3.2 The effect of cytosolic metabolite concentrations on growth rate

Many studies have shown that quantifying protein cost is an effective way of understanding cell growth and physiology (*14*, *27*, *58*). The growth of exponentially growing cells is limited by the abundances of certain proteins. The abundance of these proteins correlates with the growth rate of cells, with the increased abundance providing higher flux for higher growth rates. The amount of protein(s) required to increase the growth rate by a certain amount is the cost of that protein(s). Growth rate is limited by this cost since there is an upper limit to the amount of proteins that can be expressed in cells. About half of the proteome is fixed, and overexpressed proteins can't reach abundances higher than this limit (*58*, *59*). Ribosome-inhibiting antibiotics increase the cost of ribosomal proteins by reducing the amount of flux these proteins can provide (*59*). Similarly, when cells are limited by nutrient availability, the cost of proteins related to nutrient uptake increases,

but there's no clear mechanism that can generally explain the increased cost of nutrient limited proteins.

One possibility to explain these increased costs is by considering metabolite concentrations. It's well established that the kinetic rates of enzymes are strongly influenced by the concentrations of the substrates and products in the reactions that these enzymes catalyze (*60*). While in principle protein cost depends on standard enzyme kinematic parameters such as k_{cat} and K_m, there is also a contribution from metabolite concentrations. Since many enzymatic reactions are accelerated by high metabolite concentrations, cells can maximize their growth rate by maximizing metabolite concentrations. However, if cells can't increase their metabolite concentrations, something must be limiting them.

There is some experimental evidence suggesting how metabolite concentrations may limit growth. In steady state growth, the activity of ribosomes is limited by the effective concentration of charged tRNA (*61*). Outside of steady state growth, metabolic fluxes appear to be limited by factors other than enzyme abundance. Studies on growth transitions show that at a coarse grained level, carbon flux is limited by substrate availability (*16*, *62*). In this work, substrate availability is a coarse-grained quantity, and doesn't reflect the concentrations of any specific metabolites. However, later studies have shown that the lack of availability of key metabolites can lead to long lag times for certain growth transitions (*15*).

Many theoretical models have been proposed to explain substrate concentrations based on theories that are constrained by various mechanisms limiting metabolite concentrations. While metabolite concentrations for many enzymes appear to be saturating for many reaction-metabolite combinations, many other metabolites are at concentrations below the K_m, and may therefore be growth limiting (*63*). Furthermore, in slower growth, many reactions are sensitive to metabolite

concentrations because they are near thermodynamic equilibrium and reversible (*64*). Later work has looked at the relationship between enzymes and their limiting substrates. There is also literature where metabolites are allowed to freely vary in order to satisfy optimality constraints (*65*). Theoretical analysis of systems where total metabolite concentrations are fixed by osmolarity has been proposed (*66*). Later work on modeling multiple abiotic constraints, such as osmolarity, have been successful in predicting concentrations of individual metabolites (*67*). Other work has partially explained metabolite concentrations based on the principle of minimizing metabolite pool size and existing enzyme concentrations (*68*).

In chapter 2, we find that cells inhibited by acetate stress simultaneously accumulate large concentrations of acetate which appears to replace other useful metabolites. This effect can also be replicated by filling cells with trehalose instead of acetate. With this trehalose overdose, we provide an experimental method to perturb metabolite concentrations without targeting specific branches of metabolism.

1.4 Regulation of carbon uptake in *Bacteroides thetaiotaomicron*

Bacteroides species have a remarkable strategy for solving the challenge of taking up complex polymers into its cells. Because polymers are too big to be taken up directly into cells, those polymers must be broken down into smaller oligomers. In order to break up these polymers, polymer-degrading enzymes must be located outside of the cell. However, if these enzymes are just released into the environment, those enzymes will eventually drift too far away to be of use and any nearby organisms can "cheat" by stealing the products from those enzymes. *Bacteroides* fix this problem by keeping these enzymes fixed to their outer membranes. The large size of these membrane proteins likely presents a large physiological cost to these organisms, as membrane space is limited and so is protein synthesis rate. Expression of these enzymes is likely tightly regulated, but quantitative details of this regulation in *B. theta* are still being explored.

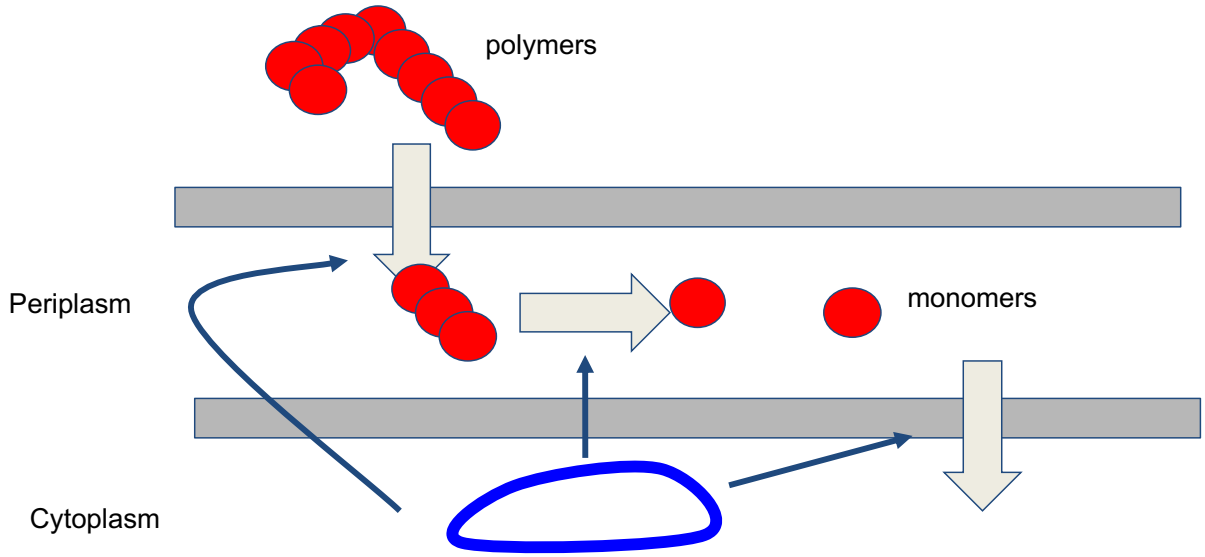

Figure 1.1 Digestion of polymers in Bacteroides thetaiotaomicron.
Polymers in the lumen of the gut are freely available for bacteria to digest. The outer membranes of Bacteroides species have enzymes that bind, hydrolyze, and import those polysaccharides as shorter oligosaccharides. Those oligosaccharides are then degraded in the periplasm and cytoplasm for use in fermentation. Adapted from (69).

1.4.1 Monod growth

Heterotrophic bacteria require an external organic carbon source for their growth. Carbon sources can range in complexity from the two-carbon molecule, acetate, to glycoproteins which consist of multiple amino acids and sugars held together by peptide and various glycosidic bonds. The model organism, *E. coli*, is capable of growing with simple carbon sources including sugars as long as other essential nutrients such as nitrogen, phosphorus, etc. are also provided. When provided an ample supply of nutrients, *E. coli*, grows exponentially with a characteristic growth rate, λ.

However, when *E. coli* is provided with a limited concentration of carbon, its growth rate is reduced compared to growth on high concentrations of the given carbon source. This phenomenon has often been quantitatively described with the Monod equation (*11*),

$$\lambda = \lambda_{max} \cdot \frac{\mathrm{c}}{\mathrm{c} + K_{\mathrm{c}}} \qquad \textit{Eq. 1.1}$$

where λ_{max} is the maximum specific growth rate for a carbon source, *c* is the concentration of the carbon source, and K_c is the Monod constant. An example of this model fit to data is shown in Figure 1.2 with the data from (*11*). The Monod equation is simply an empirical relationship derived from data and there is no clear mechanistic basis for using the equation (*11*, *70*).

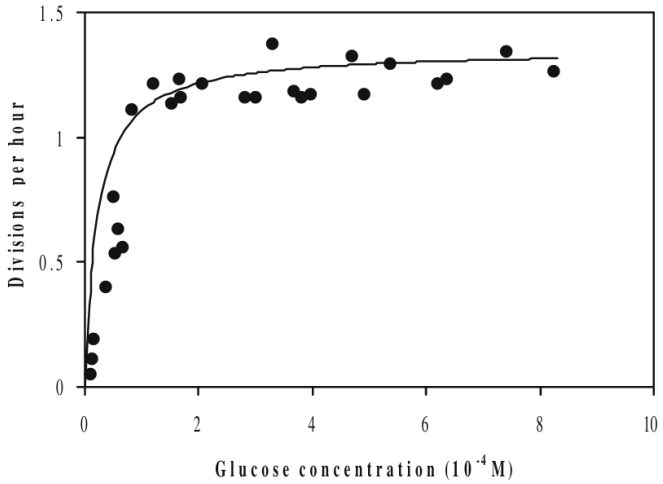

Figure 1.2 Growth rate of E. coli vs glucose concentration.
Adapted from (70). The solid line is a fit for the Monod equation (Eq. 1.1). Fit is for $\lambda_{max} = 1.35$ *doublings/hour and* $K_c = 22\ \mu M$.

Deviations from the Monod equation have been observed. One property of the Monod equation is that any non-zero concentration of nutrient can provide a non-zero growth rate. However, it's been observed that the growth of methanogenic bacteria on acetate exhibits a switch-like behavior; below 0.5 mM of acetate cells wouldn't grow, which contradicts the Monod equation (*71*). It has also been observed that bacteria have a carbon flux that isn't associated with growth. The observation has been called a maintenance flux or supply (*72*, *73*). The result of considering this maintenance flux within the context of the Monod equation is that the curve is shifted so that for some positive carbon concentration, the growth rate is zero. In chapter 3, we'll see that this equation describes the growth of *B. theta* well for single carbon sources.

$$\lambda = \lambda_{max} \cdot \frac{\mathrm{c}}{\mathrm{c} + K_{\mathrm{c}}} - \lambda_0 \qquad \textit{Eq. 1.2}$$

1.4.2 Growth on two carbon sources

When bacteria are provided two carbon sources, they can either consume them simultaneously or sequentially. In *E. coli*, the simultaneous utilization of two carbon sources has been described, allowing the growth rate on two carbon sources to be predicted from the growth parameters of cells growing on either carbon source individually (*74*).

The growth of cells is often limited by the expression of rate limiting enzymes. In *E. coli*, the uptake of carbon appears to exhibit relatively simple behavior. For many catabolic enzymes, their expression is correlated with growth rate.

$$\mathrm{E} = \mathrm{E}_{max} \cdot (1 - \lambda/\lambda_c) \qquad \textit{Eq. 1.3}$$

where E is the mass fraction of some limited catabolic enzyme, E_{max} is the maximum concentration that this limiting enzyme reaches, and λ_c is the fastest growth rate on the best carbon source where no catabolic enzymes are need, found by the x-intercept which is the same for all catabolic enzymes.

For cells growing on a single carbon source, i, the flux is related to catabolic gene expression by

$$J_i = k_i \cdot E_i \qquad \textit{Eq. 1.4}$$

where J_i is the carbon flux of carbon i, k_i is the catalytic rate constant, and E_i is the mass fraction of limited catabolic enzymes for carbon i. When growing on two carbon sources, the fluxes are additive.

$$J_{\mathrm{tot}} = k_1 \cdot E_1 + k_2 \cdot E_2 \qquad \textit{Eq. 1.5}$$

When given an adequate supply of nutrients, *E. coli* uses this supply to grow. It can be assumed that the growth rate is proportional to the flux.

$$\lambda_{12} = Y \cdot J_{tot} \qquad \textit{Eq. 1.6}$$

where Y is the efficiency of the carbon source. The efficiency, Y, won't always be constant, for example because of the excretion of acetate, however, the flux of this excretion is small enough that it won't change Y very much.

By evoking Eq. 1.3, Eq. 1.5, and Eq. 1.6, we can obtain an explicit relationship between growth rate on two carbon sources and gene expression,

$$\frac{\lambda_{12}}{1 - \lambda_{12}/\lambda_c} = Y \cdot k_1 \cdot E_1 + Y \cdot k_2 \cdot E_2. \qquad \textit{Eq. 1.7}$$

There is also a similar relationship for a single carbon source,

$$\frac{\lambda_{\mathrm{i}}}{1 - \lambda_{\mathrm{i}}/\lambda_c} = Y \cdot k_{\mathrm{i}} \cdot E_{\mathrm{i}} \qquad \textit{Eq. 1.8}$$

Combining Eq. 1.7 and Eq. 1.8 gives the growth rate composition formula,

$$\lambda_{12} = \frac{\lambda_1 + \lambda_2 - 2 \cdot \lambda_1 \cdot \lambda_2/\lambda_c}{1 - \lambda_1 \cdot \lambda_2/\lambda_c^2}, \qquad \textit{Eq. 1.9}$$

which relates the growth rate of cells grown on two carbon sources, λ_{12}, with the growth rates of the individual carbon sources, λ_i, and a parameter that describes the growth rate dependence of gene expression, λ_c. For small values of λ_1 and λ_2, $\lambda_{12} = \lambda_1 + \lambda_2$ and as λ_1 and λ_2 approach λ_c, $\lambda_{12} = \lambda_c$

In chapter 4, we show how extending Eq. 1.9 for the case where maintenance flux is non-negligible describes the growth of *B. theta* on individual sugars and how this relates to *B. theta*'s carbon uptake strategy.

1.5 Physiological role of pyrophosphate and translation

The main energy currency of cells is arguably adenosine triphosphate (ATP). Many cellular reactions involve this molecule. ATP can be hydrolyzed into adenosine diphosphate (ADP) which produces a phosphate (P_i) that can be transferred to another molecule or released as free P_i.

Alternatively, ATP can also be hydrolyzed into adenosine monophosphate (AMP) and a diphosphate or more commonly, pyrophosphate (PP_i) (Figure 1.3). The standard free energy for the release of two phosphates as PP_i is higher than releasing a single phosphate (*75*). So, for reactions that need more energy, cells have the option of freeing PP_i from ATP. PP_i is often produced by the synthesis of macromolecules, either directly or indirectly (*1*). In many organisms, PP_i is a waste product, being simply hydrolyzed into two phosphates without further usage. However, for a diverse subset of organisms, including bacteria, archaea, plants, and protists, PP_i plays a significant role in central metabolism, as a substitute for ATP.

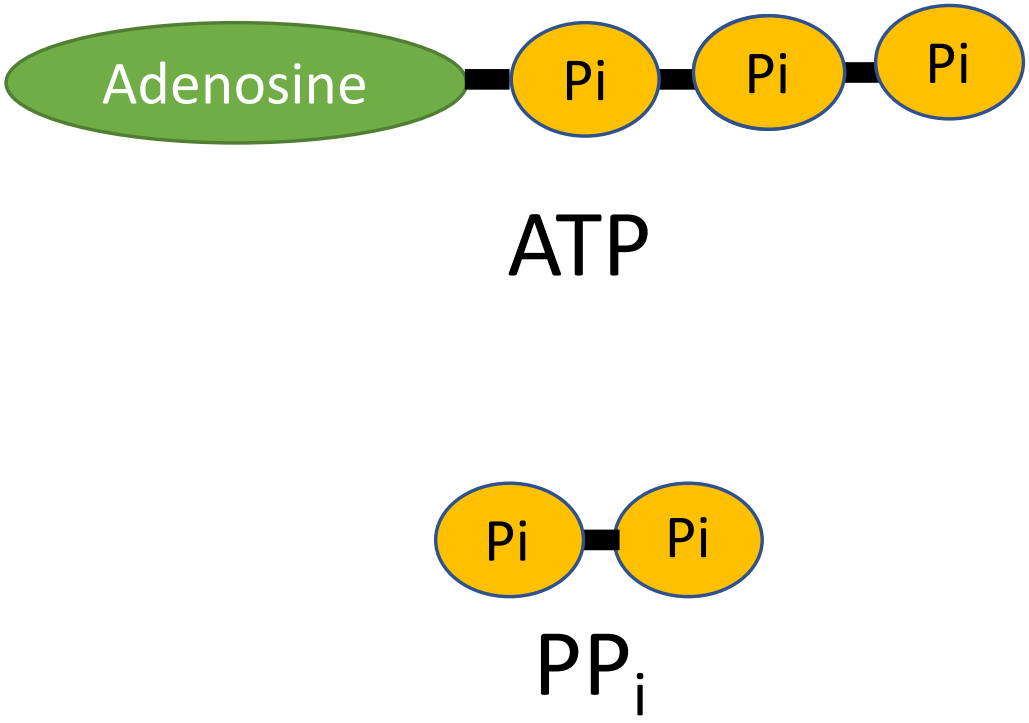

Figure 1.3 Adenosine triphosphate (ATP) and pyrophosphate (PP_i).
The bonds holding phosphates (yellow ovals) can be hydrolyzed by cells to release energy.

1.5.1 Diverse metabolism of PP_i

Experimental evidence for the use of PP_i in central carbon metabolism was first found in the anaerobic amoebozoan *Entamoeba histolytica* in 1968 (*76*). This enzyme, catalyzes the following reaction

$$phosphoenolpyruvate + \mathrm{AMP} + PP_i \rightleftharpoons pyruvate + \mathrm{ATP} + P_i$$

which is similar to the following reaction catalyzed by pyruvate kinase

$$phosphoenolpyruvate + \mathrm{ADP} + \rightleftharpoons pyruvate + \mathrm{ATP}$$

Due to this enzyme's usage of PP_i, the newly discovered enzyme was called pyruvate, phosphate dikinase (*ppdk*). Similar enzymes were isolated from plants, *Acetobacter* and *Propionibacterium* (*77–79*). These enzymes could be used in gluconeogenesis as an alternative to PEP carboxykinase, catalyzing the formation of PEP from pyruvate instead of from oxaloacetate (*78*). Around that same time, a *ppdk* was discovered in *Bacteroides symbiosus* (later *Lachnoclostridium symbiosus*) (*80*, *81*). The enzyme from *L. symbiosus*, was different from the enzyme from *E. histolytica* in that it functioned primarily in the glycolytic direction, being biased towards the right side. Surprisingly, *Bacteroides fragilis* (*B. fragilis*), a closely related organism to *B. theta*, has been found to have low levels of *ppdk* activity (*7*). It's possible that activity is in the gluconeogenic direction for this enzyme in *Bacteroides* as the gene is predicted to exist in many *B. fragilis* genomes and in the *B. theta* genome (*82*). Interestingly, the gene (BT0644) doesn't appear to be essential to growth in *B. theta* as it's deletion did not affect survivability in an insertion sequencing experiment (*83*) (Figure 1.4).

Later on, a new class of PP_i utilizing enzymes was discovered. In 1974, a 6-phosphofructokinase was discovered which produced 1,6 fructose biphosphate from PP_i instead of ATP, again in *E. histolytica* (*84*). The enzyme has also been discovered in *P. shermanii* (*85*) and

the marine bacteria *Alcaligenes* and *Pseudomonas marina* (*86*). *B. fragilis* has PP_i-dependent 6-phosphofructokinase activity, while having only negligible ATP-dependent 6-phosphofructokinase activity (*7*). Similarly, *Bacteroides* species from the rumen were found to have high PP_i-linked 6-phosphofructokinase activity relative to ATP linked 6-phosphofructokinase activity (*87*). *B. theta* is predicted to have both PP_i-dependent 6-phosphofructokinase and ATP-dependent 6-phosphofructokinase enzymes in its genome (BT0307) (*82*) (Figure 1.4). This PP_i-dependent 6-phosphofructokinase appears to be essential for growth in mice and minimal media according to an insertion sequencing experiment (*83*).

B. theta may also have other useful PP_i dependent enzymes, but their importance is unclear. A PP_i-energized sodium pump is predicted in the genome based on homology (BT3411/*hppa*) (*82*). This pump is predicted to exchange PP_i and sodium. It may function similarly to a membrane bound ATPase, which exchanges ATP and protons/sodium. While many organisms exchange protons as part of their main membrane energy currency, *B. theta* and related *Bacteroidetes* use sodium for uptake of carbon (*88*) and as an energy carrier for the electron transport chain (*82*, *89*, *90*). There are also several PP_i-binding enzymes that play small roles in biosynthesis of cofactors, but their role is minor compared to other enzymes. In *E. coli*, the enzymatic hydrolysis of PP_i is essential for growth (*91*), *B. theta* does not appear to have a similar hydrolase predicted in its genome.

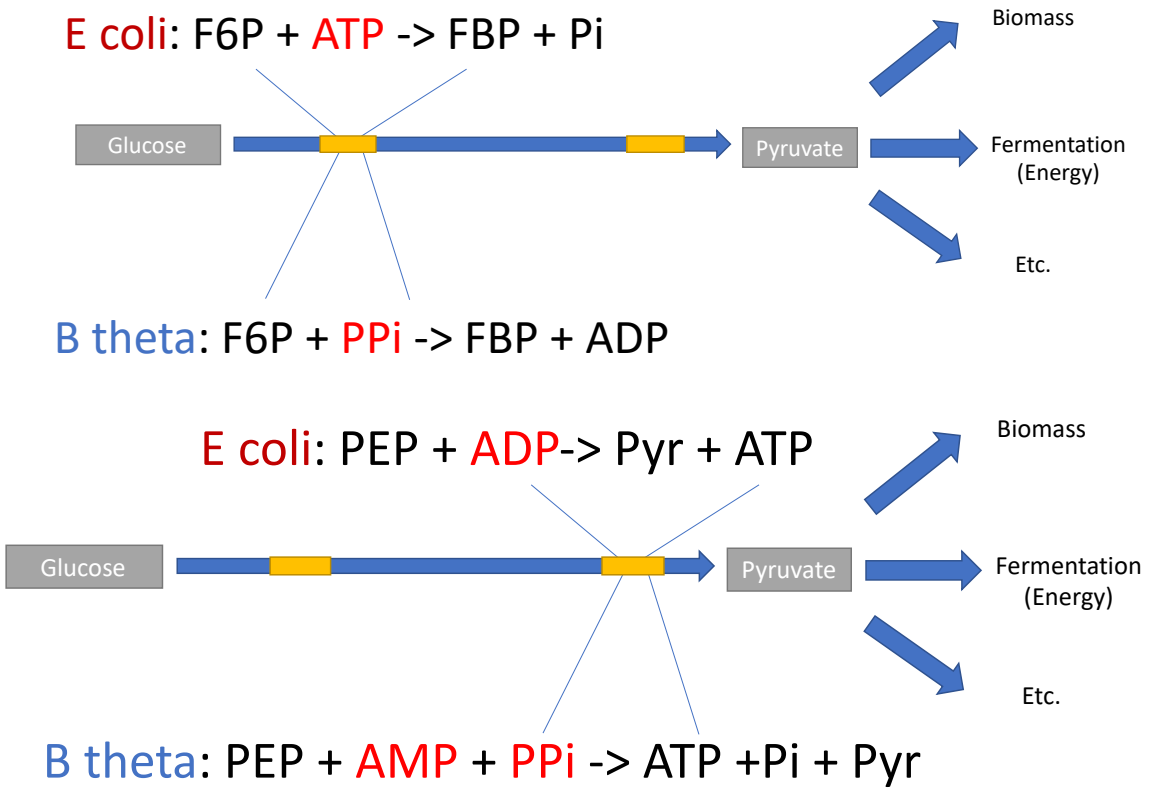

Figure 1.4 Enzymatic reactions involved in PP_i metabolism for B. theta
For each panel, E. coli (red) represents reactions that don't utilize PP_i, while B. theta (blue) reactions do utilize PP_i. Wildtype B. theta has both types of enzymes according to (82).

1.5.2 Macromolecules

Pyrophosphate also plays a prominent role in macromolecule biosynthesis, usually being released as monomers are added to the macromolecule. PP_i is produced by synthesis of DNA, RNA, protein, glycogen, and lipids (*75*, *92*) by the net hydrolysis of a nucleotide triphosphate (NTP) into a nucleotide monophosphate (NMP) and PP_i. The actual steps where this hydrolysis happens vary based on the macromolecule being synthesized. For DNA synthesis, PP_i is released by DNA polymerase during DNA synthesis (*93*). For RNA synthesis, PP_i is released by RNA polymerase as part of the translocation step during transcription (*94–96*). The synthesis of nucleotides also releases PP_i (*97*). For glycogen synthesis, the formation of ADP/UDP-glucose

from glucose-1-phosphate and ATP/UTP results in the formation of PP_i (*98*). For protein synthesis, PP_i is released during the charging of aminoacyl-tRNA with amino acids.

The reason why macromolecule synthesis involves the release of PP_i rather than the less energetic release of P_i is an open question. Theoretical calculations suggest that the free energy difference alone cannot explain the release of PP_i rather than P_i because there's enough free energy available with the less energetic reaction that doesn't involve the release of PP_i (*75*). Frequently it's suggested that PP_i acts to help reduce the error rate of nucleotide or amino acid incorporation (*99*). PP_i release helps with high-fidelity DNA replication in *Staphylococcus aureus* by acting kinetically rather than thermodynamically (*100*). For protein synthesis, it's suggested that PP_i promotes irreversibility in translation through its role in aminoacyl tRNA charging (*92*).

PP_i inhibits many of the reactions in which it takes part. DNA synthesis in *E. coli* is inhibited by a high concentration of PP_i (*101*), often leading to a decrease in fidelity of DNA synthesis (*99*). However, the decrease in fidelity is not always replicated as it appears to depend on the template used (*99*). Much of the inhibition comes from increasing PP_i from below physiological concentrations to near them (~1 mM). When increasing PP_i beyond physiological concentrations to ~8 mM, PP_i doesn't inhibit DNA synthesis significantly (*75*). RNA synthesis is also inhibited by PP_i, decreasing both the fidelity and rate for an *in vitro* system (*102*). *In vitro* studies of the effect of PP_i on protein synthesis have shown mixed roles, with the charging of some tRNAs being more strongly affected than others (*103*, *104*). For *in vivo* studies, it is not known how PP_i affects the specificity and fidelity of tRNA charging (*75*).

1.5.3 Yield and energy

Because of PP_i's similarity to ATP and PP_i's ability to replace ATP, it has been proposed that pyrophosphate is used as an energy saving molecule (*7*, *105–107*). This usefulness depends

on PP_i being freely available for cells to use, rather than directly synthesizing PP_i from ATP without using that energy (*7*, *98*, *107–109*). If the PP_i is available for free, then any ATP that PP_i replaces can be used elsewhere for another reaction. In glycolysis, these savings can be substantial since for each glucose converted to pyruvate, 2 high energy phosphate bonds, equivalent to converting 2 ATP to 2 ADP, are used to make 4 high energy phosphate bonds. One of those ATP is used to phosphorylate glucose and the other is used to phosphorylate glucose-6-phosphate. Only for the latter reaction is ATP usually used to replace PP_i. Practically there's a potential 50% increase in net energy available per glucose metabolized since PP_i used in this way can yield 3 higher energy phosphates instead of 2.

More energy saving could be included from the reaction converting PEP, AMP and PP_i to pyruvate, P_i, and ATP, depending on the direction this reaction runs in. Since each glucose makes 2 PEP, use of this enzyme to make pyruvate makes 2 ATP equivalents instead of 1 when PP_i is used. If run in the reverse direction, this reaction can be used to make PP_i if needed. Similarly, there is also another useful energy saving mechanism found in *Bacteroides* (Figure 1.5). For *Bacteroides,* in the conversion of PEP to oxaloacetate, PEP carboxykinase can yield an ATP, which differs from the pyruvate carboxylase, which doesn't save the ATP in the conversion of PEP to oxaloacetate (*7*). Additionally, *Bacteroides* has a cytochrome oxidase involved in the reduction of fumarate to succinate. This reaction could be coupled to energy generation as a part of the electron transport chain but it's unclear how much this contributes to energy yield (*110*). Ultimately, conversion of PEP to fermentation products provides *B. theta* flexibility to either create or use PP_i. Without using *ppdk*, 1 PEP can produce 1 ATP. By using *ppdk* in the glycolytic direction, 2 ATP can be produced by using 1 PP_i. Additionally, it's possible to produce PP_i in exchange for ATP by converting PEP to pyruvate and then PEP again by using pyruvate kinase

and *ppdk* in a cycle. With this cycle, it's possible to directly convert ATP and PP_i. Overall, if sufficient PP_i is available, the combined theoretical ATP yield for *Bacteroides*' glycolysis is almost double at 3-5 compared to 2-3 for *E. coli*.

PP_i's relative simplicity compared to ATP has led some to propose that PP_i could be an ancient energy currency, but there are theoretical downsides to using PP_i as a sole replacement for ATP one of which is PP_i's usefulness as an intermediate energy molecule (*92*, *105*, *106*). Also, studies on the genetic relatedness of PP_i-based enzymes suggest that these enzymes have exchanged between kingdoms and phyla through horizontal gene transfer. This frequent gene exchange solidifies the idea that PP_i plays an important role in the organisms that can find a use for it.

In chapter 4, we find that availability of PP_i benefits the yield of *Bacteroides thetaiotaomicron,* but this benefit comes at the cost of physiologically relevant concentrations of PP_i which are sufficient to inhibit protein synthesis rates.

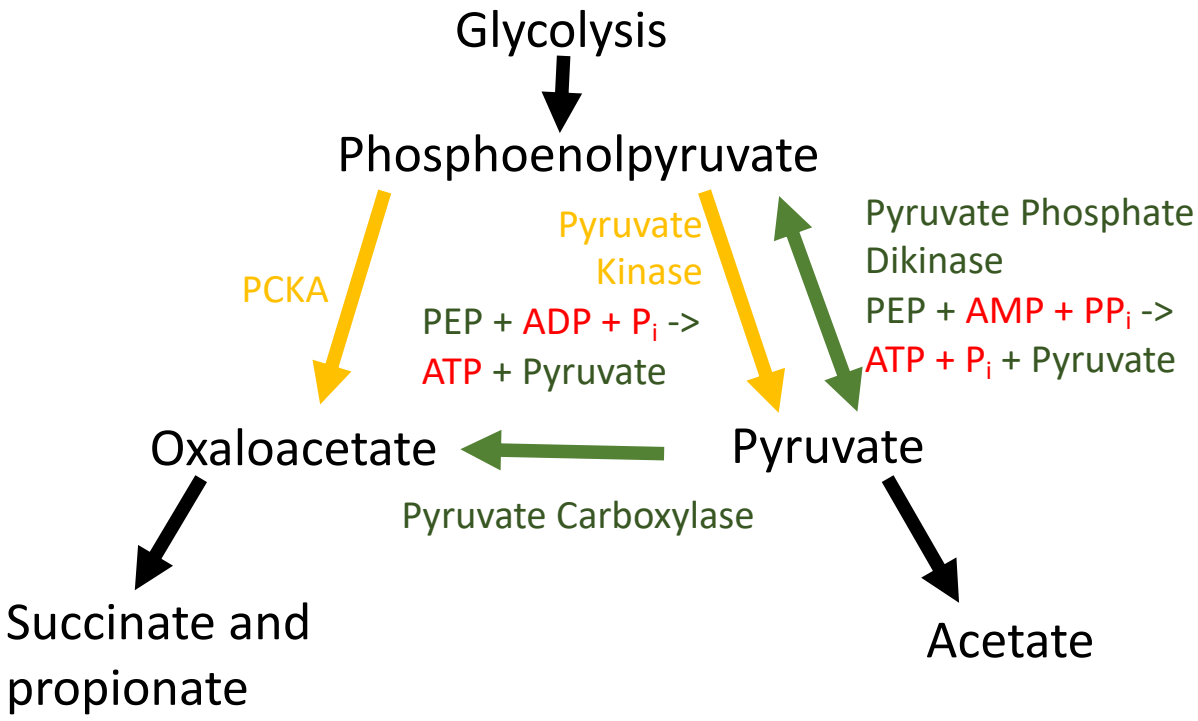

Figure 1.5 Role of PP_i in lower glycolysis for B. theta.
Glycolysis produces phosphoenolpyruvate (PEP). PEP is then converted to fermentation products as succinate, propionate, or acetate. Depending on the path taken, production of these fermentation products can either produce or consume PP_i.

Chapter 2

Tradeoff between cytoplasmic accumulation and acidification governs bacterial response to short-chain fatty acid stress

2.1 Abstract

Short-chain fatty acids (SCFAs) accumulate in the mammalian gut and other fermentative environments (*22*, *30*, *111–114*), inhibiting the growth of many bacteria (*25*, *31*, *38*, *53*, *115*). Bacterial strategy resisting SCFA stress is however unclear. Through quantitative physiological study of *E. coli* under acetate stress complemented by proteomic and metabolomic analysis, we establish that acetate accumulation reduces growth by acting as a "useless metabolite" that excludes other metabolites. This accumulation can be blocked by cytosolic acidification, which however has its own deleterious effect. Strikingly, *E. coli* acidifies its cytosol to an extent that minimizes the combined effect of acidification and acetate accumulation on cell growth. Tolerance to both stress factors would require numerous cytosolic proteins to improve their activities at acidic pH, resulting in an obligatory tradeoff between SCFA tolerance and fast growth in neutral pH as has been reported for various gut bacterial species (*38–40*, *115*).

2.2 Introduction

The mammalian gut harbors a diverse ecosystem of microbes growing at a moderately acidic pH in the range 5 – 7 due to the presence of short-chain fatty acids (SCFAs) such as acetate, propionate, and butyrate. Concentrations of these SCFAs exceed 100 mM, about half of which is

acetate (*22*, *23*). Common gut microbes such as *Bacteroidetes* and *Firmicutes* respond differently in this pH range and their differential acid responses contribute significantly to their differential abundances (*38–41*). SCFA accumulation also affects pathogenicity. *Salmonella* is, e.g., particularly sensitive to propionate, which is secreted by certain *Bacteroidetes* species (*43*). Thus, elucidating the bacterial response to SCFA is a critical element in managing and manipulating gut microbes (*32*, *48–51*). In this work, we investigate the origin of SCFA toxicity using the model enteric bacterium *E. coli*.

Acetate excretion is a common byproduct of bacterial metabolism. Acetate is excreted in both aerobic (*26*, *27*) and anaerobic conditions (*6*). Acetate as a metabolite is found in conditions varying from sludge fermenters (*28*, *29*), marine environments, soil environments, and the mammalian gut (*23*).

2.3 Effect of pH and acetate alone

We characterized the toxic effect of medium acidity by growing *E. coli* K-12 cells in minimal glucose medium set to different pH using different buffers (see 2.10.2). Growth was hardly affected down to pH 5 but dropped rapidly below that (purple symbols, Figure 2.1a). However, in the presence of acetate, cells were more strongly affected by pH, with the effect being stronger for higher concentrations of acetate (circles, Figure 2.1a).

To explore the combined effect of acetate and pH further, we performed a systematic scan of these two variables. For each fixed medium pH (from 5 to 7), the growth rate steadily decreased as the medium acetate concentration was increased, with a stronger acetate sensitivity at lower pH (Figure 2.1b). The combined effects of pH and acetate on growth rate can be collapsed onto a single curve if we plot growth rate against the concentration of acetic acid in the medium (Figure 2.1c) as shown previously for benzoic acid (*24*). The acetic acid concentration, [HAc], is calculated from the Henderson-Hasselbalch equation (*116*),

$$[\mathrm{HAc}] = [\mathrm{Ac^-}] \cdot 10^{\mathrm{pK_a - pH}}, \qquad \textit{Eq. 2.1}$$

with $\mathrm{pK_a} \approx 4.77$ (117). We next tested the toxic effect of several other weak organic acids. Similarly, to acetate, propionate and butyrate are two short-chain fatty acids (SCFA) that accumulate to high concentrations in the mammalian gut (*23*) and have very similar $\mathrm{pK_a}$ as acetate (117). Under a fixed pH, our cells responded similarly to butyrate as acetate, but exhibited somewhat increased sensitivity to propionate (blue and green circles, Figure 2.1d). In comparison, the effect of the less commonly encountered benzoate, which has similar $\mathrm{pK_a}$ (117), is much more toxic (purple, Figure 2.1d). We will focus on acetate as the quintessential SCFA in this study.

Because high concentrations of SCFAs are commonly encountered in anaerobic conditions (*22*, *23*), we also tested the acetate tolerance of anaerobically grown cells in glucose minimal medium at fixed reduced pH. Anaerobically grown cells exhibited similar growth rate as aerobically grown cells, decreasing as the acetate concentration increased (Figure 2.1e), suggesting that the cause of acetate toxicity is common to aerobiosis and anaerobiosis. We then characterized how another well-studied gut bacterium, *Bacteroides thetaiotaomicron*, responded to acetate. We grew this obligate anaerobe in glucose medium with different acetate and pH. Like *E. coli*, the response collapsed to a single curve when plotted against acetic acid (Figure 2.1f). Together, these results suggest that the toxicity to weak organic acids is a general phenomenon, although the quantitative extent of toxicity is dependent on the bacterial species and the identity of the acid.

Before we investigate the origin of acetate toxicity, we note that the biomass yield of *E. coli* growing on glucose is slightly increased by acetate despite growth reduction (Figure 2.6a-b), likely due to a small amount of acetate uptake (Figure 2.6c). Also, deleting key enzymes of acetate metabolism (Δ*acs* Δ*ackA*) (*26*) hardly showed any effect (Figure 2.6d, orange bars), suggesting that acetate exerted its effect not as an active metabolite. We also checked the role of the RpoS

(stress) regulon, which is known to alleviate growth defects for many other stresses (*118*). Surprisingly, deletion of the *rpoS* gene (Table 2.1) also exerted no effect on growth under acetate stress (Figure 2.6d, purple and pink bars).

2.4 Acetate stressed proteome

To find some clues for what cellular processes may be affected by acetate stress, we characterized the proteome of acetate-stressed cells using mass spectrometry ((*58*), Method 2.10.6) and compared the pattern of fold-changes in protein abundances due to acetate stress with previous results from cells limited in growth by a variety of bottlenecks (*58*) (Figure 2.7a-c**,** Table 2.3). The fold changes in protein levels due to acetate stress were most correlated with those with an internal bottleneck in biosynthesis, or "anabolic limitation" (Figure 2.7e). This similarity to "anabolic limitation" is also observed when proteins are grouped according to function (Figure 2.7f**,** Figure 2.8). Altogether, these results suggest that acetate exerts its toxic effect in non-specific ways on biosynthesis that cannot be shielded by *E. coli*'s stress-relief pathways.

2.5 Accumulation of acetate

We next turn to the consequence of elevated concentration of acetic acid, the source of the growth defect (Figure 2.1c). Since acetic acid is a small, lipophilic molecule that can freely diffuse across lipid membranes (*119*) relatively quickly, the concentration of acetic acid is rapidly equilibrated inside and outside the cell. Given the relationship between acetic acid and acetate ions from Eq. 2.1, a simple relation arises between the internal and external acetate concentrations (Figure 2.2a and (*120*)):

$$[\mathrm{Ac^-}]_{\mathrm{int}} = [\mathrm{Ac^-}]_{\mathrm{ext}} \cdot 10^{\Delta \mathrm{pH}} \qquad \textit{Eq. 2.2}$$

Here, $\Delta \mathrm{pH} \equiv \mathrm{pH}_{\mathrm{int}} - \mathrm{pH}_{\mathrm{ext}}$ is the differences between the intra- and extra-cellular. Because the cell can control its internal pH through proton transport and the electron transport chain (*20*), a

substantial difference between the internal and external pH can exist when the latter is set low. This pH difference would in turn result in substantial difference in the internal and external acetate concentration. Assuming that the internal pH is fixed at the unstressed value of ~7.8 (see below), Eq. 2.2 predicts a huge build-up of internal acetate across the range of acetate stress applied in our experiments (dashed line, Figure 2.2b), reaching 1 M at external concentration of ~20 mM.

We directly determined the internal acetate content for cells growing in this acetate range at medium pH=6 (Figure 2.9a,b). The accumulated acetate content is shown as red squares in Figure 2.2b (right y-axis) and charge is balanced by increased accumulation of potassium (Figure 2.9c,d), suggesting that the accumulation of potassium is associated with acetate influx. We additionally measured the cytoplasmic water content using radiolabeling (Figure 2.9e), finding it to remain at ~1 μL/OD/mL (~2x cell dry weight (*121*)), largely independent of the degree of acetate stress; thus, the measured acetate content (in nmol/OD/mL) converts simply to mM concentration (Figure 2.2b, left y-axis). The accumulated acetate was much lower than that if cells maintained their internal pH at 7.8 (compare red squares and dashed line, Figure 2.2b). Also, internal acetate scaled sub-linearly with the external acetate concentration, indicating that the internal pH and/or ΔpKa were changing under different degrees of acetate stress as reported in early studies (*53*, *120*). We confirmed a drop in internal pH for these acetate stressed cells (red triangles, Figure 2.2c) using a pH-sensitive ratiometric GFP, pHluorin (*122*) (Figure 2.10a,b), cross-validated with the classical radioactivity method (*123*, *124*) (Figure 2.10c). Given measurement of both the internal pH and acetate concentration, we calculated the internal pK_a using Eq. 2.1 and found at most a small shift of its accepted value across the range of extracellular acetate (Figure 2.10d).

The drop in internal pH could be costly, e.g., by affecting enzymatic activities (including ribosomal activity) which have limited pH ranges (see Figure 2.10e and (*125*, *126*)). To have an independent estimate of the effect of a reduced internal pH, we grew cells in glucose medium at normal pH in the absence of acetate, with the supplement of varying amounts of an uncoupler, Carbonyl cyanide m-chlorophenyl hydrazone (CCCP), which is known to reduce the internal pH (*127*). Indeed, growth decreased along with internal pH for increasing dose of CCCP (Figure 2.10f). However, growth reduction due to CCCP was about half of that due to acetate stress at the same internal pH (Figure 2.2d). Thus, the drop of internal pH alone cannot account for the observed acetate toxicity.

2.6 Acetate stressed metabolome

We next turn to the direct effect of acetate accumulation and the associated potassium ions. Despite the reduction of internal pH, the internal acetate concentration (Figure 2.2b) well exceeded the concentrations reached by typical cellular metabolites, which in total sum to a few hundred mM (*128*). As reported previously (*53*), potassium acetate accumulation was shown to decrease the level of glutamate, consistent with the notion of acetate excluding glutamate. We then looked into what happens to the abundances of other metabolites.

We quantified the relative abundances of 119 metabolites, for acetate-stressed cells and carbon-limited cells across a range of growth rates using LC-MS (*63*, *128*) (see Table 2.6 and 2.10.4). The relative abundances of most detected metabolites decreased under acetate stress (Figure 2.3a). Based on the measurements of (*63*) (2.10.4), we quantified the absolute concentrations of 72 metabolites. Summing over all the quantified pools, we found that the total concentration of these metabolites (brown stars in Figure 2.3b, including the neutralizing potassium ions associated with the large amounts of glutamate and aspartate, but not including potassium acetate), referred to collectively as “summed measured metabolite”, decreased

significantly as potassium acetate accumulated (red squares in Figure 2.3b), dropping over ~250 mM over the range where potassium acetate increased by ~250 mM. Comparing the sum of the measured metabolites to that in carbon-limited cells (blue stars in Figure 2.3c,Table 2.6,Table 2.7) which have similar water content (Figure 2.9f), the drop of metabolites in acetate-stressed cells (brown stars) is conspicuous.

The global reduction in many key metabolites under acetate stress can be rationalized by the hypothesis that the total internal metabolite concentration is fixed, e.g., to balance external osmolarity which is at 300-400 mOsm in our experiments. Consequently, when the cytoplasm is forced to accommodate large amounts of potassium acetate, a "useless metabolite" for *E. coli* from the metabolic perspective, the concentrations of normal metabolites must decrease. This decrease would provide a possible cause for growth defect under acetate stress: because many metabolite concentrations are poised near the K_m of their respective enzymes in unstressed growth conditions (*128*), a reduction of normal metabolite pools under acetate stress would reduce the metabolic flux catalyzed by these enzymes and thereby slow down growth. This mechanism of growth reduction could readily account for suggestion of biosynthesis defects found in the proteome analysis (Figure 2.7**,** Figure 2.8).

To test this "useless metabolite" hypothesis directly, we constructed strains to accumulate three distinct metabolites, trehalose, lactose, and arabinose, respectively; see Figure 2.11a-c and 2.10.1. These molecules were chosen because of their relative inactivity; in particular, trehalose is a molecule accumulated to high concentrations in osmotic stress (*129*). We measured the internal lactose, arabinose, and trehalose content accumulated (2.10.3) and established that the accumulation of these metabolites can indeed be titrated across a broad range, with a concomitant decrease in the glutamate pool (Figure 2.11d-f). Moreover, the growth rate dropped as well, while

it changed little for a control where GFP is expressed by the same system (Figure 2.11g-i). We found the accompanying cytoplasmic water content to change little (Figure 2.9g), so that the intracellular content measured (nmol/OD/mL) converts directly to concentration (mM) as with acetate stress. Notably, growth inhibition due to the overdose of lactose (Table 2.5) resulted in the proteomic phenotype similar to that of acetate stress (Figure 2.7e,g).

The concentrations of summed measured metabolites for trehalose overdosed cells are shown as purple symbols in Figure 2.3d. As predicted by the "useless metabolite" hypothesis, the summed concentration decreased as trehalose, the useless metabolite, increased. Strikingly, the amount of decrease is similar between trehalose overdose and acetate-stress (Figure 2.3d brown symbols). We also measured glutamate for the lactose and arabinose overdoses and found that, similarly to trehalose overdose and acetate stress, the concentration of glutamate decreased as lactose or arabinose accumulated, in similar ways to the effect of trehalose and potassium acetate (Figure 2.3e). Thus, regardless of the identity of the useless metabolite, its accumulation quantitatively dictates the decrease of internal metabolites, in accordance with the useless metabolite hypothesis.

We next made similar plot for growth rate against the useless metabolites (Figure 2.3f). A striking linear decrease of growth rate (λ) is obtained in each case, of the form

$$\lambda = \lambda_0 \cdot \left(1 - \frac{m}{m_c}\right) \qquad \textit{Eq. 2.3}$$

where m is the internal concentration of the useless metabolite, m_c is the inhibitory concentration where growth rate is extrapolated to vanish, and λ_0 is the stress-free growth rate. The inhibitory concentrations are surprisingly different for the different substances: accumulation of lactose led to 2x steeper reduction in growth compared to trehalose even though both are neutral disaccharides while the accumulation of arabinose led to a growth rate reduction in between the other two. Since

the effect of these useless metabolites on the internal metabolites are similar (Figure 2.3e), the results indicate that growth reduction by useless metabolites is not a sole consequence of their reduction of the normal metabolite pools. It is known that for metabolites accumulated to such high concentrations (100 mM of disaccharides correspond to ~3.4% w/v), general properties of the cytoplasm may be affected, including, e.g., the solvation and hence the activity of proteins (*130*). Trehalose and potassium acetate could be metabolites that the proteome of *E. coli* is well-adapted to, as an osmolyte for trehalose (*129*), and due to frequent exposure in the gut environment for acetate and other SCFAs (*23*). The proteome may be less adapted to lactose or arabinose as high internal concentration of lactose or arabinose is not commonly encountered, thus resulting in lower inhibitory concentration.

The fact that acetate accumulation resulted in linear growth reduction similar to the accumulation of trehalose, arabinose, and lactose (Figure 2.3f) is surprising given the change in internal pH and the growth reduction due to internal pH alone (Figure 2.2c,d). Indeed, if there is no cost to reducing the internal pH, then cells can simply set the internal pH to the same value as the external pH and thereby eliminate potassium acetate accumulation; see Eq. 2.2. Here, we hypothesize that *E. coli* actively reduces its internal pH in order to reduce potassium acetate accumulation despite the cost of reduced internal pH itself, and the observed growth defect is a result of a tradeoff between reducing potassium acetate accumulation and maintaining the internal pH (Figure 2.5a).

2.6.1 Metabolites that increase in acetate stress

While most metabolites decrease in abundance due to acetate stress, a small number of metabolites increase due to acetate stress. The metabolites that increase in acetate stress come in a few different categories (Figure 2.4). Of the metabolites that increase in concentration with acetate

stress, 46% of them are either acetylated compounds or compounds synthesized from pyruvate. Other than the few amino acids that can be used for protein synthesis, these metabolites are unlikely to be that useful and are more likely to be a side effect of the high acetate availability. The metabolites that could be useful, such as pyruvate, can't be effectively used because there are still bottlenecks elsewhere in metabolism. Other categories include metabolites in nucleotide synthesis, metabolites synthesized from glutamate, or metabolites related to methionine metabolism. We've presented the exact metabolites in a table.

Because replication of the cell requires a somewhat specific recipe of nucleotides, amino acids, lipids etc., the lack of any one of these necessary metabolites can halt growth. In that sense, even metabolites involved in central carbon metabolism such as pyruvate can't help with growth because that resource isn't allocated to where other bottlenecks are.

2.7 Combined effects of acetate and pH

We developed a mathematical model incorporating the deleterious effect of accumulating potassium acetate as a useless metabolite, described by Eq. 2.3 (with m being the internal potassium acetate concentration), and with potassium acetate accumulation affected by the internal pH via Eq. 2.1. The deleterious effect of internal pH, $\mathrm{pH_{int}}$, alone on growth (Figure 2.2d) is modeled by a parabolic dependence,

$$\lambda = \lambda_0 \cdot \left(1 - \left(\frac{\mathrm{pH_{max}} - \mathrm{pH_{int}}}{\mathrm{pH_{max}} - \mathrm{pH_{min}}}\right)^2\right) \qquad \textit{Eq. 2.4}$$

with the maximum set to $\mathrm{pH_{max}} = 7.78$, and minimum at $\mathrm{pH_{min}} = 6.42$, obtained as best-fit to data (Figure 2.12a).

The joint effect of potassium acetate accumulation and internal pH reduction is assumed to be a product of the individual effects described by Eq. 2.3 and Eq. 2.4 with the internal metabolite concentration m in Eq. 2.3 being potassium acetate, set as $2 \times [Ac^-]_{int}$, the latter given by Eq. 2.2

through the acetic acid concentration set by the external environment. The internal pH is controlled by the cell through proton import and export. The inhibitory concentration m_c for potassium acetate as a useless metabolite is the lone unknown model parameter.

As described in B.14.8B.1, this model can be solved analytically. The model predicts that for a substantial range of acetate stress, the growth rate and internal potassium acetate concentration are approximately linearly related, with an apparent inhibitory concentration,

$$m_c' \sim m_c/(\mathrm{pH_{max}} - \mathrm{pH_{min}}) \qquad \textit{Eq. 2.5}$$

when the growth rate under acetate stress is extrapolated to zero. A one-parameter fit of the model to the acetate/growth-rate data fixed the inhibitory concentration to $m_c' \approx 400\ mM$ for potassium acetate. With this parameter, the model quantitatively captured the relationship between potassium acetate, pH, and growth rate, as shown in Figure 2.12b-d. Figure 2.5b shows the comparison of the predicted growth-rate dependence on acetic acid concentration, with the dashed line indicating the expected growth defect if internal pH was not reduced. Further, Figure 2.5c shows for a number of acetic acid concentrations (different colors) what the growth rate would have been if internal pH were fixed at various levels (x-axis). Strikingly, the observed data lie closely to the growth rate maximum at each acetic acid level (circles of corresponding colors), self-consistently justifying the optimality assumption. To further test the model, we applied a "double stress", by varying the amounts of CCCP to cells growing in glucose at different fixed acetic acid concentrations. Figure 2.5d shows that the growth rate quantitatively followed the parabolic trajectories as predicted by the model, without invoking any new parameters. Together, these data establish that *E. coli* cells indeed set the internal pH to optimize the tradeoff between acetate accumulation and pH reduction.

2.8 Discussion

E. coli's strategy to partially lower its internal pH to mitigate acetate stress can be readily generalized to describe bacterial response to other weak acids (Figure 2.1d), whose intracellular concentrations are determined by the internal pH via Eq. 2.2 just like acetate. Our work indicates that the inhibitory effect of these acids is determined by a compromise of two deleterious factors, the inhibitory concentration (m_c) of the useless metabolite(s), and the minimal internal pH ($\mathrm{pH}_{\mathrm{min}}$) the cell can tolerate, as represented by the apparent inhibitory concentration given in Eq. 2.5. More detailed calculation for the half-inhibitory acetic acid concentration (Figure 2.12e,f and 4.8B.1) predicts additional weak dependence on the value of the normal pH ($\mathrm{pH}_{\mathrm{max}}$). The toxicity of different acids presumably arises from their different disruptive effects (e.g., the afore-mentioned solvent effect) as useless metabolites, with *E. coli* adapting better to the SCFAs commonly encountered in the gut compared to, say, benzoic acid, analogous to the difference between trehalose, arabinose, and lactose (Figure 2.3f).

It is noteworthy that the cellular factors determining the weak acid toxicity (m_c, $\mathrm{pH}_{\mathrm{min}}$, and $\mathrm{pH}_{\mathrm{max}}$) are *global*, in the sense that they are determined by properties of numerous cytosolic proteins and cannot be easily modified. This unique feature of the weak acid stress possibly underlies why the RpoS regulon offered no noticeable protection (Figure 2.6d). It suggests that adaptation to weak acid stress may require global modifications, e.g., lowering the minimal internal pH, which may in turn be costly to cells grown in neutral pH. This fundamental tradeoff likely underlies the basic operating strategies of the major gut microbes, exemplified e.g., by *Bacteroidetes*, which grow fast in normal pH but is sensitive to low pH, and *Firmicutes*, which grow slower in normal pH but has improved tolerance at lower pH (*38*, *39*). Understanding these

tradeoffs will be instrumental to managing and manipulating these microbes in environments ranging from the gut to bioreactors where fermentation products dominate (*48*, *131–134*).

Cells regulate their pH with many different transporters (*135*). These transporters control pH by exchanging protons for other cations such as K^+ and Na^+ or anions such as Cl^-. The role of central metabolism has been rejected based on the relative constancy of cellular pH in different growth conditions (*136*) and a clear role for ions other than protons in experiments (*135*). However, the electron transport chain moves a very large flux of protons in and out of cells. In aerobic growth, most of the ATP generated in cells comes from protons being pumped out of cells from the electron transport chain and then pumped back in by ATPases to generate ATP. Additionally, if pH were to be regulated by uptake or excretion of ions other than protons, it's unclear how the regulation of those cations is done. If those cations are imported in coordination of protons, then their import is dependent on protons. The coordination is circular; something needs to bootstrap the process.

If we do consider the electron transport chain to be important for pH regulation, then there are a few important molecules that could be helping with the regulation. The electron transport chain is run by a constant supply of NADH and oxygen. And indeed it has been shown that cells grown anaerobically that are given pulses of oxygen then export protons in response to the pulse (*137*). There's also the role of proton pumping ATPases. In addition to protons, these enzymes bind ATP and ADP. As discussed in A.6, the phosphate groups of the metabolites have pK_as around 6.8 and therefore may not work as well at low pH. This pH sensitivity is potentially very useful for pH regulation. If proton export is not pH sensitive, but proton import is pH sensitive the system is self-regulating. When cells have a low internal pH, ATP generation won't be as effective. So, proton import slows temporarily, allowing the electron transport chain to pump out more

protons and raise the pH. This type of regulation system would also explain why NADH is used in the electron transport chain but not NADPH; the regulation would work if both sides were limited by pH sensitivity of phosphate.

Notably, alkaliphiles, which have evolved in environments where acid stress is rare, don't have proton-pumping electron transport chains; they pump sodium in and out for ATP generation. *B. theta* is one such organism that has a sodium coupled electron transport chain. The inability to reduce its pH like *E. coli* does due to its different electron transport chain may be why it is more sensitive to acetate stress than *E. coli*.

2.9 Figures

Figure 2.1 Effect of pH and SCFAs on bacterial growth.
Unless otherwise indicated, E. coli K-12 NCM3722 cells were grown exponentially in glucose minimal media, at various pH fixed by phosphate buffer. Cultures were grown in either test tubes or Tecan microplate reader; see 2.10.2. a) Phosphate- or GABA-based buffers (circles or triangles, respectively) were adjusted to obtain a range of medium pH; see 2.10.2. Blue, purple, red symbols represent cultures supplemented with different concentrations of sodium acetate (NaAc) added to the medium. b) For several fixed medium pH, the growth rate of the culture was determined for a range of added sodium acetate concentrations. Excretion of acetate during growth, on the order of 1-2 mM (Figure 2.6c), was negligible. ***c)*** *The data in panel b is replotted against the concentration of acetic acid [HAc] using Eq. 2.1. d) Growth in medium fixed to pH 6 and supplemented by various weak organic acids. Each acid was added as the sodium salt at the concentration indicated on the x-axis. e) Cultures were grown anaerobically in Hungate tubes with an atmosphere of 7% CO_2 and 93% N_2, with pH fixed to 6; see 2.10.2. Various amounts of sodium acetate were added to the medium as indicated by the x-axis. Because large amounts of SCFA (totaling ~15 mM, see Figure 2.6e) were excreted over the course of growth, growth rate was not well-defined for medium with <15 mM sodium acetate added. Results of aerobic growth (red symbols) are shown for comparison. f) Effect of pH and acetate on B. thetaiotaomicron (ATCC 29148), grown in phosphate-buffered medium set to indicated pH, supplemented with vitamin B_{12}, hemin, cysteine, and various concentrations of sodium acetate; see 2.10.2 and Table 2.1. (The difference in pH before and after growth was less than 0.15. The total amount of SCFA excreted was ~5 mM, much smaller than anaerobically grown E. coli due to the lack of formic acid excretion.) Anaerobic growth was performed in a microplate reader enclosed in a custom vinyl anaerobic chamber. Data is plotted against the acetic acid concentration, calculated by Eq. 2.1. Data in panels a, d, e, and f are binned for similar x-axis values, with the bins containing data from at least 3 experiments. Error bars are calculated from the standard deviation.*

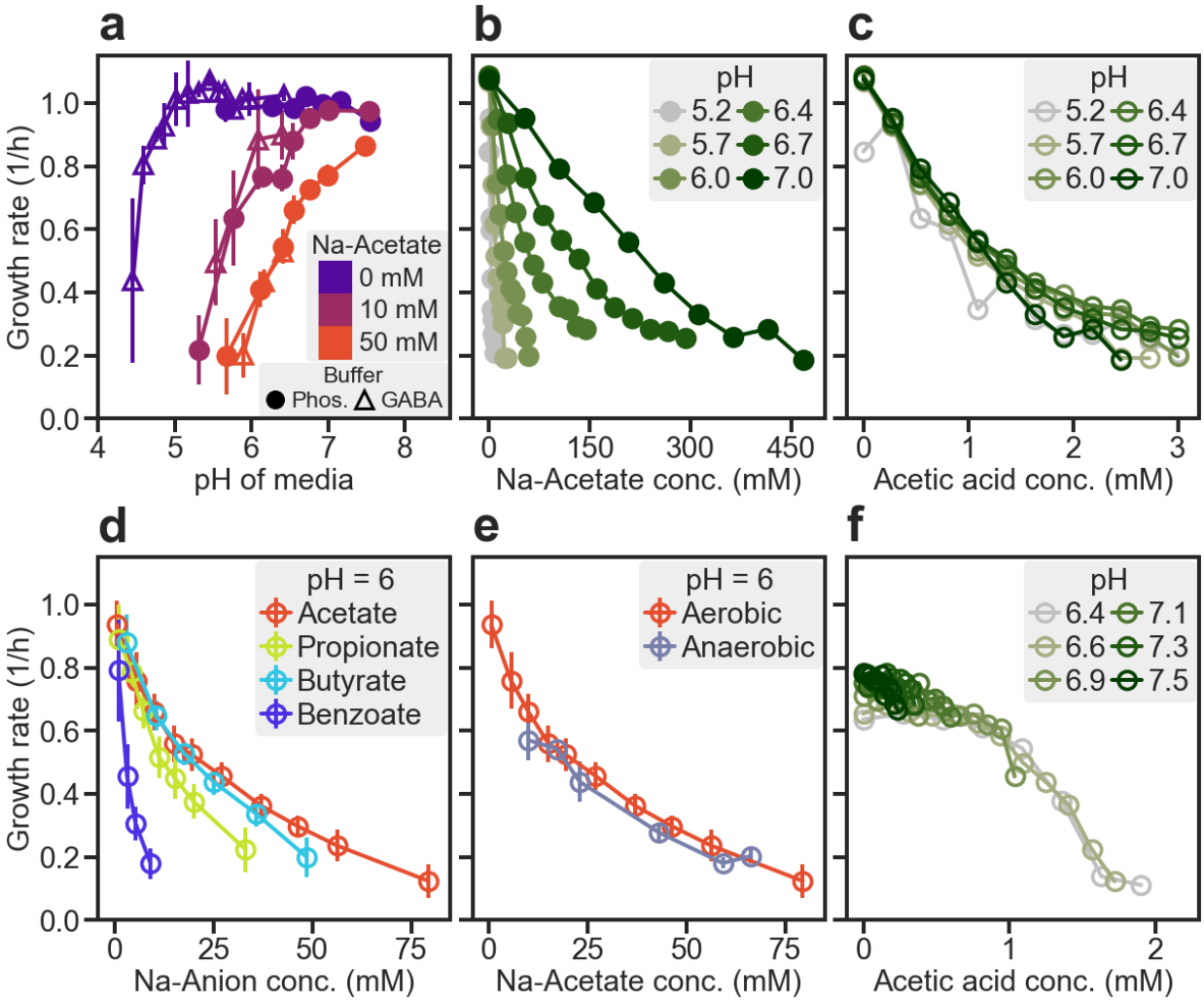
a
b
c
d
e
f
Growth rate (1/h)
pH of media
Na-Acetate
0 mM
10 mM
50 mM
Buffer
Phos.
GABA
Na-Acetate conc. (mM)
Acetic acid conc. (mM)
pH
5.2
5.7
6.0
6.4
6.7
7.0
Na-Anion conc. (mM)
pH = 6
Acetate
Propionate
Butyrate
Benzoate
Aerobic
Anaerobic
6.4
6.6
6.9
7.1
7.3
7.5

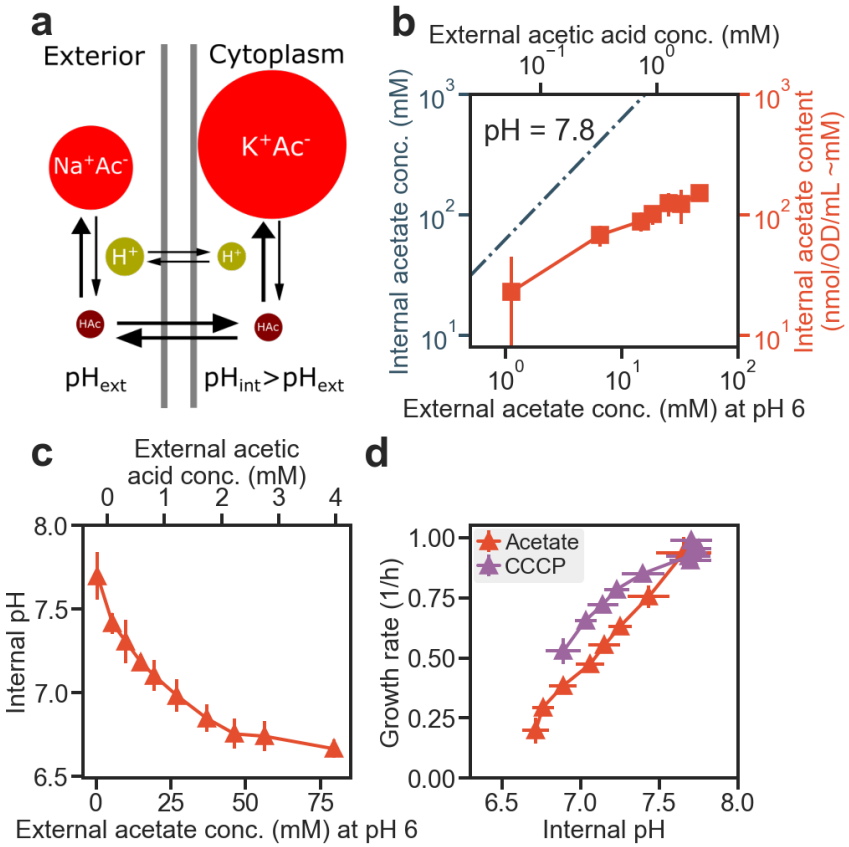

Figure 2.2 Internal acetate and internal pH in acetate stressed cells.
*a) Model of acetate equilibrium across the cell membrane. Acetate is in equilibrium with acetic acid on each side of the membrane according to Eq. 2.1. Acetic acid, due to its small size and lipophilicity, is membrane permeable. The cell controls its internal pH through transporters and the electron transport chain. A moderate difference between the internal and external pH results in a huge difference between the potassium-/sodium-acetate concentrations according to Eq. 2.2. Adapted from (*120*). b-c) Acetate stress was implemented by growing cells in phosphate buffered glucose medium (pH 6) supplemented with different concentrations of sodium acetate. b) Accumulation of internal acetate (right-axis) in NCM3722 cells was measured by rapidly filtering the culture and measuring the abundance of acetate using HPLC. The same procedure was performed with cell-free media to correct for acetate not contained in cells; see Figure 2.9a,b and 2.10.3 for details. The data is converted to internal acetate concentration (left y-axis) based on the measured water content (Figure 2.9e). The dashed line indicates the internal acetate concentrations calculated according to Eq. 2.2 for internal pH fixed at 7.8, external* $\mathrm{pH} = 6$*, and* $\Delta pK_a = 0$*. c) Internal pH was measured with the ratiometric reporter, pHluorin (*122*) for acetate stressed cells; see Figure 2.10a,b. The results here also agreed well with the classical biochemical measurement using radiolabeled acid (Figure 2.10c). d) The internal pH data in panel c is plotted against the growth rate of the culture (red triangles). Additionally, internal pH was measured for cultures of HE616 grown in varying amounts of CCCP (purple triangles) in the same phosphate buffer set to pH 6; see 2.10.2. Data in panels b and c are binned for similar x-axis values, and data in panel d is binned for similar y-axis values with the bins containing data from at least 3 experiments. Error bars are calculated from the standard deviation.*

Figure 2.3 Effect of useless metabolites.
*a) Fold changes in the 119 detected internal metabolites for cells grown with and without 20 mM acetate at pH 6. Metabolites were quantified by LC-MS following fast filtration (*128*). For the relative fold-change, a ^{13}C reference was mixed in with the collected samples; see 2.10.4. The metabolomic data are given in Table 2.6. b). For acetate stressed cells, sum of the abundances of 72 internal metabolites determined by LC-MS measurements, together with the neutralizing potassium ions for glutamate and aspartate but not including potassium acetate, are shown as brown stars (left y-axis). Data for the internal potassium acetate (red squares, right y-axis, taken to be twice of the measured internal acetate shown in Figure 2.2b. c) The sum of the measured metabolites under acetate stress (brown stars, same as in panel b) and under carbon-limited growth (blue stars), plotted against the respective growth rates. Carbon limitation was implemented by titrating glucose uptake (*27*) for cells grown in glucose minimal media (see 2.10.2, with data provided in Table 2.7). The cellular water content under these conditions are similar (Figure 2.9e,f). d) Sum of the abundances of all metabolites determined by metabolomics for trehalose overdose (purple stars, again including the neutralizing potassium ions for glutamate and aspartate) is plotted against the total trehalose content for strains HE647/HE650 (Figure 2.11**)**. The data are provided in Table 2.8. The data for acetate stress (brown stars) is the same as that shown in panel b and c but plotted here against potassium acetate (red squares in panel b). e) Effect of useless metabolites on internal glutamate, due to acetate stress (red diamonds), trehalose overdose (purple diamonds), lactose overdose (teal diamonds), and arabinose overdose (orange diamonds), in strains NCM3722, HE647/HE650, HE620, and HE639, respectively; see Figure 2.11 and Table 2.1 for description. Useless metabolites on x-axis are the measured amounts of potassium acetate, lactose, and trehalose accumulated in the respective strains. The measured acetate amount is multiplied by two to include the additional increase of potassium cations needed to neutralize the acetate anions (see Figure 2.9d). f) Same as panel e but showing the corresponding growth rates. All growth was performed in phosphate-buffered media at pH 6. Data in panels a, e and f are binned for similar x-axis values with the bins containing data from at least 3 experiments. Data in panels c and d are grouped according to the same applied stress level. Error bars are calculated from the standard deviation.*

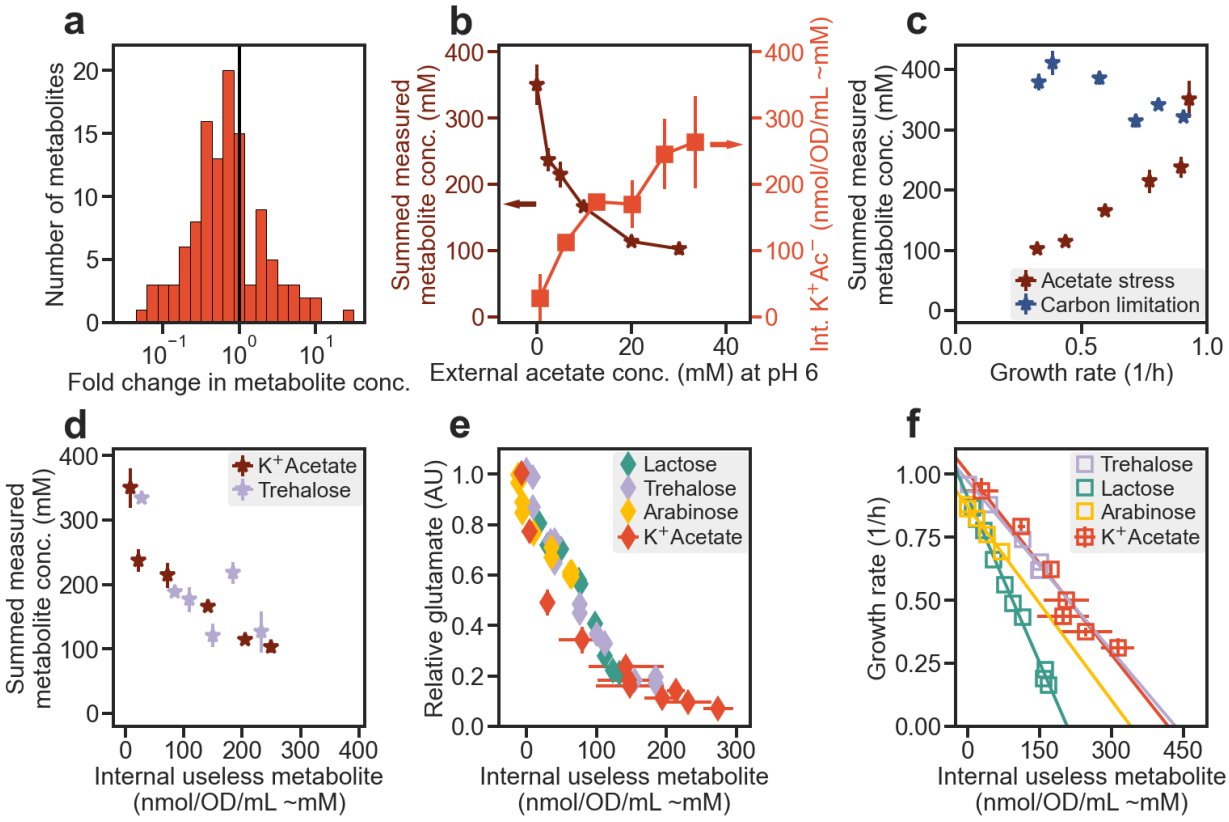
a
Number of metabolites
Fold change in metabolite conc.
b
Summed measured metabolite conc. (mM)
Int. K+Ac− (nmol/OD/mL ~mM)
External acetate conc. (mM) at pH 6
c
Summed measured metabolite conc. (mM)
Growth rate (1/h)
Acetate stress
Carbon limitation
d
Summed measured metabolite conc. (mM)
K+Acetate
Trehalose
Internal useless metabolite (nmol/OD/mL ~mM)
e
Relative glutamate (AU)
Lactose
Trehalose
Arabinose
K+Acetate
Internal useless metabolite (nmol/OD/mL ~mM)
f
Growth rate (1/h)
Trehalose
Lactose
Arabinose
K+Acetate
Internal useless metabolite (nmol/OD/mL ~mM)

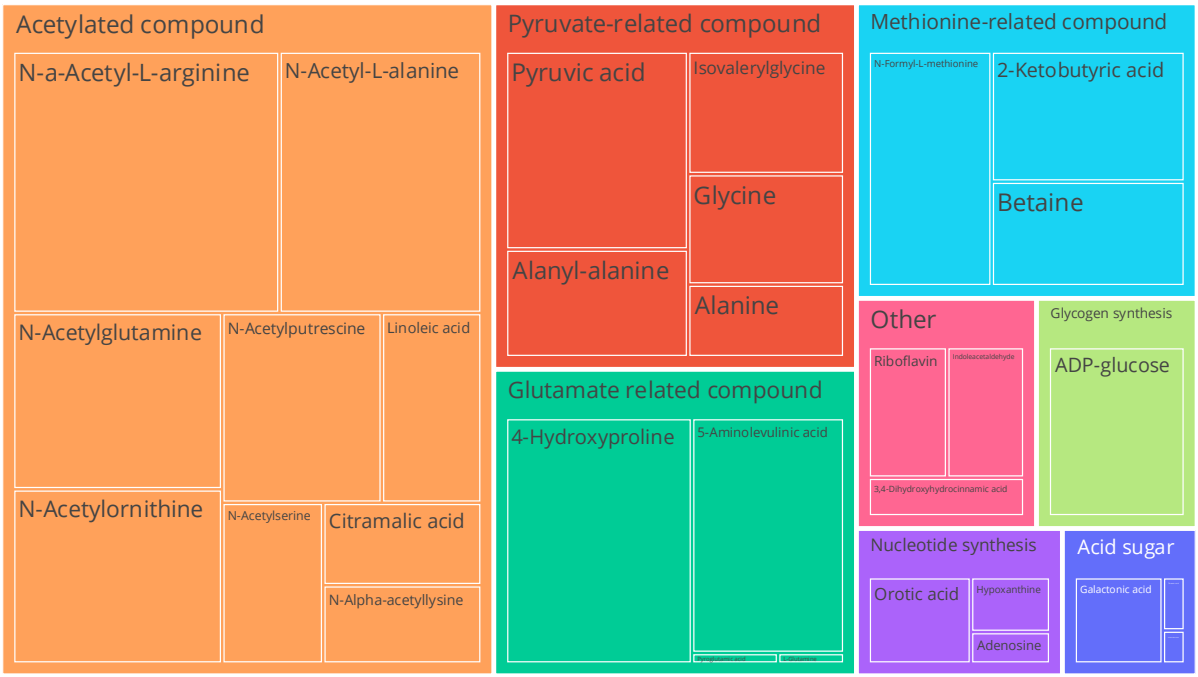

Figure 2.4 Identity of compounds that increase in acetate stress.
Treemap of metabolites that increase due to acetate stress. Metabolites are grouped by metabolic relationships. Size of boxes are proportional to the log of the fold change of metabolites for cells in high acetate compared to those in low acetate.

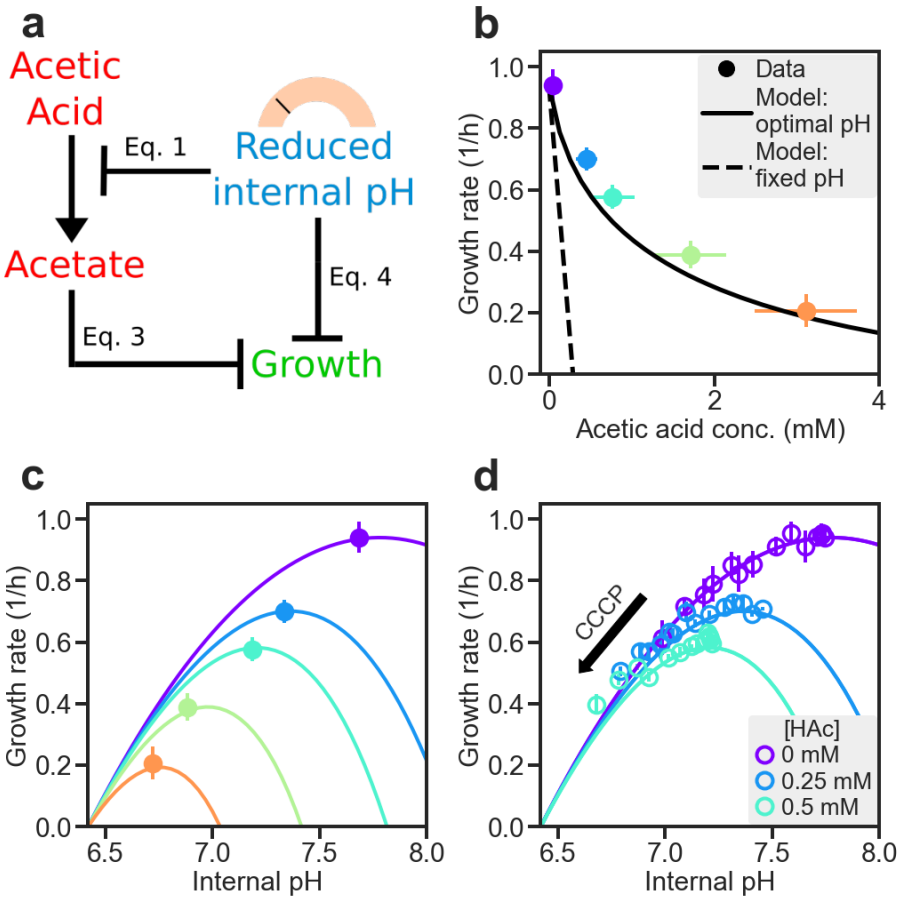

Figure 2.5 Model of acetate-pH tradeoff.
a) Schematic of the acetate-pH tradeoff model. b) The model output (solid line) quantitatively captures the effect of growth reduction by acetic acid (colored circles) with no adjustable parameter; see Figure 2.12 and 4.8B.1 for details. Dashed line shows the expected growth rate if internal pH is fixed at unstressed value of 7.78. c) Circles show the measured growth rate and internal pH for cultures in media with various acetic acid concentrations (same as Figure 2.2c). Color indicates the acetic acid concentrations shown in panel b. Solid lines show the expected growth rate if the internal pH is set to the values indicated by the x-axis. d) The lines and the filled circles are the same as those shown in panel c. Open circles are the results of experiments with combined acetate and CCCP stresses. HE616 cells harboring pHluorin were grown in glucose media buffered to pH 6, with various concentrations of sodium acetate (indicated by the colors), each with a range of CCCP concentrations to perturb the internal pH.

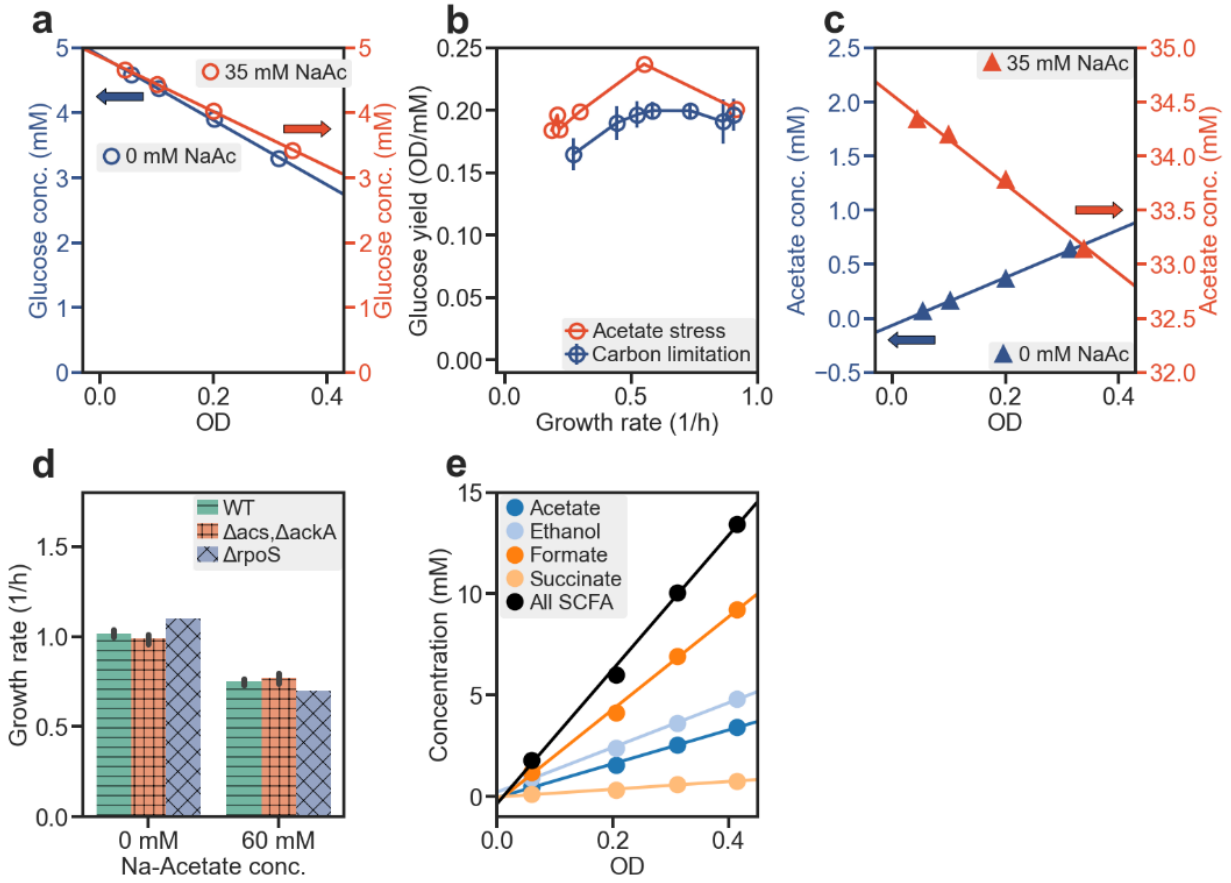

Figure 2.6 Carbon utilization in acetate stress.
a) E. coli K-12 NCM3722 cells were grown in glucose minimal medium with and without 35 mM sodium acetate (NaAc, red and blue symbols, respectively). pH was set to 6.0 using phosphate buffer. During exponential growth, samples were taken at various OD and glucose concentrations in the medium were determined using HPLC (see 2.10.3). Slope of the best-fit lines of the remaining concentrations vs OD give the glucose yields. b) Measurements described in panel a were repeated for different amounts of sodium acetate (red symbols). Blue symbols indicate control with carbon limited growth (with no acid) obtained from a titratable glucose uptake strain (27); see 2.10.3. For each data point shown, slope of the plot of glucose concentration vs OD, s, was first calculated as in panel a. Yield on glucose, obtained as $Y = -\frac{1}{s}$*, is plotted against the growth rate of the culture. c) Measurements of acetate excretion in medium with no acetate added (blue triangles, left axis), and acetate uptake (red triangles, right axis) in medium with 35 mM sodium acetate added at the beginning of the growth. Cell growth was performed in the same way as panel a (see 2.10.3). d) The effect of mutations on acetate tolerance. Two different strains derived from E. coli NCM3722 were grown (Table 2.1): Δacs-ΔackA (NQ1028, light orange), ΔrpoS (NQ1191, light purple). Cells were grown in phosphate buffered media with pH set to 6.7 without or with 60 mM sodium acetate. e) Measurements of various SCFA concentrations for cells growing anaerobically in glucose minimal media. Cultures were grown in Hungate tubes with an atmosphere of 7%* CO_2 *and 93%* N_2*, with pH set to 7; see 2.10.2. Media samples for HPLC analysis were collected at the indicated* OD_{600} *with a syringe inserted into the rubber stopper sealing the Hungate tube (see 2.10.3).*

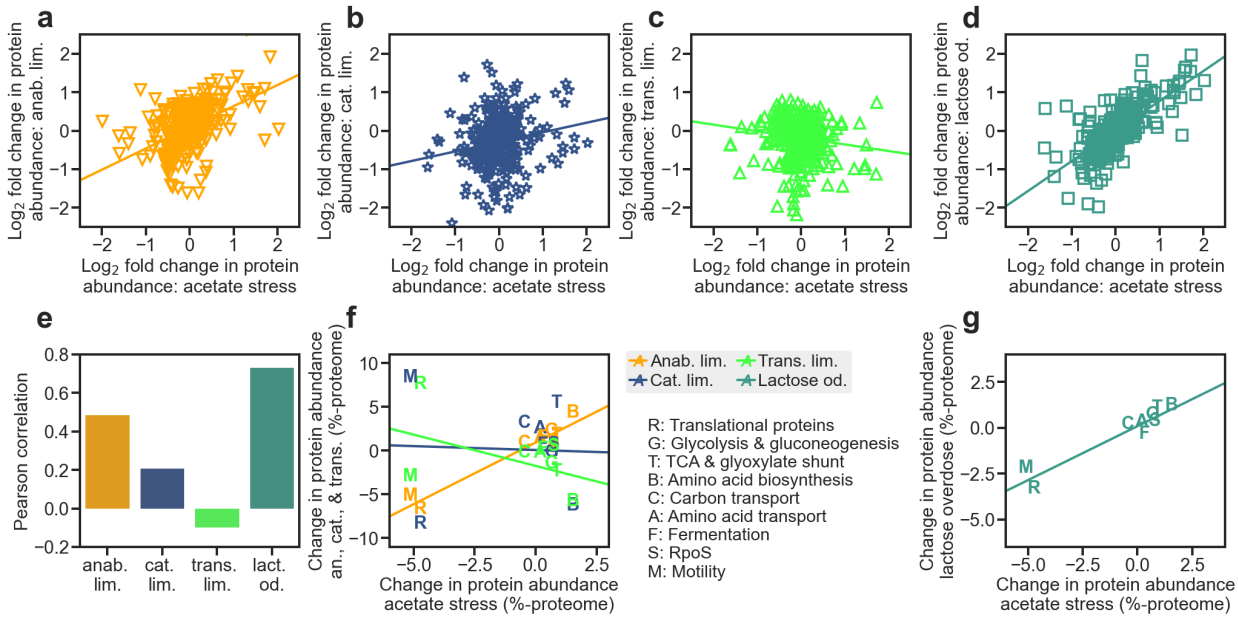

Figure 2.7 Proteome of acetate stressed cells.
a-d) show scatter plots of fold-change in the abundance of each detected proteins between reference condition (glucose minimal medium, growth rate = 0.9/h), and a condition or strain of reduced growth at ~0.4/h. x-axis: growth reduction due to acetate stress (30 mM sodium acetate at pH 6 in phosphate buffered medium); y-axis: growth reduction due to anabolic limitation (panel a), carbon limitation (panel b), translational inhibition (panel c), lactose overdose (panel d). The proteome data for anabolic limitation, carbon limitation, and translational inhibition were obtained from (58). The proteomic data for acetate stress were generated for NCM3722 cells grown in phosphate buffered glucose medium (pH 6) supplemented with 30 mM sodium acetate; the data are shown in Table 2.3. The proteomic data for lactose overdose (Figure 2.8,Figure 2.11) were generated for HE620 cells grown in 25 ng/mL cTc with 750μM lactose added to the media; the data are shown in Table 2.5. See 2.10.6. e) Pearson correlation coefficient between the fold-changes in protein abundance due to acetate stress and due to anabolic limitation (orange), catabolic limitation (blue), translational inhibition (green), and to lactose overdose (teal) shown in panels a-d. f) Scatter plots of the changes in the total abundances of proteins in each of the functional classes, between acetate stress and anabolic limitation (orange), carbon limitation (blue), and translational inhibition (green). The functional classes are as described by the legend, e.g. "R" for translational proteins. The membership of proteins belonging to each class is based on (12) and are listed in Table 2.3. The total abundances of detected proteins in each class under different growth limitations are shown in Figure 2.8 and Table 2.3,Table 2.5.

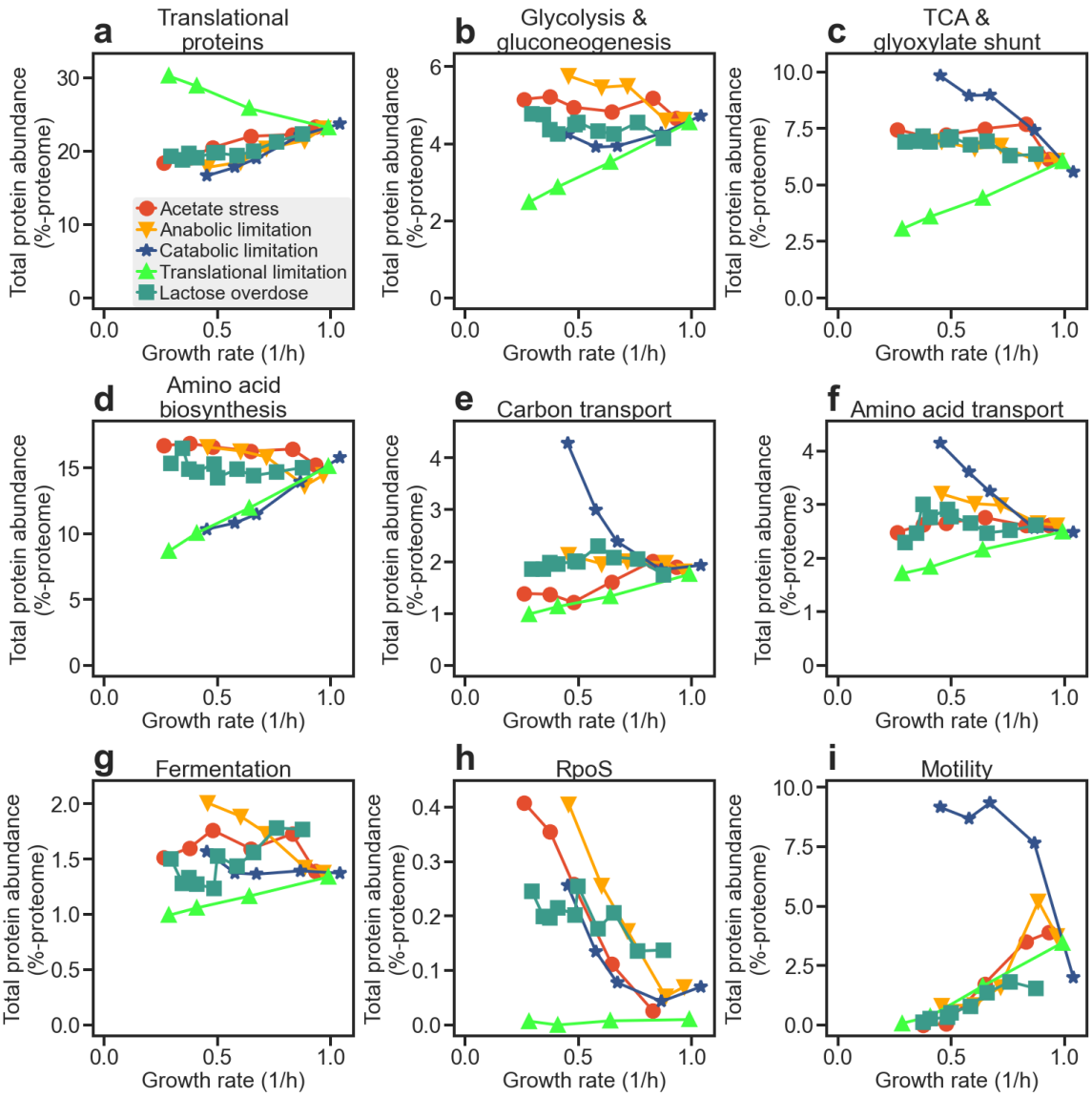

Figure 2.8 Functional grouping of proteome for acetate stressed cells.
*a-i) The proteome data shown in Figure 2.7a-d are grouped into a number of functional classes; see Table 2.3 and (*12*). The total abundance of proteins in each class, measured as the fraction of total protein mass, is plotted against the growth rate for each type of growth limitation: acetate stress (red circles), carbon limitation (blue stars), anabolic limitation (orange down-triangle), translational inhibition (green up-triangles), lactose overdose (teal squares). The proteome data for anabolic limitation, carbon limitation, and translational inhibition were obtained from (*58*). The proteomic data for acetate stress were generated for NCM3722 cells grown in phosphate buffered glucose medium (pH 6) supplemented with different concentrations of sodium acetate; the data are shown in Table 2.3. The proteomic data for lactose overdose were generated for HE620 cells grown in 25 ng/mL cTc with various concentrations of lactose added to the media; the data are shown in Table 2.5. See 2.10.6.*

Figure 2.9 Internal acetate and water content measurements.
*a) Schematic of internal acetate measurement. Cells grown in test tubes were quickly centrifuged and filtered (< 30 sec) from steady state growing cultures to separate cells from the supernatant. Supernatant-free cells were then resuspended in distilled water and lysed with chloroform. The aqueous section was collected for analysis with HPLC. To correct for the acetate left on the filter from the residual media, the same procedure was performed again with the cell-free filtrate. b) Internal acetate: subtraction of media component. Cells and cell-free filtrate were collected as described in panel a. Reported in this panel are examples for cells grown with 0 and 30 mM sodium acetate added to the media. Acetate amount measured from the filtered cells are shown as green bars with horizontal lines, and those from the filtered media are shown as orange bars with dots. The internal acetate amount is obtained from the difference of the two and shown as purple bars with crossed lines. The acetate abundance (in unit nmol/OD/ml) was obtained by normalizing by the amount of cells (in OD·mL) added to the filter. d) RNA content (2.10.3) of acetate stressed cells grown in phosphate buffered glucose minimal media at pH 6. c) To check for charge neutrality, the cellular potassium content was measured using ICP-MS (See 2.10.3); change in the total potassium content is plotted against the external acetate concentration as solid blue symbols. Although the increase in total potassium filled blue symbols) was below the increase in internal acetate (red squares), additional potassium would be released as free ions due to the decrease in RNA content (panel d), because potassium is one of the main positive counter ion neutralizing the negatively charge phosphate backbone of RNA. The open blue symbols show the total increase in the free potassium ion pool assuming that the reduction of each nucleotide residue in RNA leads to the addition of one free potassium ion. Our data suggests neutralization of acetate involves 0.5 potassium per nucleotide of the ribosome, consistent with the measured ratio of phosphate to magnesium, the other major counter ion stabilizing the ribosome e) Cytoplasmic water measurement in acetate stressed cells. Acetate stressed NCM3722 cells were grown in MES-buffered media at pH 6.3. Cytoplasmic water content was measured with radiolabeled ^{3}H-water and ^{14}C-sucrose (*138*), after they were added to steady state cultures and allowed to incubate for a brief period. The radioactivity of the two isotopes was measured from cells collected by centrifugation. Cytoplasmic water volume was calculated from the difference between estimated sucrose (extracellular + periplasmic) and water (extracellular + periplasmic + cytoplasmic). The same method was used to quantify the water content in panels f and g. f) Cytoplasmic water content for NCM3722 cells grown in MOPS minimal medium (pH 7.4) with various carbon sources. g) Cytoplasmic water content for cells accumulating internal trehalose; see Figure 2.11a.*

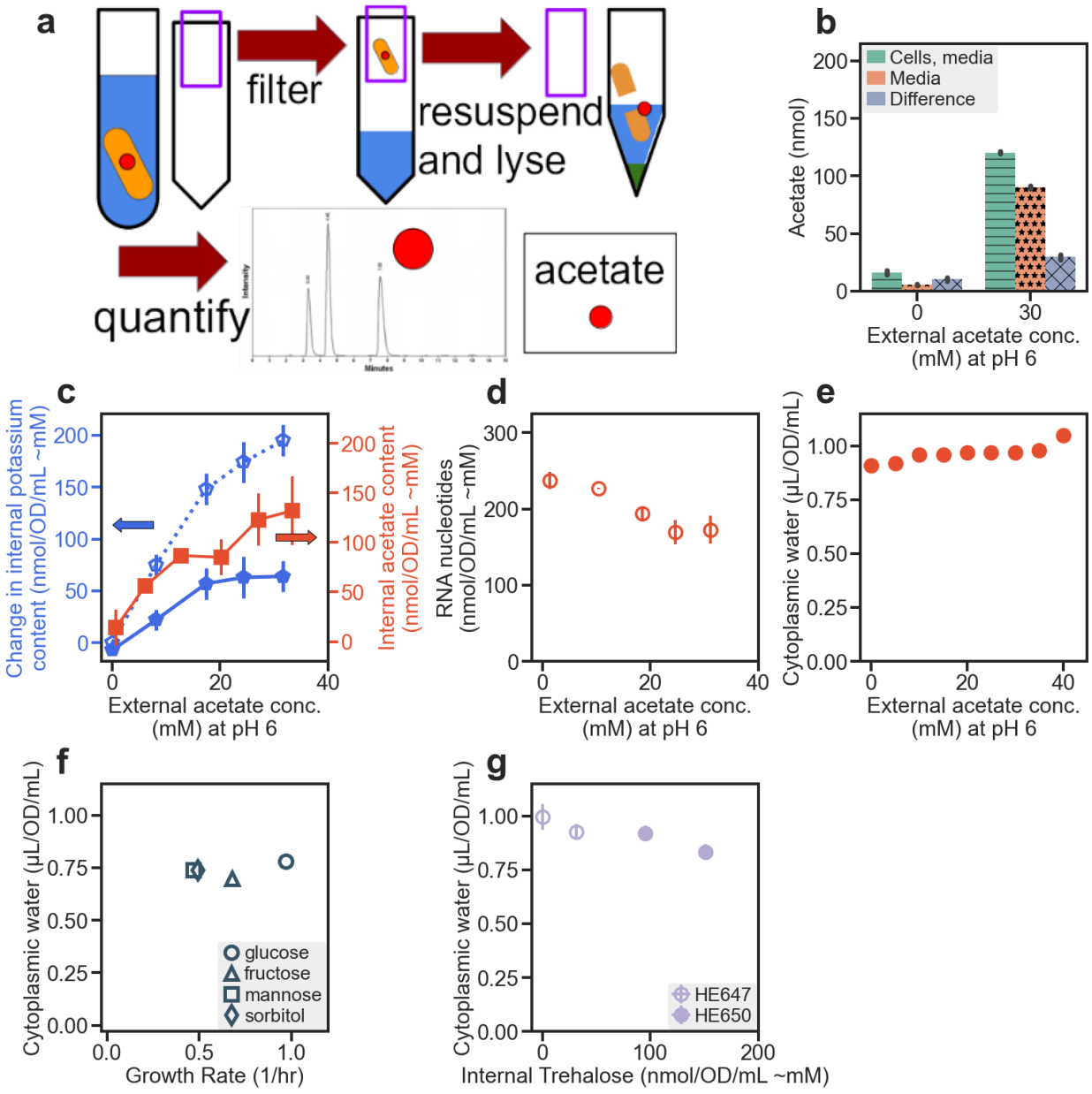
a
filter
resuspend
and lyse
quantify
acetate
b
Cells, media
Media
Difference
Acetate (nmol)
External acetate conc.
(mM) at pH 6
c
Change in internal potassium
content (nmol/OD/mL ~mM)
Internal acetate content
(nmol/OD/mL ~mM)
External acetate conc.
(mM) at pH 6
d
RNA nucleotides
(nmol/OD/mL ~mM)
External acetate conc.
(mM) at pH 6
e
Cytoplasmic water (µL/OD/mL)
External acetate conc.
(mM) at pH 6
f
Cytoplasmic water (µL/OD/mL)
glucose
fructose
mannose
sorbitol
Growth Rate (1/hr)
g
Cytoplasmic water (µL/OD/mL)
HE647
HE650
Internal Trehalose (nmol/OD/mL ~mM)

Figure 2.10 Measurement of internal pH.
*a) Fluorescence measurements were taken for exponentially growing HE616 cells harboring constitutive expression of ratiometric pHluorin (*122*) in the OD range of 0.01 and 0.2 using a Tecan Spark microplate reader. The fluorescent signals were collected for two excitation wavelengths: 390nm (y axis) and 470nm (x axis). Shown in the plot are data for two growth conditions, indicated by orange stars and grey circles (0 and 30mM sodium acetate, respectively, at pH 6 in phosphate buffered glucose media.) For each growth condition, a linear fit was made from the two signals to calculate the fluorescence ratio. This fluorescence ratio was then used to calculate the internal pH from the standard curve. b) Ratiometric pHluorin standard curve. HE616 cells grown as described in panel a were resuspended in carbon-free phosphate-buffered media fixed to a variety of pH. 10 μM CCCP was added to equilibrate the internal and external pH. For each pH, fluorescence ratio (390nm/470nm) was obtained as described in panel a for cells diluted to different densities. (The fluorescence signals settle down 15 min after CCCP addition, and the value of ratio reported here was taken an hour after CCCP addition.) c) Comparison of two internal pH measurement methods: by radiolabeled benzoic acid (black open circles – NCM3722) and by fluorescence with pHluorin (red triangles - HE616). Acetate stressed cells were grown in either MES-buffered media (radiolabeled method) at pH 6.2 or phosphate-buffered media (fluorescence method) at pH 6. Acetic acid concentration was calculated from the Henderson-Hasselbalch equation assuming a pKa of 4.77 in the medium. Internal pH for the radiolabeled method was found by measuring the fraction of radiolabeled ^{14}C-benzoic acid taken up by exponentially growing cells (*123, 124*). Data for the fluorescence method is taken from Figure 2.2c for comparison. d) For cells grown with varying concentrations of sodium acetate as shown in Figure 2.2b, we define the intercellular pK_a by the Henderson-Hasselbalch equation,* with $pK_{a,int} \equiv pH_{int} + log_{10}\left(\frac{[HAc]}{[Ac^-]_{int}}\right)$*, using the measured internal acetate concentration (Figure 2.2b) and the measured internal pH (Figure 2.2***c***). To bridge between data collected from separate experiments, internal pH and internal acetate concentrations were binned according to external acetate concentrations. Vertical lines represent the propagated standard deviation for the binned values. The average shift in the calculated* $pK_{a,int}$ *from the accepted value of 4.77 (dashed horizontal line) was noted as a small difference in the predicted and observed acetate concentration in (*139*). e) Distribution of optimal pH for 664 enzymes in BRENDA database (*140*). f) Growth rate and internal pH of HE616 cells grown in glucose medium and no acetate, with various supplement of CCCP. pH of the medium was fixed to 6.0 by phosphate buffer. Same results were obtained for medium pH fixed to 7.0. g) Growth rate vs internal pH for HE647 and HE650 cells growing in phosphate buffered glucose medium with various levels of trehalose accumulation; see Figure 2.11a. h) Internal glutamate concentration measured in CCCP limited cells. Cells grown in phosphate buffered media at pH 6 with varied concentrations of CCCP to reduce growth rate. Samples were collected with the no harvest protocol and glutamate content was measured with HPLC.*

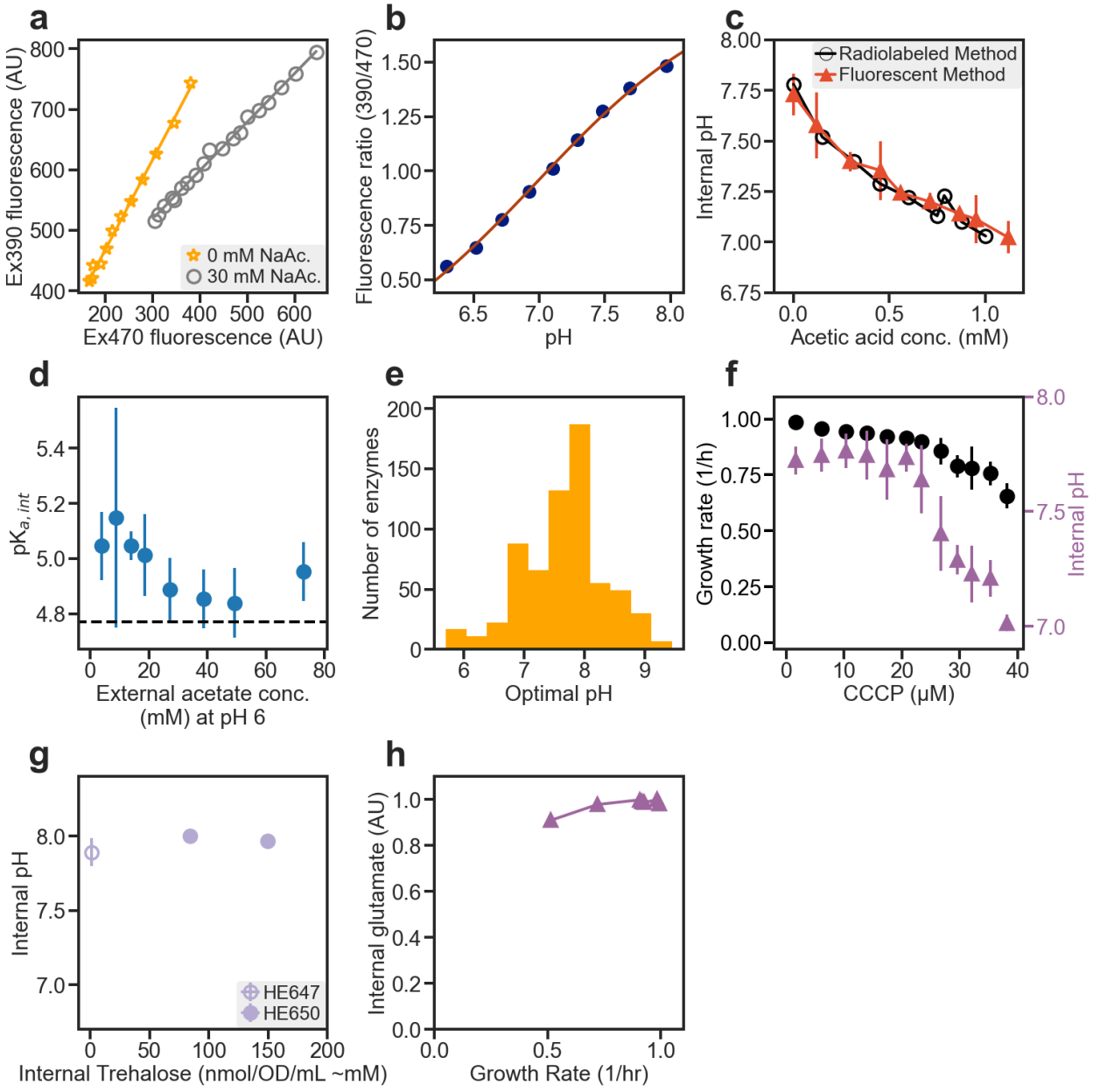
a
Ex390 fluorescence (AU)
Ex470 fluorescence (AU)
0 mM NaAc.
30 mM NaAc.
b
Fluorescence ratio (390/470)
pH
c
Radiolabeled Method
Fluorescent Method
Internal pH
Acetic acid conc. (mM)
d
pK$_{a,int}$
External acetate conc. (mM) at pH 6
e
Number of enzymes
Optimal pH
f
Growth rate (1/h)
Internal pH
CCCP (μM)
g
Internal pH
HE647
HE650
Internal Trehalose (nmol/OD/mL ~mM)
h
Internal glutamate (AU)
Growth Rate (1/hr)

Figure 2.11 Overdose of useless metabolites.
*a) Schematic of the construct for the titratable accumulation of internal trehalose. Strains HE647 and HE650 were constructed to have titratable expression of the otsBA operon, which encodes trehalose-6-phosphate synthase and trehalose-6-phosphate phosphatase (*141*) driven by the P_{Ltet} promoter (*142*). P_{Ltet} was controlled by TetR expression, which was provided by 3 copies of tetR driven by P_{Ltet} on the chromosome. The two strains differ in that otsBA is either expressed from the chromosome (HE647) or from a plasmid pZA31 (HE650). This expression system is capable of driving protein output by over 100x in response to changes in the level of an inducer, chloro-tetracycline, added to the media (*14*). b) We similarly constructed strain HE620 which allows titratable accumulation of lactose: A plasmid harboring titratable expression of lacY (encoding the Lac Permease, LacY) by the P_{Ltet} promoter is transformed into cells containing one copy of tetR driven by P_{Ltet}, which are themselves derived from NCM3722 with a chromosomally inserted tetR driven by the P_{Ltet} promoter, but with additionally the deletion of chromosomal lacIZY. Since they lack LacZ, HE620 cells in media with lactose will import lactose but not degrade it, resulting in lactose accumulation. c) The arabinose overdose strain (HE639) was designed similarly to the lactose overdose strain. A plasmid harboring titratable expression of araE (encoding the Ara Permease, AraE) by the P_{Ltet} promotor is transformed into cells containing one copy of tetR driven by P_{Ltet}. Additionally, the araBAD and araC genes were removed from the chromosome to avoid arabinose metabolism. d) The accumulation of trehalose (light purple bars, left y-axis) in trehalose titration strains (HE647 and HE650) grown in glucose minimal medium fixed to pH 6, with various inducer (cTc) concentrations and no acetate. The internal glutamate pool in these cells as measured by HPLC are shown as dark purple bars (right y-axis). e) The accumulation of lactose (triangles, left y-axis) by the lactose titration strain HE620 grown in phosphate buffered glucose media with 25 ng/mL ctc to turn on LacY. The concentration of lactose supplemented in the medium is shown as the x-axis. The corresponding internal glutamate concentrations are shown as squares (right y-axis). f) The accumulation of arabinose (squares, left y-axis) by the arabinose titration strain HE639 grown in phosphate buffered glucose media. The concentration of arabinose supplement in the medium is shown as the x-axis. The corresponding internal glutamate concentrations are shown as triangles (right y-axis). g) Growth rates of the trehalose titration strains grown in conditions described in panel c are shown as the dark purple bars. The growth rates of the control strain HE828 (identical to HE650 except that otsBA is replaced by gfp) are shown as black bars. h) Growth rates of the lactose titration strain HE620 grown in conditions described in panel e are shown as circles. The growth rates of the control strain HE829 are shown as black circles. HE829 is constructed identically to HE620 except the lacY on the plasmid was replaced with gfp. i) Growth rates of the arabinose titration strain HE639 grown in conditions described in panel f are shown as circles. The growth rates of the control strain HE839 are shown as black circles. HE839 is constructed identically to HE639 except the araE on the plasmid was replaced with gfp.*

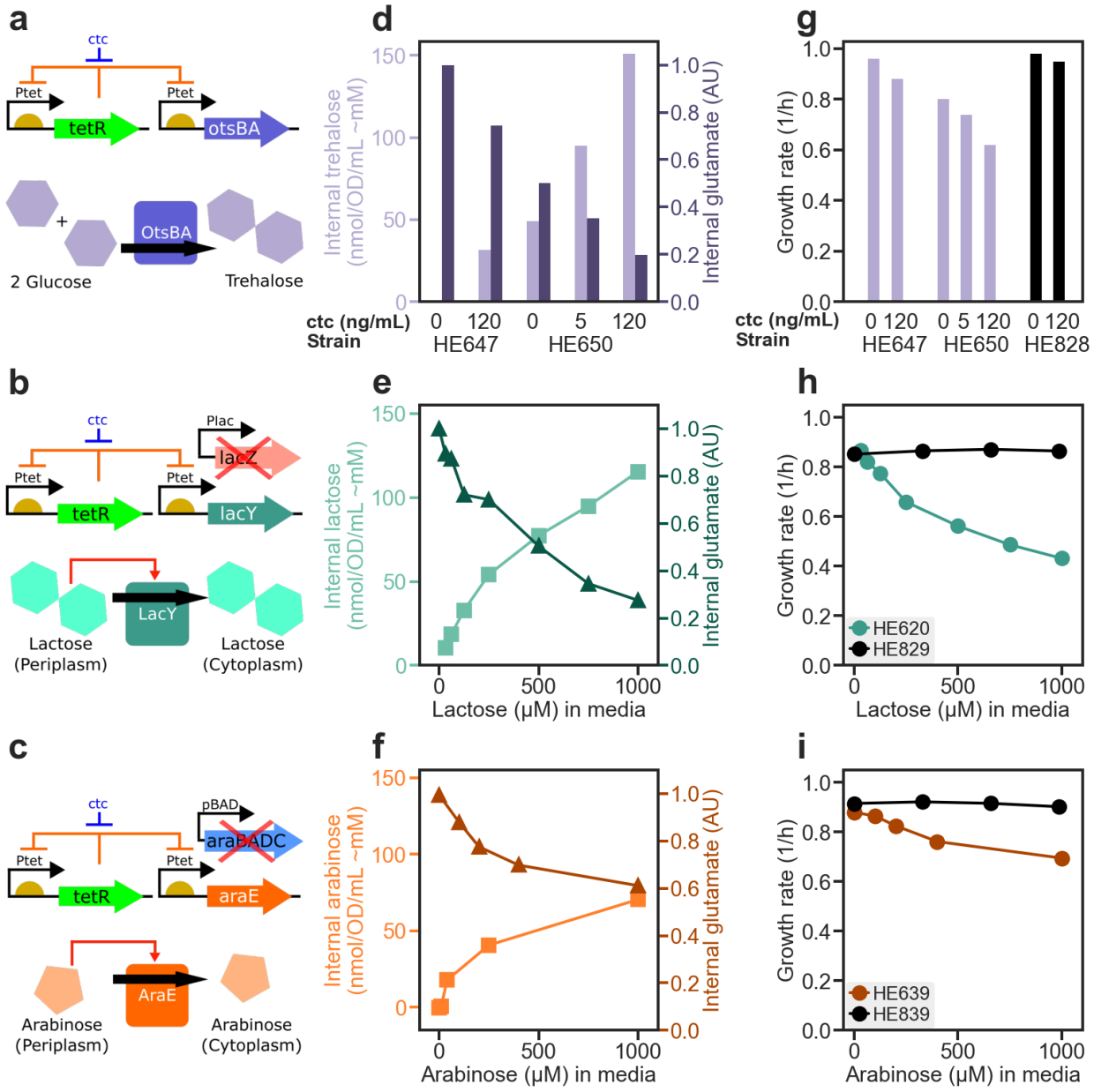
a
ctc
Ptet
Ptet
tetR
otsBA
OtsBA
2 Glucose
Trehalose
b
ctc
Plac
Ptet
Ptet
lacZ
tetR
lacY
LacY
Lactose
(Periplasm)
Lactose
(Cytoplasm)
c
ctc
pBAD
Ptet
Ptet
araBADC
tetR
araE
AraE
Arabinose
(Periplasm)
Arabinose
(Cytoplasm)
d
Internal trehalose (nmol/OD/mL ~mM)
Internal glutamate (AU)
ctc (ng/mL)
Strain
0 120 0 5 120
HE647 HE650
e
Internal lactose (nmol/OD/mL ~mM)
Internal glutamate (AU)
Lactose (μM) in media
f
Internal arabinose (nmol/OD/mL ~mM)
Internal glutamate (AU)
Arabinose (μM) in media
g
Growth rate (1/h)
ctc (ng/mL)
Strain
0 120 0 5 120 0 120
HE647 HE650 HE828
h
Growth rate (1/h)
HE620
HE829
Lactose (μM) in media
i
Growth rate (1/h)
HE639
HE839
Arabinose (μM) in media

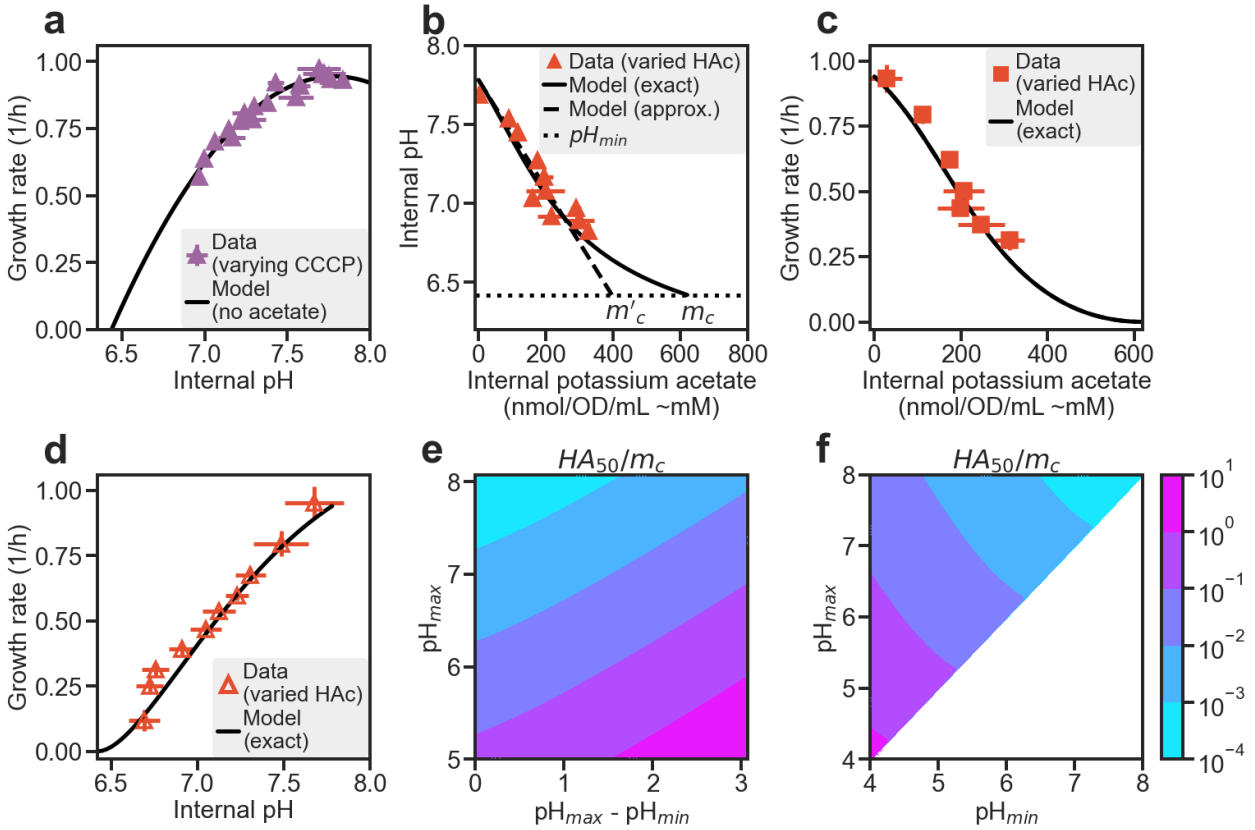

Figure 2.12 Model behavior and comparison to data.
a) The relation between growth rate and internal pH, as revealed by the CCCP experiment in the absence of acetate (same data as the purple triangles in Figure 2.3e), is well described by the quadratic form (solid line) given by Eq. B.4, with the best-fit parameters $pH_{max} = 7.78$, $pH_{min} = 6.42$, *and* $\lambda_0 = \frac{0.94}{h}$. *b) According to the solution of the model (B.1), the relation between internal pH and potassium acetate concentration is expected to be approximately linear for internal pH spanning as much as half of the range between the normal value* pH_0 *and the minimal value* pH_{min}*; see the dashed line, which extrapolates to an apparent inhibition concentration* $m'_c = \frac{2m_c}{[ln\,10\,(pH_{max}-pH_{min})]}$ *where internal pH reaches its minimal value and growth rate vanishes. Our data is best fitted by* $m_c \approx 620\,mM$ *(corresponding to* $m'_c \approx 400\,mM$*). This fixes the lone unknown parameter of the model. Using this parameter value, the exact solution of the model is shown as the solid line. c) The model with the fixed parameters accurately describes the relation between internal potassium acetate and growth rate. d) The model with the fixed parameters accurately describes the relation between internal pH and growth rate due to acetate stress. e) and f) provide two plots of the dependence of the half-inhibitory acetic acid concentration (*HA_{50}*), defined as the concentration of acetic acid (external or internal) where the growth rate is reduced to 50% of the unstressed value. The half-inhibitory concentration is plotted for different values of the cellular pH in stress-free conditions (*pH_{max}*) and minimal pH value (*pH_{min}*), and the result is expressed relative to a characteristic internal potassium acetate concentration,* m_c.

2.10 Methods

2.10.1 Strain construction

Construction of Ptet driving *tetR* at *ycaD*, *intS*, and *galK* loci on chromosome

The *tetR* structure gene was amplified from pZS4int1 (*142*) by oligos tetR-Kpn-F and tetR-Bam-R (Table 2.2). The PCR products were digested with *Kpn*I/*BamH*I and cloned into pKDT_Ptet (*143*) digested with the same enzymes, yielding pKDT_Ptet-*tetR*. Using the resultant plasmid as template, the DNA fragment (referred to as "km:rrnBT:Ptet-tetR") containing the *km* gene, the *rrnB* terminator (rrnBT) and the Ptet promoter was individually amplified using three pairs of chimeric oligos: (1) Ptet.tetR-ycaD-F and Ptet.tetR-ycaD-R, (2) Ptet.tetR-intS-F and Ptet.tetR-intS-R, and (3) Ptet.tetR-galK-F and Ptet.tetR-galK-R (Table 2.2). The PCR products were gel purified and individually integrated into the *ycaD*, *intS* and *galK* locations on the chromosome of K12 strain NCM3722 using the lambda-Red system (*144*). The Km resistant colonies were verified by PCR and subsequently by sequencing.

At the *ycaD* locus, the "km:rrnBT:Ptet-tetR" fragment is located in the *ycaC*/*ycaD* intergenic region, replacing the sequence from the -221st nucleotide to the -114th nucleotide relative to the translational start point of *ycdD*. The resultant strain is named NCM3722-1R. At the *intS* location, the "km:rrnBT:Ptet-tetR" fragment is substituted for the region from the -228th nucleotide to the +1183th nucleotide relative to the translational start point of *intS*. At the *galK* location, the "km:rrnBT:Ptet-tetR" fragment is substituted for the region from the -7th nucleotide to the +1033th nucleotide relative to the translational start point of *galK*. The three copies of Ptet-*tetR* were combined together by first flipping out the km resistance genes (*144*) and subsequently by P1 transduction, yielding strain NCM3722-3Rs (that is, HE697) (Table 2.1).

Construction of the *ackA/acs* deletion strain

The Δ*ackA* deletion allele in strain JW2293-1 (E. coli Genetic Stock Center), in which a *km* gene is substituted for *ackA*, was transferred by P1 transduction to NCM3722. The km resistance genes were then flipped out (*144*). The Δ*acs* deletion allele in strain JW4030-1 (E. coli Genetic Stock Center), in which a *km* gene is substituted for *acs*, was transferred by P1 transduction, yielding strain NQ1028 (Table 2.1).

Construction of the lacI*/lacZ/lacY* deletion strain

The *lacI*, *lacZ* and *lacY* genes were deleted using the lambda-Red method (*144*). The km resistance gene was amplified from pKD4 using chimeric oligos lacI-P1 and lacY-P2 (Table 2.2). The PCR products were electroporated into NCM3722 cells expressing lambda-Red proteins encoded by pKD46 (*144*). The Km resistant colonies were confirmed by PCR and sequencing for the replacement of the region harboring *lacI*, *lacZ* and *lacY* genes by the *km* gene. This yielded strain NCM3722 Δ*lacIZY*. The *lacIZY* deletion was transferred by P1 transduction to NCM3722-1R, yielding strain HE827 (Table 2.1). Plasmids pZA31Ptet-*lacY* (*27*) and pZA31Ptet-*gfp* (*145*) were individually transformed into HE827, yielding strain HE620 and strain HE829, respectively (Table 2.1).

Construction of Ptet driving *otsBA* on chromosome

Using plasmid pKDT:Ptet (*143*) as template, the DNA fragment (referred to as "km:rrnBT:Ptet") containing the *km* gene, the *rrnB* terminator (rrnBT) and the Ptet promoter was amplified using the primer pair Ptet.ots-P1/Ptet.ots-P2 (Table 2.2). The PCR products were integrated into the chromosome of K12 strain NCM3722 (*144*) to replace the *otsBA* promoter (from the -103th nucleotide to the +1st nucleotide relative to the translational start point of *otsB*). The chromosomal integration was confirmed first by colony PCR and subsequently by DNA

sequencing. The region carrying "km:rrnBT:Ptet-otsBA" was transferred to NCM3722-1R by P1 transduction, yielding strain HE647 (Table 2.1).

Construction of *otsBA* overexpression plasmid

The *otsBA* operon was amplified from NCM3722 chromosomal DNA using oligos otsB-Kpn-F and otsA-Bam-R (Table 2.2). Using fusion PCR, the *BamH*I restriction site GG**ATC**C (+383 to +388 downstream of the *otsA* translastional start point; ATC in bold face encoding the Isoleucine residue) on the *otsA* gene was removed by changing ATC to ATT. The modified *otsBA* operon with no *BamH*I site was digested with *Kpn*I/*BamH*I, gel purified and then ligated into the same sites of pZA31Ptet and pZE12Ptet (*142*), yielding pZA31Ptet-*otsBA* and pZE12Ptet-*otsBA*, respectively. pZA31Ptet-*otsBA* and pZE12Ptet-*otsBA* were transformed into strain HE697 (carrying three chromosomal copies of Ptet-*tetR*), yielding strains HE650 and HE654 (Table 2.1).

Construction of *araE* overexpression plasmid

The Δ*araC* deletion alleles in strain JW0063-1 (E. coli Genetic Stock Center), in which a *km* gene is substituted for *araC*, was transferred by P1 transduction to NCM3772-1R, yielding strain HE636. Because the parent strain contained was also deleted of *araBAD* (*146*), and the latter was adjacent to the *araC* locus, *ΔaraBAD* was also transferred to the recipient strain HE636.

The araE gene was PCR amplified from NCM3722 chromosomal DNA using oligos araE-Kpn-F and araE-Bam-R (Table 2.2). The amplified products were digested with KpnI and BamHI, and then ligated into the same sites of pZA31Ptet (*142*), yielding pZA31Ptet-araE, in which the araE gene is driven by the tet promoter Ptet. pZA31Ptet-*araE* (*27*) and pZA31Ptet-*gfp* (*145*) were individually transformed into HE636, yielding strain HE639 and strain HE839, respectively (Table 2.1).

Construction of pHluorin expression plasmid

The pHluorin gene, encoding pH sensitive ratiometric GFP, was amplified from the plasmid pGFPR01 (*122*) using oligos pHgfp-EcoR-F and pHgfp-Bam-R (Table 2.2). The amplified PCR products were digested with *EcoR*I and *BamH*I, purified and ligated into the same sites of pZE12Ptet, yielding pZE12Ptet-pHluorin. This recombinant plasmid was transformed into strain NCM3722-1R, yielding strain HE616 (Table 2.1). The plasmid pZA31Ptet-*gfp* (*145*) was transformed into strain HE697, yielding the control strain HE828.

2.10.2 Growth of Cells

Growth media

The phosphate-based growth media contained 20 mM glucose 10 mM NaCl, 10 mM NH_4Cl, 0.5 mM Na_2SO_4, a phosphate buffer and a 1000x micronutrient solution. The 1000x micronutrient solution contained 20 mM $FeSO_4$, 500 mM $MgCl_2$, 1 mM $MnCl_2{\cdot}4H_2O$, 1 mM $CoCl_2{\cdot}6H_2O$, 1 mM $ZnSO_4{\cdot}7H_2O$, 1 mM $H_{24}Mo_7N_6O_{24}{\cdot}4H_2O$, 1 mM $NiSO_4{\cdot}6H_2O$, 1 mM $CuSO_4{\cdot}5H_2O$, 1 mM SeO_2, 1 mM H_3BO_4, 1 mM $CaCl_2$, and 1 mM $MgCl_2$ dissolved in a 0.1 N HCl solution. The content of the phosphate buffer was changed to control the pH. At pH 6, the media was buffered with 20 mM K_2HPO_4 and 80 mM KH_2PO_4. For other pH, the proportion of K_2HPO_4 and KH_2PO_4 was used at different proportions with the total concentration summing to 100 mM. For internal potassium measurements, K_2HPO_4 and KH_2PO_4 was replaced with Na_2HPO_4 and NaH_2PO_4 and 1 mM KCl was added to provide some potassium.

The medium used for the anaerobic growth of *B. thetaiotaomicron* was the same as used for the anaerobic growth of E. coli but also included 2 mg cyanocobalamin, 2 mg hemin, and 0.6 cysteine per liter. To make the media anoxic, Hungate tubes (16 mm x 125 mm) filled with 7 mL medium were shaken at 270 rpm under a 7% CO_2, 93% N_2 atmosphere pressurized to 1.5 atm for 75 minutes. Cultures were transferred anoxically into Hungate tubes with disposable syringes.

The MOPS based growth media was the same as in (*147*). The base medium contains 40 mM MOPS and 4 mM tricine (adjusted to pH 7.4 with KOH), 0.1 M NaCl, 10 mM NH_4Cl, 1.32 mM KH_2PO_4, 0.523 mM $MgCl_2$, 0.276 mM Na_2SO_4, 0.1 mM $FeSO_4$, and the trace micronutrients described in (*148*). The MES buffered media was to the same as the MOPS media except the MOPS buffer and NaCl was replaced with 150 mM MES. In all media, carbon concentrations were added based on the number of carbon atoms in the molecule – 10 mM for C6 carbons, 20 mM for C3 carbons. Ampicillin, chloramphenicol, and kanamycin were added at concentrations of 50 mg/mL, 10 mg/mL, and 50 mg/mL, respectively.

Stresses, limitations, and overdoses: Acetate stress was applied to cells by growing cells in minimal media with various concentrations of sodium acetate. Lactose overdose was applied to cells (HE620) by titrating lactose concentrations. For the same cultures, Chloro-tetracycline (cTc) was also added to the media at a concentration of 25 ng/mL to induce expression of LacY. Trehalose overdose was applied to cells (HE647 or HE650) grown in different concentrations of cTc (0-120 ng/mL). CCCP stress was applied for cells (HE616) by titrating CCCP between 0-40 μM. Carbon limitation was implemented by titrating 3-methyl-benzylalcohol (3MBA) concentration in strains NQ1243 and NQ1390. 3MBA concentrations ranged from 0 to 600 μM.

Measurement of pH

Media pH was measured with an Orion Start A221 pH meter by Thermo Scientific with an Orion 9110DJWP pH probe by Thermo Scientific. Measurements were made according to the manufacturer's instructions.

Culture tubes

Exponential cell growth was performed in a 37°C water bath shaker at 240 rpm Cultures were grown in the following three steps: seed culture, pre-culture, and experimental culture. Cells

were first grown as seed cultures in LB broth for several hours, then as pre-cultures overnight in an identical medium to the experimental culture. Experimental cultures were started by diluting the pre-cultures to an optical density (OD) at wavelength 600 nm (OD_{600}) of ~0.01–0.02. Growth rates were calculated from at least seven OD_{600} points within a range of OD_{600} of ~0.04–0.4.

Plate reader

Seed culture and pre-culture were performed in water bath shakers as described for the growth of cells in culture tubes. Experimental culture was done in a Tecan Spark microplate reader with 96-well microplates (Greiner bio-one) with 200 µL of media. For inoculation, cells were diluted at least 1,000x into the plate media. The incubation temperature was 37°C. The plate was shaken at 280 rpm. Optical density was measured at a wavelength of 420 nm (OD_{420}). To calculate growth rate, the background OD from the opacity of the plate and media, was subtracted from raw OD measurement. Growth rates were calculated from OD_{420} from 0.02-0.2. Fluorescence was also measured for internal pH (see internal pH – fluorescence).

Anaerobic cultures

Anaerobic growth was performed similarly to aerobic growth with a few exceptions. All transfers were performed with disposable syringes to avoid oxygen contamination. For *E. coli*, aerobic seed cultures were diluted into Hungate tubes for preculture. After overnight growth, the precultures were diluted into fresh Hungate tubes for experimental culture. For *B. theta*, the seed cultures were inoculated into Hungate tubes containing 7 mL Wilkens-Chalgren broth from colonies selected from Wilkens-Chalgren agar plates. After overnight growth, these cultures were diluted into preculture tubes. And then diluted once more for the experimental cultures. To avoid atmospheric exposure from removing samples, OD measurements were performed with a Thermo Genesys 20 modified to hold Hungate tubes in place of cuvettes. The culture temperature was kept

stable during OD measurements by removing and replacing the Hungate tubes from the water bath shaker within 30 seconds. The OD_{600} measured through the Hungate tubes was equivalent to the OD_{600} measured through a cuvette for the range of 0.04-0.5.

Anerobic growth in plate reader was performed with a Tecan Spark microplate reader enclosed in a custom vinyl anaerobic chamber. Chamber was kept anaerobic with palladium catalysts and an input gas of 5% H_2, 10% CO_2, and 85% N_2. Oxygen levels were monitored with the Tecan Spark O_2 and CO_2 module to ensure the chamber stayed anaerobic during growth.

2.10.3 Assays

RNA measurement

Total RNA quantification method used was described in (*14*). RNA nucleotide amount (nmol/OD/mL) was calculated from the normalized RNA mass (µg/OD/mL) assuming that the average molecular weight of an RNA nucleotide was 339.5 g/mol, equivalent to equal parts ACGU.

Internal acetate, lactose, and trehalose measurements

Exponentially growing cells were harvested at an OD of 0.4-0.5. 600 µL of culture was collected and added to a 0.22 µm nylon filter centrifuge tube (Corning Costar Spin-X Centrifuge Tubes) and centrifuged at 20,000g for 30 seconds. Cells were quickly removed from the filter with 600 µL of deionized water. The cell-free filtrate was put aside for later. The extracted cells were then added to a 1.5 mL Eppendorf centrifuge tube containing 40 µL chloroform. The tube was vortexed for 10 seconds. Samples were stored at -20°C. The same procedure was applied for the cell-free filtrate, starting by repeating the filter step for the filtrate.

For HPLC analysis, samples were thawed and then centrifuged for 60 seconds. 80 µL of the aqueous section was placed into HPLC analysis tubes for analysis with HPLC (*39*).

The internal acetate or lactose amount, $[Ac]_{internal}$, was calculated as $[Ac]_{internal} = \frac{Ac_{cells} - Ac_{filtrate}}{\rho_{cells}}$ where Ac_{cells} is the acetate amount in the filtered cells, $Ac_{filtrate}$ is the acetate measured in the re-filtered filtrate, and ρ_{cells} is the amount of cells analyzed (in ODmL). When concentration was reported in mM, the formula was $[Ac]_{internal} = \frac{Ac_{cells} - Ac_{filtrate}}{\rho_{cells}} c_{water}$ where c_{water} was assumed to be 1 µL H_2O/OD/mL.

Trehalose pools were measured as follows. Exponentially growing cells were harvested at an OD of 0.4-0.5. A 1 mL of culture was collected on a membrane filter (Durapore membrane filters; 0.45 um; HVLP02500) which was set on a vacuum manifold and prewashed by water followed by warmed culture medium. The cells were rinsed by 2 mL warmed culture medium and transferred to 2 mL of extraction solution (40:40:20 acetonitrile:methanol:water) containing 100 nmol glycerol and 50 nmol arabinose as standards placed on a dry ice plate. Cells on the filter were suspended well in the extraction buffer by pipetting and extraction was let proceed at -20°C for 40-60 minutes. After the extracts were collected to microtubes, the filter was rinsed by 0.9 mL extraction solution and the extraction was let proceed for another 15-20 minutes. This second extracts were combined with the first extracts and stored at -80°C. On the day of HPLC measurements (*39*), the extracts were dried by speed-vac and dissolved in water.

Excreted glucose and acetate

Four samples of 200 µL were pipetted from culture tubes at regularly spaced ODs during exponential growth. For anoxically grown cultures, sample removal was done with tuberculin syringes inserted into the rubber stopper. Samples were transferred to 0.22 µm nylon filter centrifuge tubes (Corning Costar Spin-X Centrifuge Tubes) and quickly filtered by centrifugation. Samples were then stored at -20°C until HPLC analysis, which was performed according to (*39*).

Internal glutamate measurement

Measurement of amino acids were performed as in (*149–151*). Briefly, 150 µL of exponentially growing cells were added to 600 µL of ice-cold methanol with alpha amino-butyric acid as an internal standard. The samples were vortexed and then kept at 4°C for storage. The samples were then dried in a rotary vacuum desiccator and resuspended in 150 µL of H_2O for HPLC analysis. Glutamate levels were normalized by the glutamate level for unstressed cells.

Potassium

Cells for potassium measurements were grown in low potassium media where the potassium salts were replaced with sodium. 1 mM of KH_2PO_4 was used as the source of potassium. Exponentially growing cells were harvested at OD_{600}=0.4-0.5. 2 mL of culture was collected on a membrane filter (Durapore membrane filters; 0.45 µm; HVLP02500) set on a vacuum manifold. The cells were rinsed by 2.5 mL warmed potassium-free medium and transferred to 1.8 mL of 1 N HNO_3.

Cells on the filter were suspended well in the extraction buffer by pipetting and extraction was let proceed at ambient temperature for 30 minutes. After the extracts were collected to microtubes, the filter was rinsed by 1 mL of 1 N HNO_3 and the extraction was let proceed for another 15 minutes. This second extracts were combined with the first extracts and stored at -80°C. Potassium was measured in these samples with ICP-MS at the Environmental and Complex Analysis Laboratory (ECAL) at UCSD.

2.10.4 Metabolomics

Sample collection

2.5 OD_{600}·mL of exponentially growing cell culture were quickly vacuum filtered on 0.45 µm nylon filters. The cells on the filter were quickly washed 2 times with 2 mL of warm cell-free media. After washing, the filter was immediately plunged into 1.3 mL of a 40:40:20

methanol:acetonitrile:water (MAW) mixture kept on dry ice for 15 minutes. The MAW mixture without the filter was then put into a 1.5 mL Eppendorf tube and centrifuged for 60 seconds. The supernatant was put into a new tube and stored at -80°C.

To perform relative quantification with ^{13}C-labeled metabolites, cells were grown in media supplemented with ^{13}C carbon sources were collected for use as a reference. A mixed reference was used to avoid bias from any of the individual growth medium. Three conditions were collected: NCM3722 cells without an applied stress, NCM3722 cells grown with 30 mM ^{13}C-labeled sodium acetate, and HE650 cells grown with 50 ng/mL cTc (high level of trehalose overdose, see Figure 2.11). All conditions were grown in phosphate-buffered minimal media with ^{13}C-labeled glucose as the carbon source. Sample collection was the same as described above. Samples were combined in equal amounts to form the mixed ^{13}C-labeled reference.

Extracted metabolites were analyzed by LC-MS. For hydrophilic interaction chromatography, used a Vanquish UHPLC system (Thermo Fisher, San Jose, CA) and an XBridge BEH Amide column (2.1 mm x 150 mm, 2.5 mm particle size, 130 A˚pore size; Waters, Milford, MA) with a 25 min solvent gradient at flow rate of 150 µL/min. Solvent A is 95:5 water:acetonitrile with 20 mM ammonium hydroxide and 20 mM ammonium acetate, pH 9.4. Solvent B is acetonitrile. The LC gradient was 0 min, 85% B; 2 min, 85% B; 3 min, 80% B; 5 min, 80% B; 6 min, 75% B; 7 min, 75% B; 8 min, 70% B; 9 min, 70% B; 10 min, 50% B; 12 min, 50% B; 13 min, 25% B; 16 min, 25% B; 18 min, 0% B; 23 min, 0% B; 24 min, 85% B; 30 min, 85% B. LC was coupled to was a quadrupole-orbitrap mass spectrometer (Q Exactive, Thermo Fisher Scientific, San Jose, CA) via electrospray ionization. The mass spectrometer operates in negative and positive ion switching mode and scans from m/z 70 to 1000 at 1 Hz and 70,000 resolution.

Autosampler temperature was 5ºC, and injection volume was 10 µL. Data were analyzed using the El-Maven software. ^{13}C natural isotope abundance was corrected using house code (*152*).

Relative quantitation

Relative quantities were calculated as $r_{m,x} = \frac{^{12}I_{m,x}}{^{13}I_{m,x}} \frac{^{13}I_{m,ref}}{^{12}I_{m,ref}}$ where $r_{m,x}$ is the relative quantity of metabolite m in condition x, and $^{n}I_{m,x}$ is the ion count for metabolite m with atomic mass of carbon n (12 or 13) in either condition x and ref being the reference condition. $r_{m,x}$ is the relative value of metabolite m in condition x, and $r_{m,ref}$ is the relative value of metabolite m in the reference condition. The reference condition consisted of uninhibited samples from each limitation or stress.

Absolute quantitation

To compute absolute quantities of metabolites, we use the formula $[M]_{x,m} = [M]_{p,m} r_{m,x}$ where $[M]_{x,m}$ is the concentration of metabolite m in condition x, $[M]_{p,m}$ is the concentration of metabolite m as measured in (*63*) for their glucose condition.

When calculating the summed metabolite concentration including free potassium, the concentrations of glutamate and aspartate were multiplied by 2 to account for potassium associated with these negatively charged molecules.

2.10.5 Internal pH measurements

Fluorescence

Fluorescence measurements were taken for exponentially growing HE616 cells harboring constitutive expression of pHluorin in the OD range of 0.01 and 0.2 using a Tecan Spark microplate reader. Fluorescent signals were collected for two excitation wavelengths: 390nm and 470nm. The emission wavelength for both signals was 500 nm. For each growth condition, a linear fit was made from the two signals to calculate the fluorescence ratio. This fluorescence ratio was then

used to calculate the internal pH from the standard curve. In cells grown with CCCP, the fluorescence signal was adjusted to account for light absorbance from CCCP.

The following procedure was used to make the standard curve. HE616 cells grown in phosphate buffered media were resuspended in carbon-free phosphate-buffered media with 10 μM CCCP for a variety of pH. Using a Tecan Spark microplate reader, fluorescence with excitations at 390 nm and 470 nm was measured for cells at different dilutions. The fluorescence emission wavelength for both signals was 500 nm. For each pH, a linear fit was made from the two signals. The slope from this fit was used as the fluorescence ratio.

Radiolabel

Adapted from (*123*, *124*). Cells were grown in 150 mM MES medium, pH 6.3, to OD_{600} = 0.5 and a 3.2 mL of culture was transferred to a tube containing 66 μL of ^{14}C-sucrose (0.25 mM, 50 μCi/mL from Perkin Elmer Inc.) and 33 μL of either [^{3}H]-benzoic acid (0.5 mM, 0.5 mCi/ml from ARC) or ^{3}H-H_2O (1 mCi/mL from Perkin Elmer Inc.) and incubated at 37°C for 2-3 minutes. A 1 mL suspension was transferred to a microtubes containing 200 μL of 1-bromododecane and centrifuged at 21130 x g for 30 seconds. The supernatants were carefully removed, and the cells were suspended in 100 μL water. The supernatant and the cell suspension were transferred to 15 ml of scintillation cocktail (Liquiscint from National Diagnostics) and analyzed by scintillation counter. ^{14}C counts into ^{3}H channel were corrected. Impurities in ^{14}C-sucrose and ^{3}H-benzoic were removed by suspending exponentially growing NCM3722 cells followed by centrifugation and taking the supernatants. Cytoplasmic pH was calculated from the ratio of the concentrations of benzoic acid between the cytoplasm and the supernatant.

Cytoplasmic water

Adapted from (*138*). For cytoplasmic water measurements under carbon limitation and trehalose overdose, cells were grown in MOPS-buffered medium. The culture was processed essentially as described above with ^{14}C-sucrose and ^{3}H-H_2O except that oil centrifugation was done for 3 min.

2.10.6 Proteomics

Proteomics samples were taken for acetate stressed cells and lactose overdose cells. Samples were prepared as in (*61*) with the following exceptions. For the ^{15}N reference, unstressed cells growing in glucose, phosphate-based media (2.10.2) where the NH_4Cl was replaced with 10 mM $^{15}NH_4Cl$.

2.11 Acknowledgments

We are grateful to helpful discussions with many colleagues during the course of this work, including Kapil Amarnath, Jonas Cremer, Adam Feist, Harry Flint, Jun Park, Amir Zarrinpar, and the late George MacFarlane. We thank Hui (Tony) Sheng for early work on metabolomics, and Joan Slonczewski for providing JLS1105. This work is supported by the NIH through grant R01GM109069 (TH) and R35-GM136412 (JRW). JDR and YS acknowledge the support of the Ludwig Cancer Research.

Chapter 2, in full, has been submitted for publication as Tradeoff between cytoplasmic accumulation and acidification governs bacterial response to short-chain fatty acid stress. Brian R. Taylor, Vadim Patsalo, Hiroyuki Okano, Yihui Shen, Zhongge Zhang, James R. Williamson, Joshua D. Rabinowitz, Terence Hwa, 2022. The dissertation author was the primary author of this paper.

2.12 Tables

Table 2.1 Strains used in acetate study

Strain	Genotype	Description	Source
NCM3722	Wild-type E. coli K12 strain	Parent strain for all genetically modified strains	(*153*)
NQ1028	*Δacs ΔackA::kan*	Strain unable to metabolize acetate	This study
NQ1191	*ΔrpoS*	rpoS deletion strain	(*154*)
NQ1243	*ycaD*::FRT:Ptet-*xylR* PptsG::*kan*:Pu-*ptsG*	Carbon limitation strain	(*27*)
NQ1390	*ycaD*::FRT:PlacIq-*xylR* PptsG::*kan*:Pu-*ptsG*	Carbon limitation strain	(*155*)
JLS1105	pGFPR01 in W3110 background	Source of pHluorin	(*122*)
HE616	chs::Ptet-*tetR* x 1 pZE12Ptet-pHluorin	Strain used for internal pH measurements	This study
HE620	chs::Ptet-*tetR* x 1 Δ*lacIZY* pZA31Ptet-*LacY*	Lactose overdose strain	This study
HE639	YcaC/YcaD::rrnBT_Ptet_tetR ΔaraC::kan ΔaraBAD pZA31-ptet-araE	Arabinose overdose strain	This study
HE647	chs::phi(Ptet-*otsBA*) chs::Ptet-*tetR* x 1	Trehalose overdose strain	This study
HE650	chs::Ptet-*tetR* x 3 pZA31Ptet-*otsBA*	Trehalose overdose strain	This study
HE654	chs::Ptet-*tetR* x 3 pZE12Ptet-*otsBA*	Trehalose overdose strain	This study
HE697	Ptet-*tetR* x 3	Ancestor of HE647 and HE650	This study
HE827	chs::Ptet-*tetR* x 1 Δ*lacIZY*	Ancestor of HE620	This study
HE828	chs::Ptet-*tetR* x 3 pZA31Ptet-*gfp*	Trehalose overdose control strain	This study
HE829	NCM3722+1R+Δ*lacIZY* pZA31Ptet-*gfp*	Lactose overdose control strain	This study
HE839	YcaC/YcaD::rrnBT_Ptet_tetR ΔaraC::kan ΔaraBAD pZA31-Ptet-*gfp*	Arabinose overdose control strain	This study
HO1	*Bacteroides thetaiotaomicron* (ATCC 29148)	Anaerobic gut bacterium	(*82*)

Table 2.2 Oligonucleotides used in acetate study

Name	**Sequence**	**Use**
tetR-Kpn-F	aatggtaccatgtctagattagataaaagtaaagtg	Cloning *tetR* into pKDT_Ptet
tetR-Bam-R	tatggatccttaagacccactttcacatttaagttg	Cloning *tetR* into pKDT_Ptet
tetR-ver-F	ctttagaaggggaaagctggcaag	Sequencing verification of *tetR* cloning
Ptet.tetR-ycaD-F	atcagacgcgatgcattgctctgaaagcatagacgggaaatatgagtttgcttgtgtaggctggagctgcttc	Chromosomal P*tet-tetR* at the *ycaD* locus
Ptet.tetR-ycaD-R	ggtgaaaatacgcgatatcccagcggcggtattatcgatttatattacttaagacccactttcacatttaagttg	Chromosomal P*tet-tetR* at the *ycaD* locus
ycaD-ver-R	tacctgccatgtggacatgtgttc	Sequencing verification of *Ptet-tetR* at the the *ycaD* locus
Ptet.tetR-intS-F	agatttacagttcgtcatggttcgcttcagatcgttgacagccgcactccattgtgtaggctggagctgcttc	Chromosomal P*tet-tetR* at the *intS* locus
Ptet.tetR-intS-R	ctccaccttctcatcaagccagtccgcccaccattgcatcatttctctgcgttaagacccactttcacatttaagttg	Chromosomal P*tet-tetR* at the *intS* locus
intS-ver-R	tccaagtcttaatcgatcgatacttg	Sequencing verification of *Ptet-tetR* at the the *intS* locus
Ptet.tetR-galK-F	cagcagagcgtttgcgcgcagtcagcgatatccattttcgcgaatccggagttgtgtaggctggagctgcttc	Chromosomal P*tet-tetR* at the *galK* locus
Ptet.tetR-galK-R	agcttgctgtacggcaggcaccagctcttccgggatcagcgcgacgatacagttaagacccactttcacatttaagttg	Chromosomal P*tet-tetR* at the *galK* locus
galK-ver-R	tcagcactgtcctgctccttgtg	Sequencing verification of *Ptet-tetR* at the the *galK* locus
lacI-P1	atgaaaccagtaacgttatacgatgtcgcagagtatgccggtgtctcttattgtgtaggctggagctgcttc	Chromosomal deletion of *lacI*, *lacZ* and *lacY* genes
lacY-P2	catccgacattgattgcttaagcgacttcattcacctgacgacgcagcagcatatgaatatcctccttag	Chromosomal deletion of *lacI*, *lacZ* and *lacY* genes
lacY-ver-R	tcattggcatgttcaatgcgatcactc	Verification of deletion of *lacI*, *lacZ* and *lacY* genes
Ptet.ots-P1	caacaatttagcgttttttcccaccatagccaaccgccataacggttggcttgtgtaggctggagctgcttc	Chromosomal P*tet* driving *otsBA*
Ptet.ots-P2	gaattcattaaagaggagaaaggtaccggcatatttcgcggatagttcagggggtttcggttaacggttctgtcac	Chromosomal P*tet* driving *otsBA*
otsB-ver-R	cagtgcgtcaagctccaccattgag	Sequencing verification of chromosomal P*tet* driving *otsBA*
OtsB-Kpn-F	aatggtaccgtgacagaaccgttaaccgaaacccctg	Cloning *otsBA* into pZA31Ptet and pZE12Ptet
OtsA-Bam-R	ataggatccttacgcaagctttggaaaggtagcaactttatc	Cloning *otsBA* into pZA31Ptet and pZE12Ptet
Ots-R	caacaggtgataatcgtgaatccagataatgtcatc	Fusion PCR to remove *BamH*I site on *otsA*
Ots-F	gatgacattatctggattcacgattatcacctgttg	Fusion PCR to remove *BamH*I site on *otsA*
Ots-ver-F1	catgaagacgcattaatgacattag	Sequencing verification of *otsBA* cloning
Ots-ver-F2	tggtgaaacagggaatgaggatcag	Sequencing verification of *otsBA* cloning
Ots-ver-F3	aactggcgcaacttaaagcggaactg	Sequencing verification of *otsBA* cloning
araE-Kpn-F	tatggtaccatggttactatcaatacggaatctgc	Cloning *araE* into pZA31Ptet
araE-Bam-R	ttaggatcctcagacgccgatatttctcaacttctc	Cloning *arae*E into pZA31Ptet
araE-ver-F1	tcgtgtggtgctgggcattgctgtc	Sequencing verification of *araE* cloning
araE-ver-F2	tggtcgtagggctgacctttatgttc	Sequencing verification of *araE* cloning
pHgfp-EcoR-F	atagaattcattaaagaggagaaaggtaccatgagtaaaggagaagaacttttcactg	Cloning *pHluorin* into pZE12Ptet
pHgfp-Bam-R	tatggatccttatttgtatagttcatccatgccatg	Cloning *pHluorin* into pZE12Ptet
pHgfp-ver-F	tacaagacacgtgctgaagtcaag	Sequencing verification of *pHluorin* cloning

*Table 2.3 Membership of proteins belonging to different functional classes. Functional categories of proteins in the E. coli proteome used in Figure 2.7f,g and Figure 2.8 based on (*12*).*

Category	**Gene names**
AA biosynthesis	alaA alaC argA argB argC argD argE argF argG argH argI aroA aroB aroC aroD aroE aroF aroG aroH aroK aroL asd asnA asnB aspC cysC cysD cysE cysH cysI cysJ cysK cysM cysN dapA dapB dapD dapE dapF dmlA gabT gdhA glnA gltB gltD glyA hisA hisB hisC hisD hisF hisG hisH hisI ilvA ilvB ilvC ilvD ilvE ilvH ilvI ilvM ilvN leuA leuB leuC leuD lysA lysC malY metA metB metC metE metL pheA proA proB proC serA serB serC thrA thrB thrC trpA trpB trpC trpD trpE tyrA tyrB ydiB
AA-transport	abgT alaE ansP argO argT aroP artI artJ artM artP artQ brnQ cadB cstA cycA dppA dppB dppC dppD dppF dtpA dtpB dtpC dtpD eamA eamB frlA gabP gadC glnH glnP glnQ gltI gltJ gltK gltL gltP gltS hisJ leuE livF livG livH livJ livM lysP metQ mmuP mtr oppA oppB oppC oppD oppF pheP plaP potA potB potC potD potE potF potG potH potI proV proW proX proY putP puuP rhtA rhtB rhtC sgrR sstT tcyJ tcyL tcyN tcyP tdcC tnaB tyrP yahN ybaT ycaM yddG ydgI yehW yehX yehY yejA yejB yejE yejF ygjI yifK yijE yjeH yjeM
C-transport	alsA alsB alsC araF araG araH crr fruA fruB fucK fucP galE galF galK galM galP galR galS galT galU gatA gatB gatC lacY lacZ malE malF malG malK malM malP malT malX manX manY manZ melB mglA mglB mglC mtlA mtlD nagE ptsG ptsH ptsI rbsA rbsB rbsC rbsD rbsK srlA srlB srlE treB ugpA ugpB ugpC ugpE ulaA ulaB ulaC xylA xylB xylE xylF xylG xylH
Fermentation	ackA adhE fdhF frdA frdB frdC frdD hycA hycB hycC hycD hycE hycF hycG hycH hycI ldhA pflB pta
Motility	aer cheA cheB cheR cheW cheY cheZ flgA flgB flgC flgD flgE flgF flgG flgH flgI flgJ flgK flgL flgM flgN fliC fliD fliE fliF fliG fliH fliI fliJ fliK fliL fliM fliN fliO fliP fliQ fliR fliS fliT fliZ motA motB tap tar trg tsr
Sigma S	dps ecnB elaB katE osmC osmE otsA otsB wrbA
TCA and glyoxylate	aceA aceB acnA acnB fumA fumB fumC fumD fumE gltA icd lpd maeA mdh mqo sdhA sdhB sdhC sdhD sucA sucB sucC sucD ydhZ yggD
Translational proteins	sra rplA rplJ rplK rplM rplN rplO rplP rplQ rplR rplS rplB rplT rplU rplV rplW rplX rplY rpmA rpmB rpmC rplC rpmD rpmE rpmF rpmG rpmH rpmI rplD rplE rplF rplL rplI rpsA rpsJ rpsK rpsL rpsM rpsN rpsO rpsP rpsQ rpsR rpsS rpsB rpsT rpsU rpsC rpsD rpsE rpsF rpsG rpsH rpsI rpmJ aspS gltX ileS argS alaS cysS pheS pheT glyQ glyS hisS lysS lysU leuS metG asnS proS glnS serS thrS valS trpS tyrS arfB infC prfA fusA efp tsf tufA infA infB lepA prfB prfC frr
glycolysis and gluconeogenesis	eno fbaA fbaB fbp gapA glpX gpmA gpmM maeA maeB mdh pck pfkA pfkB pgi pgk ppsA pykA pykF tpiA ybhA yggF mqo

Table 2.4 Proteomic data for acetate stress.
See Supplemental file "tableS2a.xlsx". Relative and absolute proteomic data for NCM3722 cells where growth rate is limited by the addition of different concentrations of sodium acetate.

Table 2.5 Proteomic data for lactose overdose.
See Supplemental file "tableS2b.xlsx". Relative and absolute proteomic data for HE620 cells where growth rate is limited by the accumulation of lactose.

Table 2.6 Metabolomic data for NCM3722 cells under a range of acetate stress.
See Supplemental file "tableS3a.xlsx". Relative and absolute proteomic data for NCM3722 cells where growth rate is limited by the addition of different concentrations of sodium acetate.

Table 2.7 Metabolomic data for NCM3772-derived cells under carbon-limited growth.
See Supplemental file "tableS3b.xlsx". Relative and absolute metabolite measurements for cells with growth limited by controlling carbon uptake through PtsG. Strains NQ1243 and NQ1390 were grown in phosphate buffered media. Expression of PtsG was controlled by addition of 3MBA.

Table 2.8 Metabolomic data for NCM3772-derived cells under trehalose-overdose growth.
See Supplemental file "tableS3c.xlsx". Relative and absolute metabolite measurements for cells with growth limited by accumulation of trehalose by OtsAB.

Chapter 3

Carbon uptake kinetics of *Bacteroides thetaiotaomicron*

3.1 Abstract

Bacteroides thetaiotaomicron (*B. theta*) is a dominant member of the intestinal microbiota of humans and other mammals. One reason for *B. theta*'s dominance is it's abundant machinery for utilizing a large variety of complex polysaccharides as a source of carbon and energy (*82*). This machinery is organized into localized clusters of genes that coordinate to breakdown polysaccharides of great complexity (*69*). While much knowledge has been developed about the individual genes involved in polysaccharide utilization, quantitative studies are lacking. Here, we present extensive experimental characterization that leads to a quantitative model describing the growth of *B. theta* on various carbon sources, from monomers to mixtures of different monomeric carbon sources, which are the end product of polysaccharide breakdown. We find that a dominant obstacle for *B. theta*'s growth arises from a constant demand for carbon substrate that happens independently of growth. This obstacle is partially overcome by *B. theta*'s ability to utilize multiple carbon sources simultaneously.

3.2 Introduction

The mammalian gut is one of the densest natural microbial ecosystems on earth. This ecosystem would not be possible without the cooperation of the gut itself. The gut provides a stable environment of fixed temperature, fixed osmolarity, and roughly 3 square meals a day. However,

for the microbes in the gut, this environment presents its own challenges ranging from competition, antibiotics, bile acids, washout, and the immune system. Bacteria from several different phyla have evolved to stably survive in this environment. Organisms from three of these phyla are frequently found in high abundance: Bacteroidetes, Firmicutes, and Proteobacteria. The relative abundances of these different phyla have important effects on the health of the human host (*156*). Members of the *Bacteroides* phylum in particular are noteworthy due to their ability to digest different types of polysaccharides. *Bacteroides thetaiotaomicron* (*B. theta*) is one of the most well studied and abundant species of bacteria in the human gut (*157*, *158*).

One of the key features found in the genome of *B. theta* is the large presence of carbon utilization genes, commonly called polysaccharide utilization loci (PULs) (*82*). With these PULs, *B. theta* can digest a variety of polysaccharides (*159*), through a combination of membrane-bound and periplasmic hydrolases (*160–162*). *B. theta* controls the expression of many of these genes through three different known regulation systems (*159*), which monitor the presence or absence of specific sugars or polysaccharides. Breakdown of certain complex polymers has been shown to require coordination of multiple different PULs (*163*). Additionally, *B. theta* has a global carbon catabolism regulator, *BT4338* (*164*, *165*). The regulation systems of these genes work without the metabolite carbon repression system, cyclic adenosine monophosphate (cAMP), well-studied for *E. coli* and related species (*166*). However, cAMP has not been detected in *Bacteroides* species (*167*, *168*). It is currently unclear what are the quantitative constraints governing *Bacteroides* carbon catabolism.

3.3 Carbon metabolism

Our study on the physiology of *Bacteroides* carbon catabolism physiology begins with the study on single carbon sources. While polysaccharides are more relevant to the native environment of the gut, these polysaccharides are complex molecules in themselves, composing of multiple

different sugars as monomer units, arranged in varying patterns. In addition to their chemical units being different, polysaccharides may have different physical conformations that affect digestibility. For example, the polysaccharide starch can be a variety of different sizes ranging from hundreds to tens of thousands of glucose units, may be largely linear, like amylose, or highly branched, like amylopectin, and may have different secondary structures, such as is the case of resistant starch (*169*).

In order for the cell to use these polysaccharides, they must be broken up into their constituent parts. Furthermore, for many of the gene regulatory systems, single carbon sources are sufficient to upregulate the PULs (*164*). In order to gain an understanding of carbon utilization by *B. theta* and avoid the complexities presented by polysaccharides directly, we aim to understand *B. theta*'s utilization of monomers. In this chapter, we first explore the unique concentration dependence of growth rate on single carbon concentration. Then we formulate a model that describes how *B. theta* grows on two carbon sources, both of which could be the product of polysaccharide breakdown.

3.3.1 Monomers

In principle, growth of bacterial cells should be very complicated to describe, and indeed, at some levels it is. Replication of bacterial cells requires hundreds of enzymatic reactions, each described by several parameters such as enzyme turnover rate and Michaelis constants, K_m. The overall reaction rates are then determined by metabolite concentrations, which are a system property. There's no simple way to solve this problem. Yet, measurements of the growth of bacteria limited for nutrients have revealed very simple relationships. One such example is the null model of bacterial growth in simple carbon sources known as Monod growth kinetics,

$$\lambda = \lambda_0 \frac{c}{K_m + c} \qquad \textit{Eq. 3.1}$$

Where λ is the growth rate at substance concentration, c, λ_0 is the saturating growth rate, and Monod constant K_m is the concentration where the growth rate drops to half the maximum.

This equation has been proposed to model bacterial growth and has been found applicable in chemostats and batch culture for a number of organisms. Its form is similar to a Michaelis-Menten enzymatic reaction. In *E. coli* and many other organisms, the Monod constant K_m is typically very low, usually less than 100 μM for glucose (Figure 3.1). But some organisms may have higher values, such as *Mycobacterium tuberculosis*, which has a value of 5 mM which is 1000 times higher than the *E. coli* strain in Figure 3.1 (*70*).

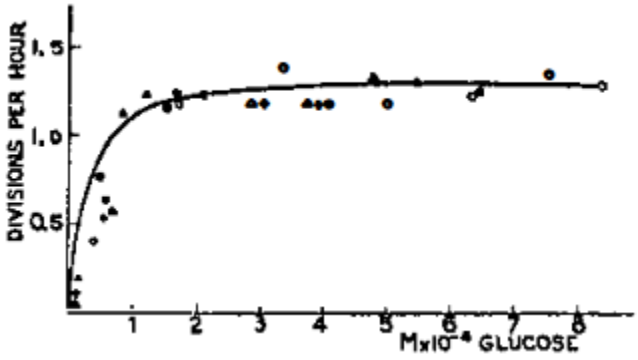

*Figure 3.1 Growth rate of E. coli as a function of glucose concentration. Taken from (*11*)*

We measured the growth rates of *B. theta* as a function of carbon concentration for 10 different sugars in concentrations ranging from 0 to 20 mM. They each exhibited simple exponential growth with different slopes for a range of high optical density in batch culture (plots of curves). Plots of growth rate vs concentration are shown in Figure 3.2. There are a few features of note from these plots. The first is that growth rate apparently reaches a maximum around 0.7/h for most carbon sources (separate bar graph). Additionally, *B. theta* is relatively insensitive to the concentrations of many sugars, with growth rate not saturating until concentrations reach 1 to 10

mM. There also appear to be nonzero sugar concentration thresholds below which yield no growth. For ribose, this phenomenon is abundantly clear with even a few mM not being sufficient for growth. The features of these growth-concentration plots make Monod growth kinetics a poor choice to describe the dependence of growth rate on monomer sugar concentration in *B. theta*.

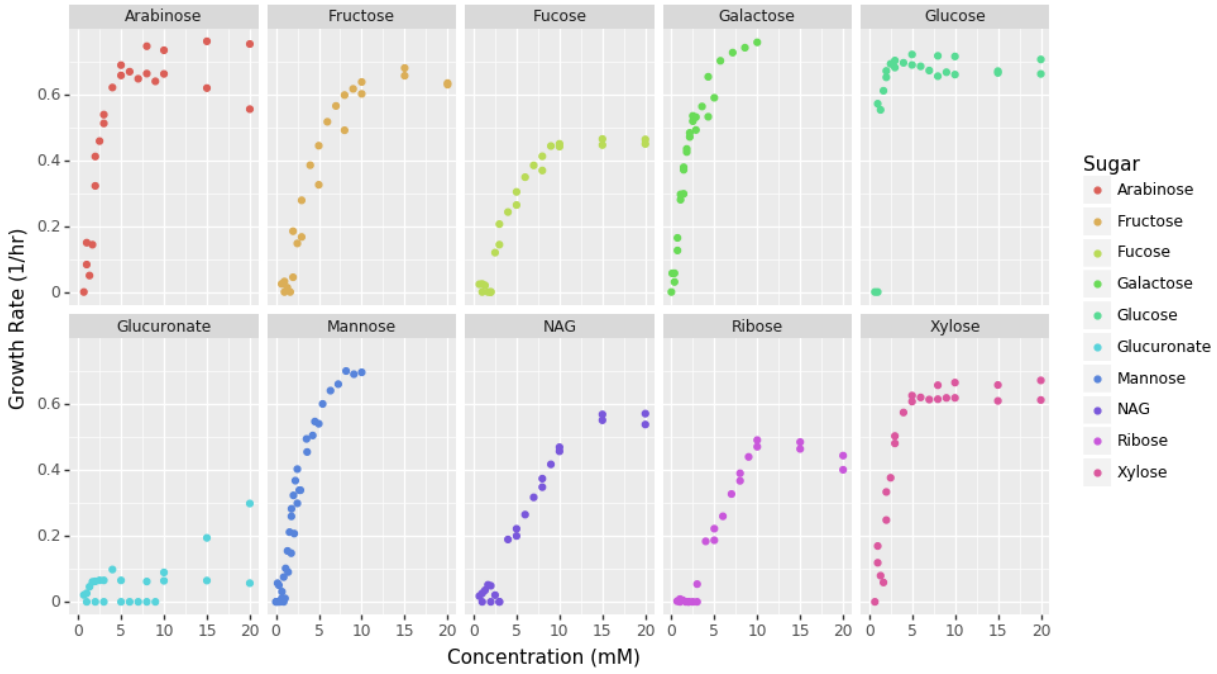

Figure 3.2 Growth of Bacteroides thetaiotaomicron on different monomer carbon sources
Cultures of Bacteroides thetaiotaomicron were grown anaerobically with minimal media. Cultures were incubated and monitored in a Tecan Spark plate reader that was incased in a custom vinyl hood to control gas concentrations. Before putting into the plate reader hood, cells were precultured anaerobically in tubes containing minimal media with 10 mM of the carbon source to be later used in the experimental culture. A 96-well plate was prepared which contained varied concentrations of the carbon sources shown in the figure above. Cells from precultures were diluted into wells with their respective carbon sources. When the whole plate was prepared, the plate was transferred from the anaerobic hood to the plate reader hood. To keep the plate reader hood anaerobic, the gas was exchanged with a gas mixture of 5% H_2, 5% CO_2, and 90% N_2. The hood also contained a palladium catalyst upon which O_2 could react with H_2.

Certain carbon substrates, however, have noticeably lower maximum growth rates, the most extreme of which is glucuronate with a maximum growth rate being around 0.1/h. Glucuronate is notable in that it is a reduced sugar. When fermenting, a reduced sugar has a

different carbon balance in its fermentation products. Therefore *B. theta* has to adjust its metabolism to compensate. We also found that *B. theta* did not support growth on gluconate, another reduced sugar (data not shown). The lack of growth on gluconate could be because gluconate is not likely found associated with polymers or because *B. theta* lacks the Entner–Doudoroff (ED) pathway needed for metabolism of gluconate (*170*, *171*). Additionally, fucose, ribose, and N-acetyl-glucosamine also have reduced maximum growth rates between 0.4-0.6/h, all of which are notable since they converting those sugars into the main glycolytic entry point, glucose-6-phosphate requires multiple reactions.

Another notable feature of these growth rate vs carbon concentration curves is that the concentrations where growth rate is half of the maximal is relatively high at concentrations of up to a few mM. This is quite a bit higher than E. coli's K_m, and the high K_ms are surprising given *B. theta'*s dedication to carbon utilization. Furthermore, there are nonzero concentrations below which *B. theta* doesn't grow. In other words, even though there is carbon in the media, *B. theta* still doesn't appear to have a growth rate.

In order to understand the lack of growth at low carbon concentrations, we can formulate a model that extends the derivation of Monod growth kinetics by considering the contribution of carbon influx to the energy flux is different for *B. theta*. To begin, we start with an expression connecting carbon flux, J, with catabolic enzyme concentration, ϕ_c, and the flux efficiency of those proteins, k_c.

$$J(c, \lambda) = k_c(c) \cdot \phi_c(\lambda) \qquad \textit{Eq. 3.2}$$

where ϕ_c, is expected to depend on growth rate, λ, and the flux efficiency, k_c, is expected to depend on the concentration of the carbon source, c, in the medium. As shown in Appendix C, the growth

rate dependence of the concentration of many catabolic enzymes in *B. theta* are linearly and negatively correlated with growth rate with the form

$$\phi_c(\lambda) = \phi_{max}\left(1 - \frac{\lambda}{\lambda_c}\right) \qquad \textit{Eq. 3.3}$$

where ϕ_{max} is the maximum mass fraction of catabolic enzymes extrapolated to zero growth, and λ_c is the growth rate where catabolic enzyme concentration approaches 0 for the best carbon source. For the flux efficiency of catabolic enzymes themselves, we assume that the expression takes on a Michaelis-Menten-like form

$$\mathrm{k_c(c)} = \kappa_c \frac{\mathrm{c}}{\mathrm{K_c + c}} \qquad \textit{Eq. 3.4}$$

where κ_c is the maximum rate of the catalytic proteins and K_c is the constant that represents the concentration where the catalytic rate is half the maximum.

In order to make progress on Eq. 3.2, we also need to understand how carbon flux changes with growth rate. Therefore, we measured the carbon flux of *B. theta* cultures that have their carbon uptake flux controlled by varying the concentration of mannose in the media (Figure 3.5). We can mathematically describe this data with a line given by

$$J = \sigma(\lambda + \lambda_0) \qquad \textit{Eq. 3.5}$$

where J is the carbon uptake flux, λ is the growth rate, and σ is the carbon yield. We define the term λ_0 as the maintenance growth rate which needs additional explanation. Conceptually, the maintenance growth rate can be thought of as the additional growth that cells could have if the maintenance flux was somehow removed. Alternatively, it can be thought of as the growth rate where half of the flux goes to maintenance, with the other half going to biomass generation.

With this phenomenological description of the flux from Eq. 3.5, we can combine Eq. 3.2, Eq. 3.3, Eq. 3.4, Eq. 3.5 into a new model that predicts the growth rate change

$$\lambda(c) = \frac{c(k_{max} - \lambda_0) - \lambda_0 K_c}{K_c + c\left(1 + \frac{k_{max}}{\lambda_c}\right)} \qquad \textit{Eq. 3.6}$$

where $k_{max} = \kappa_c \cdot \phi_{max}$. Eq. 3.6 describes a vertically-shift Monod growth kinetics. This equation has three effective parameters and has been proposed in the context of other organisms [ref]. Similar to the growth curves of Figure 3.2, the x intercept of Eq. 3.6, is nonzero, being equal to $c^* = \frac{K_c \lambda_0}{k_{max} - \lambda_0}$. The minimum growth concentration, c*, doesn't depend on the gene expression constants, ϕ_{max} and λ_c, instead depending on the maintenance growth rate and parameters related to the catalytic protein sector: the concentration constant, K_c, and maximum rate of the catalytic protein sector, κ_c. In the limit where the concentration of carbon is not limiting, the growth rate is limited by k_{max}, λ_0, and λ_c: $\lambda^{max} = \frac{(k_{max} - \lambda_0)\lambda_c}{\lambda_c + k_{max}}$. These parameter dependances can been seen in Figure 4.6, which shows how Eq. 3.6 qualitatively changes when varied for single parameters.

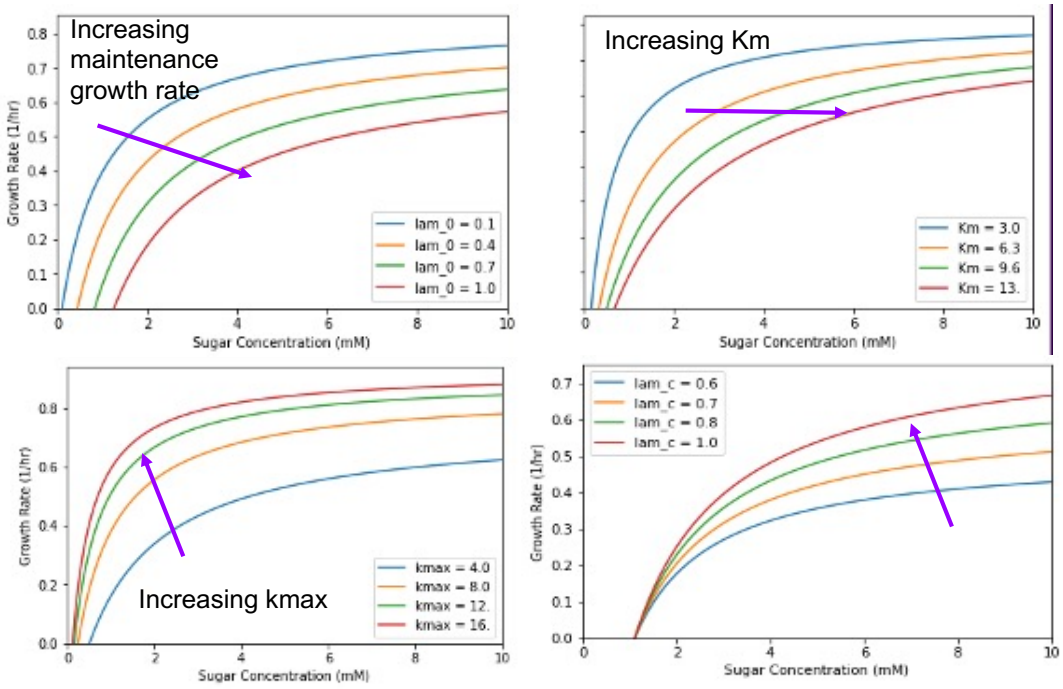

Figure 3.3 Dependence of Eq. 3.6 on model parameters.
Qualitative changes for varied λ_0, K_c, k_{max} and λ_c, respectively.

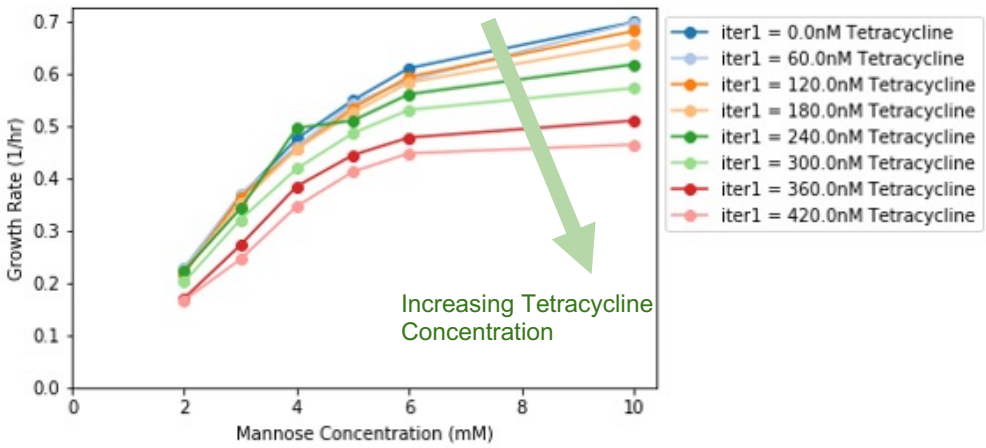

Figure 3.4 Effect of antibiotic on concentration dependence of B. theta growth.
B. theta cultures were grown in steady state with various mannose concentrations from 2 to 10 mM and various concentrations of the ribosome-inhibiting antibiotic tetracycline.

The model of Eq. 3.6 can be quantitatively tested by changing one of the parameters in that equation and checking for quantiative agreement. We perturbed the λ_c parameter by using the translation-inhibting antibioitic, tetracycline. In *E. coli* it was shown that cells respond to these antibiotics by overexpressing ribosomes, thereby reducing the available fraction of the proteome for other proteins and thus reducing λ_c. By measuring the RNA-to-protein ratio, a proxy for ribosome content, we see that these antibiotics also resulted in overexpression of ribosomes. Consistent with this, cells also have their beta-galactosidase activity reduced, which is consistant with a decrease λ_c. In Figure 3.4, we see that the data is consistant with the prediction of Eq. 3.6 for reducing λ_c.

We attempted to change the maintenance growth rate of *B. theta* cultures by adding the proton uncouplers DNP and CCCP. However, these uncouplers were surprisingly ineffective even at high concentrations. This failure might be due to the peculularities in the electron transport chain of *B. theta*, which differ from other bacteria because they do not use protons in their electron transport chain (*110*). Changing κ_c and K_c would require genetic perturbations of relevant transporters, and are currently not implementable

3.3.2 A phenomenological model describing growth on two carbon substrates

B. theta's main food source is polysaccharides, which are long chains of different monomers, most often a sugar such as glucose, galactose or arabinose. In order to consume these polysaccharides, they must be broken down into smaller units by carbohydrate-active enzymes which are unique to each glycosidic bond. One of the simplest polysaccharides is starch, which consists only of glucose monomers. But the glucose monomers are bonded together by one of two bonds. And so, a unique enzyme is required to break down each of these bonds. Additionally, part of polysaccharide degradation begins during import from the extracellular environment to the periplasm of oligomers of 1-8 monomers long, which are then degraded in the periplasm or cytoplasm (*172*). Other examples of polysaccharides include inulin, which is a polymer of mostly fructose plus some glucose, and arabinogalactan, a polymer of arabinose and galactose (*173*, *174*).

Several theories of carbon uptake have been developed. One such study found that carbon flux is mediated by protein expression, with cells that are carbon starved, upregulating carbon utilization proteins (*74*). *E. coli* can consume multiple carbon sources and indeed seems to benefit in the sense that consuming two carbon sources allows for cells to take advantage of common protein sectors (*74*). Growth of *B. ovatus* on multiple carbon sources has been observed (*174*).

Our measurements of *B. theta*'s physiology shows that it violates a key assumption of past work, namely that growth rate is directly proportional to carbon flux since there is a clear offset in the y-intercept (*74*) (Figure 3.5). Such offsets have been observed before and have been termed "maintenance flux" (*72*, *175*). Maintenance flux is defined by exclusion. It's the sugar flux that is not associated with biomass accumulation. It appears to be roughly constant.

In order to understand how flux affects growth rate, we consider a model that describes the relationship between flux and growth. Consider the growth rates, λ_1, λ_2 for two carbon sources. Similar to Eq. 3.5, the growth rates and carbon fluxes for carbon source i will be related by

$$J_i = \sigma(\lambda_i + \lambda_0) \qquad \textit{Eq. 3.7}$$

where J_i is the uptake flux of the carbon source i, λ_i is the growth rate for carbon source *i*, σ is the conversion factor between flux and growth rate, equivalent to the biomass yield, and λ_0 is the maintenance growth rate (*27*, *72*, *74*). The relationship (Eq. 3.7) between flux and growth rate differs from (*74*) by the inclusion of the maintenance growth rate, λ_0. The product $\sigma \cdot \lambda_0$ is equivalent to maintenance flux and so this maintenance growth rate, λ_0, is a derived term from the growth associated biomass yield. We can fit Eq. 3.7 to our data of *B. theta*'s flux and growth rate as shown in Figure 3.5.

Eq. 3.7 relates growth rate and uptake flux for a single carbon source. But we are interested in how growth rate depends on two carbon sources. We rearrange Eq. 3.7 to find a formula for the growth rate, λ, as a function of total carbon flux, J_{tot}

$$\lambda = \frac{J_{tot}}{\sigma} - \lambda_0 \qquad \textit{Eq. 3.8}$$

where the other parameters are the same as defined above. We note that we define the biomass yield, σ, as independent of the carbon source. This assumption will hold for sugars that interconvert without a major change in energy, such as would be the case for glycolytic carbons. For two carbon sources, Eq. 3.9 can be rewritten more explicitly as

$$\lambda_{12} = \frac{J_1}{\sigma} + \frac{J_2}{\sigma} - \lambda_0 \qquad \textit{Eq. 3.9}$$

where λ_{12} is the growth rate on combined carbon sources 1 and 2.

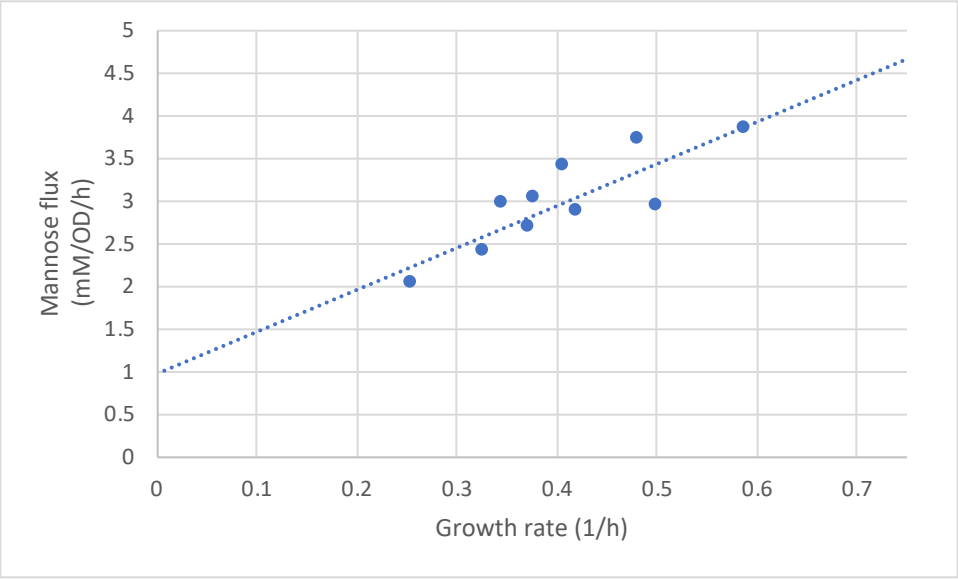

Figure 3.5 Sugar uptake flux in B. theta as a function of growth rate
Growth rates in B. theta were titrated by varying mannose concentration in the media. Mannose flux is the product of mannose uptake and growth rate. Mannose uptake was measured by calculating the slope of mannose concentration vs OD for an exponentially growing culture.

We next turn to the question of what controls the carbon fluxes themselves. Previous work has shown that the expression levels of catabolic proteins are linearly correlated with the growth rate for carbon limited cultures (*14*, *74*)

$$E_i(\lambda) = E_i^{max}\left(1 - \frac{\lambda}{\lambda_c}\right) \qquad \textit{Eq. 3.10}$$

where E_i is the mass fraction abundance of catabolic proteins for carbon source i, E_i^{max} is the proteome concentration dedicated to carbon source i as growth rate approaches 0, λ_c is the intercept where the enzyme expression goes to zero, which is the same for different carbon sources. We validate this assumption in *B. theta* with two methods. By measuring the beta-galactosidase in carbon limited growth (Figure 3.6), we see that for different carbon sources, the beta-galactosidase activity is anticorrelated with the growth rate as expected with a λ_c of around 0.8/h. By measuring the protein abundances of catabolic proteins with proteomics (*58*), we find that this correlation for abundance holds for multiple catabolic proteins (Appendix C).

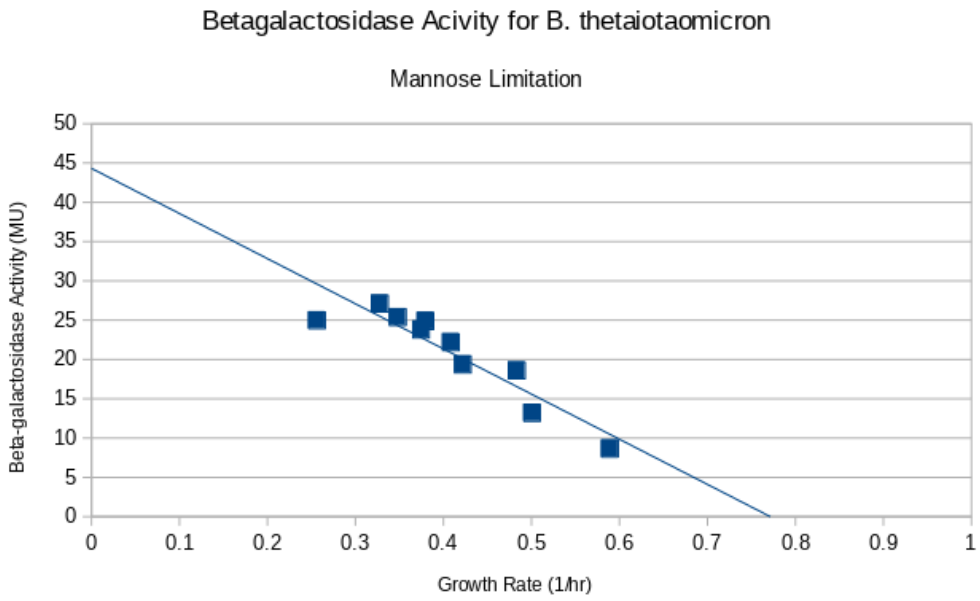

Figure 3.6 Beta-galactosidase activity as a function of growth rate.
*B. theta was grown in minimal media with growth rate reduced by controlling the initial concentrations of mannose. While the cells were still in exponential growth, samples were collected to measure beta-galactosidase activity as in (*14*,* 176*).*

To relate catabolic enzyme abundance with carbon uptake flux, we assume that carbon flux is proportional to the abundance of catabolic proteins.

$$J_i = k_i \cdot E_i \qquad \textit{Eq. 3.11}$$

where k_i is the overall turnover rate for the catabolic enzymes for carbon source i. By combining Eq. 3.11 and Eq. 3.10, and Eq. 3.7 we find that for carbon source i

$$\frac{k_i E_i^{max}}{\sigma} = \frac{\lambda_i + \lambda_0}{1 - \frac{\lambda_i}{\lambda_c}} \qquad \textit{Eq. 3.12}$$

Furthermore, we can derive a similar equation for the combined growth rate using Eq. 3.9 and Eq. 3.11

$$\frac{\lambda_{12} + \lambda_0}{1 - \frac{\lambda_{12}}{\lambda_c}} = \frac{k_1 E_1^{max}}{\sigma} + \frac{k_2 E_2^{max}}{\sigma} \qquad \textit{Eq. 3.13}$$

Combining Eq. 3.12 and Eq. 3.13 yields

$$\lambda_{12} = \frac{\lambda_1 + \lambda_2 - \frac{2 \cdot \lambda_1 \cdot \lambda_2}{\lambda_c} + \lambda_0 \cdot \left(1 - \frac{\lambda_1 \cdot \lambda_2}{\lambda_c^2}\right)}{1 - \frac{\lambda_1 \lambda_2}{\lambda_c^2} + \frac{\lambda_0}{\lambda_c}\left(2 - \frac{\lambda_1 + \lambda_2}{\lambda_c}\right)} \qquad \textit{Eq. 3.14}$$

where the variables are the same as has been described above. In the limit where the maintenance flux, λ_0, approaches 0, our result is the same as (*74*). Another notable feature of Eq. 3.14 is that λ_{12} can be positive even if the individual growth rates, λ_1 and λ_2, are equal to or less than zero. Specifically for the case where both individual growth rates are zero, the combined growth rate is

$$\lambda_{12}(\lambda_1 = 0, \lambda_2 = 0) = \frac{\lambda_0}{1 - 2\frac{\lambda_0}{\lambda_c}} \qquad \textit{Eq. 3.15}$$

which depends only on, λ_0, and λ_c. This occurs because, while the individual fluxes of sugars alone aren't sufficient to supply the maintenance flux, the two fluxes added together are sufficient. The super additivity of the growth rates is seen in Figure 3.7a, where for low growth rates, the combined growth rates are greater than the sum of the growth rates (shown by the red line). We also find that the predictions of Eq. 3.14 fits well with the measured growth rates (Figure 3.7b).

The super additivity of growth rate means that *B. theta* benefits from being able to incorporate multiple carbon sources at the same time even if their concentrations are low. *B. theta*'s ability to digest a diverse set of polysaccharides therefore likely complements the constrain put on *B. theta* by its high maintenance flux. Future work on this project will involve generalizing *B. theta*'s growth on multiple carbon sources to full polysaccharides (Figure 3.8). Specifically, it is not known if disaccharides (such as maltose) can complement monomers (such as glucose). If they can complement each other, then this will help *B. theta* maintain high enough growth rates to easily overcome the maintenance flux.

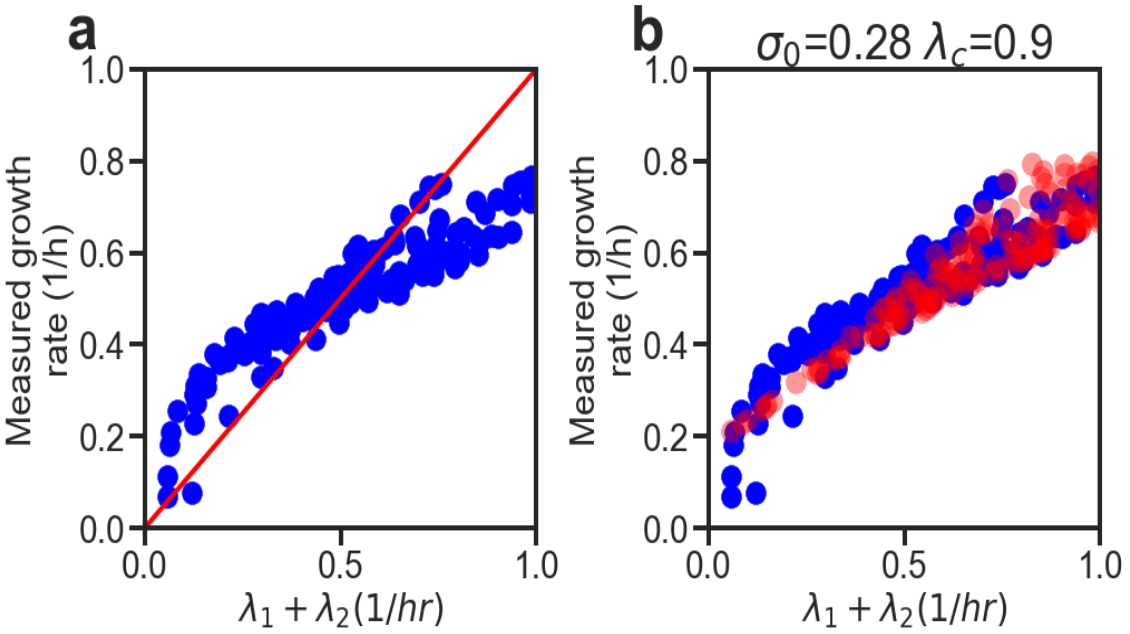

Figure 3.7 Growth rate addition for growth on mannose and galactose.
Cultures of B. theta were grown in various concentrations of mannose and galactose. X-axis represents the growth rates of cultures on mannose (without galactose) plus the growth rates of cells cultures on galactose (without mannose). Y-axis shows measured growth rates for cultures growing on a combination of mannose and galactose. a) The red line represents if the measured growth rate equaled the sum of the two individual growth rates. b) Red dots represent predicted values based on Eq. 3.14.

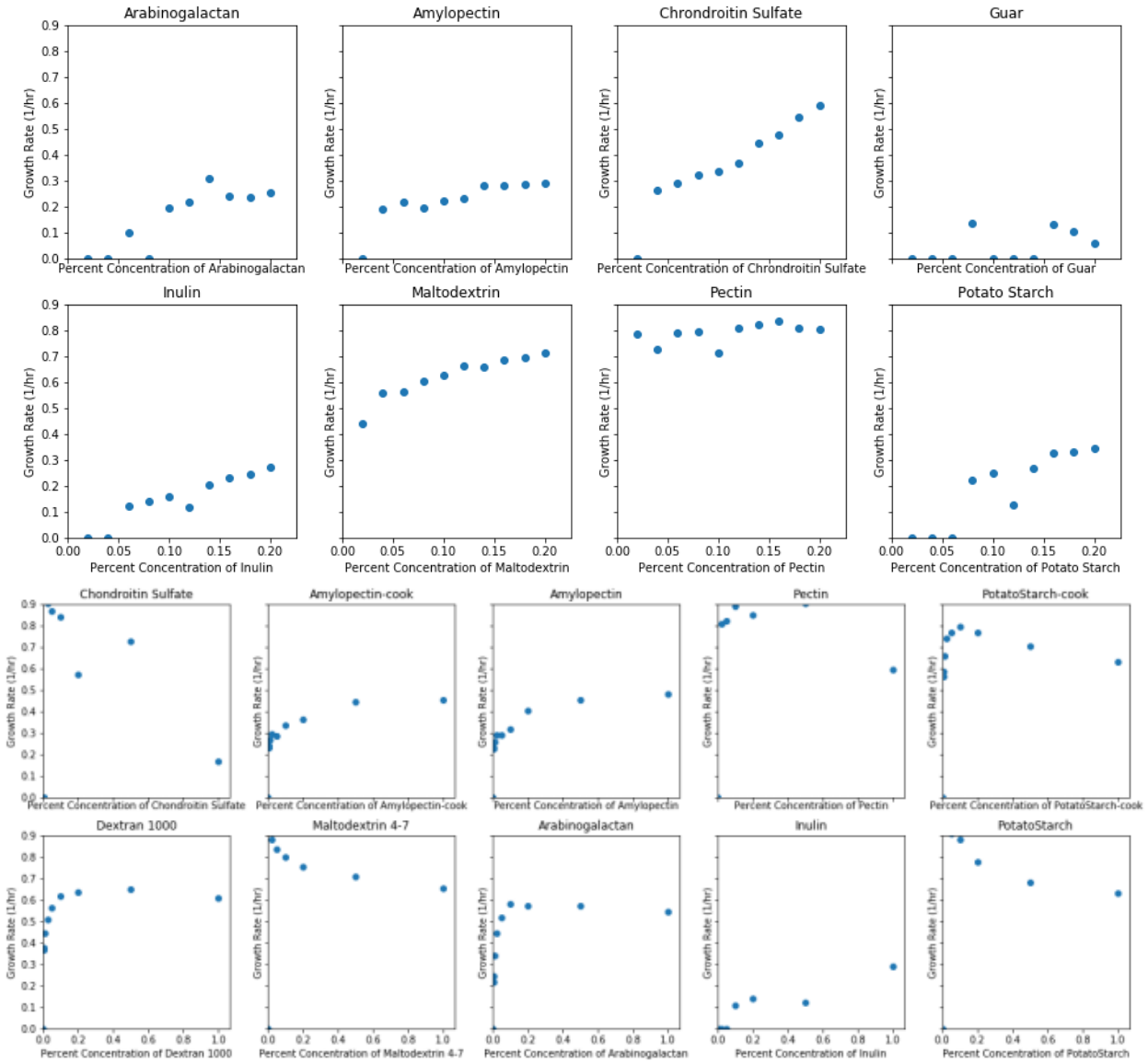

Figure 3.8 Growth of Bacteroides thetaiotaomicron on different polymers
Cultures of B. theta were grown in various concentrations of polysaccharides.

3.4 Methods

3.4.1 Growth of cells

The phosphate-based growth media contained 20 mM glucose, 10 mM NaCl, 10 mM NH_4Cl, 0.5 mM Na_2SO_4, a phosphate buffer and a 1000x micronutrient solution. The 1000x micronutrient solution contained 20 mM $FeSO_4$, 500 mM $MgCl_2$, 1 mM $MnCl_2{\cdot}4H_2O$, 1 mM $CoCl_2{\cdot}6H_2O$, 1 mM $ZnSO_4{\cdot}7H_2O$, 1 mM $H_{24}Mo_7N_6O_{24}{\cdot}4H_2O$, 1 mM $NiSO_4{\cdot}6H_2O$, 1 mM

$CuSO_4 \cdot 5H_2O$, 1 mM SeO_2, 1 mM H_3BO_4, 1 mM $CaCl_2$, and 1 mM $MgCl_2$ dissolved in a 0.1 N HCl solution. The proportion of K_2HPO_4 and KH_2PO_4 was used at different proportions with the total concentration summing to 100 mM and set the initial pH to 7.4 The medium also included 2 mg cyanocobalamin, 2 mg hemin, and 0.6 cysteine per liter. To make the media anoxic, Hungate tubes (16 mm x 125 mm) filled with 7 mL medium were shaken at 270 rpm under a 7% CO_2, 93% N_2 atmosphere pressurized to 1.5 atm for 75 minutes. Cultures were transferred anoxically into Hungate tubes with disposable syringes.

Anerobic growth in plate reader was performed with a Tecan Spark microplate reader enclosed in a custom vinyl anaerobic chamber. Chamber was kept anaerobic with palladium catalysts and an input gas of 5% H_2, 10% CO_2, and 85% N_2. Oxygen levels were monitored with the Tecan Spark O_2 and CO_2 module to ensure the chamber stayed anaerobic during growth.

3.4.2 Beta-galactosidase activity

Samples of exponentially growing cultures in Hungate tubes were sampled at different ODs. Samples were removed anoxically using syringes. The contents of the syringes were added to 1.5 mL Eppendorf tubes and frozen on dry ice. Beta-galactosidase assay was then performed as in (*14*).

3.5 Acknowledgements

Chapter 3, in part, is currently being prepared for submission for publication of the material. Brian R. Taylor, Vadim Patsalo, James R. Williamson, Terence Hwa, 2022. The dissertation author was the primary author of this paper.

Chapter 4

Tradeoff between energy efficiency and protein synthesis rate mediated by pyrophosphate

4.1 Abstract

Pyrophosphate (PP_i) is a metabolic intermediate found in all domains of life (*92*, *98*, *105*). Despite its ubiquity, many organisms treat it as a waste product, degrading the molecule into phosphate (*91*, *177*). However, some organisms use PP_i as a substitute for the energy carrier ATP (*107*). *B. theta* has multiple enzymes that fulfill this role (*82*). Here, we find that depriving *B. theta* of PP_i significantly decreases its yield, supporting PP_i's role as an energy substitute. However, this benefit of PP_i also comes at a cost as we also find increasing PP_i concentration in growing *E. coli* cells reduces their ribosomal elongation rate. We propose such a cost-benefit tradeoff underlies why many organisms do not take advantage of the free energy benefit provided by substitution of ATP with PP_i.

4.2 Contribution of pyrophosphate to yield

One of the challenges that anaerobic organisms face is that they have significantly reduced carbon yield compared to aerobic organisms. Aerobes, when utilizing a carbon source such as glucose or mannose, can efficiently turn that carbon source into biomass because the energy they need to build biomass is readily obtained when there is oxygen available to run the electron transport chain. On the other hand, anaerobes, which by definition do not use oxygen, cannot rely

on the electron transport chain without an alternative electron acceptor. The amount of energy that can be extracted from sugars via fermentation without oxygen is limited.

For *E. coli*, a facultative anaerobe that can growth with or without oxygen, the difference in extractable energy can be quite drastic; the ATP yield from one glucose molecule drops an order of magnitude from 20-30 ATP to 2-3 ATP (*6*). The reduced yield of ATP means that to meet the energy demand for biomass growth, cells must use more sugar, producing more waste products including CO_2, acetate, and others (*6*) (Figure 4.1a). When measuring the yield of biomass relative to glucose taken up, it drops 2.5 to 3-fold from 0.17 OD_{600}/mM glucose (aerobic) to 0.07-0.05 OD_{600}/mM sugar (Figure 4.1b purple and red circles respectively). The drop in biomass yield is not as high as the drop in ATP yield because a significant proportion of total carbon taken-up goes to biomass.

In contrast to anaerobic *E. coli*, *B. theta* has a high carbon yield when grown anaerobically. *B. theta*'s yield was found to be about 2x higher than anaerobic *E. coli* ranging from 0.15 to 0.10 OD_{600}/mM sugar (Figure 4.1b blue circles). To check if the difference in yield was due to biomass composition, we measured the biomass abundance of RNA, protein, and glycogen, which make up about 80-90% of cell biomass. While RNA and protein were fairly similar between the two organisms, the biomass of *B. theta* was made up of up to 20% glycogen (Table 4.2) compared to negligible amounts for E. coli. While glycogen is energetically cheaper to produce compared to RNA and protein, this amount of glycogen cannot explain the 2x difference in yield, especially as the yield difference persists even in conditions where glycogen is low. Notably, it's also been found that *B. theta* has a higher yield compared to fellow gut resident, *Agathobacter rectalis* (*39*).

It's been previously observed that there are specific energy saving features in the central metabolism of *Bacteroides*. Based on yield measurements, the ATP yield of *Bacteroides fragilis*

has been measured to be as high as 4.5 ATP/glucose, which is higher than anaerobically-grown *E. coli*'s estimated 2-3 ATP/glucose (*110*). This high ATP yield was dependent on the availability of hemin, as without hemin the ATP yield was estimated to be 1.7 ATP/glucose. The hemin allows cells to ferment glucose to a mixture of acetate, propionate, and succinate. Without the hemin, cells produce a mixture of lactate and acetate. Therefore, succinate and propionate production are important to maintaining high yields for *Bacteroides*. It's been suggested the pathway involved in propionate and succinate production allows for increased ATP yield based on three mechanisms (*7*). One is the presence of PEP carboxykinase, which allows for high energy phosphate from PEP to be used to form ATP when making oxaloacetate. This oxaloacetate can then be reduced to succinate and propionate via a membrane-bound cytochrome b and fumarate reductase, which may also produce additional energy (*7*, *110*). The third mechanism is the substitution of ATP for PP_i when phosphorylating fructose-6-phosphate. Such a mechanism would increase yield by reducing the amount of ATP used in glycolysis by one, which is a significant savings in this context as this would mean that only one ATP is used to fuel glycolysis instead of two. However, such a mechanism requires that there be a sufficient PP_i flux available.

The details of PPi flux availability are discussed in Appendix D. In short, *B. theta* appears to have excess flux of PPi available when grown in rich media conditions because having amino acid precursors available reduces the amount of PPi that *B. theta* needs. When cells are grown in minimal media, there is a net deficit of PPi, which suggests that *B. theta* has to have some additional source of PPi or make up for the deficit with ATP-utilizing enzymes. Therefore, PPi appears to be produced in sufficient amounts to alter the yield in *B. theta*.

To test if PP_i provides a significant contribution to the yield of *B. theta*, we performed some genetic modifications to perturb pyrophosphate flux. We added two different genes to *B. theta*

using a transposon-based insertion vector with the genes controlled by the *ptet* promoter (*178*). The first gene added was a pyrophosphate hydrolase from *E. coli*. This enzyme catalyzes the hydrolysis of PP_i to two phosphate ions. *B. theta* does not have a known native pyrophosphate hydrolase. Expression of this gene is expected to cause "wasteful" leakage of pyrophosphate so that there is less pyrophosphate available to replace ATP. The second gene added was *pfp* from *E. coli*. *B. theta* does have this gene in the wild type, but it appears to be expressed at a much lower level compared to pyrophosphate linked version (Appendix C). The purpose of adding this gene was to compete with the wild-type *B. theta* pyrophosphate linked phosphofructokinase so that PP_i could not be effectively utilized as an alternative source of phosphate to ATP in the phosphorylation of fructose-6-phosphate.

4.3 Tradeoff of pyrophosphate

4.3.1 Free energy consideration

While we and others have been able to establish that PP_i has a clear benefit to cells, the lack of universal adoption of PP_i as an energy source suggests that PP_i has a hidden cost. One obvious but weak cost of using PP_i as an alternative to ATP is that the standard free energy of PP_i hydrolysis is much lower than that of ATP (Figure 4.3) (21.6 kJ/mol vs 32.5 kJ/mol), which would reduce utility of PP_i as a driving force. It's likely the case that PP_i is in thermodynamic equilibrium since PP_i concentration can't be reduced from physiological levels by increasing pyrophosphatase activity in bacteria (*91*, *179*, *180*).

However, the actual free energy of a reaction can differ from the standard free energy within a physiological context since the free energy depends on the concentrations of the substrates and products in those hydrolysis reactions (*181*). However, PP_i and ATP hydrolysis share some products and substrates: phosphate and protons. So, while decreasing P_i concentrations increases the free energy for PP_i hydrolysis, the same also happens for ATP; the effects are not independent.

A decrease in P_i concentration will increase both the free energy of both PP_i hydrolysis and ATP hydrolysis. Similarly perturbing proton concentration, or pH, will have similar effects for both the PP_i and ATP hydrolysis reactions. For the hydrolysis of PP_i, increasing PP_i concentration increases the free energy independently of the ATP hydrolysis reaction.

Although we use hydrolysis as an example to illustrate the free energy difference between PP_i and ATP, the hydrolysis of these substrates will similarly be coupled to the concentrations of various metabolites that participate in these reactions. In this same vein, certain reactions may not involve the same substrates and products as the hydrolysis reactions described here. For example, afree phosphate may not be involved in a reaction if the phosphate is used to phosphorylate some molecule. Controlling the concentrations of these reactants and products gives cells using PP_i another way to perturb the free energy of specific reactions.

4.3.2 Effect of PP_i on enzymes

For cells that want to maintain a high free energy of PP_i, the relative concentrations of PP_i must also be kept high. But what are the consequences of high PP_i? It's known that high PP_i concentrations can negatively affect cell growth (*91*). While much has been discussed biochemically about the role of PP_i on various different reaction kinetics, it's not clear which of those reactions are affecting cell growth.

One observation of growth in *B. theta* is that translation appears to be inhibited compared to *E. coli*. The evidence for this comes from the relative ribosome levels between the two organisms. Ribosome content is linearly correlated with growth rate when that growth rate is controlled by quality of nutrients such as carbon or nitrogen source (*59*). The slope of the linear correlation is related to the speed of translational elongation. For a given growth rate, cells with slower translating ribosomes have higher levels of ribosomes (*61*, *182*). Figure 4.4 shows the mass

fraction of ribosomes in *E. coli* for anaerobic and aerobic conditions, with growth rate limited by carbon uptake. For both conditions, ribosome content is linearly correlated with growth rate, having a positive slope. Similarly for *B. theta* limited by carbon, there is also a linear correlation. However, in contrast to *E. coli*, the slope for *B. theta* is noticeable steeper. The steeper slope suggests that the ribosomes of *B. theta* cells are translating at slower rates, particularly for faster growth.

The ribosomal mass fraction data suggests that *B. theta* has slower translating ribosomes. However, it's unclear if PP_i can directly inhibit translation rate in growing cells. To explore this possibility, we use *E. coli* as a model organism to study the effects of PP_i on translation rate.

In *E. coli*, it's possible to increase the concentration of PP_i by titrating the levels of the PP_i hydrolase, *ppa* (*91*). In our construct (HE750), control of *ppa* was placed under the ptet promoter (Figure 4.5above). The ptet promoter can be controlled by titrating the inducer for the promoter, choro-tetracycline (cTc). By titrating cTc, we were able to reduce the growth rate down to zero from wild type growth rate (Figure 4.5a). The decrease in growth rate was accompanied by an increase in PP_i concentrations (Figure 4.5b teal circles) ranging from 1 mM to 8 mM. In contrast, the PP_i concentration of WT cells whose growth rate was decreased by limiting carbon uptake stayed below 1mM, consistent with previous measurements of PP_i in *E. coli* (Figure 4.5b black circles) (*177*, *180*).

Since we are able to control PP_i with this method, we can investigate how PP_i concentration affects ribosomes by measuring the translational elongation rates in growing cultures (*61*, *183*, *184*). Translational elongation rates can be measured by measuring the length of time it takes for cultures to synthesize a protein after that protein is induced. In our case, we induce β-galactosidase activity from the lac promoter by addition of isopropyl ß-D-1-thiogalactopyranoside (IPTG) to

exponentially growing cultures (Figure 4.6a). There is an initial lag with no change in activity, followed by an increase in activity that scales with time like t^2 (*183*). The time it takes to produce the first molecule, T_{init} can then be calculated by projecting back from the square root of the change in activity (Figure 4.6b).

Consistent with PP_i inhibiting translational elongation rate, we find that translational elongation rate decreases as PP_i increases (Figure 4.7a teal circles). In a condition with 4 mM PP_i, the translation elongation rate is decreased two-fold from 16 aa/s to 8 aa/s. This decrease in translational elongation rate is substantial as slow growing cells that are nutrient limited still maintain translational elongation rates near 12 aa/s for intermediate growth rates while the translational elongation rate for *ppa* titration cultures decreases to 8 aa/s for a similar growth rate (Figure 4.7b).

The reduction in translational elongation rate due to increased PP_i concentration is consistent with the hypothesis that PP_i is inhibiting tRNA charging. Looking at how translational elongation rate decreases with growth rate, we see that the decrease is similar to fusidic acid treatment and osmotic stress (Figure 4.7b) (*61*, *185*). Fusidic acid inhibits translational elongation by preventing rapid turnover of elongation factor G (EF-G) from the ribosome by binding to the EF-G-ribosome complex (*186*, *187*). Fusidic acid slows down translation by acting reversibly, inhibiting translation by slowing down elongation, which differs from other translation inhibiting antibiotics that act irreversibly, such as tetracycline or chloramphenicol by nearly completely stalling ribosomes (*61*). In hyper-osmotically stressed cells, there is also a near linear decrease of translational elongation rate with growth rate. While an exact mechanism of action has not been found for this decrease, a coarse-grained study suggests that this decrease is due to charged tRNA availability, which become diffusion limited in the crowded hyper-osmotic environment (*185*).

These similarities to hyper-osmotic stress and fusidic acid stress are in contrast to other translation rate inhibiting antibiotics, such as chloramphenicol or tetracycline, which inhibit translational synthesis by stalling individual ribosomes. For these antibiotics, the inhibition of ribosomes inactivates individual ribosomes on long timescales, leading to a low active ribosome fraction. By measuring RNA/protein ratio of PP_i stressed cells (Figure 4.7c), and calculating active ribosome fraction, we find that the active ribosome fraction remains fairly high (Figure 4.7d). The ribosomes that avoid being stalled for these antibiotics have translation rates that are faster, despite the slower overall synthesis, which is also inconsistent with the behavior of translation rate at reduced growth rate for the *ppa* titration (Figure 4.7b) (*61*).

4.4 Discussion

The results presented here support two opposing roles for PP_i in *B. theta* cells (Figure 4.8). The first is that PP_i supply is necessary for *B. theta* to maintain its relatively higher yield since it's possible to reduce the carbon yield of *B. theta* by reducing the available PP_i flux by either adding a protein to hydrolyze PP_i or bypass its utilization in glycolysis. Furthermore, through experiments in *E. coli*, we've shown that high concentrations of PP_i inhibit ribosomal protein synthesis by decreasing translational elongation rate, likely because tRNA charging is inhibited. To our knowledge, this is the first study showing that PP_i has a physiological cost on growing cells, specifically through inhibiting translation rate.

Rate-yield tradeoffs are common in organisms (*27*, *188*, *189*). Evolved strains of *E. coli* show a rate-yield tradeoff (*175*). Yet it's surprising that *B. theta* would sacrifice translation rate given its ability to consume diverse sources of carbon that are readily available in the gut. It's also been noted that other organisms with plenty of access to sugar also use PP_i (*92*).

Why would *B. theta* put so much effort into maintaining high yield when ignoring yield could be beneficial? For example, we can see that the growth rate of *E. coli* is higher than that of

B. theta. That means that when in competition for the same food source, *E. coli* would outcompete *B. theta*. In principle, a mutant of *B. theta* could evolve to grow faster while sacrificing yield. Being stingy doesn't help if they can't grow fast enough to survive.

While the ecological relevance of increasing yield is not always clear, there is at least one problem that anaerobic organisms face when growing at high densities: inhibition from their own fermentation products. Increasing yield is synonymous with decreasing excreted organic acids. As long as the carbon source is completely consumed, an increased amount of carbon going into biomass means that less carbon goes into fermentation acids. It's been previously reported that *Bacteroidetes* are significantly more inhibited by SCFA stress than their *Firmicutes* competitors. Therefore, the protein synthesis tradeoff may be acceptable because they avoid inhibiting themselves. In essence, the benefit of high yield isn't necessarily the growth of more cells but reduced waste. Such a mechanism of action may allow *B. theta* and other *Bacteroides* to stably establish themselves within their niche (*190*, *191*).

The rate-yield tradeoff may also have to do with complexity of carbon sources in the gut. Given that protein expression is limited by a set fraction (*59*), limiting the rate of one sector of enzymes may be useful if the rates of flux are constrained (*27*). Since many *Bacteroides ssp.* express large hydrolases on their membranes, membrane space itself may be limiting. Therefore, increasing yield reduces the amount of carbon that's required for growth, which allows for more growth even with the same amount of flux. If there are tradeoffs to pyrophosphate utilization, the theory that PP_i exists today as a fossil is untenable. Given that horizontal gene transfer is so prevalent in microorganisms, transfers of single genes that are beneficial to organisms should be stably maintained within the population, outcompeting the bad genes.

It's also interesting to note that many gut bacteria appear to have a dependence on amino acids for their growth, given our finding that supplemental amino acids positively affect the PP_i supply. Even *B. theta* requires cysteine as a sulfur source for fast growth, if it uses hydrogen sulfide as a sulfur source it grows slowly. In general, the more glycolysis required for growth, the more strained the PP_i supply will be since the PP_i supply is limited by the relative to the amount of macromolecule biosynthesis. This limits the usefulness of PP_i to a certain range of yields. If ATP yield is too high, like with aerobic growth, PP_i may be costly to keep at high concentrations because it could inhibit translation. If ATP yield is too low, then the amount of PP_i produces from macromolecule synthesis won't be enough to supply glycolysis. A low ATP yield may be overcome slightly by being provided a supply of amino acids, but those amino acids may not always be available. It seems then that *B. theta* operates in a goldilocks zone, with *B. theta* trying to keep its yield higher that 2 ATP per glucose so that there's enough PP_i to go around.

Our study as it stands has some limitations. All of the work on translation rates was done in E. coli. While we do see that *B. theta* does have higher levels of ribosomes for similar growth rates as *E. coli*, we don't know if this difference in ribosomes represents a difference in translational elongation rate. Furthermore, even if *B. theta* does have a reduced translational elongation rate, we would need to show that changing the PP_i pool also changes translation rate.

4.5 Figures

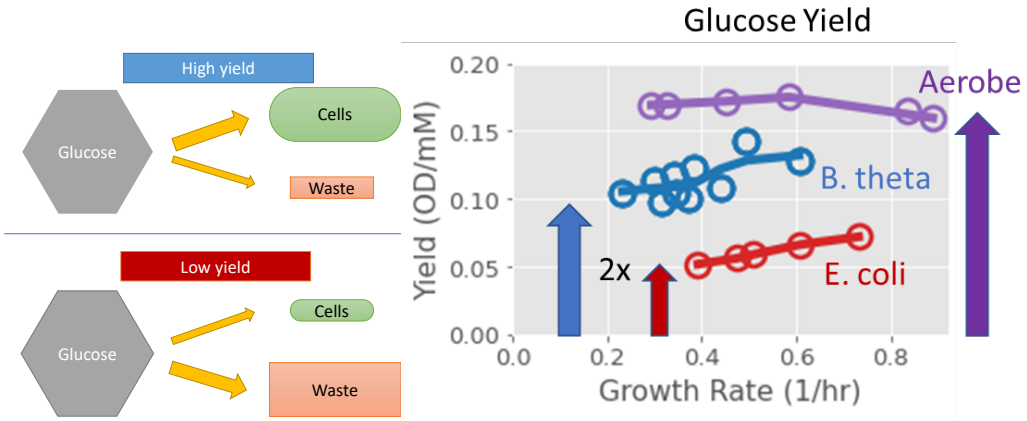

Figure 4.1 Yield of B. theta compared to E. coli.
Cultures were grown in minimal media. B. theta was grown in minimal media with varying mannose concentrations to reduce growth rate. E. coli cultures were grown in minimal media either aerobically or anaerobically. Growth rate was reduced by titrating expression of the glucose transporter ptsG (27). During exponential growth, samples were taken at various ODs and glucose concentrations in the medium were determined using HPLC. Slope of the best-fit lines of the remaining concentrations vs OD give the glucose yields. Yield on glucose, obtained as $Y = -\frac{1}{s}$*, is plotted against the growth rate of the culture.*

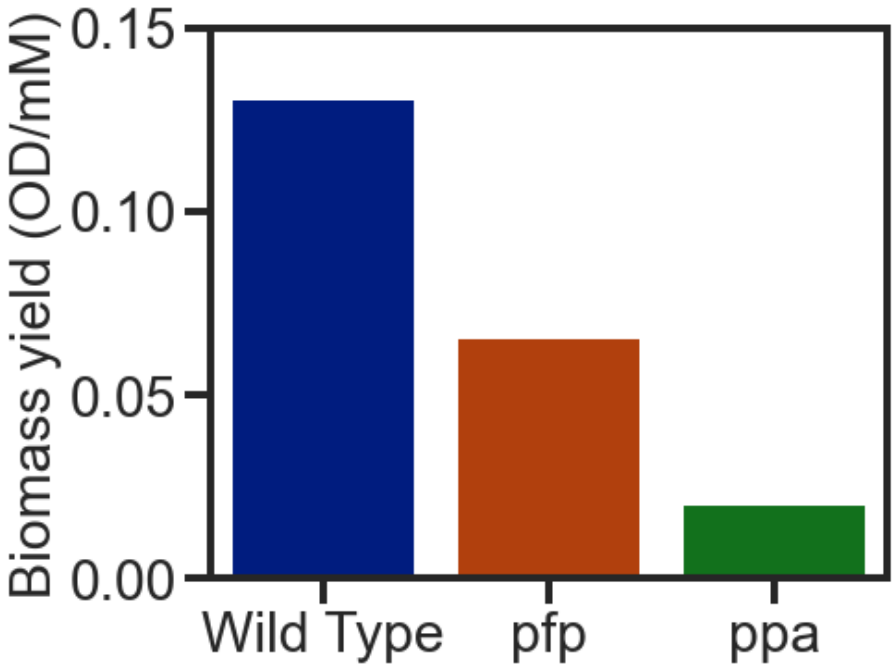

Figure 4.2 Change in yield from PP_i *flux perturbation.*
*Yield was measured based on the final OD of B. theta cultures grown in rich media with 3 mM glucose after 14 hours of incubation. The two genetically modified strains consist of the pfkA and ppa genes from E. coli with a constitutive synthetic promoter which were inserted into the chromosome of B. theta (*178*).*

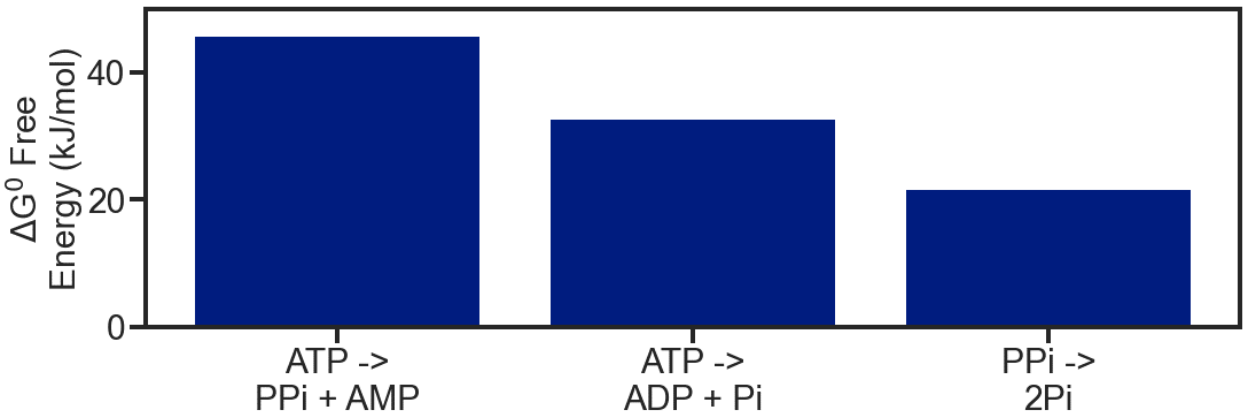

Figure 4.3 High energy phosphate bond free energies.
The standard Gibbs free energy changes for hydrolysis of ATP to AMP, ATP to ADP, and PP_i to phosphate are taken from (75).

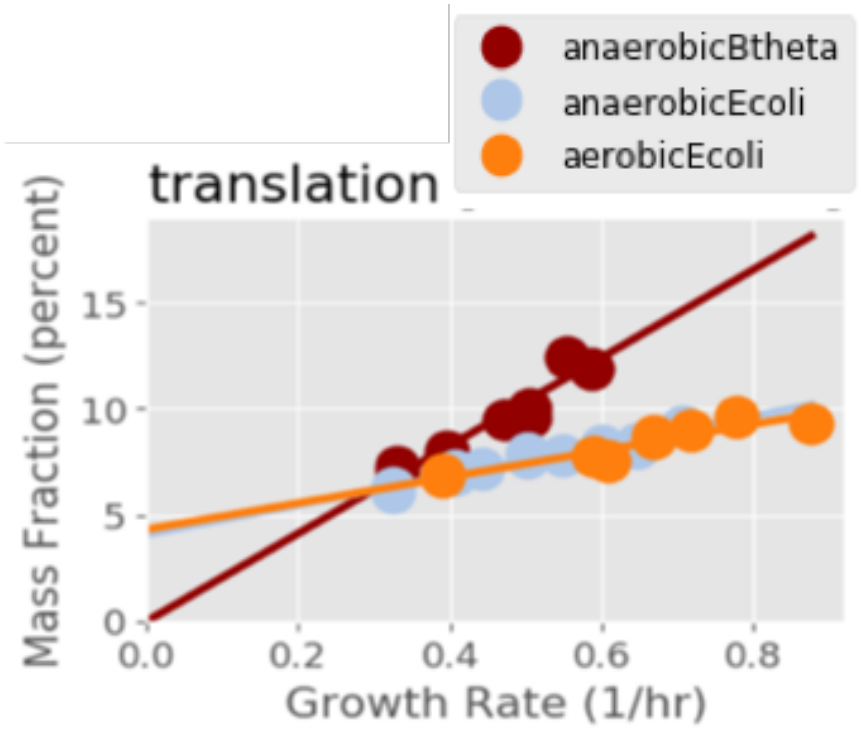

Figure 4.4 Translation gap in B. theta.
Cultures were grown in minimal media. B. theta was grown in minimal media with varying mannose concentrations to reduce growth rate. E. coli cultures were grown in minimal media either aerobically or anaerobically. Growth rate was reduced by titrating expression of the glucose transporter ptsG (27). Samples of exponentially growing cultures were collected for proteomics. Mass fractions represent the summed peptide abundances divided by the total protein abundance for the ribosomal proteins reported in Table 4.5.

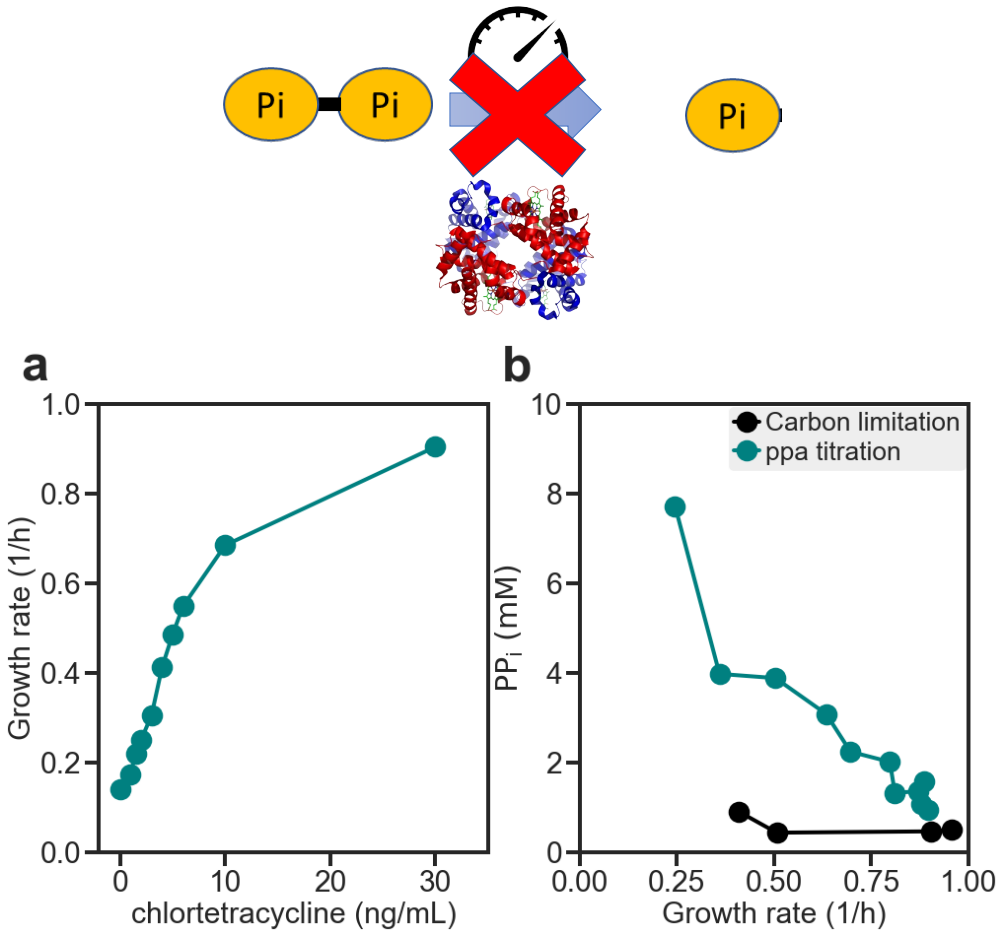

Figure 4.5 Titratable control of PPi pool in E. coli.
a) Titratable control of growth in HE751, a strain with ppa under the control of the ptet promoter, with cTc. b) PP_i concentrations measured in exponentially growing cultures. In carbon limitation, growth rate was limited in NCM3722 cultures by use of different carbon sources (glucose, mannose, and acetate in decreasing growth rate). In ppa titration, growth rate was limited by cTc concentration in HE750 as described in panel a.

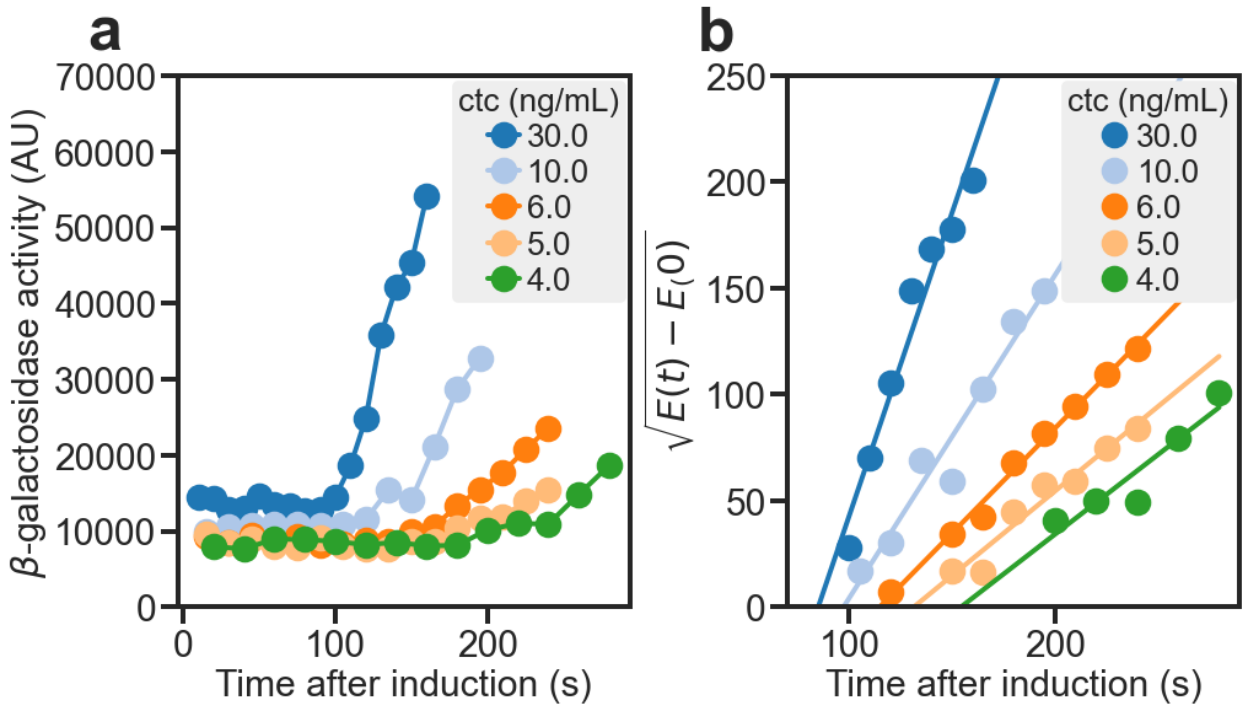

Figure 4.6 β-galactosidase translation elongation rate assay.
a) Induction of LacZ activity over time for HE750 cultures grown in various concentrations of cTc. At time 0, IPTG is added to exponentially growing cultures. b) The square root of lacZ activity above basal level were plotted against time after induction to obtain the lag time for the synthesis of the first LacZ molecule T_{first}. The translational elongation rates were caclulated as $\epsilon = L_{lacZ}/(T_{first} - T_{init})$ where L_{lacZ} is the length of LacZ monomer (1024aa) and T_{init} being the time taken for the initiation steps (10s).

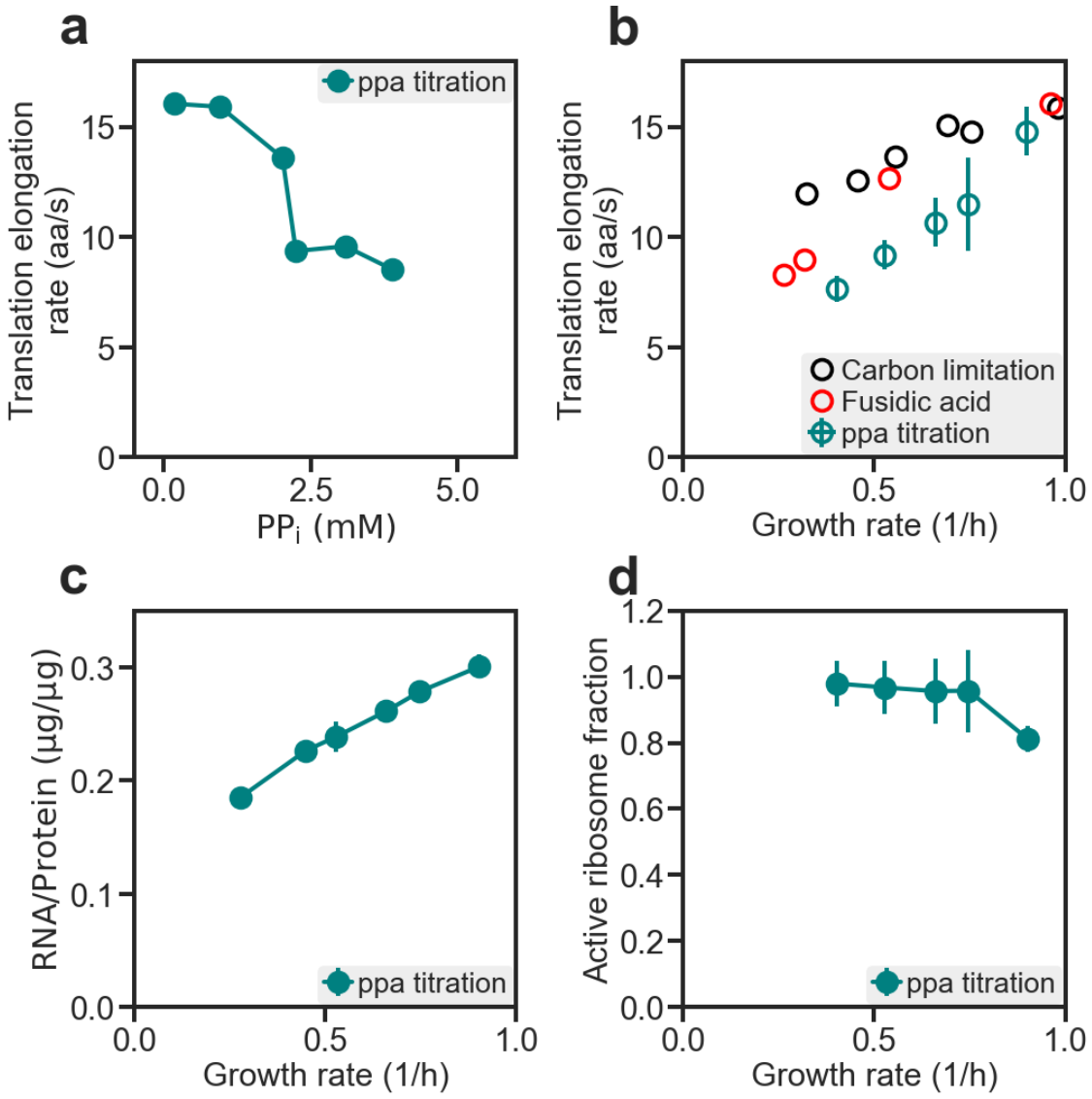

Figure 4.7 Translation rate at different PPi concentrations
In all panels, cultures with ppa limitation had their growth rate reduced by titrating cTc concentration in HE750 strain (See Figure 4.5a). a) Translational elongation rates and PP_i concentrations were measured for exponentially growing HE750 cultures grown in various cTc concentrations. b) Translation elongation rate was measured for NCM3722 cultures with growth rate limited by carbon source (carbon limitation), various cTc concentration in HE750 (ppa titration), or concentrations of fusidic acid in NCM3722 strain (Fusidic acid, data taken from (Dai et al., 2016)). c) RNA and protein content was measured for HE750 cultures grown in various cTc concentrations. d) Active ribosome fraction, f_{active} is calculated as $f_{active} = \frac{\lambda}{k \cdot R/P}\sigma$ where λ is the growth rate of the culture, k is the translation elongation rate, R/P is the RNA/protein ratio, and σ is a proportionality constant.

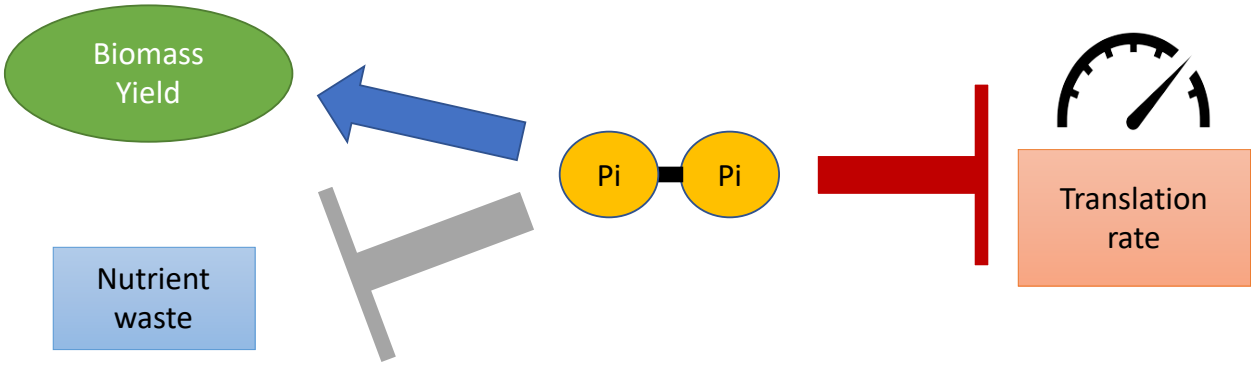

Figure 4.8 Opposing roles of PP_i in B. theta.
PP_i has two effects in B. theta. On the one hand, it benefits cells by increasing biomass yield and reducing nutrient waste. On the other, PP_i reduces the translational elongation rate of ribosomes.

4.6 Acknowledgements

Chapter 4, in part, is currently being prepared for submission for publication of the material. Brian R. Taylor, Vadim Patsalo, Zhongge Zhang, James R. Williamson, Terence Hwa, 2022. The dissertation author was the primary author of this paper.

4.7 Methods

4.7.1 Growth of cells

Culture media

The phosphate-based growth media contained 20 mM glucose 10 mM NaCl, 10 mM NH_4Cl, 0.5 mM Na_2SO_4, a phosphate buffer and a 1000x micronutrient solution. The 1000x micronutrient solution contained 20 mM $FeSO_4$, 500 mM $MgCl_2$, 1 mM $MnCl_2{\cdot}4H_2O$, 1 mM $CoCl_2{\cdot}6H_2O$, 1 mM $ZnSO_4{\cdot}7H_2O$, 1 mM $H_{24}Mo_7N_6O_{24}{\cdot}4H_2O$, 1 mM $NiSO_4{\cdot}6H_2O$, 1 mM $CuSO_4{\cdot}5H_2O$, 1 mM SeO_2, 1 mM H_3BO_4, 1 mM $CaCl_2$, and 1 mM $MgCl_2$ dissolved in a 0.1 N HCl solution. The content of the phosphate buffer was changed to control the pH. At pH 6, the media was buffered with 20 mM K_2HPO_4 and 80 mM KH_2PO_4. For other pH, the proportion of K_2HPO_4 and KH_2PO_4 was used at different proportions with the total concentration summing to

100 mM. For internal potassium measurements, K_2HPO_4 and KH_2PO_4 was replaced with Na_2HPO_4 and NaH_2PO_4 and 1 mM KCl was added to provide some potassium.

The medium used for the anaerobic growth of *B. thetaiotaomicron* was the same as used for the anaerobic growth of *E. coli* but also included 2 mg cyanocobalamin, 2 mg hemin, and 0.6 cysteine per liter. Rich media included 2% tryptone. To make the media anoxic, Hungate tubes (16 mm x 125 mm) filled with 7 mL medium were shaken at 270 rpm under a 7% CO_2, 93% N_2 atmosphere pressurized to 1.5 atm for 75 minutes. Cultures were transferred anoxically into Hungate tubes with disposable syringes.

Culture tubes

Exponential cell growth was performed in a 37°C water bath shaker at 240 rpm. Cultures were grown in the following three steps: seed culture, pre-culture, and experimental culture. Cells were first grown as seed cultures in LB broth for several hours, then as pre-cultures overnight in an identical medium to the experimental culture. Experimental cultures were started by diluting the pre-cultures to an optical density (OD) at wavelength 600 nm (OD_{600}) of ~0.01–0.02. Growth rates were calculated from at least seven OD_{600} points within a range of OD_{600} of ~0.04–0.4.

Plate reader

Seed culture and pre-culture were performed in water bath shakers as described for the growth of cells in culture tubes. Experimental culture was done in a Tecan Spark microplate reader with 96-well microplates (Greiner bio-one) with 200 µL of media. For inoculation, cells were diluted at least 1,000x into the plate media. The incubation temperature was 37°C. The plate was shaken at 280 rpm. Optical density was measured at a wavelength of 420 nm (OD_{420}). To calculate growth rate, the background OD from the opacity of the plate and media, was subtracted from raw OD measurement. Growth rates were calculated from OD_{420} from 0.02-0.2.

Anaerobic cultures

Anaerobic growth was performed similarly to aerobic growth with a few exceptions. All transfers were performed with disposable syringes to avoid oxygen contamination. For *E. coli*, aerobic seed cultures were diluted into Hungate tubes for pre-culture. After overnight growth, the pre-cultures were diluted into fresh Hungate tubes for experimental culture. For *B. theta*, the seed cultures were inoculated into Hungate tubes containing 7 mL Wilkens-Chalgren broth from colonies selected from Wilkens-Chalgren agar plates. After overnight growth, these cultures were diluted into pre-culture tubes. And then diluted once more for the experimental cultures. To avoid atmospheric exposure from removing samples, OD measurements were performed with a Thermo Genesys 20 modified to hold Hungate tubes in place of cuvettes. The culture temperature was kept stable during OD measurements by removing and replacing the Hungate tubes from the water bath shaker within 30 seconds. The OD_{600} measured through the Hungate tubes was equivalent to the OD_{600} measured through a cuvette for the range of 0.04-0.5.

Anerobic growth in plate reader was performed with a Tecan Spark microplate reader enclosed in a custom vinyl anaerobic chamber. Chamber was kept anaerobic with palladium catalysts and an input gas of 5% H_2, 10% CO_2, and 85% N_2. Oxygen levels were monitored with the Tecan Spark O_2 and CO_2 module to ensure the chamber stayed anaerobic during growth.

4.7.2 Pyrophosphate measurement

Pyrophosphate samples were collected using the $CaCl_2$ precipitation method (*192*). 5mL of exponentially growing cells at OD 0.4-0.5 were mixed with 500uL 3N perchloric acid and immediately placed onto dry ice. After overnight storage at -20°C, samples were thawed and centrifuged at 5000 rpm for 10 minutes at 4°C. The supernatant was then collected and put into a new tube. Then 450 μL 3N NaOH was added to neutralize the samples, bringing the pH to about

8-8.5. Then 10 μL of a 100 mM $CaCl_2$ solution was added followed by mixing and 250 μL of a 1M NaF solution. After 10 minutes on ice, a precipitate would form. The precipitate was centrifuged for 10 minutes at 5000 rpm at 4°C and washed with 5 mL of ice-cold deionized water. Then samples were centrifuged and washed 2 more times. Finally, the pellet was dissolved in 400 μL 0.5 N H_2SO_4.

For the PP_i measurement, 200 μL of sample was mixed with 100 μL of MT mix, which consisted of 4mL of 40mM $(NH_4)_6Mo_7O_{24}$, 1mL 5N H_2SO_4, and 50 μL triethylamine. After a precipitate formed in the mixture, the sample was centrifuged at maximum speed and the supernatant was put into a new tube. Then 50 μL 5 NH_2SO_4 was added to the tube and the tube was centrifuged again. Next, 16 μL of beta-mercaptoethanol was added for color development. After about 10 minutes of color development, OD at 650 nm was measured. PP_i amount was determined by a standard curve.

4.7.3 RNA measurement

Total RNA quantification method used was described in (*14*). RNA nucleotide amount (nmol/OD_{600}/mL) was calculated from the normalized RNA mass (μg/OD_{600}/mL) assuming that the average molecular weight of an RNA nucleotide was 339.5 g/mol, equivalent to equal parts ACGU.

4.7.4 Protein measurement

Protein quantification method used was described in (*14*).

4.7.5 Glycogen measurement

For sample collection, samples growing in steady state were collected into tubes. Cells were pelleted via centrifugation and washed with 150 mM NaCl solution. The pelleting and centrifugation were performed twice. Then the pellets were frozen on dry ice and stored at -20°C.

Glycogen was measured with the phenol-sulfuric acid assay (*193*). Briefly, pellet samples were resuspended in a mixture of phenol, followed by concentrated sulfuric acid. The samples, warm from the mixture of sulfuric acid and water were then incubated at 90°C for 10 minutes. Then, 200 μL of samples were loaded into 96-well plates and the OD spectrum was measured for between 300 and 700 nm with a Tecan Spark plate-reader. Because this assay is sensitive to both pentoses and hexoses, the pentose contribution was subtracted based on the spectrum from a standard curve made from samples containing arabinose. Glycogen was quantified from the remaining hexose contribution.

4.7.6 Translation rate measurements

Translation rates were measured as in (*184*). As in the publication, an initiation time of 10s was assumed for all translation rate calculations.

4.7.7 Strain construction

Construction of titratable *ppa* in *E. coli*

Using plasmid pKDT:Ptet (*143*) as a template, the DNA fragment (referred to as "km:rrnBT:Ptet") containing the *km* gene, the *rrnB* terminator (rrnBT) and the Ptet promoter was amplified using the primer pair Ptet.ppa-P1/Ptet.ppa-P2. The PCR products were integrated into the chromosome of K12 strain NCM3722 (*144*) to replace the *ppa* promoter (from the -103th nucleotide to the +1st nucleotide relative to the translational start point of *ppa*). The chromosomal integration was confirmed first by colony PCR and subsequently by DNA sequencing. The region carrying "km:rrnBT:Ptet-ppaBA" was transferred to NCM3722-1R by P1 transduction.

Construction of *ppa* and *pfp* in *B. theta*

DNA fragments containing the *ppa* and *pfp* genes from K12 strain MG1655 were inserted into the multiple cloning site of plasmid pNBU2_erm_P1T_DP-A21 (*178*). Each plasmid was then

transformed into *E. coli* strain S17-1. Each strain was grown with wild-type *Bacteroides thetaiotaomicron* (HO1) for biparental mating (*191*). After selection on erythromycin antibiotic plates, colonies were screened for integration of the genes into the *B. theta* genome by colony PCR.

4.7.8 Proteomics

Proteomics were performed as in (*61*).

4.8 Tables

Table 4.1 PP_i yields from biosynthesis of macromolecules.
*For protein, rRNA, mRNA, and glycogen, the PP_i yield from macromolecules with precursors provided was calculated based on one PP_i produced per monomer unit. For lipids, it was assumed that one fatty acid produced 3 PP_i (*97*). Molecular weights of lipids in E. coli is based on median lipid (*194*). When precursors are included for glycogen or lipids, there would be no change in PP_i yield because the PP_i produced comes from the synthesis of the polymers rather than the monomers. For mRNA synthesis, turnover is assumed to be high. Therefore, PP_i yield from synthesis of precursors is negligible. For rRNA synthesis, the synthesis of precursors creates PP_i (*97*). The yield of PP_i for synthesis of protein without precursors is calculated in Table 4.3. The difference between with and without precursors comes from the use of PP_i in glycolysis when synthesizing the precursors. PP_i is also produced when synthesizing specific amino acids (Table 4.4).*

Macromolecule	**Molecular weight per monomer (g/mol)**	**PP_i per biomass (µmol PP_i/mg macromolecule)**	**PP_i with precursors (µmol PP_i/mg macromolecule)**
Protein	110	3.6	9.1
rRNA	324	6.9	3.1
Glycogen	164	6.1	6.1
Lipids	734	3.8	3.8
mRNA	324	3.1	3.1

Table 4.2 PPi yields in different conditions.
RNA, protein, and glycogen content were measured as described in methods. mRNA was estimated based on assuming that mRNA synthesis rate was equal to rRNA synthesis rate. rRNA synthesis rate is the rRNA content times the growth rate of cells. Lipid content was estimated to be 10% of total biomass. Net PP_i yield was calculated from the macromolecule numbers in this table and the yields in Table 4.1.

Condition	**RNA (µg/OD_{600}mL)**	**Protein (µg/OD_{600}mL)**	**Glycogen (µg/OD_{600}mL)**	**mRNA ***	**Lipids ***	**PP_i (µmol PP_i / OD_{600}mL)**
Minimal media	80	330	70			2.50
Rich media	120	300	70			4.40

Table 4.3 Net PP_i debt in minimal vs rich media.

Condition	**PP_i (µmol PP_i / OD_{600}mL)**	**Mannose Uptake**	**Mannose used in biomass**	**Mannose left over for energy**	**Net PP_i debt**
Minimal Media	2.50	6.5	3.2	3.2	-0.74
Rich Media	4.40	4.3	1.0	3.2	1.14

Table 4.4 PP_i produced or used in the synthesis of amino acids.

	Glucose used	**PP_i used through pfp**	**PP_i made**	**Net**
alanine	0.5	0.5	0	0.5
arginine	1.5	1.5	1	0.5
asparagine	0.5	0.5	0	0.5
aspartate	0.5	0.5	0	0.5
cysteine	0.5	0.5	1	-0.5
glutamate	1	1	0	1
glutamine	1	1	0	1
glycine	0.5	0.5	0	0.5
histidine	1	0	2	-2
isoleucine	1	1	0	1
leucine	1.5	1.5	0	1.5
lysine	1	1	0	1
methionine	1	1	1	0
phenylalanine	1.67	1.67	0	1.67
proline	1	1	0	1
serine	0.5	0.5	0	0.5
threonine	0.5	0.5	0	0.5
tryptophan	1.17	1.17	1	0.17
tyrosine	1.67	1.67	0	1.67
valine	1	1	0	1
Average PP_i used in biosynthesis (µmol PP_i/µmol aa)		0.9	0.3	0.6
Average PP_i used in biosynthesis (µmol PP_i/mg protein)				5.45
PPi generated in peptide elongation (µmol PP_i/mg protein)				9.09
net PPi (µmol PPi/mg protein)				3.63

Table 4.5 List of uniprot proteins involved in translation for B. theta and E. coli.

E. coli	*B. theta*
P0A7J3, P0DTT0, P0A7K2, P0A7M9, P60422, P62399, P0A7L0, P0AG55, P0A7J7, P60723, P61175, P0A7L8, P27431, P0A7L3, P60624, P0A7N9, P0ADY3, P0ADZ0, P0ADY7, P60438, P68919, P0A7K6, P0A7N4, P0A7M6, P0A7M2, P0C0R7, A0A2Z5XFS5, Q8X776, Q8XDN1, Q8XBP2, P21507, P42641, P0A7G2, P0C018, P0A850, P0AG24, P0ADZ4, P37634, P0A7X6, P0AAT6, P0A9P6, P0AD89, P25519, P21693, P0AG48, P75782, Q2EEQ2, P0A7Q6, P76104, P0A7Q1, P02413, P0A7N1, P0AG51, P0AG44, P75876, P39286, P0ADR6, P0A7R1, P0A7Y0, P0A7P5, P0A7S9, P0A7U3, P0A8A8, P75864, P0AA10, Q8FEY4, P0A898, P0A7S3, P0A8X0, P0ADK8, Q47149, P0ABU2, Q47157, P0A8H6, P39199, P0AGK4, P69348, P0AD49, P0AGL5, P0A707, P0A705, P69222, P0ACG8, P0A6P5, P36675	Q89ZK5, Q8A015, Q8A2E8, Q8ABA7, Q8A8I1, Q8A9A2, Q8A0H8, Q8A8H7, Q8A5I9, Q8A417, Q8A4N6, Q8A472, Q8AA33, Q8A7G2, Q8A251, Q8A9B8, Q8A277, Q8A466, Q8AA41, Q8A4A1, Q8A482, Q8A5I1, Q8A499, Q8A136, Q8A487, Q8A473, Q89Z76, Q8A583, Q8A467, Q89Z89, Q8A849, Q8A339, Q8AAU4, Q89ZN2, E7MCA7, Q8A7Q0, Q8A5G6, Q8A0Z6, Q8A478, Q8AAJ0, Q8A462, Q8A2B4, Q8A8L7, Q8A3C1, Q8A2S8, Q8A5V8, Q89ZP8, Q89YZ3, Q8A3V8, Q8A194, Q8A538, Q8A6Z6, Q8A5S1, Q8A3W5, Q8A9H9, Q8A7Q1, Q8A0L3, Q8A276, Q89YP0, Q8A138, Q8A2A3, Q8A4A3, Q8A477, Q8A8M2, Q8A0Z5, Q8A475, Q8AAN9, Q8ABV5, Q8A486, Q8A490, Q8A493, Q8A135, Q8A474, Q8A5S7, Q8A488, Q8A476, Q8AAP0, Q89ZR2, Q8A484, Q8A4V8, Q8A479, Q8A483, Q89YZ1, Q8A418, Q8A492, Q8A494, Q8A9A0, Q8A682, Q8A491, Q9RQ15, Q8A5J0, Q8A495, Q8A468, Q8A5S5, Q8A1F6, Q8A465, Q8A999, Q8A733, Q8AAZ8, Q8A485, Q89ZR3, Q8A481, Q8A4A0, Q8A5S6, Q8A0Z4, Q8A2M2, Q8A489, Q8A480, Q8AAP1, Q8A2A1, Q8A498, Q8A120

Appendix A

Additional experimental results for acetate stress

A.1 Kinetics of acetate accumulation

In order to understand acetate stress outside of steady state growth, we performed an experiment acetate was suddenly added to the medium of exponentially growing cultures, an experiment we call acetate downshift. Surprisingly, cultures exposed to this acetate downshift adapt quickly, recovering within minutes. In the initial phase after the downshift, there is a sudden decrease in OD_{600} by about 5%, possibly happening either from a change in cell volume (*195*) or sudden lysis of a small fraction of cells. From the initial drop to about 10 minutes after the acetate addition, there is very little change in OD_{600}. Then, after the initial lag, the instantaneous growth rate of the culture reaches around 0.3/h, which is near the steady-state growth rate (Figure A.2a).

Despite the fast initial recovery of growth, there is a substantial perturbation to metabolism for cells exposed to a sudden acetate stress. The quickest change happens with the excretion of the amino acid, glutamate. Shortly after acetate addition, A small amount of glutamate is excreted, but then disappears from the media within less than 4 minutes, likely taken up by the cells (Figure A.2a). Alanine is excreted, reaching a maximum of 30 μM in the media after approximately one doubling (Figure A.2b). But as cells start to adapt, the cells begin to take up the alanine after 120 minutes. No other amino acid was detected in the media in significant quantities.

There is also a very sudden decrease in internal amino acids from the acetate downshift. Glutamate, the most abundant metabolite in growing cells and used for the synthesis of most amino acids, drops to under 10% of its steady state concentration within four minutes of the acetate addition (Figure A.2c). Similarly, glutamine, another amino acid used in amino acid synthesis,

decreases to 30% of its steady state concentration, also within four minutes of the acetate addition (Figure A.2d). The changes we see with these two important amino acids suggest that the biosynthesis part of the metabolome shifts quickly to the acetate addition.

In contrast to the quick change in internal metabolites, the acetate downshift leads to a large disruption in carbon utilization. Healthy, aerobic, *E. coli* cultures typically only excrete acetate and carbon dioxide as long as carbon is available in excess. However, after the acetate downshift, cells begin excreting pyruvate, reaching almost 3 mM in the media after growing one doubling (Figure A.3a). Additionally, cells start to excrete small amounts of acetate as well, increasing the concentration of acetate by about 0.2 mM after one doubling (Figure A.3b). The excretion of pyruvate is substantial, equivalent to about 16 mM of pyruvate per OD_{600} of cell growth during the transition. Steady-state growing cells take up only 5 mM of glucose per OD_{600}, which is equivalent to 10 mM pyruvate per OD_{600} since one glucose can be converted to two pyruvate molecules via glycolysis. Cells increase their uptake of glucose to compensate for the increased excretion of pyruvate, reaching 12 mM glucose per OD_{600}, which is over double the uptake for steady-state growing cells (Figure A.3c). This drop in biomass yield resolves for acetate stressed cells that have been grown long enough to adapt.

The heavy excretion of pyruvate suggests that the cell has to deal with an immediate bottleneck in metabolism around pyruvate and acetyl-CoA, leading to a buildup of these metabolites that then are excreted. Alpha-ketoacids, such as pyruvate, are known to control the expression of catabolism related genes including the beta-galactosidase, *lacZ*. For *lacZ*, alpha-ketoacids suppress expression through repressing synthesis of cyclic-AMP (cAMP) (*14*). Synthesis of *lacZ*, quantified by beta-galactosidase activity, stops after the acetate downshift, not resuming until after an hour after the shift (Figure A.3d). This pause in *lacZ* synthesis is consistent

with the bottleneck in pyruvate metabolism leading to a building of metabolites around pyruvate due to the acetate downshift.

If the cell is filled excess carbon in the form of acetate and pyruvate, excreting it instead of metabolizing it, this suggests that there's a bottleneck in amino acid synthesis that's compounded by pyruvate stealing nitrogen from other amino acids to create alanine. Alanine is synthesized from pyruvate from one of two possible transamination reactions: one originating from glutamate the other from valine. This hypothesis is supported by the small adaptation we find in the proteome, where catabolic proteins are expressed less and anabolic proteins are expressed more, which is similar to cultures where glutamate flux is limited. Curiously, the adaptation to the proteome doesn't appear to lead to any change in the growth rate since the growth rate change happens quickly after the acetate shift. So, it's not immediately clear how the proteome adaptation benefits the cells. However, there is a likely benefit that comes from increasing yield. Given that adapted cells don't excrete alanine, pyruvate, and acetate, this suggests that the proteome is adjusted to prevent this excretion. These three metabolites are located near each other metabolically as pyruvate can be turned into alanine or acetyl-CoA in one step. A surprising part of the transient is the acetate excretion. Even though cells are filled with acetate, they aren't prepared to utilize the acetate initially (*53*). However, when given enough time for the proteome to adapt, the cell's response to being filled with acetate is to use it. This adaptation is seen in transitions between glycolytic and gluconeogenic carbon sources, where cells take a long to adapt because the sudden depletion of key metabolites that come from glycolysis (*15*). In the acetate downshift described here in this appendix, glycolytic metabolites are still available since glucose is still available and no lag results. Yet the proteome of these cells eventually adapts to this high carbon environment.

There are several exporters coded in the E. coli genome that could be used to export the metabolites that we find in the media. For glutamate, the amino acid exporter, *yddG*, has been shown to export glutamic acid among other amino acids (*196*). Export of alanine has been demonstrated from *alaE* (*197*). The formic acid channel, *focA*, has been shown to export other carboxylic acids including acetate and pyruvate (*198*).

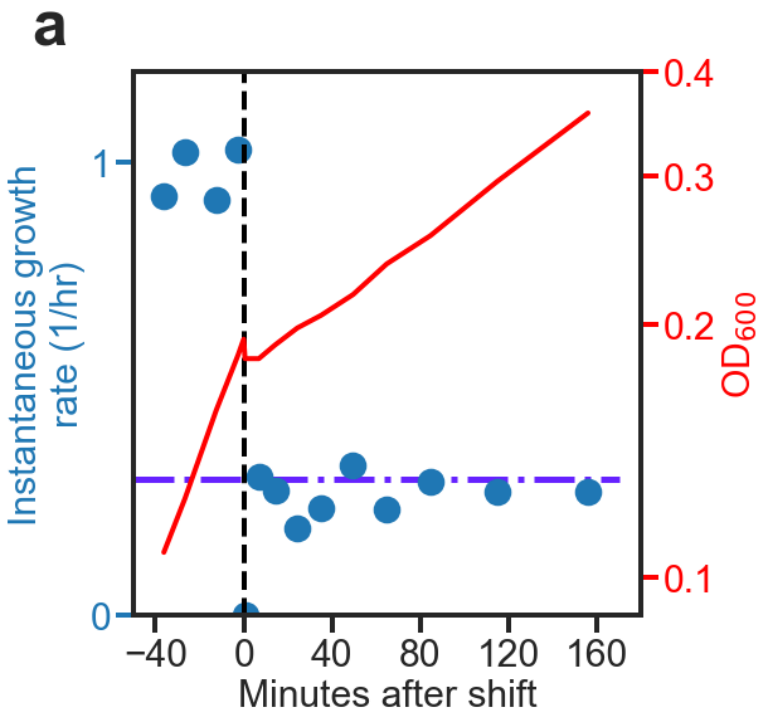

Figure A.1 Growth kinetics of acetate downshift.
Exponentially growing cultures in MES buffered media were exposed at time 0 to a sudden addition of 40 mM acetate pipetted into the media. Instantaneous growth rate for each timepoint was calculated from the logarithmic derivative of OD_{600} averaged with the measurements before and after to reduce scatter.

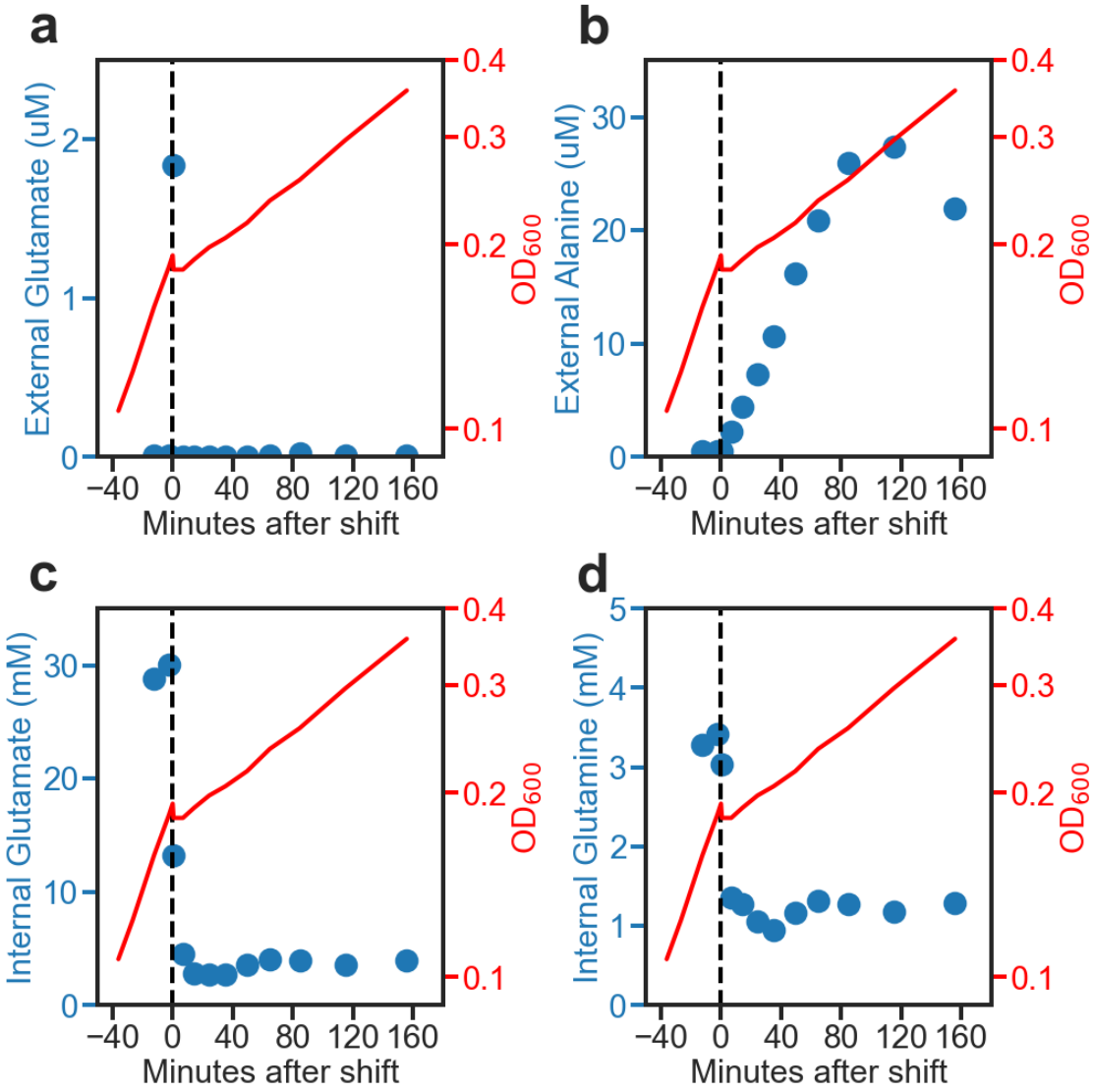

Figure A.2 Metabolites in acetate downshift (part 1).
Exponentially growing cultures in MES buffered media were exposed at time 0 to a sudden addition of 40 mM acetate pipetted into the media. Samples were collected for metabolite measurement by HPLC. For all panels, OD600 is shown by the red line. The blue circles are a) Internal glutamate. b) Internal glutamine c) External glutamate

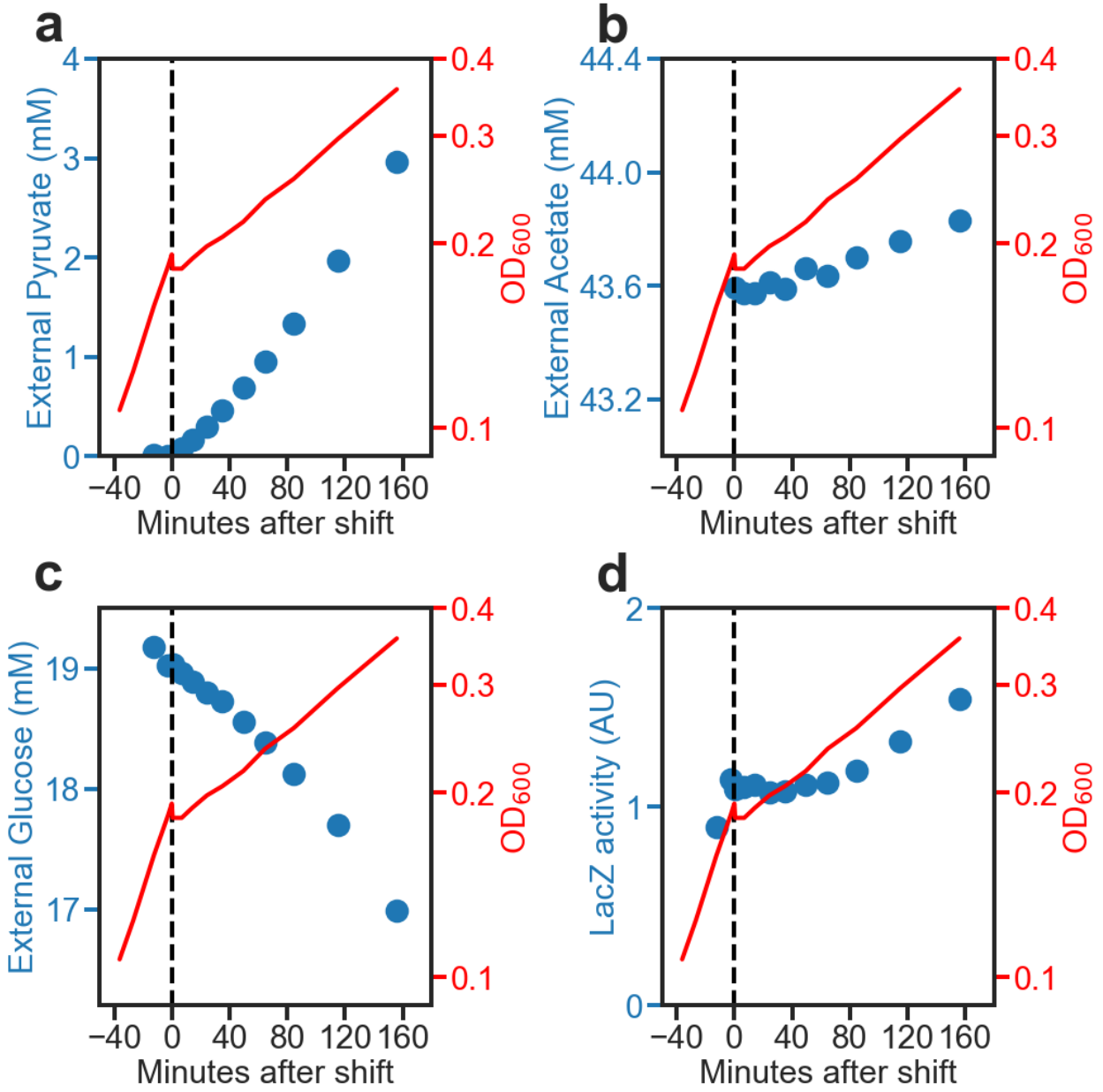

Figure A.3 Metabolites in acetate downshift (part 2).
Exponentially growing cultures in MES buffered media were exposed at time 0 to a sudden addition of 40 mM acetate pipetted into the media. Samples were collected for metabolite measurement by HPLC. For all panels, OD600 is shown by the red line. The blue circles are a) external pyruvate b) external acetate c) external glucose d) beta-galactosidase activity.

A.2 Effect of acetate on ribosome proteins

Protein synthesis is necessary for cell growth. Proteins are synthesized by ribosomes, which are large, complicated proteins and are potentially sensitive to many different perturbations.

In cells limited for nutrients, ribosome content is linearly correlated with growth rate (*59*). But when ribosomes are inhibited, ribosomal content increases to make up for the decreased flux through the ribosome. Therefore, increased ribosomal content is an indirect barometer of translation rate. Slow-growing cells have reduced demand for ribosomes, but cells still maintain a higher content than necessary. As a result, the translation rate decreases. Ribosome content can be approximated by measuring the total RNA of the cell since ribosomes are approximately 2/3 RNA by weight.

We measured RNA and protein content in cells grown in different concentrations of acetate. While RNA/protein content decreases due to acetate, when compared the content with nutrient-limited cells, RNA/protein is increased (Figure A.4a), which suggests that ribosomes are inhibited by the effects of acetate stress, relative to the rest of the proteome. However, the increase in ribosome abundance does not necessarily indicate that ribosomes are translating slower, it could also suggest that a certain fraction of ribosomes is becoming inactive (*61*, *185*).

To confirm that ribosomes were indeed inhibited, we directly measured the translational elongation rates. The translational elongation rates were measured with the lacZ induction method (*61*, *183*, *184*). In this method, translation of lacZ is induced by adding IPTG to the culture medium of an exponentially growing culture. Then, the increase in lacZ activity is monitored to estimate the time it takes for the first molecule to appear (Figure 4.6). We measured translational elongation rate this way for acetate stressed cells and compared the rates with cells limited by nutrients (Figure A.4b). The translational elongation rates of cells were decreased for acetate stressed cultures compared to carbon limited cultures. The active ribosome fraction, f_{active}, does not appear to be different between acetate stress and carbon limitation (Figure A.4c). The translational elongation

rate of *E. coli* has been shown have a Michaelis-Menten type relationship with ternary complex concentration (*61*)

$$\frac{1}{k} = \frac{1}{k_{on} \cdot [TC_{eff}]} + \frac{1}{k_{max}} \qquad \textit{Eq. A.1}$$

where k is the translational elongation rate, k_{max} is the maximum translational elongation rate, k_{on} is the rate of ternary complex binding with ribosomes, and $[TC_{eff}]$ is the effective concentration of ternary complexes. The ternary complex concentration is approximately proportional to the RNA/protein ratio.

For cells limited by nutrient availability or translation inhibiting antibiotics, Eq. A.1 describes translational elongation rates fairly well (*61*) (Figure A.4d black circles). However, for acetate stress cells, there is a significant deviation from Eq. A.1 (Figure A.4d red circles). This deviation also happens for cell that are osmotically stressed (*185*). As it turns out, the constant that changes can be investigated by holding the stress fixed while perturbing $[TC_{eff}]$. In our case, we changed $[TC_{eff}]$ by applying the translation inhibiting antibiotic, chloramphenicol for three different acetate concentrations: 0, 10, and 20 mM sodium acetate in media at pH 6. Chloramphenicol increases the RNA/protein ratio for these acetate stress cultures (Figure A.5a). Furthermore, translation rate also increases from chloramphenicol (Figure A.5b). Due to the increase and RNA/protein and increase in translational elongation rate, the fraction of active ribosomes decreases for the chloramphenicol and acetate stress (Figure A.5c). The increase in RNA/protein suggests that ternary complex concentration increases as the two are proportional to each other.

In order to find which constants of Eq. A.1 change due to acetate stress, we can plot the translational elongations rates and effective ternary complex concentrations on a Lineweaver-Burk plot. The results of this analysis are mixed (Figure A.5d). For cells grown in 10 mM sodium acetate

and various chloramphenicol concentrations, there is a decrease in the maximum translational elongation rate, k_{max}, without a change in the on rate for ternary complex and ribosome binding. However, for cultures grown in 20 mM sodium acetate and various chloramphenicol concentrations, Lineweaver-Burk plot shows that there is in increase in k_{max} and a decrease in k_{on}, which is qualitatively different from the result for 10 mM sodium acetate. It's possible that there is another change happening to ribosomes that isn't captured by the Michalis-Menten formulation of Eq. A.1. Alternatively, there is a change happening in the conversion from RNA/protein to $[TC_{eff}]$. Regardless, these results establish that one of the effects of acetate stress on cells is that the translational elongation rate of cells decreases.

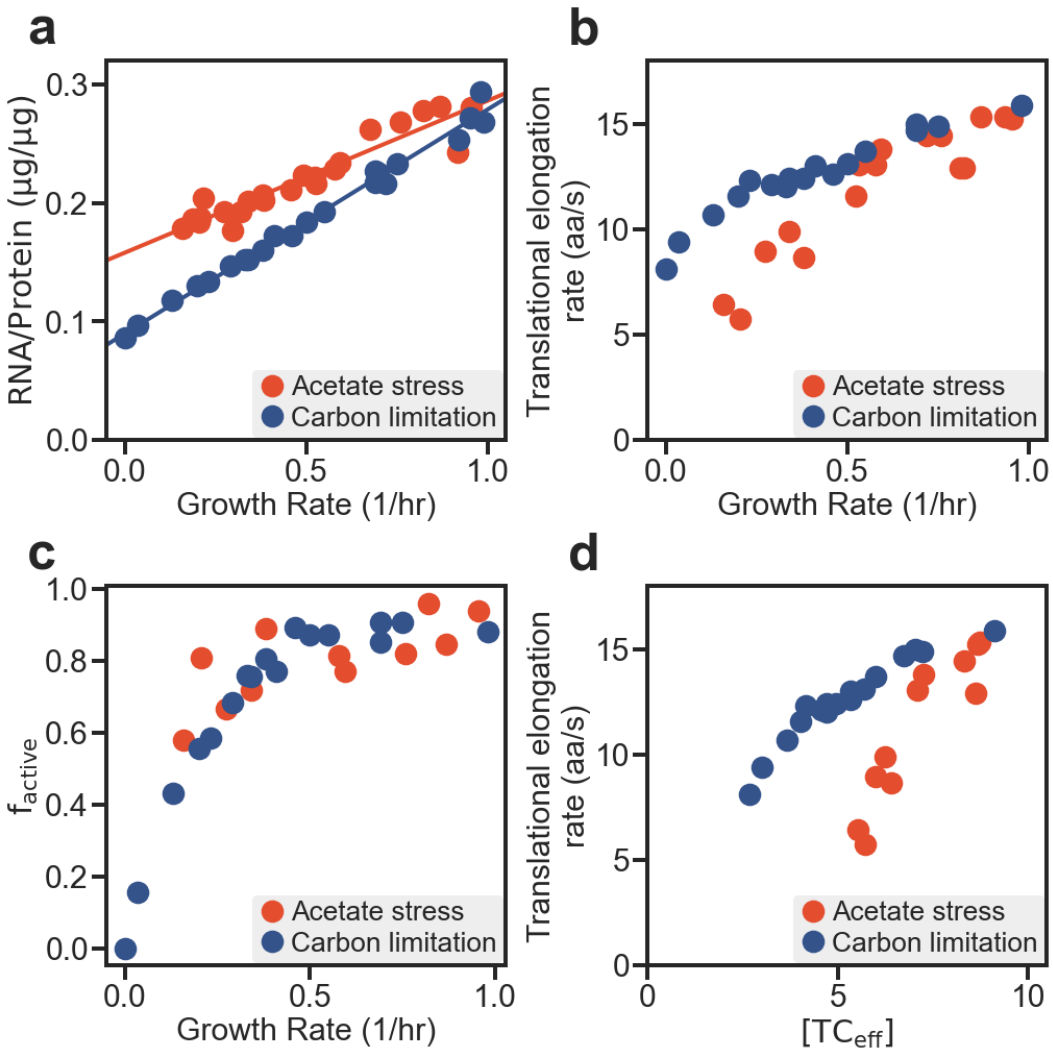

Figure A.4 Effect of acetate stress on ribosomes compared to nutrient limited cells.
*For all panels, acetate stressed cells were grown in various sodium acetate concentrations in phosphate-based media set to pH 6. Carbon limited cells were grown in MOPS minimal media with various carbon sources to limit growth. Data for carbon limitation taken from (*61*). a) RNA and protein content was measured for exponentially growing cultures. b) Translational elongation rate was measured by the lacZ induction method (*61, 183*). c) Active ribosome fraction, f_{active} is calculated as $f_{active} = \frac{\lambda}{k \cdot R/P}\sigma$ where λ is the growth rate of the culture, k is the translation elongation rate, R/P is the RNA/protein ratio, and σ is a proportionality constant. d) The effective ternary complex concentration, $[TC_{eff}]$ was calculated based on $[TC_{eff}] = C \cdot (R/P)$ where C is 31 µM from (*61*).*

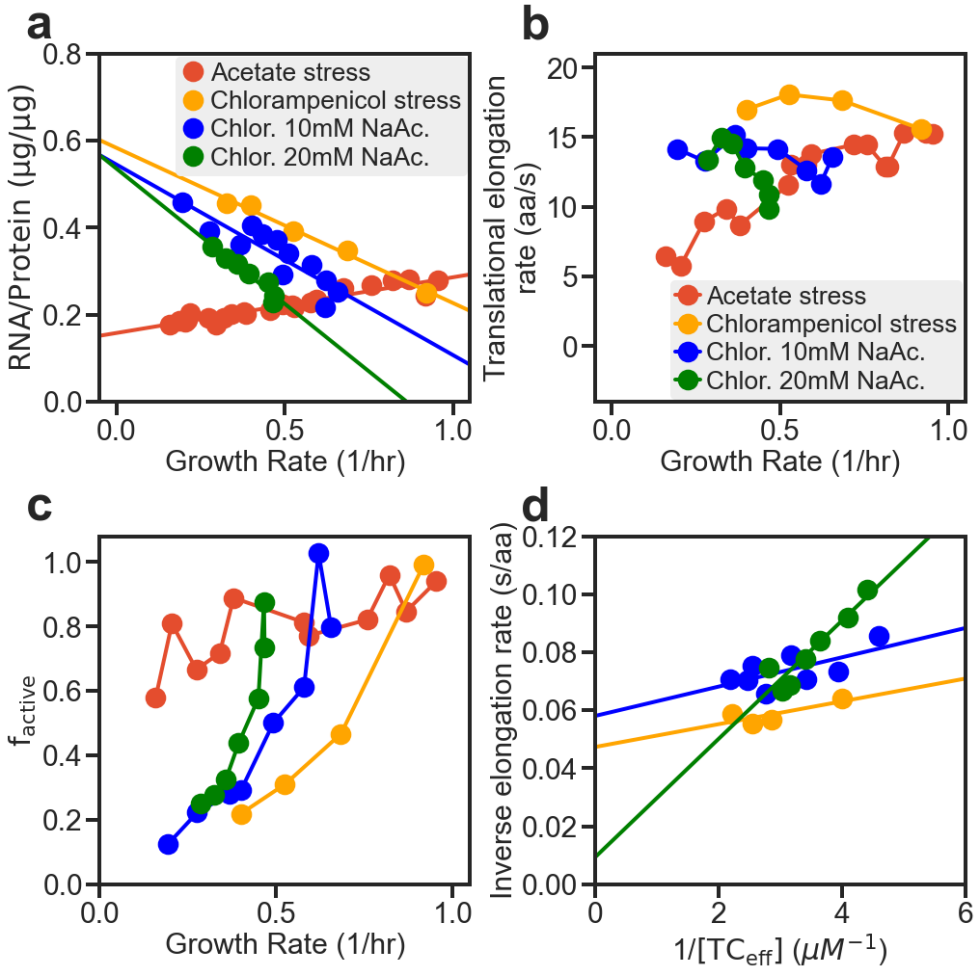

Figure A.5 Effect of acetate stress on ribosomes with antibiotics.
*All cultures were grown in phosphate-based media set to pH 6. Acetate stressed cultures were grown in various sodium acetate concentrations to limit growth rate. For all chloramphenicol stressed cells (gold, blue, and green circles), acetate concentration was kept fixed (0, 10, or 20 mM NaAc) while chloramphenicol concentration was varied to reduce growth rate. a) RNA and protein content was measured for exponentially growing cultures. b) Translational elongation rate was measured by the lacZ induction method (*61, 183*). c) Active ribosome fraction, f_{active} is calculated as $f_{active} = \frac{\lambda}{k \cdot R/P}\sigma$ where λ is the growth rate of the culture, k is the translational elongation rate, R/P is the RNA/protein ratio, and σ is a proportionality constant. d) Lineweaver-Burk plot of elongation rate and [TC_{eff}]. The slope of the linear correlation denotes the binding rate between the ternary complexes and the ribosome, and the y intercept denotes $1/k_{max}$ the maximum elongation rate.*

A.3 Strain dependent effects

It's well known that different strains of bacteria have different tolerances to various stresses. This is likely to be the case for acetate stress as well. Therefore, in order to validate the

strain in our study, NCM3722, as a good model organism for studying acetate stress, we compare NCM3722 with other strains of *E. coli*. We can compare two different types of bacteria. One is other strains of *E. coli* used in laboratories. The other is strains of *E. coli* recently isolated from the environment, that have not gone through any "domestication" process.

We compared two lab strains with the main strain of our study, NCM3722. One strain is designated BOP27, which is alternatively named MG1655 (*153*, *199*). This strain is commonly used in physiological studies (*153*). However, it's known to have certain defects that have accumulated during storage including low expression of *pyre* leading to a pyrimidine limitation in minimal media, an *fnr* deletion, and poor growth on certain carbon sources (*153*). As a result, BOP27 grows slowly compared to NCM3722 in minimal media (Figure A.6). Furthermore, when acetate is included in the growth media, BOP27 grows slower than NCM3722.

The derivative strain, BOP1000, is improved from BOP27 by curing some of its defects found through adaptive laboratory evolution (*199*). As a result, this strain grows much faster than BOP27 at a growth rate similar to NCM3722 of about 0.9/h compared to 0.75/h for BOP27. However, when grown in high acetate concentrations, BOP1000 is more affected by acetate than NCM3722, growing at a growth rate that is nearly similar to BOP27 at an acetate concentration of 15 mM at pH of 6.

We also compared the acetate tolerance of NCM3722 with *E. coli* strains recently isolated from humans. Again NCM3722 fairly well compared to the other strains (Figure A.7 blue triangles). The isolated strains had a wide range of growth rates, both with and without acetate. Without acetate, the strains didn't grow at a growth rate much higher than 1/h, while some grew very slowly at about 0.2/h. This growth rate is equivalent to fairly high inhibition from acetate for NCM3722. Since these cultures were grown in minimal media, it may be the case that these strains

were not tolerant to growing without certain amino acids or vitamins, leading to their relatively slow growth rates. Interestingly, these slower growing strains were isolated from relatively downstream locations in the intestinal tract, coming from either the rectum (AZ61, AZ125) or feces (AZ39). The relative decrease in growth rate for these strains in acetate stress was fairly low compared to NCM3722, decreasing by 2-fold compared to NCM3722's 4-fold for acetate concentrations around 50 mM. There were also several strains that performed similarly to NCM3722, growing well both with and without acetate (AZ73, AZ76, AZ116, AZ122, and AZ259). Some of these strains (AZ116 and AZ122) were isolated the terminal ileum, which is near the entrance to the colon, where most fermentation takes place. Interestingly, there was one strain that grew well without acetate, reaching a grown rate near 1.0/h, but was much more sensitive to acetate compared to other fast growing strains (AZ55). This strain was isolated from the duodenum, which being far from the colon is an environment without much SCFAs, likely leading to this strain's poor tolerance to these acids.

Overall, the lab strain, NCM3722 seems well adapted to acetate stress compared to other strains of *E. coli*, making this strain a good choice for studying the limits of acetate tolerance. Because of the diversity in tolerance to acetate for these different *E. coli* strains, there are likely genetic and physiological reasons for why these different strains are more or less tolerant to acetate stress. Understanding these origins is an actively explored research topic.

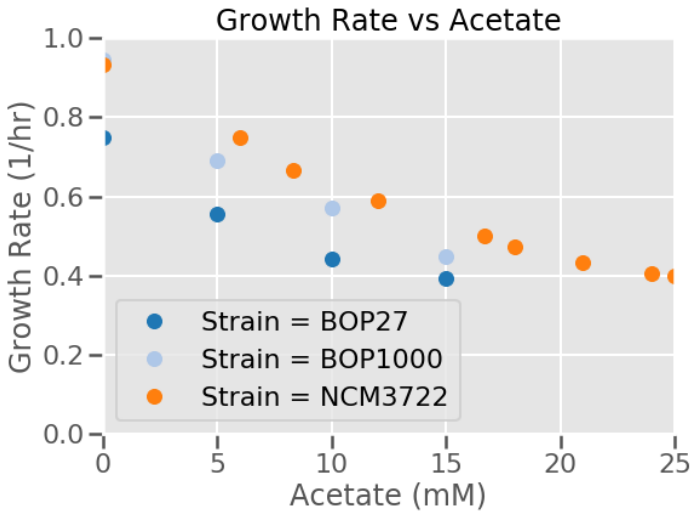

Figure A.6 Comparison of lab strains with the strain focused on for this study, NCM3722.
Cultures were grown in phosphate based minimal media a pH of 6 in various concentrations of sodium acetate as indicated on the x-axis. Strains indicated are the commonly studied strain MG1655 (BOP27) and a version of this strain that was evolved for grown on glucose minimal media (BOP1000). Cultures were grown in Tecan microplate reader.

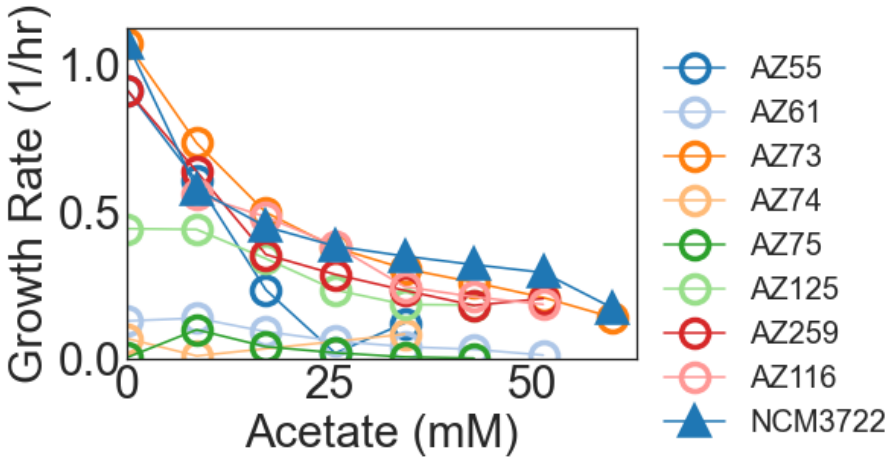

Figure A.7 Comparison of microbes isolated from human gut with the strain focused on for this study, NCM3722.
Cultures were grown in phosphate based minimal media a pH of 6 in various concentrations of sodium acetate as indicated on the x-axis. Except for the lab strain, NCM3722, the AZ strains were isolated from various locations from human samples. Cultures were grown in Tecan microplate reader.

A.4 Effects of carbon quality

Ultimately, specific molecular mechanisms can't tell the whole story for why cells are inhibited by acetate. As an example, methionine supplementation has been reported to help with

acetate tolerance (*54*, *55*). In our strain, we don't see much of an effect for methione, but there is a small effect for other amino acids (Figure A.8). Aspartate, glutamine, and glutamate appear to have the most positive effect while addition of leucine decreases the steady state growth rate. In (*55*), a multitude of additives help with growth on acetate. It's likely that part of this effect is related to defects in BW25113's growth in minimal media alone, particularly with pyrimidine metabolism. Since our strain is curred of these defects (*199*), we focused on multiple amino acids.

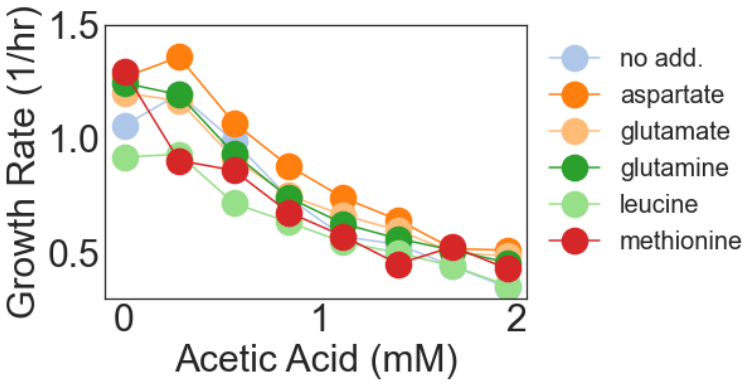

Figure A.8 Growth of NCM3722 in acetate stress with single amino acid supplements. Cultures of NCM3722 were grown in phosphate based minimal media a pH of 6 in various concentrations of sodium acetate. Cultures were grown in Tecan microplate reader. Acetic acid reported is calculated according to the Henderson-Hasselbalch equation. Amino acids were added as indicated in the legend at concentrations of 1mM.

To get a large enough measureable effect, we performed the same experiment but in rich media, where more amino acids were supplied. We see that tolerance to acetate is significantly improved depending on the nutrients that were supplied, with the best nutrient condition providing the best tolerance (Figure A.9a). Futhermore, this affect seems to scale with the growth rate of cultures that aren't stressed with acetate (Figure A.9b). This increased tolerance to acetate is unlikely to be explained by the acidification of the cytoplasm since neither pH_{max} or pH_{min} change very much despite the large growth rate change (Figure A.9c,d). However, the measured internal acetate, like the external acetate, scales with nutrient quality (Figure A.10a,b). Cells grown in richer media, can acculate proportionally more acetate before their growth slows down. Similarly,

trehalose overdosed cells also can accumulate more trehalose when grown in richer media (Figure A.10c,d). This suggests that the increased tolerance to acetate experienced by cells growing in richer medium is related to the useless metabolite effect rather than pH effect.

Cells with better nutrient availability are able to accumulate more trehalose or acetate, thus connecting acetate stress to nutrient quality. However, our measurements don't take into account internal water content, which is known to be affected by nutrient quality, with faster growing cells having greater water content (*147*). This would mean that internal acetate concentrations would trend towards being equivalent despite the amount of acetate per weight of biomass being higher. While water content is roughly fixed for acetate stressed cells growing in glucose minimal media (see chapter 2), it's unknown how the water content changes for acetate stressed cells growing in rich media. It's also unclear why cells growing in better nutrients can tolerate higher concentrations of acetate and trehalose. One possibly explaination is that cells growing in unstressed rich media may have higher total concentrations of nutrients, but this effect is confounded by water content diluting the effect from accumulated nutrients. Since any increase in nutrient content would be cancelled out by increased water content, there would be no improvement in catalytic rate of metabolic enzymes. More understanding is warrented for how useless metabolites affect cells in rich and poor media conditions.

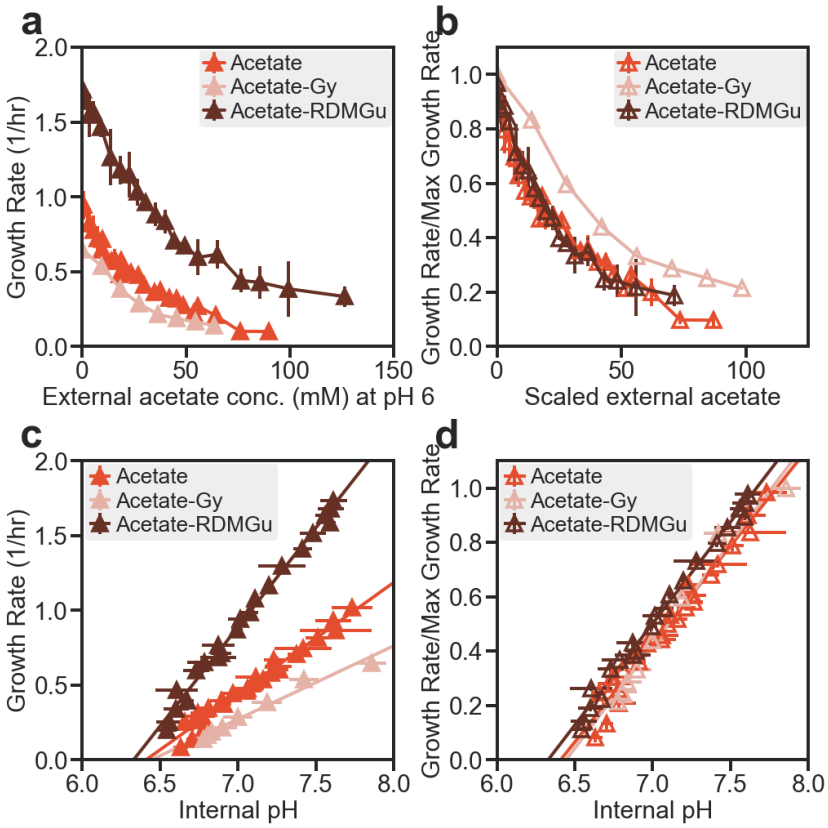

Figure A.9 Effect of carbon quality on growth rate and internal pH for acetate stress.
*E. coli K-12 NCM3722 cells were grown exponentially in glucose minimal media, at various pH fixed by phosphate buffer. Where indicated, scaled quantities are the quantities in the previous panel divided by the growth rate for unstressed cells in a given nutrient condition. Cultures were grown in a Tecan Spark plate-reader. Internal pH was measured with the ratiometric reporter, pHluorin (*122*); see Figure 2.10a,b. The results here also agreed well with the classical biochemical measurement using radiolabeled acid (Figure 2.10c).*

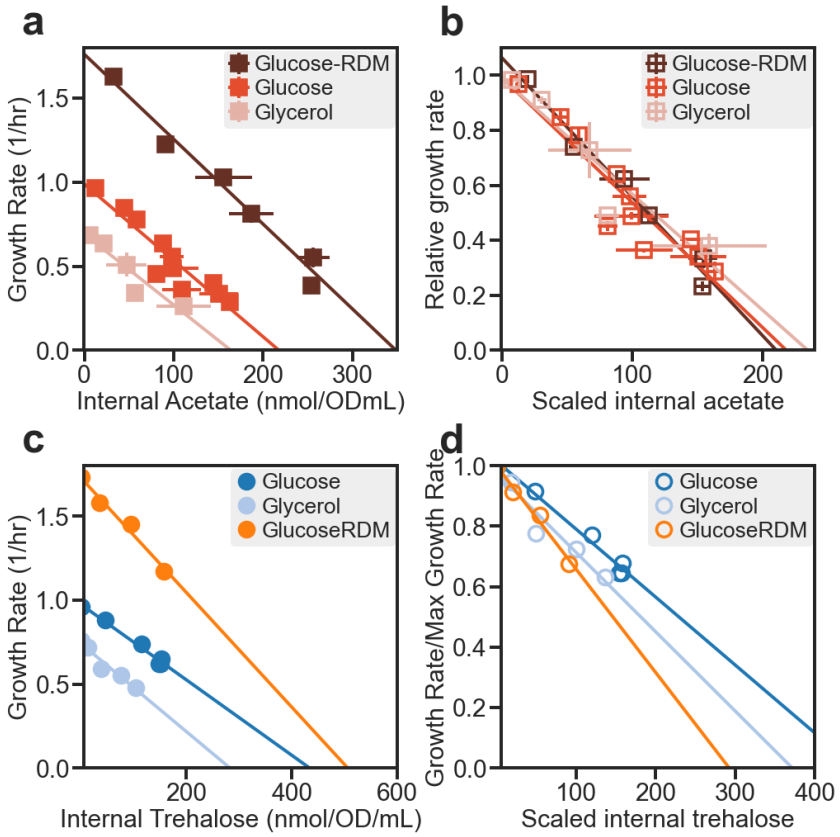

Figure A.10 Effect of carbon quality on internal acetate and trehalose.
E. coli K-12 NCM3722 cells were grown exponentially in glucose minimal media, at various pH fixed by phosphate buffer. Cultures were grown in test tubes to collect samples for either internal acetate or internal trehalose measurements. Where indicated, scaled quantities are the quantities in the previous panel divided by the growth rate for unstressed cells in a given nutrient condition.

A.5 Stress from organic acids other than acetate

There are many other organic acids that are toxic to E. coli and other organisms. Some organic acids are alternative biproducts of metabolism. This category includes compounds such as lactate, formate, pyruvate. Other organic acids have specific activity as inhibitors. This category includes compounds such as benzoic acid and sorbic acid. It's unknown how many of these inhibitors other than acetate affect cells. However, according to the equilibrium theory proposed by Russell, most acids should accumulate at the same concentrations of acetate. Primary results show that there are likely diverse mechanisms of action from organic acids, which are informed by equilibrium theory.

We first begin with measurements of organic acids that are related to metabolism. Although these organic acids are typically not found in high concentrations in the gut, these organic acids can be excreted in large concentrations in certain conditions. For example, formate is excreted anaerobically as a byproduct of acetate and ethanol metabolism. Lactate is excreted typically at low pH. Pyruvate is excreted in response to sudden application of acetate. We measured growth rates of E. coli growing in these organic acids at pH 6. Surprisingly these acids are weaker than acetate for the same pH. This weakness is somewhat surprising given that these acids are stronger than acetate in the sense that they have lower pK_a's. In order to understand the effects of these acids further, we compared their effects to NaCl, which acts as an osmolyte that doesn't enter cells. The growth rate behavior of NaCl is most similar to sodium pyruvate.

It's likely that if these was entering the membrane of cells, we might find that internal pH would be changing in response to these acids. So, we measured internal pH. The response of internal pH was fairly similar to that of acetate stress for most acids. However, pyruvate again was an outlier, having a pH that was higher than the other acids. Again, comparing the internal pH to osmotic stress from NaCl, we see that pyruvate is quite similar.

Furthermore, we computed the predicted internal anion concentration according to the equation predicted. In this case we see very high predicted internal anion concentrations, much higher than the typical metabolite concentrations found inside the cell. It's not a given that cells are accumulating anions at these high of concentrations. Furthermore, the similarity of pyruvate stress to NaCl stress indicates that pyruvate is more likely acting as an osmolyte rather than a semipermeable acid.

We can then ask why pyruvate isn't entering inside cells like acetate would. Pyruvic acid is unlikely to cross the membrane at high fluxes for the following reasons. The concentration of

pyruvic acid at pH 6 is going to be about 60 times less than that of acetate because the pK_a is 2.93 (pyruvate) vs 4.7 (acetate). Furthermore, diffusion rate of small molecules across lipid membranes has been shown to be related to logP, the water/octanol partition coefficient, and molecule size. Both factors suggest that pyruvic acid diffusion is slower than acetic acid diffusion since pyruvic acid 1.5 times larger than acetic acid and has a slightly lower logP (-.6 vs -.28). Despite the similarity to NaCl stress, we can see that there is a small deviation from the osmotic stress at high pyruvate concentrations, likely because the pyruvate inside the cell reaches a high enough point where it no longer benefits the cell, with that excess becoming "useless".

The other organic acids that we measure, lactate and formate, are likely intermediate cases in between acetate and pyruvate. We can apply the same argument about membrane permeability as we did for pyruvate. Notably these acids have low pK_a's. However formic acid is much smaller than acetate, which would help with permeability, but formic acid is known to dimerize under certain conditions, which would increase the effective size of formic acid, thereby limiting its permeability.

We next turn to the organic acid benzoic acid. This acid is stronger than acetic acid but is more lipophilic with a logP of 1.87 compared to acetic acid's -0.28, suggesting that it should cross the membrane easily. Benzoate is much stronger than acetate. However, the behavior on internal pH is similar to other organic acids. The internal benzoate is predicted to be much lower than for acetate. So, we measured benzoate content in cells. The measured benzoate roughly matched that predicted from the equilibrium equation (Figure A.12). The low accumulation of benzoate suggests that a mechanism other than anion toxicity is inhibiting cells. In yeast, sodium benzoate inhibits the activity of the phosphofructokinase enzyme (*200*, *201*). But it's unclear if that mechanism is

applicable to *E. coli*. Further investigation would be required for organic acids that inhibit via mechanisms other than accumulation of useless metabolites.

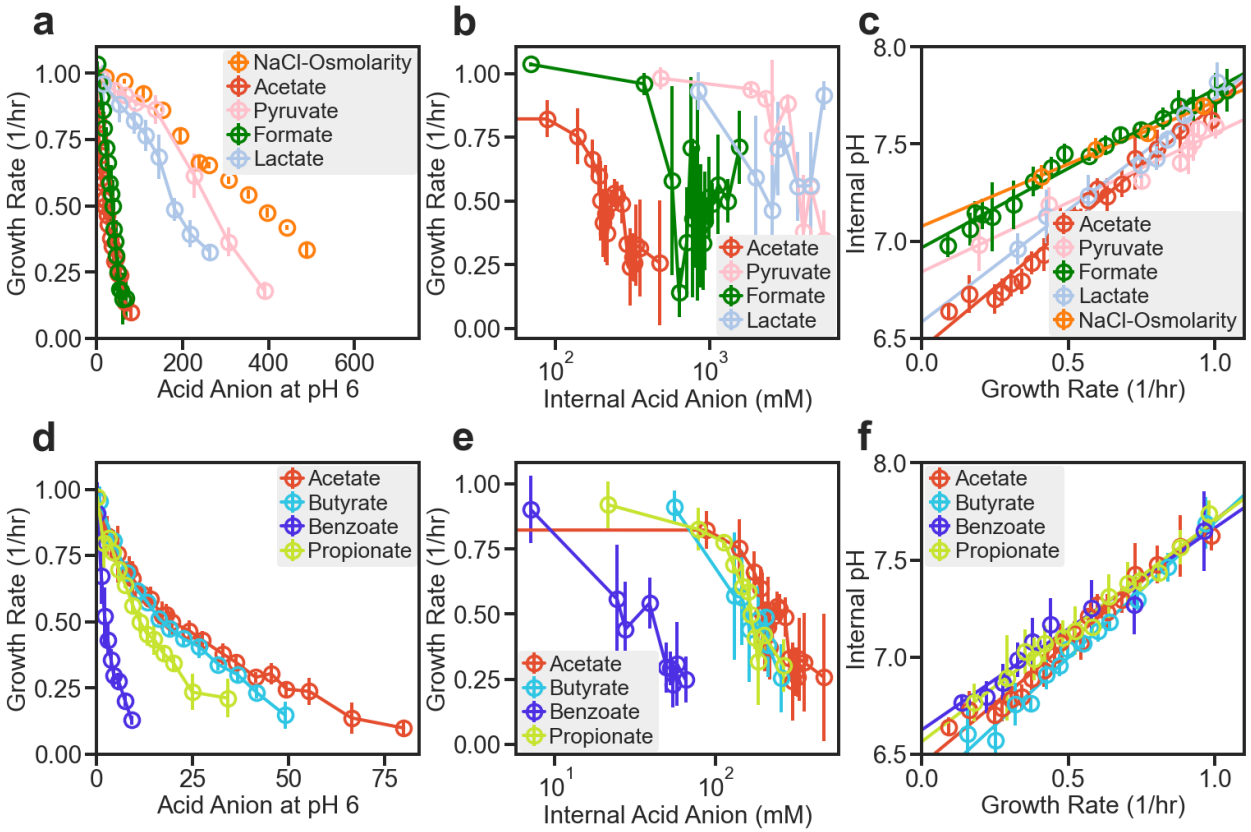

Figure A.11 Sensitivity of E. coli to organic acids other than acetate.
E. coli K-12 NCM3722 cells were grown exponentially in glucose minimal media, at various pH fixed by phosphate buffer. Cultures were grown in Tecan microplate reader. a) and d) Growth in medium fixed to pH 6 and supplemented by various weak organic acids or NaCl for osmolarity condition. Each acid was added as the sodium salt at the concentration indicated on the x-axis. Data are binned for similar x-axis values, with the bins containing data from at least 3 experiments. Error bars are calculated from the standard deviation. b) and e) Internal acid anion is the concentration of acids accumulated calculated according to Eq. 2.1 c) and f) Internal pH was measured with the ratiometric reporter, pHluorin (122) for acetate stressed cells; see Figure 2.10a,b. The results here also agreed well with the classical biochemical measurement using radiolabeled acid (Figure 2.10c).

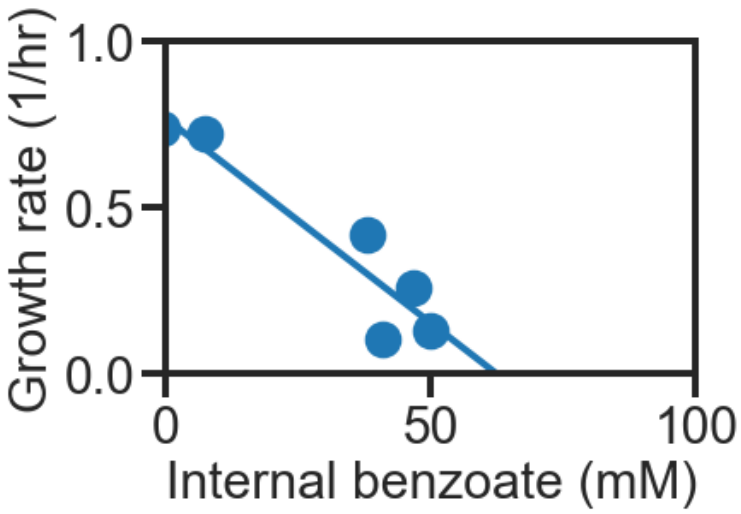

Figure A.12 Internal benzoate for benzoate stressed cells.
Benzoate stress was implemented by growing cells in phosphate buffered glucose medium (pH 6) supplemented with different concentrations of sodium benzoate. Accumulation of internal benzoate in NCM3722 cells was measured by rapidly filtering the culture and measuring the abundance of benzoate using HPLC. The same procedure was performed with cell-free media to correct for benzoate not contained in cells; see Figure 2.9a,b and 2.10.3 for details.

A.6 Origin of sensitivity to low internal pH

While it's commonly accepted that enzyme catalytic rates are effect by changes in pH, it's not immediately clear why E. coli enzymes should be affected by pH so strongly. Indeed, for a given enzyme it's not immediately clear how it will be affected by pH. pH has been shown to affect proteins by disrupting their catalytic sites and overall protein structure. Given the global effect that reduced cytoplasmic pH has on *E. coli*, it's possible there is a global constraint on how proteins are affected by pH.

One possible origin is the titratability of individual residues of a protein. Common to all amino acids is the amino acid groups themselves. The amino acid group contains an acidic carbon and a basic nitrogen. Deprotonation or protonation, respectively, of these atoms effectively transform these molecules into different molecules; a single proton affects how other molecules interact with the "transformed" molecules since most molecular interactions are electrostatic in nature.

However, it's unlikely that the titratability of amino acids groups could explain E. coli's sensitivity to internal pH. The pK_a of the COOH and NH_2 groups are around 2 and 9.5 respectively. Our strain of E. coli grows with cytoplasmic pH between 8 to 6.5. The deprotonation of the COOH carbon happens at too low of a pH, 2, compared to the final inhibition pH of 6.5. It could be possible that there is some effect from the NH_2 group, but the mechanism would be odd. At normal pH (~8) there would be about 5% of NH_2 groups unprotonated. Reducing the pH would protonate the NH_2 molecules such that there is less than 0.5% of NH_2 groups unprotonated. Requiring a small, random fraction of NH_2 groups be unprotonated for maximal catalytic activity doesn't seem likely.

One other alternative is to look at the side chain of the residues as those could have pK_as close to neutrality. The obvious candidate is histidine with a pK_a of 6.5. And indeed the binding forces of interactions of histidine change between their protonated and unprotonated form (*202*). Notably, histidine is found in fairly small abundance (<1% of residues), but histidine residues are localized in the active sites in 50% of all enzymes (*203*). However, its known that the pK_as of active sites can be modified when in the folded state (*204–206*). For example the pK_a of histidine folded within a protein has been measured to be decreased by 1.5 (*203*). Often the titratable groups of proteins exhibit non-Henderson-Hasselbalch behavior (*207*). Additionally, for many cases histidine can be replaced with alternative amino acids that serve a similar purpose. On evolutionary timescales, the problem should be easy to solve.

We can also eliminate other biomolecules. RNA and DNA are acidic with pK_as less than 2. Lipids contain COOH and NH_2 groups, which are for the most part in the pK_a range outside of neutrality. For the limited lipids that do have pK_as around 7, they can be avoided by the organism if necessary.

If proteins and other macromolecules are unlikely to be responsible for pH sensitivity, then an alternative is metabolites. Unlike proteins, metabolites are pretty much fixed on evolutionary timescales. Central carbon metabolism is roughly the same for all domains of life. There are a limited number of biosynthetic pathways for central carbon metabolites. And it's not like there are limited evolutionary constraints for biochemical pathways as secondary metabolism is quite diverse. Furthermore, metabolites contain a titratable group that proteins don't: phosphate. Individual phosphate has 3 protonation sites with pK_as of 2, 6.8, and 12.5. When phosphate is attached to carbon groups the highest pKa site is removed. So, the phosphate connected to one carbon atom has pK_as around 2 and 6.8. This agrees with our observation that growth stops around pH 6.5. Indeed, many carbon-phosphates have pK_as around 6.5. Furthermore, many important cofactors such as ATP, ADP, AMP, NADPH, and NADP+ have phosphates with pK_as in this range. Furthermore, the Gibbs free energy of ATP hydrolysis is decreased at low pH, which would create an additional problem in ATP utilization (*208*). Given the generality of these phosphate-containing metabolites, the internal pH of almost all living organisms could be constrained by the pK_a of phosphate.

Even if the pK_as of these phosphate groups is in a range consistent with the pH of growth inhibition, we can ask why this would decrease catalytic activity, again with the criteria that the reasoning must be stable over evolutionary timescales. Since protonated molecules are effectively different molecules from their unprotonated forms, enzymes can only bind to one form since optimized enzymes can only be optimized for one form of molecule. The consequence of this is the specialization of enzymes for growth either above the pKa or below the pKa. It may even be possible to evolve to optimize both, but there will likely be tradeoffs for that.

One counterpoint may be that if enzymes can change the pKa of individual amino acids, then the same could happen with metabolites. However, in order to apply an electric field that could influence the pKa of a metabolite (i.e. protonate or deprotonate it), the enzyme would have to bind the alternative form, which would again be a form of specialization.

Appendix B

Mathematical details of acetate and useless metabolite stress

B.1 Mathematical details of model

As described in the main text and Figure 2.5a, the accumulation of potassium acetate in the cell is controlled by the internal pH. Potassium acetate accumulation itself exerts an inhibitory effect on cell growth as a useless metabolite. This effect can be reduced by lowering the internal pH. But the pH reduction independently reduces growth rate as well (Figure 2.2d). Here we develop a simple model to study the consequence of this tradeoff.

The reduction of growth from useless metabolites is described by Eq. 2.3 and Figure 2.3f. For a useless metabolite at concentration m, we write the growth rate as $\lambda = \lambda_0 \cdot \beta(m)$, where λ_0 is the unstressed growth rate and

$$\beta(m) = 1 - \frac{m}{m_c}, \qquad \textit{Eq. B.1}$$

with m_c being the inhibitory concentration where growth vanishes. The value of m_c is not known for potassium acetate as a useless metabolite, but we will estimate it later. When the useless metabolite is potassium acetate, the intracellular concentration is dependent on the internal pH through the Henderson-Hasselbalch equation Eq. 2.1,

$$m = 2 \times HA \cdot 10^{pH_{int} - pK_{a,int}} \qquad \textit{Eq. B.2}$$

where HA is the concentration of acetic acid which has equilibrated across the cell membrane, pH_{int} is the internal pH value of the cell, and $pK_{a,int} \approx 4.97$ is the effective pKa value in the cell

according to the data in Figure 2.10d. A factor of 2 is included to account for the potassium associated with acetate.

When cells experience a reduction in internal pH (without useless metabolite accumulation), they also suffer a growth reduction. We describe the data in Figure 2.2d with a quadratic form, $\lambda = \lambda_0 \cdot \gamma(pH)$, where

$$\gamma(pH) = 1 - \left(\frac{pH_{int} - pH_{max}}{pH_{max} - pH_{min}}\right)^2. \qquad \textit{Eq. B.3}$$

Here pH_{max} is the internal pH value of unstressed cells, and pH_{min} is the internal pH at which growth stops. Figure 2.12a shows that the data is well described by the form in Eq. B.3, with the values $pH_{max} = 7.78$, $pH_{min} = 6.42$, and $\lambda_0 = \frac{0.94}{h}$.

To model the combined effect of potassium acetate and internal pH, we have to make an assumption on the function form of the growth rate λ: If $m = 0$ so that $\beta = 1$, then $\lambda = \lambda_0 \cdot \gamma(pH_{int})$ and if $pH_{int} = pH_{max}$ such that $\gamma = 1$, then $= \lambda_0 \cdot \beta(m)$. Here we make assume the joint effect to be described by a simple product form, which is the simplest form satisfying the above constraint,

$$\lambda(HA, pH_{int}) = \lambda_0 \cdot \beta\big(m(HA, pH_{int})\big) \cdot \gamma(pH_{int}), \qquad \textit{Eq. B.4}$$

where $m(HA, pH_{int})$ is given by Eq. B.2.

The only unspecified variable in Eq. B.4 is the internal pH, pH_{int},which is under the control of the cell. For a fixed stress level imposed by an external acetic acid concentration HA, the growth rate given by Eq. B.4 has a unique maximum in the range $pH_{min} < pH_{int} < pH_{max}$ (see Figure 2.5c). In our model, we assume that the cell sets the internal pH at a level pH_{int}^* which maximizes the growth rate. The value of pH_{int}^* is obtained by setting $\frac{\partial \lambda}{\partial pH_{int}} = 0$ where λ comes from Eq. B.4:

$$2 \times HA \cdot 10^{pH^*_{int} - pK_{a,int}} = \frac{m_c}{1 + \frac{\ln 10}{\tilde{\gamma}(pH^*_{int})}}. \qquad \textit{Eq. B.5}$$

here

$$\tilde{\gamma}(pH_{int}) \equiv \frac{\gamma'(pH_{int})}{\gamma(pH_{int})} = \frac{2(pH_{max} - pH_{int})}{(\Delta pH)^2 - (pH_{max} - pH_{int})^2} \qquad \textit{Eq. B.6}$$

and $\Delta pH \equiv pH_{max} - pH_{min} \approx 1.36$.

As mentioned already, we do not know the parameter m_c for potassium acetate as a useless metabolite. We can fix this parameter by fitting the relation between internal pH and the internal potassium acetate concentration found by substituting Eq. B.2 into Eq. B.5. Denoting the internal acetate concentration corresponding to the value of pH^*_{int} by m^*, we obtain:

$$m^* = \frac{m_c}{1 + \ln 10 \cdot \tilde{\gamma}(pH^*_{int})} \qquad \textit{Eq. B.7}$$

This relationship is plotted in Figure 2.12b (solid line). The data is well described for $m_c \approx 620\ mM$.

Notably, the relation between m^* and pH^*_{int} is approximately linear over its range. So, we explored a linear solution as well. To do so, let us simplify the notation first: Let $h \equiv \frac{(pH_{max} - pH^*_{int})}{\Delta pH}$ and let $x = \tilde{\gamma} \cdot \Delta pH$. Then Eq. B.7 is a quadratic equation for $h(x)$, i.e., $x \cdot (1 - h^2) = 2h$, with the solution

$$h = \frac{x}{1 + \sqrt{1 + x^2}} \approx \begin{cases} x/2 + O(x^3) & \text{for } x \ll 2, \\ x/(1 + x) & \text{for } x \gg 1. \end{cases} \qquad \textit{Eq. B.8}$$

Further using $x = \frac{\frac{bm^*}{m_c}}{1 - \frac{m^*}{m_c}}$ from Eq. B.7 where $b \equiv \Delta pH \ln 10 \approx 3.1$, we obtain

$$h(m^*) = \frac{bm^*}{m_c - m^* + \sqrt{m_c^2 - 2m^* m_c + (1+b^2)(m^*)^2}}$$

Eq. B.9

$$pH^*{}_{int} \approx pH_{max} - \frac{(\Delta \mathrm{p}H)^2\, m^*}{2m_c \ln 10} + O\left(\frac{m^*}{m_c}\right)^2 \quad \text{for } m^* \ll \frac{m_c}{\left(1+\frac{b}{2}\right)} \approx 0.37 m_c.$$

The linear (small-x) solution in Eq. B.9 is plotted in Figure 2.12b as a dashed line. We see that the exact solution is well approximated by the small-x solution (dashed line) over the regime where data is available. The linear form of the pH-acetate relation shows that for much of the data range, the inhibitory concentration m_c is shifted to a smaller value, $m_c' = \frac{2m_c}{\Delta pH \ln 10}$, which is the intersection of the dashed and dotted line in Figure 2.12b, where $pH^* \to pH_{min}$ (or $h \to 1$) and growth rate vanishes. From the best-fit parameter $m_c \approx 620\, mM$, we obtain $m_c' \approx 400\, mM$. The difference between the two parameters reflects the additional cost due to pH reduction.

Using Eq. B.9, we can express the growth rate $\lambda^* = \lambda_0 \cdot (1+h^2)\left(1 - \frac{m^*}{m_c}\right)$ in term of the internal potassium acetate alone. Figure 2.12c shows that the approximate linear decrease of growth rate against the internal potassium acetate concentration, shown also in main text Figure 2.3f, recovered here as the small-x expansion. The dotted line is obtained using the approximate linear relation between m^* and h^*, i.e., for

$$\lambda^* \approx \lambda_0 \cdot \left(1 - \frac{m^*}{m_c}\right)\left(1 - \left(\frac{(\Delta pH)^2\, m^*}{2m_c \ln 10}\right)^2\right), \qquad \textit{Eq. B.10}$$

which has $\lambda^* \to 0$ as $m^* \to m_c'$, the apparent inhibition concentration.

The exact relation between growth rate and internal pH, plotted as the solid line in Figure 2.12d, is obtained from substituting the metabolite concentration from Eq. B.7 into Eq. B.4 as

$$\lambda^* = \lambda_0 \frac{1-h^2}{1+\frac{2h}{[b(1-h^2)]}}. \qquad \textit{Eq. B.11}$$

Finally, the dependence of the growth rate on the acetic acid concentration, shown as the solid line in Figure 2.5b, is obtained as an implicit function defined by $\lambda^*(h)$ in Eq. B.11 and $HA(h)$ from Eq. B.5:

$$HA(h) = \frac{m_c}{2} \frac{e^{bh} 10^{pK_{a,int} - pH_{max}}}{1+\frac{b(1-h^2)}{2h}} \qquad \textit{Eq. B.12}$$

We can ask what parameters the cell can change to increase tolerance to acetate. To do this, we solve the half-inhibitory acetic-acid concentration, HA_{50}, which is the acetic acid concentration where the growth rate is halved. To find HA_{50}, first we solve the value $h_{50}(b)$ where $\lambda^* = 0.5\lambda_0$ using Eq. B.11, and then insert $h_{50}(b)$ into Eq. B.12. For $\lambda^* = \frac{\lambda_0}{2}$, we find $h_{50} \approx \frac{b}{2+b\sqrt{2}}$. Substituting this dependence of $h_{50}(b)$ into Eq. B.12, we obtain

$$HA_{50} = \frac{m_c}{2} \frac{e^{\left(\frac{b^2}{2+b\sqrt{2}}\right)} 10^{pK_{a,int} - pH_{max}}}{1+\frac{b\left(1-\left(\frac{b^2}{2+b\sqrt{2}}\right)^2\right)}{2\left(\frac{b^2}{2+b\sqrt{2}}\right)}} \qquad \textit{Eq. B.13}$$

$$HA_{50} \approx \frac{m_c}{2}\sqrt{2} \frac{10^{\left(\frac{1}{\sqrt{2}}-1\right)pH_{max} - \frac{pH_{min}}{\sqrt{2}} + pK_{a,int}}}{\sqrt{2} + 1 - 2\ln^2 10\,(pH_{max} - pH_{min})^2} \qquad \text{for } \Delta pH \gg \frac{1}{\sqrt{2}\ln 10} \qquad \textit{Eq. B.14}$$

Eq. B.13 and Eq. B.14 show that up to a substance-specific effect represented by m_c, the half-inhibitory concentration HA_{50} is dependent on both the value of the stress-free pH (pH_{max}) and the minimal pH (pH_{min}), with $\log_{10}\left(\frac{A_{50}}{m_c}\right) \sim -0.29pH_{max} - 0.71pH_{min}$. Thus HA_{50}

increases (i.e., the cell becomes more tolerant to acetate) with either decrease in the normal (max) pH or decrease in the minimal pH, but with the latter being about twice as potent as the former. The full dependence of $\frac{HA_{50}}{m_c}$ on $pH_{max} - pH_{min}$ and on pH_{max}, based on the exact solution, is shown in Figure B.1, and the dependence on pH_{min} and pH_{max} is shown in Figure B.1b. Contour plots are shown in Figure 2.12e,f.

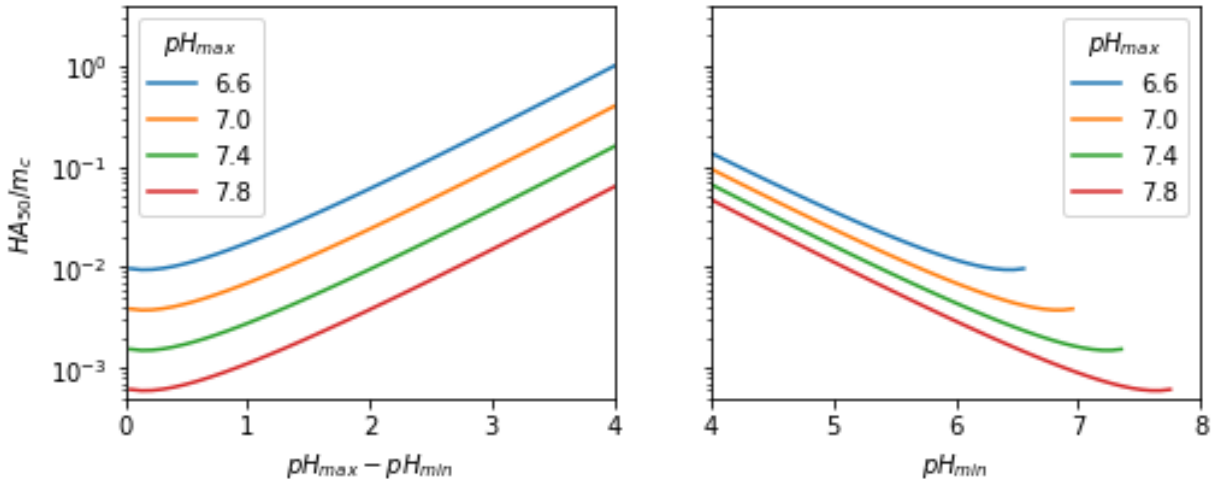

Figure B.1 The dependence of the half-inhibitory acetic acid concentration on model parameters. a) HA_{50} expressed in term of the substrate-specific characteristic concentration m_c given by Eq. B.13, for various values of stress-free pH (pH_{max}) and the viable pH range $pH_{max} - pH_{min}$. b) Same quantity as that plotted in panel b, but for various values of the stress-free pH (pH_{max}) and the minimal pH (pH_{min}).

B.2 Useless metabolite stress and growth laws

Previous studies have shown that growth rate is correlated with protein flux. It's often been assumed that metabolites are not limiting. Indeed, this is supported by strong correlations between protein content and growth flux. However, other studies have shown that protein content is not the sole determinant of flux. Ribosomes in particular are limited by tRNA concentrations, especially in nutrient limited concentrations but also in osmotically stressed conditions.

We begin our discussion by considering a simple enzymatic reaction system. We model the growth of the cell as a set of reactions. Each reaction flux, v_i, is described as a Michaelis-Menton type reaction for enzyme i

$$v_i = v_{cat,i} \cdot \phi_i \cdot \frac{c_i}{c_i + K_{m,i}} \qquad \textit{Eq. B.15}$$

where $v_{cat,i}$ is the maximum flux, ϕ_i is the protein mass fraction, c_i is the metabolite, and $K_{m,i}$ is the Michaelis-Menton constant for enzyme i. In the case where the metabolite, c_i, is much higher than $K_{m,i}$, the reaction flux is determined by the maximum flux and protein mass fraction i.e. $v_i = v_{cat,i} \cdot \phi_i$. In this limit, there is a unique solution given if one assumes flux balance and a maximum total protein concentration i.e.

$$v_i = v_j \text{ and } \sum_{i=1}^{n} \phi_i = \phi_{max} \qquad \textit{Eq. B.16}$$

for all reactions i and j. Then the growth rate is defined by

$$\lambda = \left(\sum\nolimits_{i=1}^{n} \frac{1}{v_i} \right)^{-1} \qquad \textit{Eq. B.17}$$

Which is a similar form to (*59*).

Returning to the metabolite limited case, if there are no constraints on metabolite concentrations, then the metabolite concentration that provides the maximum flux for cells approaches infinity. In our useless metabolite stress, we find that metabolite concentrations decrease overall. The exclusion of useful metabolites suggested from Figure 2.3d-f hints that the total concentration of metabolites is constrained for our cells. Following Eq. B.1,

$$\lambda \sim \sum\nolimits_{i=1}^{n} c_i = m_{max} \qquad \textit{Eq. B.18}$$

Where m_{max} is the total concentration of metabolites.

With the maximum substrate concentration set, we can find the substrate concentrations, m_i, that give the maximum growth rate by setting the derivative of growth rate with respect to each substrate concentration to 0 and solving for the m_i

$$\frac{d\lambda}{dm_i} = 0 \qquad \textit{Eq. B.19}$$

Assuming the Michaelis-Menten kinetics, the functional form of growth rate from Eq. B.17 and 12 is

$$\lambda = \phi_{max}\left(\sum_{i=1}^{n}\frac{m_i + k_{m,i}}{v_{cat,i}m_i}\right)^{-1} \qquad \textit{Eq. B.20}$$

With the maximum metabolite constraint, one substrate concentration can be eliminated. Without loss of generality, let's go with the last one, $m_n = m_{max} - \sum_{i=0}^{n-1} m_j$

$$\lambda = \phi_{max}\left(\frac{K_{m,n} + m_{max} - \sum_{\mathrm{j}=0}^{n-1} m_j}{v_{cat,n}\left(m_{max} - \sum_{\mathrm{j}=0}^{n-1} m_j\right)} + \sum_{\mathrm{j}=1}^{n-1}\frac{m_j + K_{m,\mathrm{j}}}{v_{cat,j}m_j}\right)^{-1} \qquad \textit{Eq. B.21}$$

We can exclude cases where λ = 0 so that finding the zero can by simplified by rewriting the derivative

$$\frac{\partial\lambda}{\partial m_i} = -\lambda^2\frac{\partial\lambda^{-1}}{\partial m_i} = 0 \Leftrightarrow \frac{\partial\lambda^{-1}}{\partial m_i} = 0 \qquad \textit{Eq. B.22}$$

For an arbitrary m_j the derivative of λ^{-1} is then calculated as

$$\frac{\partial\lambda^{-1}}{\partial m_j} = \frac{K_{m,n}}{v_{cat,n}\left(m_{max} - \sum_{i=0}^{n-1} m_i\right)^2} - \frac{K_{m,j}}{v_{cat,j}m_j^2} = 0 \qquad \textit{Eq. B.23}$$

This equation can then be simplified by resubstituting $m_n = m_{max} - \sum_{j=0}^{n-1} m_j$ after computing the derivative. Without loss of generality, any metabolite concentration pair of j and n is related to another by

$$m_n^2 = \frac{v_{cat,\mathrm{n}} K_{m,\mathrm{i}}}{v_{cat,\mathrm{i}} K_{m,\mathrm{n}}} m_i^2 \qquad \textit{Eq. B.24}$$

The metabolite concentrations can then be written in terms of the total metabolite concentration, m_{max} and no other metabolite.

$$m_j = m_{max} \sqrt{\frac{v_{cat,j}}{K_{m,j}}} \left(\sum_{i=1}^{n} \sqrt{\frac{v_{cat,i}}{K_{m,i}}} \right)^{-1} \qquad \textit{Eq. B.25}$$

A few things are of note for this solution of metabolite concentrations, m_j. First thing is that every substrate concentration scales with the maximum total concentration, independently of the details of the kinetics. So, every reaction gets an equal piece of the pie. Additionally, there is a cost to adding reactions because every reaction added dilutes the pool for the other metabolites. So, removing reactions by adding metabolites should help increase the available pool. Experimentally, reactions could be removed by adding building blocks such as amino acids or vitamins to the media.

Under these constraints, we can solve for the growth rate. Substituting the new values for m_j from into equation (6)

$$\lambda = \phi_{max} \left(\sum_{j=1}^{n} \frac{m_{max} \sqrt{\frac{v_{cat,j}}{K_{m,j}}} \left(\sum_{i=1}^{n} \sqrt{\frac{v_{cat,i}}{K_{m,i}}} \right)^{-1} + K_{m,j}}{v_{cat,j} m_{max} \sqrt{\frac{v_{cat,j}}{K_{m,j}}} \left(\sum_{i=1}^{n} \sqrt{\frac{v_{cat,i}}{K_{m,i}}} \right)^{-1}} \right)^{-1} \qquad \textit{Eq. B.26}$$

We can then simplify this equation by separating two terms, one independent and one dependent on m_{max}. This simplifies to

$$\boxed{\lambda = \lambda_\infty \phi_{max} \frac{m_{max}}{\frac{\lambda_\infty}{\kappa} + m_{max}}} \qquad \textit{Eq. B.27}$$

where $\lambda_\infty \equiv \left(\sum_{j=1}^{n} \frac{1}{v_{cat,j}}\right)^{-1}$ and $\kappa \equiv \left(\sum_{i=1}^{n} \sqrt{\frac{v_{cat,i}}{K_{m,i}}}\right)\left(\sum_{j=1}^{n} \frac{\sqrt{K_{m,j}^3}}{\sqrt{v_{cat,j}^3}}\right)$ are parameters that have no dependence of metabolite concentrations, only being dependent on the Michaelis-Menton parameters of the enzymes. The first parameter, λ_∞, is the maximum possible growth rate which can be obtained for unlimited metabolites and depends on the maximum kinetic rates of the enzymes. The second parameter is metabolite concentration dependent, set by the product of κ, an effective K_m, and m_{max}, the total metabolite concentration in the cell.

We can compare this formula to the behavior seen in the useless metabolite stress. Unlike the typical curve of Michalis-Menton functions, the useless metabolite limitation produces a straight line vs growth rate. A straight line is still compatible with a Michalis-Menton function. For Eq. B.27, if we take the limit where $m_{max} << \lambda_\infty/\kappa$, then the equation simplifies to a linear form

$$\lambda = \phi_{max} m_{max} \kappa \left(1 - \frac{\kappa}{\lambda_\infty} m_{max}\right) \qquad \textit{Eq. B.28}$$

or alternatively (only taking solutions that are first order in m_{max}

$$\lambda = \phi_{max} m_{max} \qquad \textit{Eq. B.29}$$

But when does the constraint $m_{max} << \lambda_\infty/\kappa$ arise for the cell? Or in other words, is the following number much larger than the total concentration of metabolites in E. coli cells? Based on dimensional scaling, this value should scale mostly with total K_m of the individual reactions. This scaling may not necessarily hold depending on the distributions of these numbers. It looks like unequal values mean higher $\frac{\lambda_\infty}{\kappa} \sim \sum_{j=1}^{n} k_{m,j}$ values. So, the total kms should give an underestimate of this λ_∞/κ parameter. Because calculating the total kms is much easier than calculating λ_∞/κ directly, it could give an independent estimate of how straight the Michalis-Menton curve should be.

Within this formulation, we can find the relationship between protein abundances and metabolite concentrations. Protein mass fraction ϕ_i for an enzyme i is related to growth rate by $\lambda = \phi_i \cdot v_i$. Therefore, by using the expression for growth rate, the protein mass fraction is

$$\phi_i = \frac{\lambda_\infty \phi_{max}}{v_{i,max}} \frac{m_{max} + \frac{(K_{m,i})^{3/2}}{\sqrt{v_{i,max}}\alpha}}{m_{max} + \frac{\lambda_\infty}{\kappa}} \qquad \textit{Eq. B.30}$$

where $\alpha \equiv \sum_{i=1}^{n} \sqrt{\frac{v_{max,i}}{K_{m,i}}}$.

We can take the derivative of ϕ_i with respect to m_{max} to more clearly see how ϕ_i depends on enzyme parameters.

$$\frac{d\phi_i}{dm_{max}} = \frac{\lambda_\infty \phi_{max}}{v_i \alpha} \frac{\left(\frac{\alpha\lambda_\infty}{\kappa}\right) - (k_{m,i})^{3/2}(v_i)^{-1/2}}{\left(m_{max} + \frac{\lambda_\infty}{\kappa}\right)^2} \qquad \textit{Eq. B.31}$$

The change of protein fraction depends on the relative values of $\left(\frac{\alpha\lambda_\infty}{\kappa}\right)$ and $(k_{m,i})^{3/2}(v_i)^{-1/2}$, which are global and local parameters, respectively. If m_{max} is decreased, ϕ_i decreases if $(k_{m,i})^{3/2}(v_i)^{-1/2} < \left(\frac{\alpha\lambda_\infty}{\kappa}\right)$. Biologically speaking, this means that proteins with high effective K_ms relative to the "global" K_m will be anticorrelated with changing m_{max}. In other words, when total metabolites are limiting, enzymes with high K_ms will be overexpressed as those proteins are the most sensitive to concentrations of the metabolite they require. And they get more inefficient if they don't have a pool available for them to use. At high m_{max} the proteome would be relatively dominated by proteins with low K_ms relative to the total flux required for growth.

Enzymes with multiple metabolites

In the previous section, we assumed that all cellular reactions were just of the Michaelis-Menton type. However, most reactions involve more than one metabolite, either being a reversible

reaction where the product can inhibit production of the substrate or there are multiple substrates (*60*, *209*).

The simplest equation of a reaction involving two substrates is

$$v_{ab} = \frac{v_{cat,ab}}{K_{m,ab}} m_a m_b \qquad \textit{Eq. B.32}$$

where v_{ab} is the reaction flux for the reaction involving substrates a and b, $K_{m,ab}$ is the substrate constant, m_a is the concentration of metabolite a, m_b is the concentration of metabolite b. If we fix the metabolite concentration for this reaction such that $m_{max} = m_a + m_b$, and substitute one of the metabolite concentrations with m_{max}, then we find that maximizing this reaction flux happens when the two metabolite concentrations are equal, $m_a = m_b = \frac{m_{max}}{2}$. Furthermore, for the slightly more complicated reaction where the flux can be saturated by the metabolites,

$$v_{ab} = v_{cat,ab} \frac{m_a m_b}{m_a m_b + K_{m,ab}} \qquad \textit{Eq. B.33}$$

the same condition on the metabolite concentrations applies, $m_a = m_b = \frac{m_{max}}{2}$. Overall flux is more sensitive to the total concentration of metabolites for these two types of equations since this flux changes with the square of m_{max} instead of linearly.

Similarly, we can consider the case where there are two reactions, with a single metabolite shared between those two reactions. We call the separate metabolites m_a and m_b and the shared metabolite m_c. Then for reaction i where i is either a or b,

$$v_i = v_{cat,ic} \frac{m_i m_c}{m_i m_c + K_{m,ic}} \qquad \textit{Eq. B.34}$$

Again, by setting the reaction fluxes equal and the derivatives equal to zero, we find that for when the total metabolite pool is constrained by m_{max}, the shared metabolite is $m_c = \frac{m_{tot}}{2}$ and

$m_a = \frac{m_{max}}{2\left(\sqrt{\frac{v_{cat,ac}K_{m,bc}}{v_{cat,bc}K_{m,ac}}}+1\right)}$ and $m_b = \frac{m_{max}}{2\left(\sqrt{\frac{v_{cat,bc}K_{m,ac}}{v_{cat,ac}K_{m,bc}}}+1\right)}$. The shared metabolite, m_c, uses half of the total metabolites. So, one prediction that could come of this observation is that metabolites that are involved in multiple reactions will be in relatively higher abundance than metabolites involved in single reactions. Examples of these metabolites include glutamate, which is involved in the transamination of most amino acids, ATP, which is involved in many reactions of both catabolism and anabolism, and NADPH, which is involved in the biosynthesis of multiple molecules. Because each metabolite concentration scales linearly with m_{max}, the growth rate again simply scales with the square of the metabolite concentration.

Appendix C

Condition dependent physiology of anaerobic *E. coli* and *Bacteroides thetaiotaomicron*

C.1 Proteome of B theta growing on different sugars

To understand the *B. theta* proteome, we performed proteomics of *B. theta* growing on 6 different sugars. For *B. theta* growing on these different sugars, their growth rates are similar (*15*). Using absolute abundances, we averaged the overall abundance of the peptides to understand the most abundant peptides in the genome. Looking at the top 10 most abundant proteins, many proteins are involved in metabolism and protein synthesis.

Proteins involved in protein synthesis include elongation factor Tu, elongation factor-G, EF-Ts, 50s and 30s proteins subunits. Surprisingly, several proteins are chaperone proteins. Typically, chaperone proteins assist in protein folding during synthesis and are expressed during stress such as excessive heat. However, our samples were collected in physiological conditions which shouldn't introduce problems with folding. This suggests that *B. theta* uniquely has issues with translation.

Many of *B. theta*'s highly expressed are involved in metabolism. As *Bacteroides* are adapted to low oxygen conditions, their metabolism is based around fermentation/anaerobic respiration. Correspondingly, those abundant proteins are involved in glycolysis or fermentation. The most abundant of these proteins is pyruvate carboxy kinase, which makes up about 3% of the proteome. This enzyme is fairly special to *Bacteroides*. The enzyme, *pckA* is beneficial to use because it conserves ATP when converting PEP to OAA, which is a step involved in succinate

excretion. Also unique to *Bacteroides* is the expression of pyruvate phosphate dikinase (*ppdk*) and pyrophosphate-fructose 6-phosphate (*pfp*).

Several abundant proteins of *B. theta* are also uncharacterized. Most notable of these proteins is *BT0173* and *BT0174*. While these proteins are uncharacterized according to Uniprot, many *Bacteroides* contain this protein in their genome. With *BT0173*, this homology shows up in the form of a GGGtGRT protein motif. *BT0174* is more interesting, being labeled as a *nifU* homologue. *nifU* homologues are involved in a variety of processes, but the most likely reason for *nifU* homologues is iron sulfur cluster building. *B. theta* contains many iron-sulfur clusters, some of which may be involved in metabolism (*210*). They are particularly sensitive to oxygen. The larger of the two, *BT0173* contains that GGGtGRT motif. Family members are found in bacteria. Proteins in this family are approximately 330 amino acids in length and contain many highly conserved residues including a GGGtGRT motif.

C.2 Physiology of carbon limited growth

To better understand the physiology of these two bacteria, we limited growth by controlling the supply of glycolytic carbon sources (referred to as carbon limited growth) while still maintaining steady-state growth. Steady-state cells are well-defined physiologically since they grow with a well-defined growth rate. We present two ways to implement carbon limited growth in bacteria for a given carbon source. One way is to change the concentration of a carbon source. With *E. coli* growing on glucose, the maximum growth rate can be achieved. However, the Km is too low for practical growth (*11*). The alternative way to implement carbon limited growth is to control the expression of uptake proteins. For *E. coli*, we implement this by using glucose as the carbon source and titrating the expression of *ptsG*, a glucose transporter (*27*).

Bacteria consume carbon when they grow. In general, this carbon consumption depends on the conditions of the media and on the organism. We find that for many different growth

conditions, the consumption of carbon from the media is linearly correlated to the growth of cells (Figure 3.5). The linear consumption allows us to define the uptake as the amount of carbon consumed per unit of biomass produced. This uptake quantity allows us to define relevant parameters for characterizing the physiology of these cells. The multiplicative inverse of the uptake is the yield of cells. The yield relates how much carbon is needed to produce a given quantity of cells, expressed here relative to OD_{600} which has been shown to scale with biomass (*121*).

We observed a large decrease in the yield of E. coli in the anaerobic condition compared to the aerobic condition. As shown in Figure 4.1, this difference persists across the growth conditions. For both conditions, the yield decreases as growth rate also decreases. Comparing the fastest growth rates for each oxygen condition, the yield is 0.08 OD/mM Glucose vs 0.2 OD/mM Glucose in anaerobic and aerobic condition, respectively. This yield difference is expected as the ATP yield per glucose is much lower for fermentative metabolism compared to aerobic metabolism (*121*).

It's been previously observed that carbon yield is dependent on growth rate, with slower growing cells typically have smaller yields. By transforming the yield to flux, there is a linear correlation between carbon uptake flux and growth rate. The parameters of the linear fit can be interpreted physiologically. The slope of the line is the maximum uptake rate that can be achieved by fast growing cells. The y-intercept is called the maintenance flux. It represents a constant cost of carbon uptake that is independent of biomass accumulation.

We also present a method for implementing carbon limited growth in *B. theta* without using genetic tools. In general, *B. theta* has a similar maximum growth rate for a variety of sugars (*15*). However, the K_ms for these sugars varied. Unfortunately, the K_m for glucose was relatively low.

Therefore, we chose mannose as the sugar to control carbon uptake because of its higher K_m compared to glucose.

The yield of *B. theta* in anaerobic growth was higher than the yield of *E. coli* in anaerobic growth. In the respective reference conditions, the yield of *B. theta* as 0.14 OD/mM hexose (mannose) compared to 0.08OD/mM hexose (glucose) anaerobic yield of *E. coli*. Similarly, the projected maintenance flux in E. coli is over 5 times higher at 4.9 mM/OD/h compared to *B. theta*'s 0.8mM/OD/hr. These differences in uptake suggest that *B. theta* has evolved to be very energy efficient even without the benefit of oxygen. The yield numbers of *B. theta* are closer to aerobic *E. coli*'s aerobic yield than anaerobic *E. coli*'s anaerobic yield, further illustrating *B. theta*'s efficiency.

C.3 Genomic Comparison of E. coli and B. theta

In order to further compare *E. coli* and *B. theta*, we plan to analyze their respective genomes at a gene level and higher. These genomes of these two organisms have been published (*82*, *211*). Being a common laboratory organism, *E. coli* has a well annotated genome with a variety of databases characterizing gene functions and relationships between those genes. However, even though B. theta and related Bacteroides are some of the most studied gut bacteria, relatively less attention has been placed on annotating the *B. theta* genome. For example, while 97.4% of *E. coli* genes have at least gene ontology (GO) annotation, only 80.5% of *B. theta* genes have at least one GO annotation. Furthermore, the mean number of annotations for each gene in *E. coli* is 5.4 while the mean for *B. theta* is 2.9. There is a similar bias towards *E. coli* annotation for COG (clusters of orthologous groups) and EC labels as well (Figure C.2). This difference presents an obstacle for analysis for comparing the two genomes as any comparison using these tools would be biased.

To avoid this category bias, we consider two methods. One is to use GO pathways as a guide for annotating conserved pathways. For example, ribosomal, glycolytic, and TCA cycle

genes are typically highly conserved and so are more likely to be successfully annotated. The other method is to find homologue pairs between the two organisms for comparison purposes. To find homologues, we blastp each species' genome against each other and find pairs that matched based on an e-value cutoff of 10^{-5} (Figure C.2). Matches from one genome to the other that didn't match uniquely, i.e. a singular match, were ignored for further analysis. This algorithm generated 836 homologous pairs of proteins between the two organisms. This set of homologues is also useful for ad hoc labeling the *B. theta* genome using the labels from the *E. coli* genome. If the matches do successfully represent homologues, it is likely their functions are similar. The annotation from our well annotated organism, *E. coli*, can then be applied to the less annotated organism, *B. theta*. The matched homologues can be used to validate the completeness of the annotations.

C.4 Quantitative proteomic mass spectrometry

To further understand *E. coli* and *B. theta* physiology, we took quantitative proteomic measurements to measure gene expression levels between the two organisms and to see how those genes change in response to carbon limited growth. To estimate the completeness of our proteomics measurements, we can estimate the mass fractional abundance of ribosomes using data from our total RNA measurements. Because most of RNA in steady state *E. coli* cells are part of ribosomal complexes, we assume that the fraction of RNA to ribosomes is relatively constant even as growth rate changes. Previous studies have found that the ratio of rRNA to protein is about 0.76 in *E. coli* (*58*). As shown in Figure C.3, we find that the measured RNA/Protein ratio fits well with the ribosome mass fraction via mass spec.

C.5 Carbon limitation proteomics of E. coli and B. theta

We start with comparing non-growth-limited conditions for *E. coli* and *B. theta*. Figure C.4 shows that *E. coli* grown in aerobic and anaerobic conditions in glucose minimal media does not differ much in proteome allocation, with the proteins overall being well correlated. In comparison

Figure C.4, shows that while *B. theta* and *E. coli* genes are correlated ($r^2 = 0.413$), the correlation is weaker.

We can further compare the *E. coli* and *B. theta* proteome by looking at protein synthesis and central carbon pathways. To group proteins into these pathways, we use Gene Ontology (GO) enrichment analysis. Figure C.5 shows how the mass fractions of these different pathways changes as cells become more carbon limited. Results for *E. coli* are presented in both aerobic and anaerobic conditions while results for *B. theta* are in anaerobic conditions.

Looking at the tricarboxylic acid cycle, the summed mass fractions of these proteins make up a significant portion of the *E. coli* aerobic proteome, ranging from 5% to 8%. In contrast, *E. coli* grown anaerobically has significantly reduced expression, ranging from 2 to 4%. Similar to anaerobically grown *E. coli*, *B. theta*, grown in anaerobic conditions, expresses low levels of the tricarboxylic acid cycle proteins, ranging from 1-2.5%. The tricarboxylic acid (TCA) cycle, when ran as a cycle, generates significant amounts of NADH. In aerobic growth, NADH can be used along with oxygen to produce energy and NAD. In anaerobic growth, NADH must be recycled without oxygen, so organisms growing anaerobically would not be able to use the TCA cycle without an electron acceptor for NADH. Therefore, the reduced expression of TCA cycle proteins for both *E. coli* and *B. theta* is consistent with reduced flux through the TCA pathway. Both organisms need some expression for amino acid precursor synthesis, producing useful precursor amino acids such as aspartate and glutamate.

We also see significant differences in glycolytic gene expression between aerobic and anaerobic *E. coli* (Figure C.5), again, likely due to the shift in metabolism caused by lack of oxygen. *E. coli* growing anaerobically resorts to fermentative metabolism, which has a lower

energy yield. To maintain ATP flux for biosynthesis, more carbon must be imported for the same growth rate.

Surprisingly, *B. theta* has lower levels of glycolytic genes (5-8%) compared to anaerobically grown *E. coli* (8-10%) (Figure C.5). B. theta has a higher biomass yield compared to anaerobically grown *E. coli* (Figure 4.1). So, it does not need to import as much carbon through glycolysis to make energy. Why does *B. theta* have a higher yield than anaerobically grown *E. coli*? We propose *B. theta* achieves is energy efficiency from its ability to utilize pyrophosphate (PPi) to replace ATP in some reactions. *B. theta* has high levels of enzymes that can utilize PP_i Figure C.9). In addition, *B. theta* has an alternative oxaloacetate synthesis gene, *pckA*, which produces ATP (*7*).

We also examined the complete set of amino acid biosynthesis genes with GO. This was done by summing the set of all proteins that contained the biosynthetic pathways for each of the 20 amino acids that E. coli uses for synthesis. Expression of amino acid biosynthesis genes is flat over the growth rate change for both organisms. Expression in *E. coli* is also similar for both oxygen conditions, suggesting that amino acid biosynthesis is not limited or enhanced by oxygen availability. Notably, *B. theta* expresses half as many amino acid biosynthesis genes as *E. coli*. Because the proportion of protein relative to dry mass is similar between the two organisms, this difference suggests that *B. theta* is more efficient at synthesizing amino acids. Part of this difference can come from the methionine biosynthesis genes.

C.6 Growth Limitations in *B. theta*

We present 4 growth limitations to *B. theta*. These limitations are antibiotic, low carbon, low nitrogen, and low carbon dioxide. Carbon and nitrogen are input nutrients for the gut. The ratio of carbon to nitrogen that makes it to the colon can influence the point where they are limited, respectively. *B. theta* is known to require CO_2 for optimal growth (*212*).

The limitation imposed on at the hexose sugar level was implemented by titrating the concentration of mannose available. The CO_2 limitation was imposed by controlling levels of bicarbonate added to a Hungate tube with a fixed volume and pH. The nitrogen limitation was imposed by substituting the preferred nitrogen source, ammonia, with a titratable source, N-acetylglucosamine. The limitation was imposed on translation by adding the ribosome inhibiting antibiotics, tetracycline, at sub-inhibitory concentrations. We were able to obtain a large range of growth rates with these 4 limitations ranging for 0.7/h to 0.2/h (Figure C.6).

C.7 Excreted metabolites

In addition to mannose uptake, we measured the excreted fermentation products of B. theta under the four limitations. The fluxes for the detected products are presented in Figure C.7. Overall, we detected 6 excreted metabolites: succinate, propionate, formate, acetate, lactate, and ethanol. In the reference condition, the largest flux is going through acetic acid excretion at 2 mM/OD/h acetate. Formate and propionate are excreted at about 1 mM/OD/hr. Succinate is excreted at about 0.7 mM/OD/hr. We did not detect any production of lactate or ethanol in reference condition.

As cells become growth limited, the excreted products follow similar trends for the carbon, nitrogen, tetracycline limitations. As the growth rate is decreased by the limitations, the flux of the excreted products, similarly decreases because the demand for energy is decreased. However, the CO_2 limitation has a different metabolite profile. As cells are inhibited, they start producing increased fluxes of acetate and formate. In addition, new metabolite products are made including lactate and ethanol. These new products likely come from the decreased ability to produce succinate and propionate because producing these two molecules requires the input of CO_2. Many amino acids such as aspartate are synthesized through this same pathway, so the production of lactate and ethanol are possibly the result of keeping amino acid synthesis high enough.

C.8 Figures

protName	locus	pmf
Glyceraldehyde-3-phosphate dehydrogenase (EC 1....	BT_4263	3.453
Elongation factor Tu (EF-Tu)	BT_2740	2.549
Phosphoenolpyruvate carboxykinase (ATP) (PCK) (...	BT_2790	1.879
Fructose-bisphosphate aldolase	BT_1691	1.785
60 kDa chaperonin (GroEL protein) (Protein Cpn60)	BT_1829	1.445
50S ribosomal protein L7/L12	BT_2735	1.365
Elongation factor G (EF-G)	BT_2729	1.118
Chaperone protein DnaK (HSP70) (Heat shock 70 k...	BT_4615	1.097
Putative tetratricopeptide repeat family protein	BT_0900	1.044
TPR domain protein	BT_2844	1.015
Uncharacterized protein	BT_0173	1.009
Pyruvate-flavodoxin oxidoreductase (EC 1.2.7.-)	BT_1747	0.953
Malate dehydrogenase (EC 1.1.1.37)	BT_3911	0.919
Elongation factor Ts (EF-Ts)	BT_3878	0.914
Phosphoglycerate kinase (EC 2.7.2.3)	BT_1672	0.868

Figure C.1 Abundant proteins of B. theta.
Pmf is percent mass fraction. Locus is the gene identifier. B. theta cells were grown in minimal media in carbon rich conditions. Samples were collected and assayed for proteomics quantification.

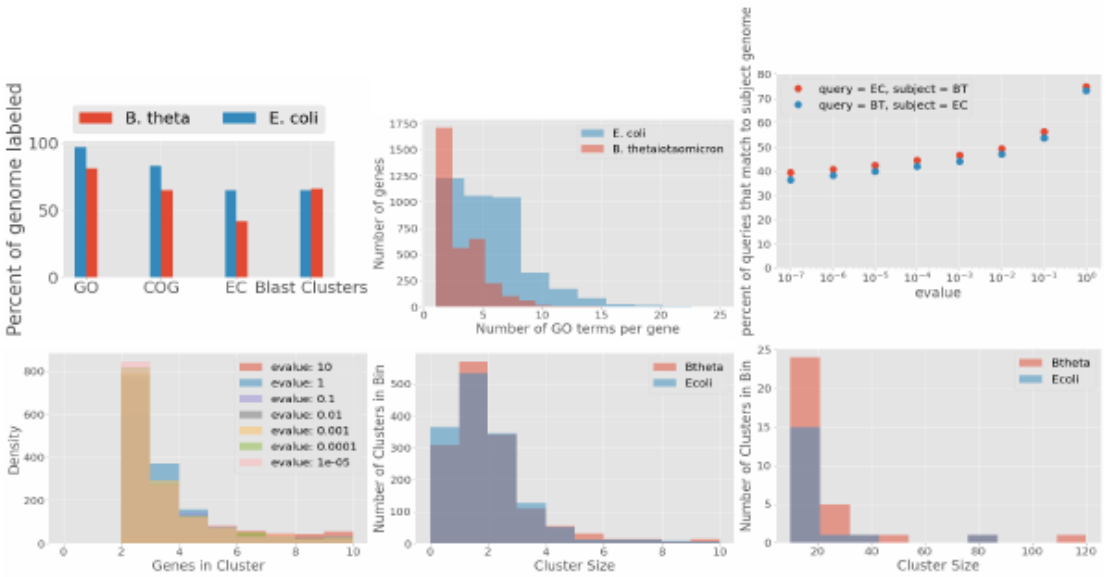

Figure C.2 Comparison of functional grouping for E. coli *and* B. theta *proteins.*
a) Genome coverage for GO, COG, EC and blast clusters was compared between E. coli and B. theta. b) Coverage of GO terms per gene was plotted as a histogram for E. coli and B. theta. c) Dependence of cluster matches for different evalue cutoffs used in the blastp analysis. d) dependence of how the number of genes per blastp cluster changes for different evalue cutoffs used for blastp clustering.

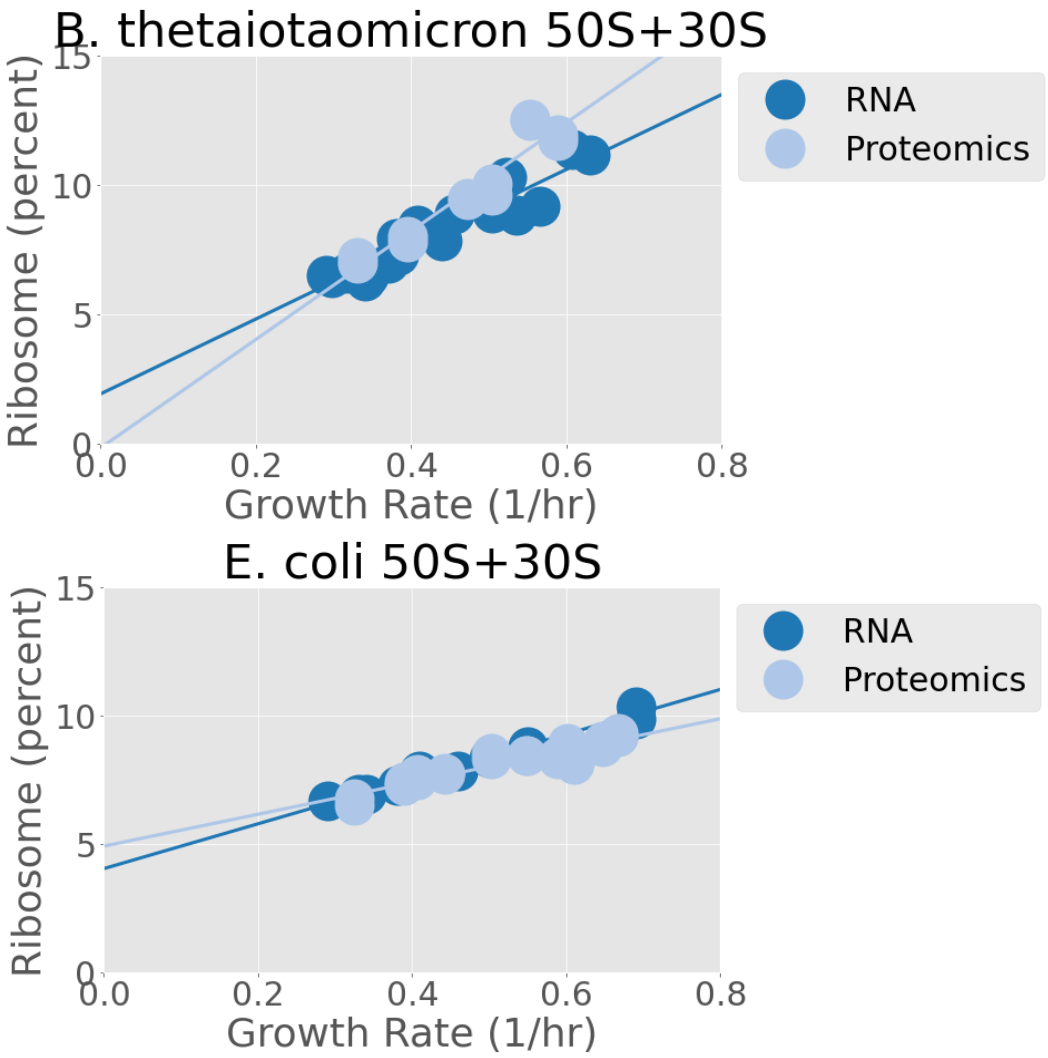

Figure C.3 Comparison of ribosomal proteins from proteomics and RNA-to-protein ratio measurement for E. coli *and* B. theta*.*
E. coli and B. theta samples were grown anaerobically in minimal media for varying levels of carbon limitation. RNA-to-protein ratio was converted to protein mass fraction by multiplying by a factor of 0.34 since the RNA-to-protein ratio is about 0.76 (58).

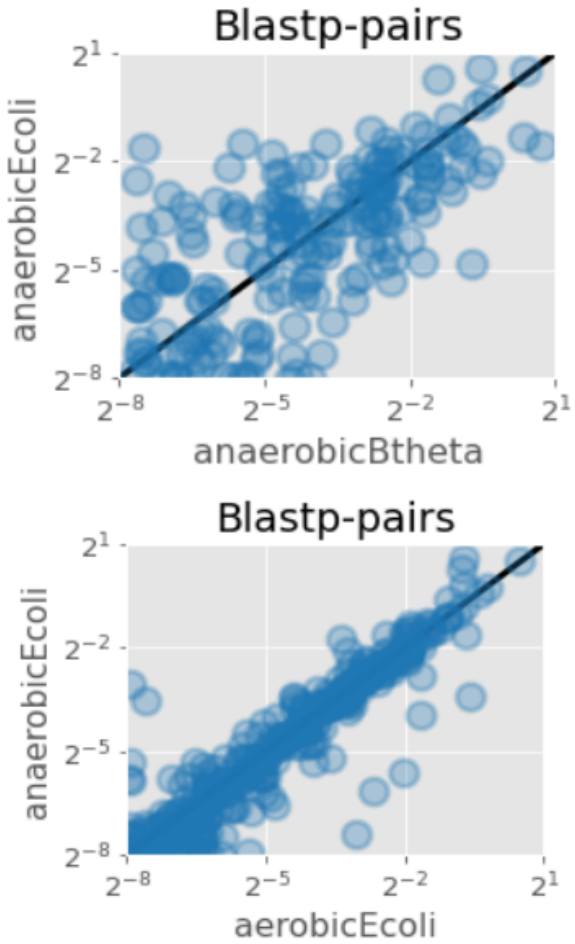

Figure C.4 Blastp pairwise comparison of protein mass fraction abundances in E. coli and B. theta reference condition.
Each sample is the proteomics reference condition for nonlimiting growth in minimal media. Each point is a protein matched by blastp, with the values on the different axes being the protein mass fraction quantified by proteomics.

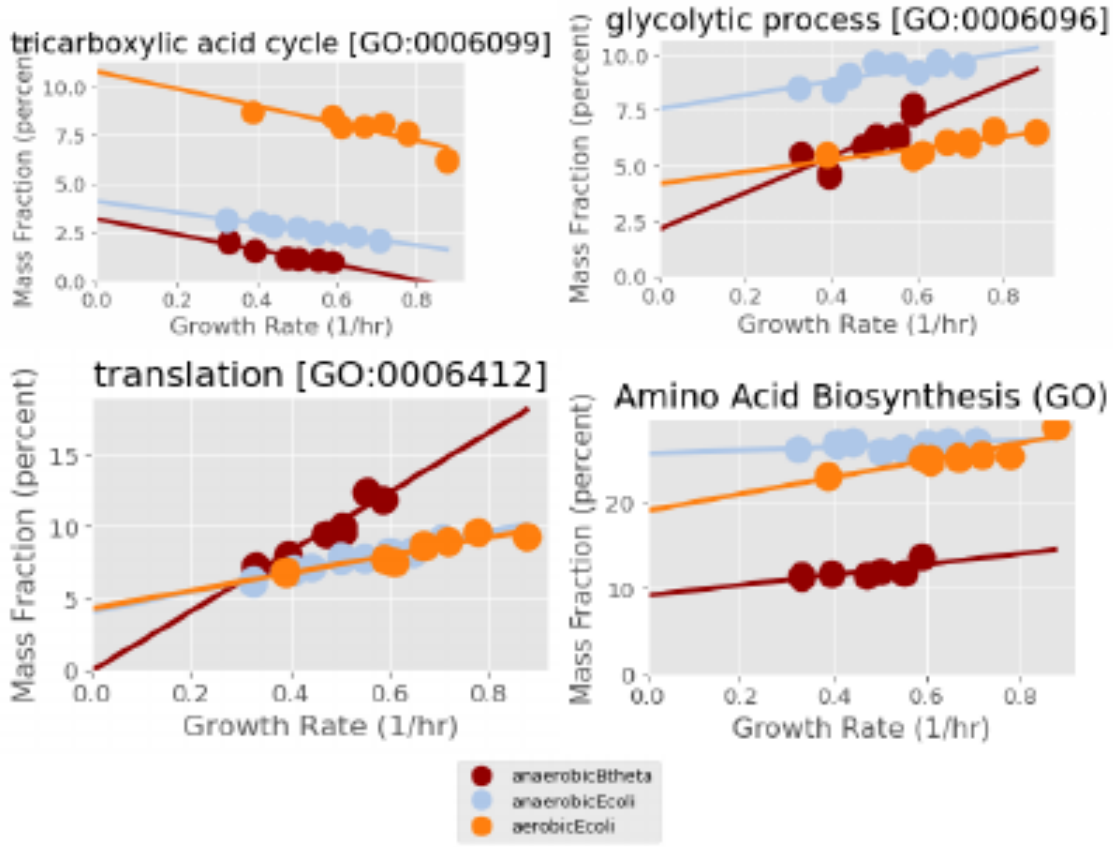

Figure C.5 Functional groupings of B. theta *and* E. coli *proteins for carbon limited growth. Growth rates of B. theta and E. coli were grown in carbon limiting conditions. Proteomics samples were collected, and proteins were quantified as mass fractions. For each grouping, the percent reported is the summed mass fraction of the proteins in that grouping.*

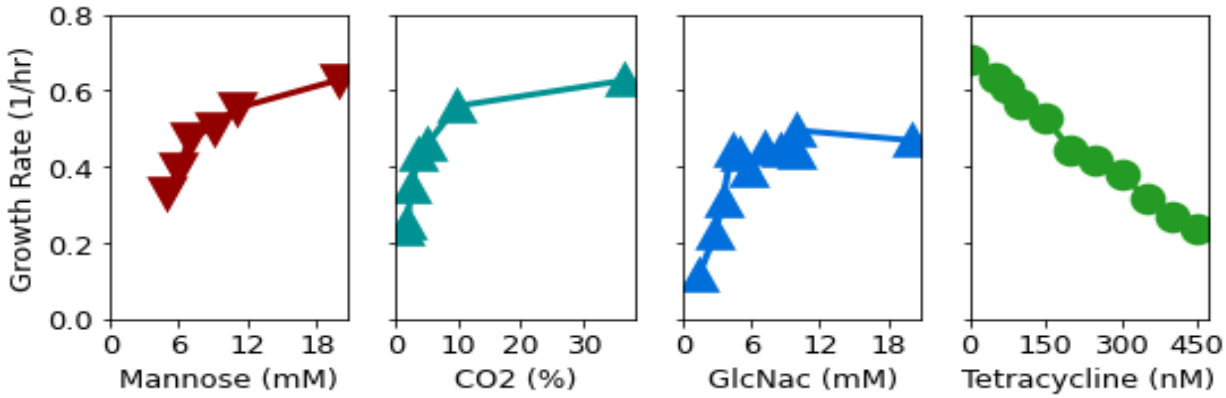

Figure C.6 Controllable limitation of nutrient availability in B. theta.
In all conditions, cells were grown in anaerobic Hungate in minimal media limited for various nutrients, or for the ribosomal titration, limited by antibiotic concentration. Carbon limitation was implemented by titration mannose concentration, carbon dioxide limitation was implemented by setting CO_2 and bicarbonate concentration. Glcnac limitation was performed for cells with Glcnac as the sole nitrogen source.

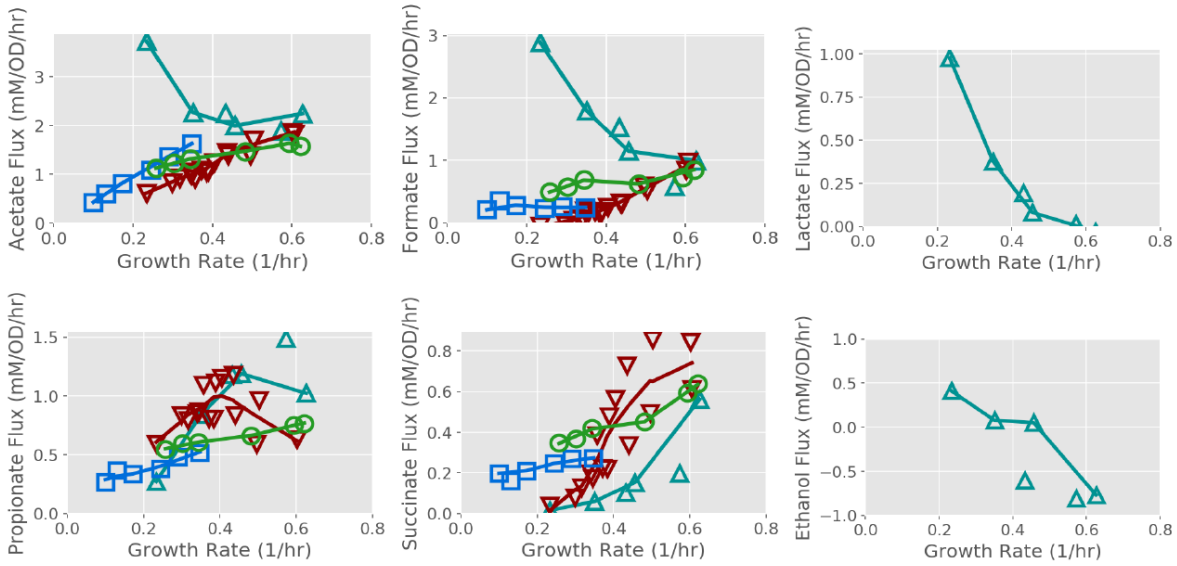

Figure C.7 Excretion fluxes from B. theta in different conditions.
Growth rates were controlled as described in Figure C.6. Fluxes of excreted fermentation products were measured by collecting samples at various OD_{600} and calculating the slope of the linear fit for change in concentration of product vs OD_{600}. The flux was calculated as this slope times the growth rate.

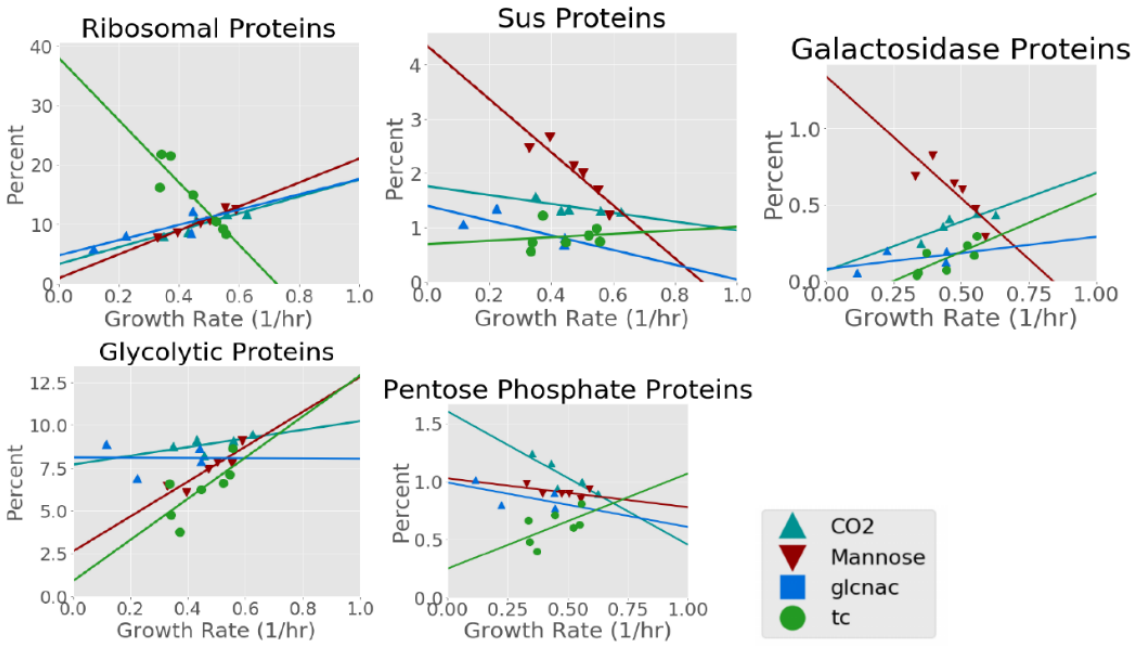

Figure C.8 Proteome response of different protein groups in different conditions.
Growth rates of B. theta were controlled as described in Figure C.6. Proteomics samples were collected, and proteins were quantified as mass fractions. For each grouping, the percent reported is the summed mass fraction of the proteins in that grouping.

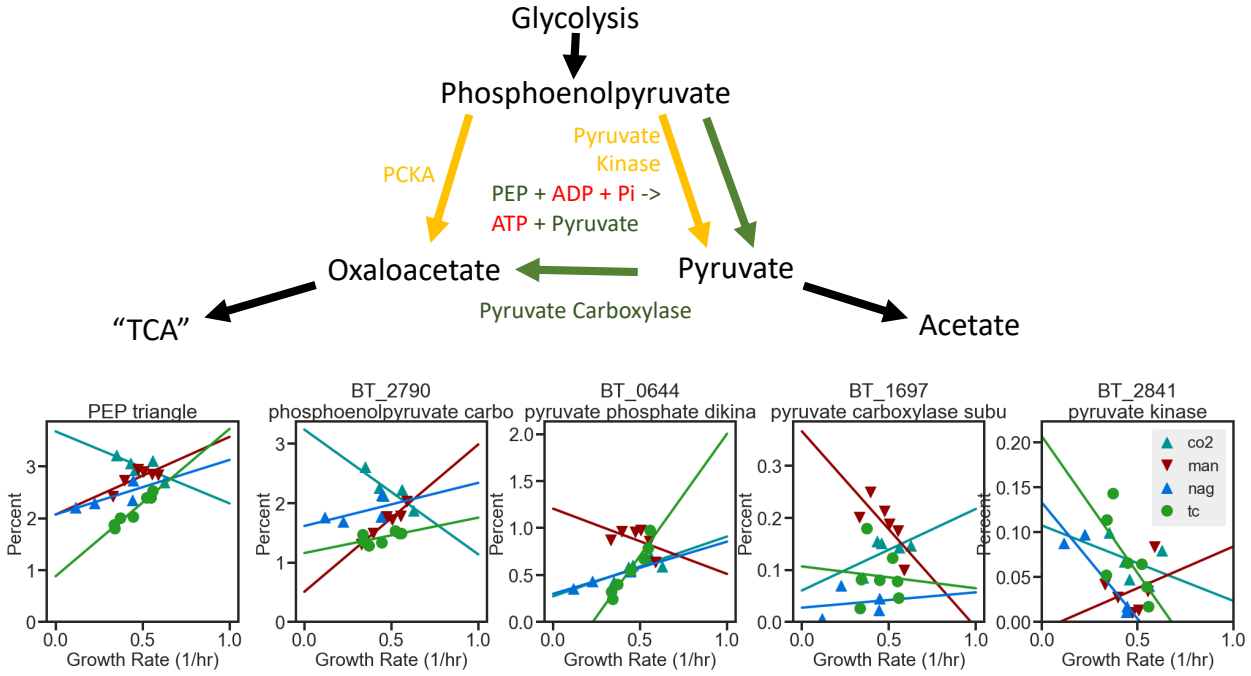

Figure C.9 Proteomics around PEP triangle of B. theta.
Growth rates of B. theta were controlled as described in Figure C.6. Proteomics samples were collected, and proteins were quantified as mass fractions. For each grouping, the percent reported is the summed mass fraction of the proteins in that grouping.

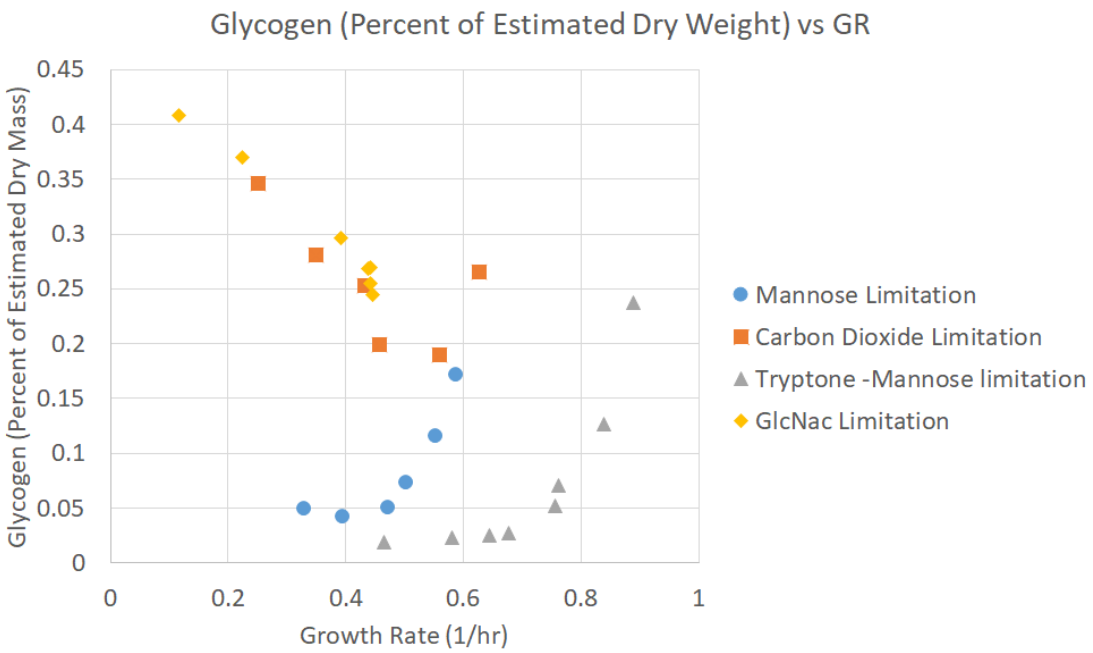

Figure C.10 Biomass composition of Bacteroides thetaiotaomicron.
*Glycogen was measured in Bacteroides thetaiotaomicron for a variety of conditions. Mannose limitation (blue circles) was implemented by titration the concentration of mannose in the growth media. Carbon dioxide limitation was implemented by changing the supplemented concentrations of bicarbonate, which then determines carbon dioxide concentration. Tryptone-mannose limitation (grey triangles) was implemented by titration mannose concentration with a fixed tryptone concentration of 2%. GlcNac limitation was implemented by titration n-acetyl-glucosamine concentration while keeping mannose concentration fixed in a media without ammonium chloride. Percentage of dry weight was estimated from 400 ug/OD_{600}/mL (*121*).*

Appendix D

Pyrophosphate flux

D.1 Estimation of net PP_i flux of growing cells

In order for ATP to adequately substitute for PP_i, there needs to be sufficient flux available to match the demand. We therefore performed calculations to shed light on the availability of PP_i cells. PP_i flux has been computed for several organisms including *E. coli* (*97*), *T. vaginalis* (*98*), and others (*213*, *214*). Most of the PP_i flux comes from the synthesis of macromolecules such as RNA, DNA, proteins, glycogen, and lipids (Figure C.10). Further PP_i flux comes from synthesis of amino acids, nucleotides and other precursors. Cofactors maybe also be a source of PP_i, but since not much of these molecules are synthesized relative to overall flux, their contribution can be ignored. In order to gain a simplified understanding of this PP_i flux, we focus our analysis on synthesis of macromolecules and central carbon metabolism.

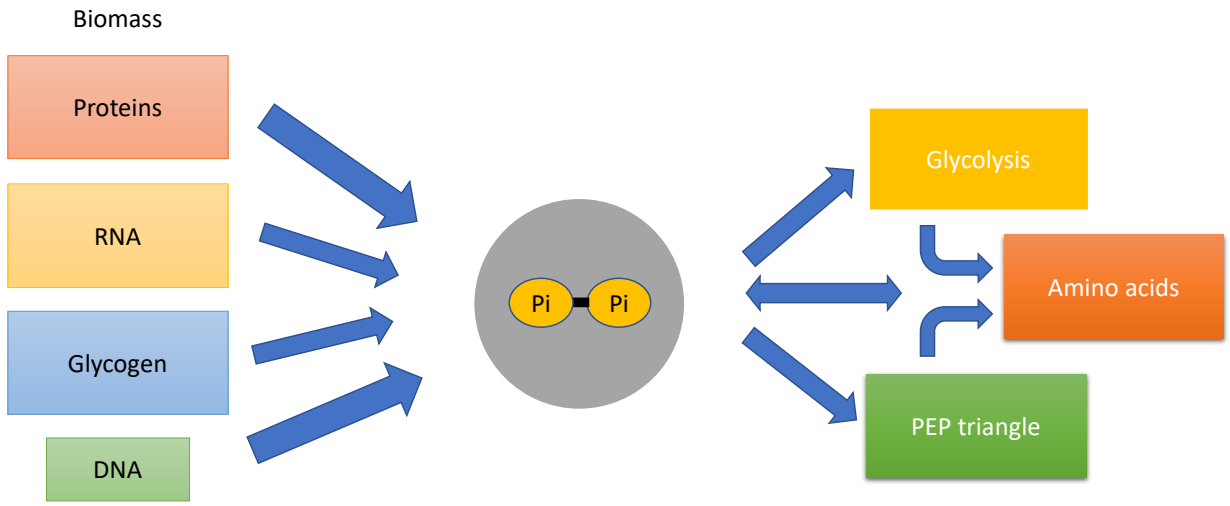

Figure D.1 Input and output of the pyrophosphate pool

When considering the net flux of PP_i from synthesis of macromolecules, we need to consider cases where precursors are either provided or not provided as the overall flux will change accordingly. The simplest case for analysis is when the precursors are provided since we don't have to keep track of the PPi flux change due to the synthesis of the precursors. We consider 4 main types of macromolecules that the cell can have: protein, RNA, glycogen, and lipids. DNA is ignored as it's a small fraction of the total mass of macromolecules in bacteria (*121*). RNA itself also includes different types of RNA, such as mRNA, tRNA, and rRNA. For the purpose of this analysis, we break down RNA into two categories: stable RNA and unstable RNA. Stable RNA includes RNA that isn't degraded on fast time scales. This type of RNA includes rRNA and tRNA which are stably folded. There is also unstable RNA such as mRNA, which is constantly synthesized and degraded. Because this mRNA is being constantly turned over during exponential growth, we cannot easily estimate the synthesis rate of this type of RNA by measuring the steady state abundance. Furthermore, the constant degradation means that most of the PPi will be generated in the process of synthesizing the polymers of unstable RNA as the precursor pool will be reused by cells. Assuming there is negligible degradation of the other macromolecules, their synthesis rates can be estimated by measuring their total abundance.

The estimated fluxes of PP_i from synthesis of macromolecules are shown in Table 4.1. For synthesis without precursors of all macromolecules except for lipids, it was assumed that each monomer of the macromolecule contributed one PP_i. For lipids, there are three PP_i formed for every fatty acid synthesized (*97*). To find the estimated PP_i per weight of macromolecule, we assumed that the molecular weight of protein, RNA, and glycogen was 110, 324, and 164 g/mol respectively.

We can then estimate the net fluxes of PP_i when included precursors. However, to do this requires understanding the fluxes of PP_i in central metabolism as that is the pathway through which many of these precursors are formed. Those molecules will be formed from sugars that are processed through glycolysis and branches of the TCA cycle (which won't be a cycle for *B. theta*). The precursors for glycogen synthesis won't be affected by this as glucose-6-phosphate can be used to synthesize glycogen. The precursors for RNA nucleotide synthesis bypass glycolysis by moving through the pentose phosphate pathway. Overall, synthesis of RNA nucleotides produces an additional one PP_i per monomer of RNA. The synthesis of guanosine also produces an additional PP_i. Assuming that all nucleotides are used equally frequently, this means that synthesis of RNA starting from glucose precursors yields an additional 1.25 PP_i per monomer of RNA.

The adjustment of the flux for proteins without precursors requires careful consideration since there are 20 amino acids that must be accounted for. All amino acid precursors except for histidine pass through glycolysis. Furthermore, there are also additional reactions that consume or product PPi for specific amino acids.

When considering flux through glycolysis, we assume that the PP_i utilizing phosphofructokinase is utilized rather than the ATP utilizing form. This assumption is supported by the finding that *Bacteroides* cells have high activity of the PP_i utilizing phosphofructokinase and low activity of the ATP utilizing form (*7*). Furthermore, we find that the proteome of *B. theta* has higher expression of the PP_i utilizing form vs ATP utilizing form.

There's another glycolytic PP_i utilizing enzyme that *B. theta* has that will affect PP_i flux through glycolysis. This enzyme converts PEP to pyruvate by consuming PP_i and producing ATP. In *B. theta*, it's unknown what direction the *ppdk* enzyme goes in. This complication is further complicated by how *ppdk* isn't clearly essential. One factor is the free energy of PEP hydrolysis is

very high at -61 kJ/mol (*92*). Yet many studies assume or find that PP_i runs in the gluconeogenic direction (*213*). Additionally, a study in *Bacteroides* failed to find significant activity of *ppdk* (*7*). Therefore, we leave the utilization of *ppdk* open as a free variable to explore what direction this enzyme acts in.

With these assumptions regarding glycolytic usage of PP_i, it's possible to estimate the PP_i flux from protein synthesis where the cell also synthesizes its own precursors. The net estimate is shown in Table 4.4. For each amino acid, this table has 3 columns. The first is the total amount of glucose equivalents used to synthesis one amino acid. The second is the amount of PP_i that would be used in glycolysis assuming pfp was used. For all amino acids except for histidine, this is the same column. The third column is the secondary reactions which either produce or consume PP_i (*97*). From this, the net PP_i produced or consumed can be calculated for each amino acid. If we assume equal coverage of amino acids, the amino acid biosynthesis significantly changes the net PPi flux associated with protein biomass production, reducing from 9.1 to 3.6 μmol PP_i/mg protein.

Overall, the absence of precursors leads to a significant decrease in available PP_i flux. In Table 4.2, we calculate the net fluxes based on the biomass composition in cells grown in rich and minimal media. The only difference between these media is the presence of 2% tryptone, which is a source of amino acids. As a result of the two differences, pyrophosphate production increases by 75% from 2.5 to 4.4 μmol PP_i/mg protein. If we also incorporate the uptake of sugars into the calculation, this difference still holds with there being a net deficient 0.73 μmol PP_i/mg protein in minimal media conditions vs a surplus of 1.14 μmol PP_i/mg protein in rich media conditions Table 4.3.

The difference in PP_i yield between the rich media and minimal media conditions allows us to speculate on the role *ppdk* in the physiology of *B. theta*. Ultimately cells have to match PP_i

pyrophosphate production and utilization to avoid buildup of pyrophosphate. Without the ability to freely hydrolyze PP_i, cells still need some way to utilize excess pyrophosphate while still being flexible when PPi is relatively scarce. The combination of pyruvate kinase and *ppdk* could fill such a role. When PPi is freely available, *ppdk* can provide pyruvate flux. When PPi is scarcer, pyruvate kinase can provide such a role or *ppdk* can run in reverse to provide additional PP_i flux.

There are some possible limitations to our calculation. We didn't have a good estimate for mRNA synthesis rate. While in *E. coli*, mRNA synthesis rate appears to scale with rRNA synthesis, it's unclear if the same will hold for *B. theta*. It's also possible that at slower growth rates, PP_i utilizing enzymes could be replaced by ATP utilizing enzymes. We also don't know how lipids change as lipid content wasn't measured. We also include cysteine in our minimal media, which can provide some amino acids, as cysteine can be broken down into pyruvate.

REFERENCES

1. R. L. Morris, T. M. Schmidt, Shallow breathing: bacterial life at low O2. *Nat Rev Microbiol*. **11**, 205–212 (2013).

2. A.-M. Reimers, H. Knoop, A. Bockmayr, R. Steuer, Cellular trade-offs and optimal resource allocation during cyanobacterial diurnal growth. *Proc Natl Acad Sci USA*. **114**, E6457–E6465 (2017).

3. M. Tiso, A. N. Schechter, Nitrate Reduction to Nitrite, Nitric Oxide and Ammonia by Gut Bacteria under Physiological Conditions. *PLoS ONE*. **10**, e0119712 (2015).

4. A. Bernalier, J. Dore, M. Durand, in *Colonic Microbiota, Nutrition and Health*, G. R. Gibson, M. B. Roberfroid, Eds. (Springer Netherlands, Dordrecht, 1999; http://link.springer.com/10.1007/978-94-017-1079-4_3), pp. 37–53.

5. K. M. Dombek, L. O. Ingram, Ethanol production during batch fermentation with Saccharomyces cerevisiae: changes in glycolytic enzymes and internal pH. *Appl Environ Microbiol*. **53**, 1286–1291 (1987).

6. D. P. Clark, The fermentation pathways of *Escherichia coli*. *FEMS Microbiology Letters*. **63**, 223–234 (1989).

7. J. M. Macy, L. G. Ljungdahl, G. Gottschalk, Pathway of Succinate and Propionate Formation in *Bacteroides fragilis*. *J Bacteriol*. **134**, 84–91 (1978).

8. A. D. Baughn, M. H. Malamy, The strict anaerobe Bacteroides fragilis grows in and benefits from nanomolar concentrations of oxygen. *Nature*. **427**, 441–444 (2004).

9. J. A. Imlay, Iron-sulphur clusters and the problem with oxygen. *Mol Microbiol*. **59**, 1073–1082 (2006).

10. Dependency on Medium and Temperature of Cell Size and Chemical Composition during Balanced Growth of Salmonella typhimurium | Microbiology Society, (available at https://www.microbiologyresearch.org/content/journal/micro/10.1099/00221287-19-3-592).

11. J. Monod, THE GROWTH OF BACTERIAL CULTURES, 24 (1949).

12. M. Mori, Z. Zhang, A. Banaei-Esfahani, J.-B. Lalanne, H. Okano, B. C. Collins, A. Schmidt, O. T. Schubert, D.-S. Lee, G.-W. Li, R. Aebersold, T. Hwa, C. Ludwig, From coarse to fine: the absolute Escherichia coli proteome under diverse growth conditions. *Molecular systems biology*. **17**, e9536 (2021).

13. M. Scott, T. Hwa, Bacterial growth laws and their applications. *Current Opinion in Biotechnology*. **22**, 559–565 (2011).

14. C. You, H. Okano, S. Hui, Z. Zhang, M. Kim, C. W. Gunderson, Y.-P. Wang, P. Lenz, D. Yan, T. Hwa, Coordination of bacterial proteome with metabolism by cyclic AMP signalling. *Nature*. **500**, 301–306 (2013).

15. M. Basan, T. Honda, D. Christodoulou, M. Hörl, Y.-F. Chang, E. Leoncini, A. Mukherjee, H. Okano, B. R. Taylor, J. M. Silverman, C. Sanchez, J. R. Williamson, J. Paulsson, T. Hwa, U. Sauer, A universal trade-off between growth and lag in fluctuating environments. *Nature*. **584**, 470–474 (2020).

16. D. W. Erickson, S. J. Schink, V. Patsalo, J. R. Williamson, U. Gerland, T. Hwa, A global resource allocation strategy governs growth transition kinetics of Escherichia coli. *Nature*. **551**, 119–123 (2017).

17. D. F. Evans, G. Pye, R. Bramley, A. G. Clark, T. J. Dy, Measurement of gastrointestinal pH profiles in normal ambulant human subjects. *Gut*. **29**, 1035–1041 (1988).

18. I. R. Booth, P. Cash, C. O'Byrne, Sensing and adapting to acid stress, 10.

19. U. Kanjee, W. A. Houry, Mechanisms of Acid Resistance in *Escherichia coli*. *Annu. Rev. Microbiol*. **67**, 65–81 (2013).

20. J. L. Slonczewski, M. Fujisawa, M. Dopson, T. A. Krulwich, Cytoplasmic pH Measurement and Homeostasis in Bacteria and Archaea. *Advances in Microbial Physiology*. **55**, 1–317 (2009).

21. H. Yan, T. Fukamachi, H. Saito, H. Kobayashi, Expression and Activity of Kdp under Acidic Conditions in Escherichia coli. *Biological & Pharmaceutical Bulletin*. **34**, 426–429 (2011).

22. J. H. Cummings, Short chain fatty acids in the human colon. *Gut*. **22**, 763–779 (1981).

23. J. H. Cummings, E. W. Pomare, W. J. Branch, C. P. Naylor, G. T. Macfarlane, Short chain fatty acids in human large intestine, portal, hepatic and venous blood. *Gut*. **28**, 1221–1227 (1987).

24. C. V. Salmond, R. G. Kroll, I. R. Booth, The Effect of Food Preservatives on pH Homeostasis in Escherichia coIi. *Journal of General Microbiology*. **130**, 2845–2850 (1984).

25. J. B. Russell, Factors That Alter Rumen Microbial Ecology. *Science*. **292**, 1119–1122 (2001).

26. A. J. Wolfe, The Acetate Switch. *Microbiol Mol Biol Rev*. **69**, 12–50 (2005).

27. M. Basan, S. Hui, H. Okano, Z. Zhang, Y. Shen, J. R. Williamson, T. Hwa, Overflow metabolism in Escherichia coli results from efficient proteome allocation. *Nature*. **528**, 99–104 (2015).

28. M. S. Barredo, L. M. Evison, Effect of propionate toxicity on methanogen-enriched sludge, Methanobrevibacter smithii, and Methanospirillum hungatii at different pH values. *Appl Environ Microbiol*. **57**, 1764–1769 (1991).

29. H. Yuan, Y. Chen, H. Zhang, S. Jiang, Q. Zhou, G. Gu, Improved Bioproduction of Short-Chain Fatty Acids (SCFAs) from Excess Sludge under Alkaline Conditions. *Environ. Sci. Technol.* **40**, 2025–2029 (2006).

30. G. L. Kleman, W. R. Strohl, Acetate metabolism by Escherichia coli in high-cell-density fermentation. *Applied and Environmental Microbiology*. **60**, 3952–3958 (1994).

31. G. Raba, S. Adamberg, K. Adamberg, Acidic pH enhances butyrate production from pectin by faecal microbiota. *FEMS Microbiology Letters*. **368**, fnab042 (2021).

32. S. Sanna, N. R. van Zuydam, A. Mahajan, A. Kurilshikov, A. Vich Vila, U. Võsa, Z. Mujagic, A. A. M. Masclee, D. M. A. E. Jonkers, M. Oosting, L. A. B. Joosten, M. G. Netea, L. Franke, A. Zhernakova, J. Fu, C. Wijmenga, M. I. McCarthy, Causal relationships among the gut microbiome, short-chain fatty acids and metabolic diseases. *Nat Genet*. **51**, 600–605 (2019).

33. B. Dalile, L. Van Oudenhove, B. Vervliet, K. Verbeke, The role of short-chain fatty acids in microbiota–gut–brain communication. *Nat Rev Gastroenterol Hepatol*. **16**, 461–478 (2019).

34. P. Louis, H. J. Flint, Formation of propionate and butyrate by the human colonic microbiota. *Environ Microbiol*. **19**, 29–41 (2017).

35. P. Guilloteau, L. Martin, V. Eeckhaut, R. Ducatelle, R. Zabielski, F. Van Immerseel, From the gut to the peripheral tissues: the multiple effects of butyrate. *Nutr. Res. Rev.* **23**, 366–384 (2010).

36. L. Brooks, A. Viardot, A. Tsakmaki, E. Stolarczyk, J. K. Howard, P. D. Cani, A. Everard, M. L. Sleeth, A. Psichas, J. Anastasovskaj, J. D. Bell, K. Bell-Anderson, C. R. Mackay, M. A. Ghatei, S. R. Bloom, G. Frost, G. A. Bewick, Fermentable carbohydrate stimulates FFAR2-dependent colonic PYY cell expansion to increase satiety. *Molecular Metabolism*. **6**, 48–60 (2017).

37. A. J. Brown, S. M. Goldsworthy, A. A. Barnes, M. M. Eilert, L. Tcheang, D. Daniels, A. I. Muir, M. J. Wigglesworth, I. Kinghorn, N. J. Fraser, N. B. Pike, J. C. Strum, K. M. Steplewski, P. R. Murdock, J. C. Holder, F. H. Marshall, P. G. Szekeres, S. Wilson, D. M. Ignar, S. M. Foord, A. Wise, S. J. Dowell, The Orphan G Protein-coupled Receptors GPR41 and GPR43 Are Activated by Propionate and Other Short Chain Carboxylic Acids *. *Journal of Biological Chemistry*. **278**, 11312–11319 (2003).

38. S. H. Duncan, P. Louis, J. M. Thomson, H. J. Flint, The role of pH in determining the species composition of the human colonic microbiota. *Environmental microbiology*. **11**, 2112–2122 (2009).

39. J. Cremer, M. Arnoldini, T. Hwa, Effect of water flow and chemical environment on microbiota growth and composition in the human colon. *Proc Natl Acad Sci USA*. **114**, 6438–6443 (2017).

40. G. Falony, M. Joossens, S. Vieira-Silva, J. Wang, Y. Darzi, K. Faust, A. Kurilshikov, M. J. Bonder, M. Valles-Colomer, D. Vandeputte, R. Y. Tito, S. Chaffron, L. Rymenans, C. Verspecht, L. De Sutter, G. Lima-Mendez, K. D'hoe, K. Jonckheere, D. Homola, R. Garcia, E. F. Tigchelaar, L. Eeckhaudt, J. Fu, L. Henckaerts, A. Zhernakova, C. Wijmenga, J. Raes, Population-level analysis of gut microbiome variation. *Science*. **352**, 560–564 (2016).

41. R. A. Quinn, W. Comstock, T. Zhang, J. T. Morton, R. da Silva, A. Tran, A. Aksenov, L.-F. Nothias, D. Wangpraseurt, A. V. Melnik, G. Ackermann, D. Conrad, I. Klapper, R. Knight, P. C. Dorrestein, Niche partitioning of a pathogenic microbiome driven by chemical gradients. *Science Advances*. **4**, eaau1908 (2018).

42. S.-Y. Park, C. Rao, K. Z. Coyte, G. A. Kuziel, Y. Zhang, W. Huang, E. A. Franzosa, J.-K. Weng, C. Huttenhower, S. Rakoff-Nahoum, Strain-level fitness in the gut microbiome is an emergent property of glycans and a single metabolite. *Cell*. **185**, 513-529.e21 (2022).

43. A. Jacobson, L. Lam, M. Rajendram, F. Tamburini, J. Honeycutt, T. Pham, W. V. Treuren, K. Pruss, S. R. Stabler, K. Lugo, D. M. Bouley, J. G. Vilches-Moure, M. Smith, J. L. Sonnenburg, A. S. Bhatt, K. C. Huang, D. Monack, A Gut Commensal-Produced Metabolite Mediates Colonization Resistance to Salmonella Infection. *Cell Host & Microbe*. **24**, 296–307 (2018).

44. C. Bourriaud, R. J. Robins, L. Martin, F. Kozlowski, E. Tenailleau, C. Cherbut, C. Michel, Lactate is mainly fermented to butyrate by human intestinal microfloras but inter-individual variation is evident. *Journal of Applied Microbiology*. **99**, 201–212 (2005).

45. S. P. Wang, L. A. Rubio, S. H. Duncan, G. E. Donachie, G. Holtrop, G. Lo, F. M. Farquharson, J. Wagner, J. Parkhill, P. Louis, A. W. Walker, H. J. Flint, Pivotal Roles for pH, Lactate, and Lactate-Utilizing Bacteria in the Stability of a Human Colonic Microbial Ecosystem. *mSystems*. **5** (2020), doi:10.1128/mSystems.00645-20.

46. T. L. Miller, M. J. Wolin, E. C. de Macario, A. J. Macario, Isolation of Methanobrevibacter smithii from human feces. *Appl Environ Microbiol*. **43**, 227–232 (1982).

47. J. L. Rychlik, T. May, The Effect of a Methanogen, Methanobrevibacter smithii , on the Growth Rate, Organic Acid Production, and Specific ATP Activity of Three Predominant Ruminal Cellulolytic Bacteria. *Current Microbiology*. **40**, 176–180 (2000).

48. G. A. M. Cresci, J. W. Lampe, G. Gibson, Targeted Approaches for In Situ Gut Microbiome Manipulation. *Journal of Parental and Enteral Nutrition*. **44**, 581–588 (2020).

49. C.-J. Guo, B. M. Allen, K. J. Hiam, D. Dodd, W. Van Treuren, S. Higginbottom, K. Nagashima, C. R. Fischer, J. L. Sonnenburg, M. H. Spitzer, M. A. Fischbach, Depletion of microbiome-derived molecules in the host using Clostridium genetics. *Science*. **366**, eaav1282 (2019).

50. J. Frampton, K. G. Murphy, G. Frost, E. S. Chambers, Short-chain fatty acids as potential regulators of skeletal muscle metabolism and function. *Nat Metab*. **2**, 840–848 (2020).

51. S. Liu, E. Li, Z. Sun, D. Fu, G. Duan, M. Jiang, Y. Yu, L. Mei, P. Yang, Y. Tang, P. Zheng, Altered gut microbiota and short chain fatty acids in Chinese children with autism spectrum disorder. *Sci Rep*. **9**, 287 (2019).

52. F. Diez-Gonzalez, J. B. Russell, Effects of carbonylcyanide-m-chlorophenylhydrazone (CCCP) and acetate on Escherichia coli O157:H7 and K-12: uncoupling versus anion accumulation. *FEMS Microbiology Letters*. **151**, 71–76 (2006).

53. A. J. Roe, D. McLaggan, I. Davidson, C. O'Byrne, I. R. Booth, Perturbation of Anion Balance during Inhibition of Growth of Escherichia coli by Weak Acids. *Journal of Bacteriology*. **180**, 767–772 (1998).

54. A. J. Roe, C. O'Byrne, D. McLaggan, I. R. Booth, Inhibition of Escherichia coli growth by acetic acid: a problem with methionine biosynthesis and homocysteine toxicity. *Microbiology*. **148**, 2215–2222 (2002).

55. N. R. Sandoval, T. Y. Mills, M. Zhang, R. T. Gill, Elucidating acetate tolerance in E. coli using a genome-wide approach. *Metabolic Engineering*. **13**, 214–224 (2011).

56. C. Kirkpatrick, L. M. Maurer, N. E. Oyelakin, Y. N. Yoncheva, R. Maurer, J. L. Slonczewski, Acetate and Formate Stress: Opposite Responses in the Proteome of *Escherichia coli*. *J Bacteriol*. **183**, 6466–6477 (2001).

57. S. Pinhal, D. Ropers, J. Geiselmann, H. de Jong, Acetate Metabolism and the Inhibition of Bacterial Growth by Acetate. *J Bacteriol*. **201** (2019), doi:10.1128/JB.00147-19.

58. S. Hui, J. M. Silverman, S. S. Chen, D. W. Erickson, M. Basan, J. Wang, T. Hwa, J. R. Williamson, Quantitative proteomic analysis reveals a simple strategy of global resource allocation in bacteria. *Mol Syst Biol*. **11**, 784 (2015).

59. M. Scott, C. W. Gunderson, E. M. Mateescu, Z. Zhang, T. Hwa, Interdependence of Cell Growth and Gene Expression: Origins and Consequences. *Science*. **330**, 1099–1102 (2010).

60. J. M. Berg, J. L. Tymoczko, G. J. Gatto, L. Stryer, *Biochemistry* (W.H. Freeman & Company, a Macmillan Education Imprint, New York, Eighth edition., 2015).

61. X. Dai, M. Zhu, M. Warren, R. Balakrishnan, V. Patsalo, H. Okano, J. R. Williamson, K. Fredrick, Y.-P. Wang, T. Hwa, Reduction of translating ribosomes enables Escherichia coli to maintain elongation rates during slow growth. *Nat Microbiol*. **2**, 1–9 (2016).

62. M. Mori, S. Schink, D. W. Erickson, U. Gerland, T. Hwa, Quantifying the benefit of a proteome reserve in fluctuating environments. *Nat Commun*. **8**, 1225 (2017).

63. J. O. Park, S. A. Rubin, Y.-F. Xu, D. Amador-Noguez, J. Fan, T. Shlomi, J. D. Rabinowitz, Metabolite concentrations, fluxes and free energies imply efficient enzyme usage. *Nat Chem Biol*. **12**, 482–489 (2016).

64. J. O. Park, L. B. Tanner, M. H. Wei, D. B. Khana, T. B. Jacobson, Z. Zhang, S. A. Rubin, S. H.-J. Li, M. B. Higgins, D. M. Stevenson, D. Amador-Noguez, J. D. Rabinowitz, Near-equilibrium glycolysis supports metabolic homeostasis and energy yield. *Nat Chem Biol*. **15**, 1001–1008 (2019).

65. H. Dourado, M. Mori, T. Hwa, M. J. Lercher, On the optimality of the enzyme–substrate relationship in bacteria. *PLOS Biology*. **19**, e3001416 (2021).

66. S. Schuster, R. Heinrich, Minimization of intermediate concentrations as a suggested optimality principle for biochemical networks. *J. Math. Biol*. **29**, 425–442 (1991).

67. A. Akbari, J. T. Yurkovich, D. C. Zielinski, B. O. Palsson, The quantitative metabolome is shaped by abiotic constraints. *Nat Commun*. **12**, 3178 (2021).

68. N. Tepper, E. Noor, D. Amador-Noguez, H. S. Haraldsdóttir, R. Milo, J. Rabinowitz, W. Liebermeister, T. Shlomi, Steady-State Metabolite Concentrations Reflect a Balance between Maximizing Enzyme Efficiency and Minimizing Total Metabolite Load. *PLOS ONE*. **8**, e75370 (2013).

69. E. C. Martens, R. Roth, J. E. Heuser, J. I. Gordon, Coordinate Regulation of Glycan Degradation and Polysaccharide Capsule Biosynthesis by a Prominent Human Gut Symbiont. *Journal of Biological Chemistry*. **284**, 18445–18457 (2009).

70. Y. Liu, Overview of some theoretical approaches for derivation of the Monod equation. *Appl Microbiol Biotechnol*. **73**, 1241–1250 (2007).

71. M. S. M. Jetten, A. J. M. Stams, A. J. B. Zehnder, Acetate threshold values and acetate activating enzymes in methanogenic bacteria. *FEMS Microbiology Ecology*. **6**, 339–344 (1990).

72. S. J. Pirt, The maintenance energy of bacteria in growing cultures, 8 (1965).

73. P. van Bodegom, Microbial Maintenance: A Critical Review on Its Quantification. *Microb Ecol*. **53**, 513–523 (2007).

74. R. Hermsen, H. Okano, C. You, N. Werner, T. Hwa, A growth-rate composition formula for the growth of *E. coli* on co-utilized carbon substrates. *Mol Syst Biol*. **11**, 801 (2015).

75. J. K. Heinonen, *Biological Role of Inorganic Pyrophosphate* (Springer US, Boston, MA, 2001; http://link.springer.com/10.1007/978-1-4615-1433-6).

76. R. E. Reeves, A New Enzyme with the Glycolytic Function of Pyruvate Kinase. *Journal of Biological Chemistry*. **243**, 3202–3204 (1968).

77. M. D. Hatch, C. R. Slack, A new enzyme for the interconversion of pyruvate and phosphopyruvate and its role in the C4 dicarboxylic acid pathway of photosynthesis. *Biochemical Journal*. **106**, 141–146 (1968).

78. H. J. Evans, H. G. Wood, The mechanism of the pyruvate, phosphate dikinase reaction. *Proc Natl Acad Sci U S A*. **61**, 1448–1453 (1968).

79. M. Benziman, N. Eizen, Pyruvate-Phosphate Dikinase and the Control of Gluconeogenesis in Acetobacter xylinum. *Journal of Biological Chemistry*. **246**, 57–61 (1971).

80. R. E. Reeves, Pyruvatephosphate dikinase from Bacteroides symbiosus. *Biochemical Journal*. **125**, 531–539 (1971).

81. R. E. Reeves, R. A. Menzies, D. S. Hsu, The Pyruvate-Phosphate Dikinase Reaction. *Journal of Biological Chemistry*. **243**, 5486–5491 (1968).

82. J. Xu, M. K. Bjursell, J. Himrod, S. Deng, L. K. Carmichael, H. C. Chiang, L. V. Hooper, J. I. Gordon, A genomic view of the human-Bacteroides thetaiotaomicron symbiosis. *Science*. **299**, 2074–2076 (2003).

83. A. L. Goodman, N. P. McNulty, Y. Zhao, D. Leip, R. D. Mitra, C. A. Lozupone, R. Knight, J. I. Gordon, Identifying Genetic Determinants Needed to Establish a Human Gut Symbiont in Its Habitat. *Cell Host & Microbe*. **6**, 279–289 (2009).

84. R. E. Reeves, D. J. South, H. J. Blytt, L. G. Warren, Pyrophosphate:d-Fructose 6-Phosphate 1-Phosphotransferase: A NEW ENZYME WITH THE GLYCOLYTIC FUNCTION OF 6-PHOSPHOFRUCTOKINASE. *Journal of Biological Chemistry*. **249**, 7737–7741 (1974).

85. W. O'Brien, S. Bowien, H. Wood, Isolation and characterization of a pyrophosphate-dependent phosphofructokinase from Propionibacterium shermanii. *Journal of Biological Chemistry*. **250**, 8690–8695 (1975).

86. M. H. Sawyer, P. Baumann, L. Baumann, Pathways of d-fructose and d-glucose catabolism in marine species of Alcaligenes, Pseudomonas marina, and Alteromonas communis. *Arch. Microbiol*. **112**, 169–172 (1977).

87. A. M. Roberton, P. G. Glucina, Fructose 6-phosphate phosphorylation in Bacteroides species. *J Bacteriol*. **150**, 1056–1060 (1982).

88. P. B. Hylemon, J. L. Young, R. F. Roadcap, P. V. Phibbs, Uptake and Incorporation of Glucose and Mannose by Whole Cells of *Bacteroides thetaiotaomicron*. *Appl Environ Microbiol*. **34**, 488–494 (1977).

89. V. Meuric, A. Rouillon, F. Chandad, M. Bonnaure-Mallet, Putative respiratory chain of Porphyromonas gingivalis. *Future microbiology*. **5**, 717–734 (2010).

90. A. Y. Mulkidjanian, M. Y. Galperin, K. S. Makarova, Y. I. Wolf, E. V. Koonin, Evolutionary primacy of sodium bioenergetics. *Biology Direct*. **3**, 13 (2008).

91. J. Chen, A. Brevet, M. Fromant, F. Lévêque, J. M. Schmitter, S. Blanquet, P. Plateau, Pyrophosphatase is essential for growth of Escherichia coli. *J Bacteriol*. **172**, 5686–5689 (1990).

92. J. L. E. Wimmer, K. Kleinermanns, W. F. Martin, Pyrophosphate and Irreversibility in Evolution, or why PPi Is Not an Energy Currency and why Nature Chose Triphosphates. *Frontiers in Microbiology*. **12**, 2999 (2021).

93. J. Kottur, D. T. Nair, Pyrophosphate hydrolysis is an intrinsic and critical step of the DNA synthesis reaction. *Nucleic Acids Research*. **46**, 5875–5885 (2018).

94. R. S. Johnson, M. Strausbauch, Pyrophosphate (PPi) release during transcription elongation by E. coli RNA polymerase (RNAP). *The FASEB Journal*. **21**, A656–A656 (2007).

95. J. Y. Kang, T. V. Mishanina, R. Landick, S. A. Darst, Mechanisms of Transcriptional Pausing in Bacteria. *Journal of Molecular Biology*. **431**, 4007–4029 (2019).

96. S. M. Uptain, C. M. Kane, M. J. Chamberlin, BASIC MECHANISMS OF TRANSCRIPT ELONGATION AND ITS REGULATION. *Annu. Rev. Biochem*. **66**, 117–172 (1997).

97. J.-H. Klemme, Regulation of Intracellular Pyrophosphatase-Activity and Conservation of the Phosphoanhydride-Energy of Inorganic Pyrophosphate in Microbial Metabolism. *Zeitschrift für Naturforschung C*. **31**, 544–550 (1976).

98. E. Mertens, Pyrophosphate-dependent phosphofructokinase, an anaerobic glycolytic enzyme? *FEBS Letters*. **285**, 1–5 (1991).

99. T. A. Kunkel, R. A. Beckman, L. A. Loeb, On the fidelity of DNA synthesis. Pyrophosphate-induced misincorporation allows detection of two proofreading mechanisms. *Journal of Biological Chemistry*. **261**, 13610–13616 (1986).

100. S. P. Fagan, P. Mukherjee, W. J. Jaremko, R. Nelson-Rigg, R. C. Wilson, T. L. Dangerfield, K. A. Johnson, I. Lahiri, J. D. Pata, Pyrophosphate release acts as a kinetic checkpoint during high-fidelity DNA replication by the Staphylococcus aureus replicative polymerase PolC. *Nucleic Acids Research*. **49**, 8324–8338 (2021).

101. Enzymatic Synthesis of Deoxyribonucleic Acid: XXVIII. The pyrophosphate exchange and pyrophosphorolysis reactions of deoxyribonucleic acid polymerase. *Journal of Biological Chemistry*. **244**, 3019–3028 (1969).

102. J. D. Kahn, J. E. Hearst, Reversibility of nucleotide incorporation by Escherichia coli RNA polymerase, and its effect on fidelity. *Journal of Molecular Biology*. **205**, 291–314 (1989).

103. R. K. Airas, F. Cramer, Pyrophosphate-caused inhibition of the aminoacylation of tRNA by the leucyl-tRNA synthetase from Neurospora crassa. *Eur J Biochem*. **160**, 291–296 (1986).

104. A. M. Khvorova, Yu. A. Motorin, A. D. Wolfson, Crucial role of pyrophosphate in the aminoacylation of *E. coli* $tRNA^{Phe}$ by yeast phenylalanyl-tRNA synthetase. *FEBS Letters*. **311**, 139–142 (1992).

105. F. Lipmann, in *Molecular Evolution and Protobiology*, K. Matsuno, K. Dose, K. Harada, D. L. Rohlfing, Eds. (Springer US, Boston, MA, 1984; https://doi.org/10.1007/978-1-4684-4640-1_11), pp. 133–135.

106. E. Mertens, ATP versus pyrophosphate: glycolysis revisited in parasitic protists. *Parasitology Today*. **9**, 122–126 (1993).

107. R. E. Reeves, How useful is the energy in inorganic pyrophosphate? *Trends in Biochemical Sciences*. **1**, 53–55 (1976).

108. J. T. Keltjens, R. Erp, R. J. Mooijaart, C. Drift, G. D. Vogels, Inorganic pyrophosphate synthesis during methanogenesis from methylcoenzyme M by cell-free extracts of Methanobacterium thermoautotrophicum (strain DeltaH). *Eur J Biochem*. **172**, 471–476 (1988).

109. H. G. Wood, W. E. O'Brien, G. Michaels, in *Advances in Enzymology - and Related Areas of Molecular Biology*, A. Meister, Ed. (John Wiley & Sons, Inc., Hoboken, NJ, USA, 2006; https://onlinelibrary.wiley.com/doi/10.1002/9780470122907.ch2), pp. 85–155.

110. J. Macy, I. Probst, G. Gottschalk, Evidence for cytochrome involvement in fumarate reduction and adenosine 5'-triphosphate synthesis by Bacteroides fragilis grown in the presence of hemin. *J Bacteriol*. **123**, 436–442 (1975).

111. S. Lucas, Y. Omata, J. Hofmann, M. Böttcher, A. Iljazovic, K. Sarter, O. Albrecht, O. Schulz, B. Krishnacoumar, G. Krönke, M. Herrmann, D. Mougiakakos, T. Strowig, G. Schett, M. M. Zaiss, Short-chain fatty acids regulate systemic bone mass and protect from pathological bone loss. *Nat Commun*. **9**, 55 (2018).

112. Y. Chen, J. J. Cheng, K. S. Creamer, Inhibition of anaerobic digestion process: a review. *Bioresource technology*. **99**, 4044–4064 (2008).

113. J. G. Pan, J. S. Rhee, J. M. Lebeault, Physiological constraints in increasing biomass concentration of Escherichia coli B in fed-batch culture. *Biotechnology Letters*. **9**, 89–94 (1987).

114. R. L. Shahab, S. Brethauer, M. P. Davey, A. G. Smith, S. Vignolini, J. S. Luterbacher, M. H. Studer, A heterogeneous microbial consortium producing short-chain fatty acids from lignocellulose. *Science*. **369**, eabb1214 (2020).

115. M. Tramontano, S. Andrejev, M. Pruteanu, M. Klünemann, M. Kuhn, M. Galardini, P. Jouhten, A. Zelezniak, G. Zeller, P. Bork, A. Typas, K. R. Patil, Nutritional preferences of human gut bacteria reveal their metabolic idiosyncrasies. *Nat Microbiol*. **3**, 514–522 (2018).

116. L. Henderson, Concerning the relationship between the strength of acids and their capacity to preserve neutrality. *American Journal of Physiology*. **21**, 173–179 (1908).

117. G. Kortüm, W. Vogel, K. Andrussow, Dissociation constants of organic acids in aqueous solution. *Pure and Applied Chemistry*. **1**, 187–536 (1960).

118. A. Battesti, N. Majdalani, S. Gottesman, The RpoS-Mediated General Stress Response in *Escherichia coli*. *Annu. Rev. Microbiol*. **65**, 189–213 (2011).

119. T. X. Xiang, B. D. Anderson, Permeability of acetic acid across gel and liquid-crystalline lipid bilayers conforms to free-surface-area theory. *Biophysical Journal*. **72**, 223–237 (1997).

120. J. B. Russell, Another explanation for the toxicity of fermentation acids at low pH: anion accumulation versus uncoupling. *Journal of Applied Bacteriology*. **73**, 363–370 (1992).

121. M. Basan, M. Zhu, X. Dai, M. Warren, D. Sévin, Y. Wang, T. Hwa, Inflating bacterial cells by increased protein synthesis. *Mol Syst Biol*. **11**, 836 (2015).

122. K. A. Martinez, R. D. Kitko, J. P. Mershon, H. E. Adcox, K. A. Malek, M. B. Berkmen, J. L. Slonczewski, Cytoplasmic pH Response to Acid Stress in Individual Cells of Escherichia coli and Bacillus subtilis Observed by Fluorescence Ratio Imaging Microscopy. *Appl. Environ. Microbiol*. **78**, 3706–3714 (2012).

123. H. Rottenberg, The measurement of transmembrane electrochemical proton gradients. *J Bioenerg Biomembr*. **7**, 61–74 (1975).

124. I. R. Booth, W. J. Mitchell, W. A. Hamilton, Quantitative analysis of proton-linked transport systems. The lactose permease of Escherichia coli. *Biochemical Journal*. **182**, 687–696 (1979).

125. W. W. Cleland, The use of pH studies to determine chemical mechanisms of enzyme-catalyzed reactions. *Methods in Enzymology*. **87**, 390–405 (1982).

126. B. E. H. Maden, R. E. Monro, Ribosome-Catalyzed Peptidyl Transfer: Effects of Cations and pH Value. *European Journal of Biochemistry*. **6**, 309–316 (1968).

127. F. Diez-Gonzalez, J. B. Russell, Effects of carbonylcyanide-m-chlorophenylhydrazone (CCCP) and acetate on Escherichia coli O157:H7 and K-12: uncoupling versus anion accumulation. *FEMS Microbiology Letters*. **151**, 71–76 (1997).

128. B. D. Bennett, E. H. Kimball, M. Gao, R. Osterhout, S. J. Van Dien, J. D. Rabinowitz, Absolute metabolite concentrations and implied enzyme active site occupancy in Escherichia coli. *Nat Chem Biol*. **5**, 593–599 (2009).

129. P. I. Larsen, L. K. Sydnes, B. Landfald, A. R. Strøm, Osmoregulation in Escherichia coli by accumulation of organic osmolytes: betaines, glutamic acid, and trehalose. *Archives of microbiology*. **147**, 1–7 (1987).

130. N. K. Jain, I. Roy, *Protein Science*, in press, doi:10.1002/pro.3.

131. F. D. Vadder, P. Kovatcheva-Datchary, D. Goncalves, J. Vinera, C. Zitoun, A. Duchampt, F. Bäckhed, G. Mithieux, Microbiota-generated metabolites promote metabolic benefits via gut-brain neural circuits. *Cell*. **156**, 84–96 (2014).

132. M. L. Patnode, Z. W. Beller, N. D. Han, J. Cheng, S. L. Peters, N. Terrapon, B. Henrissat, S. L. Gall, L. Saulnier, D. K. Hayashi, A. Meynier, S. Vinoy, R. J. Giannone, R. L. Hettich, J. I. Gordon, Interspecies Competition Impacts Targeted Manipulation of Human Gut Bacteria by Fiber-Derived Glycans. *Cell*. **179**, 59–73 (2019).

133. R. U. Sheth, V. Cabral, S. P. Chen, H. H. Want, Manipulating bacterial communities by in situ microbiome engineering. *Trends in Genetics*. **32**, 189–200 (2016).

134. J. L. Foo, H. Ling, Y. S. Lee, M. Woo, Microbiome engineering: Current applications and its future. *Biotechnology journal*. **12**, 1600099 (2017).

135. I. R. Booth, Regulation of Cytoplasmic pH in Bacteria. *MICROBIOL. REV*. **49**, 20 (1985).

136. I. R. Booth, R. G. Kroll, Regulation of cytoplasmic pH (pH1) in bacteria and its relationship to metabolism. *Biochemical Society Transactions*. **11**, 70–72 (1983).

137. J. M. Gould, W. A. Cramer, Relationship between oxygen-induced proton efflux and membrane energization in cells of Escherichia coli. *Journal of Biological Chemistry*. **252**, 5875–5882 (1977).

138. J. B. Stock, B. Rauch, S. Roseman, Periplasmic space in Salmonella typhimurium and Escherichia coli. *Journal of Biological Chemistry*. **252**, 7850–7861 (1977).

139. J. B. Russell, F. Diez-Gonzales, The Effects of Fermentation Acids on Bacterial Growth. *Advances in Microbial Physiology*. **39**, 205–234 (1997).

140. A. Change, L. Jeske, S. Ulbrich, J. Hormann, J. Koblitz, I. Schomburg, M. Neumann-Schall, D. Jahn, D. Schomburg, BRENDA, the ELIXIR core data resource in 2021: new developments and updates. *Nucleic Acids Research*. **49**, 498–508 (2020).

141. M. Rimmele, W. Boos, Trehalose-6-phosphate hydrolase of Escherichia coli. *Journal of Bacteriology*. **176**, 5654–5664 (1994).

142. R. Lutz, H. Bujard, Independent and tight regulation of transcriptional units in Escherichia coli via the LacR/O, the TetR/O and AraC/I1-I2 regulatory elements. *Nucleic acids research*. **26**, 1203–1210 (1997).

143. S. Klumpp, Z. Zhang, T. Hwa, Growth rate-dependent global effects on gene expression in bacteria. *Cell*. **139**, 1366–1375 (2009).

144. K. A. Datsenko, B. L. Wanner, One-step inactivation of chromosomal genes in Escherichia coli K-12 using PCR products. *Proceedings of the National Academy of Sciences*. **97**, 6640–6645 (2000).

145. E. Levine, Z. Zhang, T. Kuhlman, T. Hwa, Quantitative characteristics of gene regulation by small RNA. *PLoS Biol*. **5**, e229 (2007).

146. T. Baba, T. Ara, M. Hasegawa, Y. Takai, Y. Okumura, M. Baba, K. A. Datsenko, M. Tomita, B. L. Wanner, H. Mori, *Molecular Systems Biology*, in press, doi:10.1038/msb4100050.

147. S. Cayley, B. A. Lewis, H. J. Guttman, M. T. Record, Characterization of the cytoplasm of Escherichia coli K-12 as a function of external osmolarity. *Journal of Molecular Biology*. **222**, 281–300 (1991).

148. F. C. Neidhardt, P. L. Bloch, D. F. Smith, Culture Medium for Enterobacteria. *Journal of Bacteriology*. **119**, 736–747 (1974).

149. T. P. Ikeda, A. E. Shauger, S. Kustu, Salmonella typhimurium Apparently Perceives External Nitrogen Limitation as Internal Glutamine Limitation. *Journal of Molecular Biology*. **259**, 589–607 (1996).

150. L. N. Csonka, T. P. Ikeda, S. A. Fletcher, S. Kustu, The accumulation of glutamate is necessary for optimal growth of Salmonella typhimurium in media of high osmolality but not induction of the proU operon. *J Bacteriol*. **176**, 6324–6333 (1994).

151. H. Okano, T. Hwa, P. Lenz, D. Yan, Reversible Adenylylation of Glutamine Synthetase Is Dynamically Counterbalanced during Steady-State Growth of Escherichia coli. *Journal of Molecular Biology*. **404**, 522–536 (2010).

152. X. Su, W. Lu, J. D. Rabinowitz, Metabolite Spectral Accuracy on Orbitraps. *Anal. Chem*. **89**, 5940–5948 (2017).

153. E. Soupene, W. C. van Heeswijk, J. Plumbridge, V. Stewart, D. Bertenthal, H. Lee, G. Prasad, O. Paliy, P. Charernnoppakul, S. Kustu, Physiological Studies of Escherichia coli Strain MG1655: Growth Defects and Apparent Cross-Regulation of Gene Expression. *J Bacteriol*. **185**, 5611–5626 (2003).

154. S. J. Schink, E. Biselli, C. Ammar, U. Gerland, Death Rate of E. coli during Starvation Is Set by Maintenance Cost and Biomass Recycling. *Cell Systems*. **9**, 64-73.e3 (2019).

155. K. Kochanowski, H. Okano, V. Patsalo, J. R. Williamson, U. Sauer, T. Hwa, Global coordination of metabolic pathways in Escherichia coli by active and passive regulation. *Mol Syst Biol*. **17**, e10064 (2021).

156. P. D. Cani, Human gut microbiome: hopes, threats and promises. *Gut*. **67**, 1716–1725 (2018).

157. H. M. Wexler, Bacteroides: the Good, the Bad, and the Nitty-Gritty. *Clinical Microbiology Reviews*. **20**, 593–621 (2007).

158. A. G. Wexler, A. L. Goodman, An insider's perspective: Bacteroides as a window into the microbiome. *Nat Microbiol*. **2**, 1–11 (2017).

159. N. D. Schwalm, E. A. Groisman, Navigating the Gut Buffet: Control of Polysaccharide Utilization in Bacteroides spp. *Trends in Microbiology*. **25**, 1005–1015 (2017).

160. K. L. Anderson, A. A. Salyers, Biochemical evidence that starch breakdown by Bacteroides thetaiotaomicron involves outer membrane starch-binding sites and periplasmic starch-degrading enzymes. *J Bacteriol*. **171**, 3192–3198 (1989).

161. A. A. Salyers, J. R. Vercellotti, S. E. West, T. D. Wilkins, Fermentation of mucin and plant polysaccharides by strains of Bacteroides from the human colon. *Appl Environ Microbiol*. **33**, 319–322 (1977).

162. A. A. Salyers, M. O'Brien, Cellular location of enzymes involved in chondroitin sulfate breakdown by Bacteroides thetaiotaomicron. *J Bacteriol*. **143**, 772–780 (1980).

163. J. Briliūtė, P. A. Urbanowicz, A. S. Luis, A. Baslé, N. Paterson, O. Rebello, J. Hendel, D. A. Ndeh, E. C. Lowe, E. C. Martens, D. I. R. Spencer, D. N. Bolam, L. I. Crouch, Complex N-glycan breakdown by gut Bacteroides involves an extensive enzymatic apparatus encoded by multiple co-regulated genetic loci. *Nat Microbiol*. **4**, 1571–1581 (2019).

164. N. D. Schwalm, G. E. Townsend, E. A. Groisman, Multiple Signals Govern Utilization of a Polysaccharide in the Gut Bacterium Bacteroides thetaiotaomicron. *mBio*. **7**, e01342-16 (2016).

165. G. E. Townsend, W. Han, N. D. Schwalm, X. Hong, N. A. Bencivenga-Barry, A. L. Goodman, E. A. Groisman, A Master Regulator of Bacteroides thetaiotaomicron Gut Colonization Controls Carbohydrate Utilization and an Alternative Protein Synthesis Factor. **11**, 14 (2020).

166. K. H. Cho, D. Cho, G.-R. Wang, A. A. Salyers, New Regulatory Gene That Contributes to Control of Bacteroides thetaiotaomicron Starch Utilization Genes. *J Bacteriol*. **183**, 7198–7205 (2001).

167. P. B. Hylemon, P. V. Phibbs, Evidence against the presence of cyclic AMP and related enzymes in selected strains of Bacteroides fragilis. *Biochemical and Biophysical Research Communications*. **60**, 88–95 (1974).

168. L. S. Siegel, P. B. Hylemon, P. V. Phibbs, Cyclic adenosine 3',5'-monophosphate levels and activities of adenylate cyclase and cyclic adenosine 3',5'-monophosphate phosphodiesterase in Pseudomonas and Bacteroides. *J Bacteriol*. **129**, 87–96 (1977).

169. M. g. Sajilata, R. S. Singhal, P. R. Kulkarni, Resistant Starch–A Review. *Comprehensive Reviews in Food Science and Food Safety*. **5**, 1–17 (2006).

170. A. Flamholz, E. Noor, A. Bar-Even, W. Liebermeister, R. Milo, Glycolytic strategy as a tradeoff between energy yield and protein cost. *Proceedings of the National Academy of Sciences*. **110**, 10039–10044 (2013).

171. N. J. Sweeney, D. C. Laux, P. S. Cohen, Escherichia coli F-18 and E. coli K-12 eda mutants do not colonize the streptomycin-treated mouse large intestine. *Infection and Immunity*. **64**, 3504–3511 (1996).

172. J. A. Shipman, K. H. Cho, H. A. Siegel, A. A. Salyers, Physiological Characterization of SusG, an Outer Membrane Protein Essential for Starch Utilization by *Bacteroides thetaiotaomicron*. *J Bacteriol*. **181**, 7206–7211 (1999).

173. G. T. Macfarlane, S. Hay, S. Macfarlane, G. R. Gibson, Effect of different carbohydrates on growth, polysaccharidase and glycosidase production by *Bacteroides ovatus* , in batch and continuous culture. *Journal of Applied Bacteriology*. **68**, 179–187 (1990).

174. G. T. MacFarlane, G. R. Gibson, Co-utilization of polymerized carbon sources by Bacteroides ovatus grown in a two-stage continuous culture system. *Appl Environ Microbiol*. **57**, 1–6 (1991).

175. C. Cheng, E. J. O'Brien, D. McCloskey, J. Utrilla, C. Olson, R. A. LaCroix, T. E. Sandberg, A. M. Feist, B. O. Palsson, Z. A. King, Laboratory evolution reveals a two-dimensional rate-yield tradeoff in microbial metabolism (2018), doi:10.1101/414912.

176. J. Miller, Experiments in Molecular Genetics. Cold Spring Harbor, NY: Cold Spring Harbor Laboratory Press (1972).

177. E. Kukko, J. Heinonen, The Intracellular Concentration of Pyrophosphate in the Batch Culture of Escherichia coli. *Eur J Biochem*. **127**, 347–349 (1982).

178. B. Lim, M. Zimmermann, N. A. Barry, A. L. Goodman, Engineered Regulatory Systems Modulate Gene Expression of Human Commensals in the Gut. *Cell*. **169**, 547-558.e15 (2017).

179. E. Kukko, H. Saarento, Diphosphate concentration does not correlate with the level of inorganic diphosphatase inEscherichia coli. *Folia Microbiol*. **29**, 282–287 (1984).

180. E. Kukko-Kalske, M. Lintunen, M. K. Inen, R. Lahti, J. Heinonen, Intracellular PPi concentration is not directly dependent on amount of inorganic pyrophosphatase in Escherichia coli K-12 cells. *J Bacteriol*. **171**, 4498–4500 (1989).

181. C. S. Henry, L. J. Broadbelt, V. Hatzimanikatis, Thermodynamics-Based Metabolic Flux Analysis. *Biophysical Journal*. **92**, 1792–1805 (2007).

182. T. Ruusala, D. Andersson, M. Ehrenberg, C. G. Kurland, Hyper-accurate ribosomes inhibit growth. *The EMBO Journal*. **3**, 2575–2580 (1984).

183. R. Schleif, W. Hess, S. Finkelstein, D. Ellis, Induction Kinetics of the L -Arabinose Operon of *Escherichia coli*. *J Bacteriol*. **115**, 9–14 (1973).

184. M. Zhu, X. Dai, Y.-P. Wang, Real time determination of bacterial in vivo ribosome translation elongation speed based on LacZα complementation system. *Nucleic Acids Research*. **44**, e155 (2016).

185. X. Dai, M. Zhu, M. Warren, R. Balakrishnan, H. Okano, J. R. Williamson, K. Fredrick, T. Hwa, Slowdown of Translational Elongation in Escherichia coli under Hyperosmotic Stress. *mBio*. **9**, e02375-17 (2017).

186. A. Okura, T. Kinoshita, N. Tanaka, FORMATION OF FUSIDIC ACID-G FACTOR-GDP-RIBOSOME COMPLEX AND THE RELATIONSHIP TO THE INHIBITION OF GTP HYDROLYSIS. *J. Antibiot*. **24**, 655–661 (1971).

187. H.-S. Seo, S. Abedin, D. Kamp, D. N. Wilson, K. H. Nierhaus, B. S. Cooperman, EF-G-Dependent GTPase on the Ribosome. Conformational Change and Fusidic Acid Inhibition. *Biochemistry*. **45**, 2504–2514 (2006).

188. M. Novak, T. Pfeiffer, R. E. Lenski, U. Sauer, S. Bonhoeffer, Experimental Tests for an Evolutionary Trade-Off between Growth Rate and Yield in E. coli. *The American Naturalist*. **168**, 242–251 (2006).

189. S. A. Frank, The trade-off between rate and yield in the design of microbial metabolism. *Journal of Evolutionary Biology*. **23**, 609–613 (2010).

190. J. J. Faith, J. L. Guruge, M. Charbonneau, S. Subramanian, H. Seedorf, A. L. Goodman, J. C. Clemente, R. Knight, A. C. Heath, R. L. Leibel, M. Rosenbaum, J. I. Gordon, The Long-Term Stability of the Human Gut Microbiota. *Science*. **341**, 1237439 (2013).

191. E. S. Shepherd, W. C. DeLoache, K. M. Pruss, W. R. Whitaker, J. L. Sonnenburg, An exclusive metabolic niche enables strain engraftment in the gut microbiota. *Nature*. **557**, 434–438 (2018).

192. S. Lee, K. K. Y. Yuen, K. A. Jolliffe, J. Yoon, Fluorescent and colorimetric chemosensors for pyrophosphate. *Chem. Soc. Rev*. **44**, 1749–1762 (2015).

193. S. S. Nielsen, in *Food Analysis Laboratory Manual*, S. S. Nielsen, Ed. (Springer US, Boston, MA, 2010; https://doi.org/10.1007/978-1-4419-1463-7_6), *Food Science Texts Series*, pp. 47–53.

194. J. Gidden, J. Denson, R. Liyanage, D. M. Ivey, J. O. Lay, Lipid Compositions in Escherichia coli and Bacillus subtilis During Growth as Determined by MALDI-TOF and TOF/TOF Mass Spectrometry. *Int J Mass Spectrom*. **283**, 178–184 (2009).

195. A. L. Koch, Shrinkage of growing Escherichia coli cells by osmotic challenge. *Journal of Bacteriology*. **159**, 919–924 (1984).

196. H. Tsuchiya, S. Doki, M. Takemoto, T. Ikuta, T. Higuchi, K. Fukui, Y. Usuda, E. Tabuchi, S. Nagatoishi, K. Tsumoto, T. Nishizawa, K. Ito, N. Dohmae, R. Ishitani, O. Nureki, Structural basis for amino acid export by DMT superfamily transporter YddG. *Nature*. **534**, 417–420 (2016).

197. H. Hori, H. Yoneyama, R. Tobe, T. Ando, E. Isogai, R. Katsumata, Inducible l-Alanine Exporter Encoded by the Novel Gene ygaW (alaE) in Escherichia coli. *Applied and Environmental Microbiology*. **77**, 4027–4034 (2011).

198. W. Lü, J. Du, N. J. Schwarzer, E. Gerbig-Smentek, O. Einsle, S. L. A. Andrade, The formate channel FocA exports the products of mixed-acid fermentation. *Proceedings of the National Academy of Sciences*. **109**, 13254–13259 (2012).

199. R. A. LaCroix, T. E. Sandberg, E. J. O'Brien, J. Utrilla, A. Ebrahim, G. I. Guzman, R. Szubin, B. O. Palsson, A. M. Feist, Use of Adaptive Laboratory Evolution To Discover Key Mutations Enabling Rapid Growth of Escherichia coli K-12 MG1655 on Glucose Minimal Medium. *Appl. Environ. Microbiol.* **81**, 17–30 (2015).

200. N. A. Santiesteban-López, M. Rosales, E. Palou, A. López-Malo, Growth Response of Escherichia coli ATCC 35218 Adapted to Several Concentrations of Sodium Benzoate and Potassium Sorbate. *Journal of Food Protection*. **72**, 2301–2307 (2009).

201. A. D. Warth, Mechanism of action of benzoic acid on Zygosaccharomyces bailii: effects on glycolytic metabolite levels, energy production, and intracellular pH. *Appl Environ Microbiol*. **57**, 3410–3414 (1991).

202. S.-M. Liao, Q.-S. Du, J.-Z. Meng, Z.-W. Pang, R.-B. Huang, The multiple roles of histidine in protein interactions. *Chem Cent J*. **7**, 44 (2013).

203. A. L. Hansen, L. E. Kay, Measurement of histidine pKa values and tautomer populations in invisible protein states. *Proceedings of the National Academy of Sciences*. **111**, E1705–E1712 (2014).

204. M. D. Joshi, G. Sidhu, I. Pot, G. D. Brayer, S. G. Withers, L. P. McIntosh, Hydrogen bonding and catalysis: a novel explanation for how a single amino acid substitution can change the ph optimum of a glycosidase11Edited by M. F. Summers. *Journal of Molecular Biology*. **299**, 255–279 (2000).

205. M. D. Joshi, G. Sidhu, J. E. Nielsen, G. D. Brayer, S. G. Withers, L. P. McIntosh, Dissecting the Electrostatic Interactions and pH-Dependent Activity of a Family 11 Glycosidase †,‡. *Biochemistry*. **40**, 10115–10139 (2001).

206. J. E. Nielsen, in *Methods in Enzymology* (Elsevier, 2009; https://linkinghub.elsevier.com/retrieve/pii/S0076687908038093), vol. 454, pp. 233–258.

207. A. R. Klingen, E. Bombarda, G. M. Ullmann, Theoretical investigation of the behavior of titratable groups in proteins. *Photochem Photobiol Sci*. **5**, 588–596 (2006).

208. C. Bergman, Y. Kashiwaya, R. L. Veech, The Effect of pH and Free Mg2+ on ATP Linked Enzymes and the Calculation of Gibbs Free Energy of ATP Hydrolysis. *J. Phys. Chem. B*. **114**, 16137–16146 (2010).

209. I. M. Keseler, A. Mackie, A. Santos-Zavaleta, R. Billington, C. Bonavides-Martínez, R. Caspi, C. Fulcher, S. Gama-Castro, A. Kothari, M. Krummenacker, M. Latendresse, L. Muñiz-Rascado, Q. Ong, S. Paley, M. Peralta-Gil, P. Subhraveti, D. A. Velázquez-Ramírez, D. Weaver, J. Collado-Vides, I. Paulsen, P. D. Karp, The EcoCyc database: reflecting new knowledge about Escherichia coli K-12. *Nucleic Acids Research*. **45**, D543–D550 (2017).

210. V. Pascal Andreu, M. A. Fischbach, M. H. Medema, Computational genomic discovery of diverse gene clusters harbouring Fe-S flavoenzymes in anaerobic gut microbiota. *Microb Genom*. **6** (2020), doi:10.1099/mgen.0.000373.

211. Complete Genome Sequence of Escherichia coli NCM3722, , doi:10.1128/genomeA.00879-15.

212. D. Caspari, J. M. Macy, The role of carbon dioxide in glucose metabolism of Bacteroides fragilis. *Arch. Microbiol*. **135**, 16–24 (1983).

213. E. K. Holwerda, J. Zhou, S. Hon, D. M. Stevenson, D. Amador-Noguez, L. R. Lynd, J. P. van Dijken, Metabolic Fluxes of Nitrogen and Pyrophosphate in Chemostat Cultures of Clostridium thermocellum and Thermoanaerobacterium saccharolyticum. *Applied and Environmental Microbiology*. **86**, e01795-20 (2020).

214. J. Zhou, D. G. Olson, D. A. Argyros, Y. Deng, W. M. van Gulik, J. P. van Dijken, L. R. Lynd, Atypical Glycolysis in Clostridium thermocellum. *Applied and Environmental Microbiology*. **79**, 3000–3008 (2013).